INVESTIGATION OF THE POTENTIAL OF PV IN TROLLEYGRIDS

STUDY OF THE EFFECT OF KEY PERFORMANCE INDICATORS ON THE INTEGRATION OF PHOTOVOLTAIC (PV) SYSTEMS IN TROLLEYGRIDS

ARNHEM AND GDYNIA CASE STUDIES

A thesis submitted to the Delft University of Technology in partial fulfillment
of the requirements for the degree of

Master of Science in Sustainable Energy Technologies

by

Alice Saffirio

June 2021

Alice Saffirio: *Investigation of the Potential of PV in Trolleygrids* (2021)

The work in this thesis was made in the:

DC Systems, Energy Conversion & Storage
Department of Electrical Sustainable Energy
Faculty of Electrical Engineering, Mathematics and Computer Science (EEMCS)
Delft University of Technology

Supervision: Ir. Ibrahim Diab
Dr.ir. Gautham Ram Chandra Mouli
Prof.dr.ir. Pavol Bauer
Dr.ir. Rudi Santbergen

ABSTRACT

The transport sector in the EU is responsible for 30% of its yearly energy consumption and 27% of its greenhouse gas emissions, as oil and gas products still have a leading role in the transport sector supply [16]. The use of electricity from renewable energy sources (RES) for transport, however, is a possible and mature alternative to fossil fuels and combustion motors. One of the most effective electrification solutions for the urban transport is offered by the trolleybus grids [19]. These transportation networks can become more sustainable and efficient by the direct integration of RES and storage. Among the several RES possibilities, solar photovoltaic (PV) energy is the most promising and also most studied source for this type of application because of its modularity and cost, offering the possibility of distributed green generation at the different substations of the grid. Moreover, both the trolleygrid and the PV are DC, which removes one power conversion step.

A recent study on the Arnhem grid in the Netherlands, however, has shown that distributed PV necessitates large storage and/or large exchange with the grid – a situation that is defined as low "PV Utilization" (PVU) [54]. Fortunately, some substations did offer the interesting potential of a high PVU. In order to understand the feasibility of supplying trolleygrids with PV, it is necessary to identify which parameters impact the PVU, and in which manner.

This thesis allows to draw some estimations for the feasibility of the application of PV in the trolleybus grids. This is done by identifying a set of Key Performance Indicators (KPIs) and studying their correlation to the PVU for two trolleybus grids, namely Arnhem (the Netherlands) and Gdynia (Poland). The selected KPIs are: Sunshine duration, yearly irradiance, substation load demand, number of sections fed by one substation, section length, bus traffic density under a section, and the HVAC (heating, ventilation, air conditioning) requirement of the bus brought on by the local weather.

To estimate the load on the grid substations, first, velocity profiles of the buses were created from available measurements and introducing random traffic lights and bus stops probability. These profiles were translated into a bus power demand using a vehicle model (courtesy of HAN University of Applied Sciences) and a developed HVAC model. This, coupled with the timetables, created the input to a MATLAB trolleygrid model. The PV system output was obtained from a MATLAB PV model and local weather data for each city. The PV system integration potential was assessed in terms of both how much of the PV energy is used (PVU) and the fraction of the load that is covers (Load Coverage, LC).

The results of the simulation show different trends for the studied parameters. Sunshine duration and yearly irradiance levels between the two cities have a strong impact on the LC, with a maximum variation of 10 percentage points, while they do not affect noticeably the PVU, with 1 percentage point variation. The spread-out Arnhem layout causes an increase in the number of the substations in grid, and a reduction of their size. This was found to be a disadvantage when integrating PV in trolleygrids, when compared to the denser Gdynia grid. As a matter of fact, the increase in power demand and in the number of sections supplied by one substation, both cause an improvement of the PV utilization and the load coverage. Although the average section length does not seem to show a PVU or LC trend, the higher bus traffic under a substation is found to present higher PVU and LC values. It is also observed that removing the HVAC system from the substation supply brings reductions of in the PVU and LC reaching up to 35 and 14 percentage points, respectively. This was not an expected result, as the yearly heating demand curve and the yearly PV generation curve present opposite trends.

In conclusion, it was found that the potential of integrating PV into the trolleygrid in Gdynia is higher than that in Arnhem, with better results both in terms of PV utilization and load coverage. The more centralised traction system found in Gdynia, with higher average demand of the substations, average number of sections and of buses supplied by a substation, together with the higher number of lines and buses running in this grid and the better environmental conditions all favour the integration of PV when compared to the Arnhem trolleygrid.

Additionally, the introduction of Stationary Storage coupled with the PV systems at substation level is studied, and it is found that it can improve substantially the performance of the PV systems, reaching values of PV utilization in the range of 90% or higher and levels of load coverage of approximately 40%. The enhancement of PVU and LC is high especially for smaller substations which see increases by up to 60 and 30 percentage points, respectively. This shows that, coupled with storage, PV integration is still feasible for substations with unfavourable KPIs values.

ACKNOWLEDGEMENTS

I am grateful to Ibrahim Diab and Dr.ir. Gautham Ram Chandra Mouli for the opportunity of working in this research group. I believe that the project I worked on for my Master Thesis with the DCSE&S group has a big potential within the energy transition scope. Not only I found the topic very interesting and inspiring, but the elevated number of challenges faced made it also very engaging. I would like to thank my daily supervisor Ibrahim Diab for the continuous support provided throughout the whole project. A special thanks also to my supervisor, Dr.ir. Gautham Ram Chandra Mouli, who consistently allowed this project to be my own work, but steered me in the right the direction. I would like to thank Prof.dr.ir. Pavol Bauer too, for the time spent on my project and the feedback provided on my work. I would also like to acknowledge the precious inputs to the project coming from Mikołaj Bartłomiejczyk, Marcin Wolek and Abhishek Tomar.

I must also express my gratitude to my parents and to all my family for providing me with unfailing support and continuous encouragement throughout my years of study. Thank you for always believing in me and for backing me up in all my decisions.

Finally, thank you to all my friends, close and far. Thank you Kristin, Tati, Chatu, Martijn, Svenja and all the Gezellig group, you made my final university years so rich of experiences and emotions. A special thanks to my flatmates, my Dutch family, always available to help me and encourage me. A 'thank you' also goes to my friends from Italy, Carolina, Sara, Carola, Ginni and Sara, 'le 7 Meraviglie' group, Manfra, Andrea, Luca and Stefano, who have always been supportive although the distance.

This accomplishment would not have been possible without you.

Thank you.

My warmest regards,

Alice

CONTENTS

LIST OF FIGURES

LIST OF TABLES

NOMENCLATURE

Abbreviations

AC	Alternating Current
aprx	Approximation
BESS	Battery Energy Storage System
BESSU	BESS Utilization
Cap	Capacity
cf	Capacity Factor
DC	Direct Current
DHI	Diffuse Horizontal Irradiance
DNI	Direct Normal Irradiance
DoD	Depth of Discharge
EoS	End of Section
GHG	Green House Gases
GHI	Global Horizontal Irradiance
HVAC	Heating, Ventilation, Air Conditioning system
KPI	Key Performance Indicator
LC	Load Coverage
LV	Low Voltage
MV	Medium Voltage
PV	Photovoltaic
PVU	PV system Utilization
SC	Super-capacitor
SD	Sunshine Duration
SOC	State of Charge
STC	Standard Test Conditions
SVF	Sky View Factor

Symbols

λ	Thickness	[m]
ρ	Air density	$[\frac{kg}{m^2}]$
τ	Transmissivity	[-]
θ_M	PV module tilt angle	[°]
c_p	Air heat capacity	$[\frac{J}{kgK}]$
G	Irradiance	$[\frac{W}{m^2}]$
h_o	Inner surface convection coefficient	$[\frac{W}{m^2K}]$
h_o	Outer surface convection coefficient	$[\frac{W}{m^2K}]$
I	Current	[I]
k	Thermal conductivity	$[\frac{W}{mK}]$
l_s	Distance between parallel connections	[m]
$l_{parallel}$	Length of the line connected in parallel between the bus and the supply point	[m]
l_{single}	Bus distance from the closest parallel connection before it	[m]
l_{total}	Bus distance from supply point	[m]
M	Metabolic Heat Load	[W]
P_{bus}	Bus Power	[kW]
$P_{discharge}$	Battery discharge power	[kW]
P_{grid}	Grid power requirements	[kW]
P_{load}	Load power demand	[kW]
P_{PV}	PV generated power	[kW]
Q	Heat Load	[W]
R	Resistance	[Ω]

RH	Relative Humidity	[-]
S	Surface	[m]
T	Temperature	[K]
T_M	Module Temperature	[K]
T_a	Air Temperature	[K]
T_{ground}	Ground Temperature	[K]
T_{sky}	Sky Temperature	[K]
V	Voltage	[V]
v	Velocity	$[\frac{m}{s}]$
V_{bus}	Bus Voltage	[V]
V_{supply}	Supply voltage	[V]

1 INTRODUCTION

The introduction chapter is used to give the main definitions and a general explanation of the problem that this master thesis project will contribute to solving. First, the reasons and the interest in the research project are explained. Then, a brief overview of the trolleybus traction system is given, followed by an explanation of how PV and storage are integrated in the grid. Finally, the objectives of the research project are outlined.

1.1 Research interest and purpose

The transport sector in EU is responsible for 30% of total energy consumption and 27% of greenhouse gas emissions [16]. Looking at the pie charts in Figure 1.1, it is possible to notice that the transport sector has 19% and 29% share of the Total Final Consumption (TFC) of the Netherlands and Poland respectively [35]. These two countries are taken as reference, since Arnhem and Gdynia are located respectively in the former and in the latter. The trolleybus grids used for the two case studies are located in these two cities. Among all sectors that emit CO_2, the transport sector is the second fastest growing, after industry, and it represents from 22% to 24% of global Greenhouse gas (GHG) emissions from fossil fuel sources [63].

In Europe, the total amount of carbon dioxide emissions coming from road traffic in urban environment accounts for 40% [16]. Taking into consideration these data and the instability of liquid fuel prices, which has a negative impact on countries' economies, it becomes necessary to introduce and increase the share of alternative energy sources in transportation. The use of electricity for transport is a possible and mature alternative to liquid fuel and combustion motors. However, oil products still have a leading role in the transport supply, with a share of 93% of the total final consumption of the transport sectors of the Netherlands and Poland [35], as can be seen from the pie charts in Figure 1.2. Today, electric vehicles have increased in use, from scooters to buses Electricity, however, still has a minor contribution of the energy consumption of this sector, supplying 2% and 1% of the transport energy demand in the Netherlands and in Poland [35]. Up to today, the most effective way of supplying electricity to

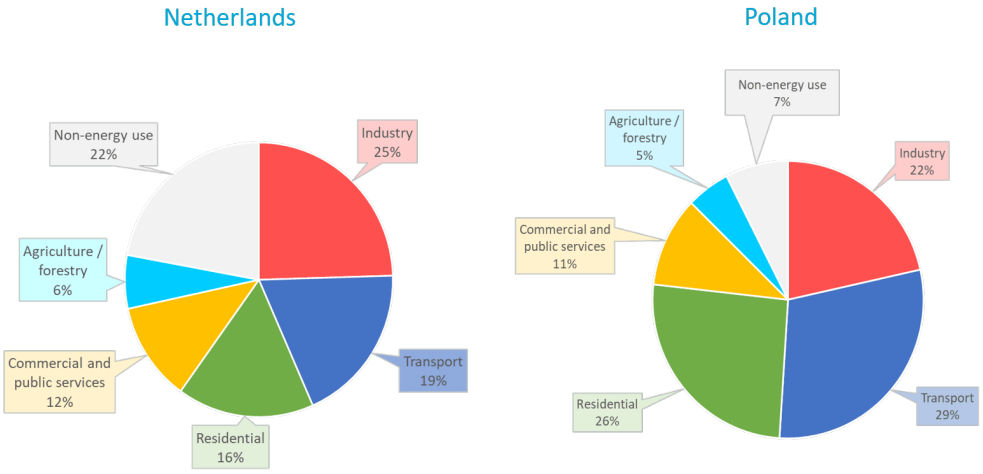

Figure 1.1: Total Final Consumption (TFC) per sector of the two countries of interest: the Netherlands (Arnhem trolleygrid) and Poland (Gdynia trolleygrid) [35]

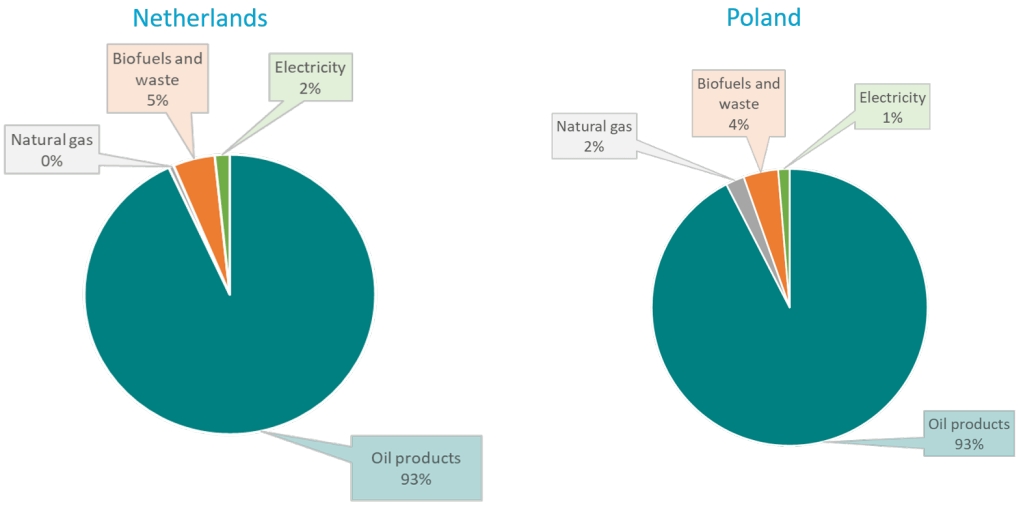

Figure 1.2: Total Final Consumption (TFC) per source of the Transport Sector of the two countries of interest: the Netherlands (Arnhem trolleygrid) and Poland (Gdynia trolleygrid) [35]

urban means of transport is still through overhead lines of rail vehicles (unipolar) and trolleybuses (bipolar) [19].

The need of renovation of urban transportation systems also stems from the continuous increase of car dependency of European populations. Towns and cities in Europe are facing mobility challenges due to urbanization and increase of the population density in urban areas. The strong dependency on cars to cover all types of routes and distances has consequences on high GHG emissions in the cities, but also on space consumption. As a matter of fact, buses perform better both in terms of sustainability, also due to the higher passenger capacities, and in terms of space-efficiency [25]. In the contest of renovation, the electrification of urban transport and the reduction of emissions find possible solutions in the existing trolleybus structures. The renovation of these systems towards more sustainable and greener solution can include both the introduction of renewable sources of energy to supply the grid and of storage systems to increase the efficiency and reliability of the system. By observing the charts in Figure 1.3, the dependence of the two countries of interest on Coal, Oil and Gas for electricity generation is clear. The reason behind proposing alternative solutions to supply the trolleybus systems, is found in these pie charts. The electrification of urban transport is partially answering the need of renovation of the urban transportation, since the electricity is mainly generated by highly emitting sources of energy. The electrification of transports can alleviate a number of contemporary issues connected to urban environments when inducing the reduction of the health hazards and olfactory discomfort to passengers caused but the tailpipe emissions of the vehicles, because of lower heat and noise emissions and the lack of motor vibration [31]. Electric vehicles also have higher efficiencies and cause lower emissions, in [43] it is demonstrated that fully-electric buses have the potential to reduce carbon dioxide emissions by up to 75%. However, it is necessary that renewable energy sources in the electricity mix is increased, in order to increase on a long-term basis the sustainability of electric mobility.

The renovation of trolleybus systems towards more sustainable solutions, through the integration of renewable sources of energy, answers to the need of electrification and reduction of emissions of the fast growing transport sector. The integration of storage can facilitate the transition to renewable sources providing a solution for the mismatch between load and demand and for voltage regulation. Between the multiple possibilities of supplying the loads through renewable energy systems, PV energy is the most promising and also most studied source for this type of application. Its modularity and urban friendly characteristics, make it an interesting option to supply through zero-emission sources the trolleybus grids.

After discussing the reasons why trolleybuses are interesting to research upon and why we the focus will be on the integration of renewable sources in the trolleygrids, in the next sections the reader finds an introduction of the system. First, the trolleybus system is presented, followed by an introduction on what introducing PV and storage in the grids actually means.

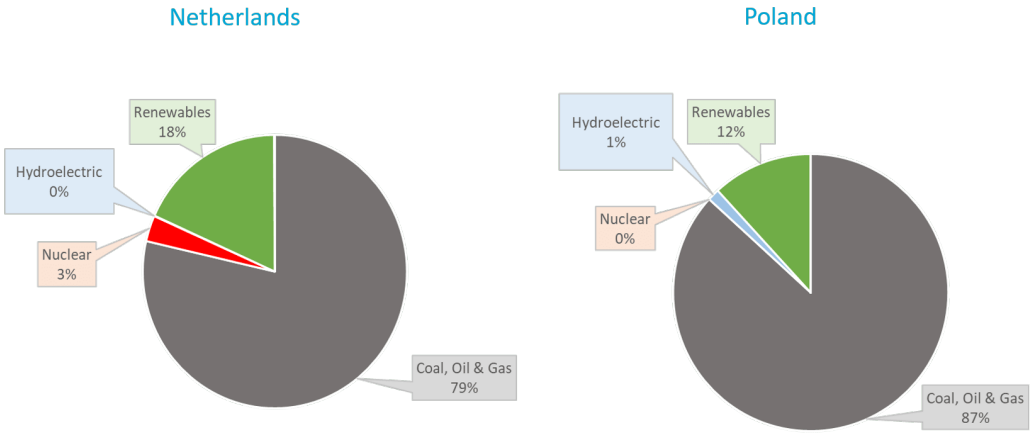

Figure 1.3: Electricity generation per source of the two countries of interest: the Netherlands (Arnhem trolleygrid) and Poland (Gdynia trolleygrid) [35]

1.2 What is a Trolleybus and what is a Trolleybus grid?

Trolleybuses are electric road vehicles used in urban context, which are powered by means of an overhead catenary line. This is formed by power cables that are installed above the roads travelled by the buses. In Figure 1.4, a schematic representation of the structure of a trolleybus traction grid is provided. The direct current (DC) traction network (overhead cables) is divided into power supply sections to which electrical power is supplied from traction substations. The supply areas are galvanically separated from each other and cannot exchange power between them. This division of the overhead cables is necessary to reduce the voltage drops along the lines and for maintenance purposes, since it allows to operate the system also when a portion of it is disconnected [66].

As can be seen in Figure 1.4, the sections are individually powered by feeders (subterranean power wires), which can vary in relation to the specific grid characteristics (distance of the substation from the grid, type of installation, temperatures, etc.). The DC busbars of the substations, together with the catenary and the feeder cables form what is called the low voltage (LV) DC traction grid. The substations of the trolleybuses are supplied by medium voltage (MV) AC power grids. In the traction substation both voltage reduction from medium to low voltage and transformation from AC to DC occur [12], respectively through a transformer and a rectifier. The voltage is decreased from the medium voltage of the AC grid, between 6 and 35 kV, to the DC voltage required. The nominal DC voltage amounts to 600 V or 725 V, which represent the standard input voltages of the vehicles. However, due to the voltage drops in the catenary lines and in the feeder cables the nominal output voltage from the substations is kept higher, in the range of approximately 10% [12]. This value can vary according to the distance of the substation from the catenary lines, to the power requirements, and other characteristics of the grid and the cables which can increase/reduce the voltage drops along the lines.

Trolleybuses are equipped with electrical motors which covert the electric energy supplied through the pantographs by the overhead power cables to kinetic energy. Electrical machines are capable of operating with bidirectional flows, which means that trolleybus traction motors can also convert kinetic energy into electric energy [18]. This happens when the vehicles are braking, and the speed of the vehicle is decreased, causing a reduction of the vehicle's kinetic energy. This energy can either be dissipated or transformed in electric energy (generator mode of the traction motor). The generated energy, increased in voltage by the traction inverter, is partly used to power bus auxiliaries or is directed to the overhead lines. The connection of the buses to the catenary lines allows bidirectional flow of electricity to and from the buses. In the case of absence of a consumer, in a conventional system without storage accumulators, the energy is sent to the braking resistors and dissipated as heat. In [18] M. Bartłomiejczyk and M. Połom identify three ways to re-use recovered energy: it can be consumed by auxiliaries, by other vehicles or accumulated in storage systems. A flow diagram is provided in Figure 1.6, to show the flow of recuperated energy. Consumption for non-traction purposes of the

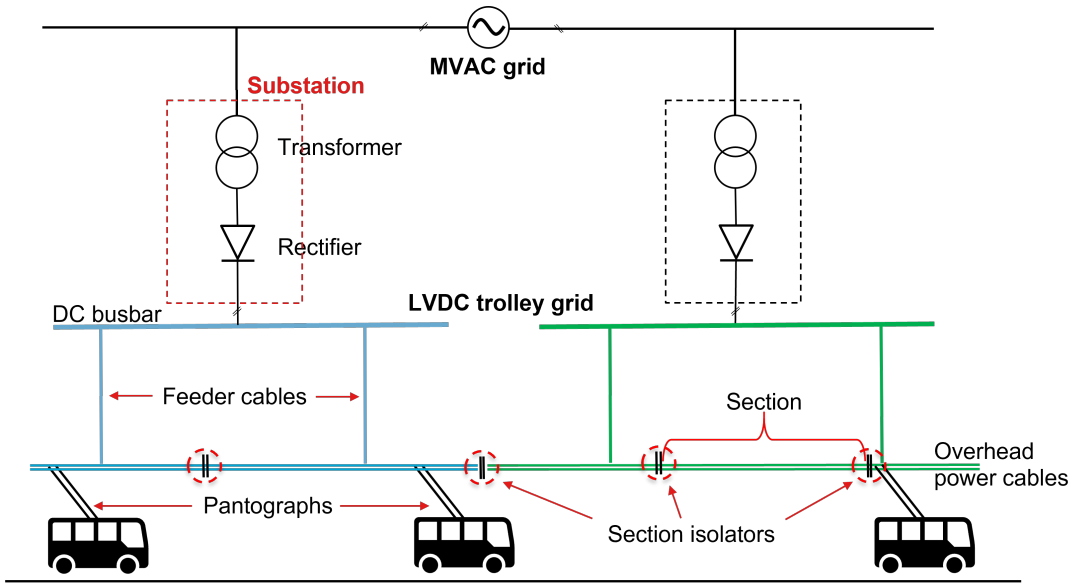

Figure 1.4: Schematics of a trolleybus traction system (LVDC grid and connection to MVAC grid) - reworked from [54]

vehicle is the most effective form of energy recovery utilization. What is not used from the auxiliaries should be returned to the supply system [18].

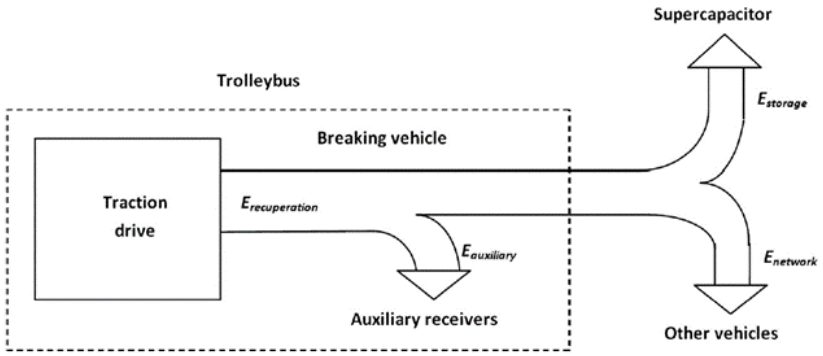

Figure 1.5: Braking vehicle - recouped energy flow [18]

In order to effectively return electric energy to the supply system the generated voltage must be higher than the one in the overhead lines. Therefore, high substation voltage levels can significantly reduce the utilization of recovered energy. The other condition to share recovered braking energy with other buses is that the sender and the consumer should be in the same power supply section of the grid. As discussed in the previous paragraph, the sections are galvanically isolated between them, and therefore power exchange is not allowed. For this reason, in supply sections with high traffic density, the recuperation efficiency can reach values of 40%. However, in supply area with low traffic the energy re-use system fails. In case of low traffic intensity or hilly areas, traction substations should be equipped with a storage system to increase recuperation efficiency. In [41], Yasunori Kume *et al.* study the effects of introducing LI-ion batteries in a railway system to temporarily store the regenerative power. A maximum reduction of 25.2% for the peak demand is achieved in their study due to the storage integration. In [34], Hitoshi Hayashiya *et al.* compare different methods to re-use regenerative braking energy in terms of the effect and of the cost that it introduces in the system. The authors concluded that the most promising solution to use recouped energy in DC traction power supply systems is the introduction of energy storage systems, through which 600 MWh per year are estimated to be saved, accounting for 4-8% reduction of the total traction power of the studied railway traction grid.

Another method to improve energy consumption efficiency by increasing the utilization of braking energy in a railway traction system is proposed in [38]. The authors present a strategy to restore the regenerative braking energy to the AC utility grid through reversible substations. The results obtained in [38] showed that introducing bidirectional substations to harvest recouped energy can have beneficial effects also on the power quality. However, substations in trolleygrids are usually unidirectional, which means they are characterised by unidirectional diode rectifiers which do not allow to send energy back to the medium voltage grid [51, 64]. It is a crucial element to take into consideration, since reversible substations would allow to send back to the MVAC grid the energy in excess in the LV trolleybus DC grid.

In order to exchange power between them, two buses have to be in sections supplied by the same substation. In conventional power supply systems, as explained in [9], each section of the overhead contact line is supplied from one substation only. Supply areas are galvanically isolated from each other and cannot exchange power between them. The utilization of recuperation energy from a braking vehicle could be improved if supply areas were to be joined with neighbouring substations, allowing the flow of recuperated energy between sections. In [9], Mikołaj Bartłomiejczyk presents the findings from his study on bilateral power supply in the trolleybus grid in Gdynia, Poland. In Figure 1.6, one can find a comparison between a standard supply system and a bilateral supply system. As shown in the pictures, allowing power flow between sections not only increases the chance in finding a consumer of regenerated energy but allows also to reduce voltage losses in the overhead catenary lines. As a matter of fact, through bilateral supply one section can be fed from two substations or from two supply points of the same substation, reducing like this the load currents in the lines. The findings of this study on bilateral power supply, conducted by Mikołaj Bartłomiejczyk, is that in lines with higher traffic and higher usage of braking energy recovery, the implementation of bilateral supply significantly reduces the voltage drops and the transmission losses. While, in lines with low traffic conditions and low capability of re-using regenerated energy, the bilateral connection brings to noticeable increases in recuperation effectiveness and a slight reduction of energy transmission losses.

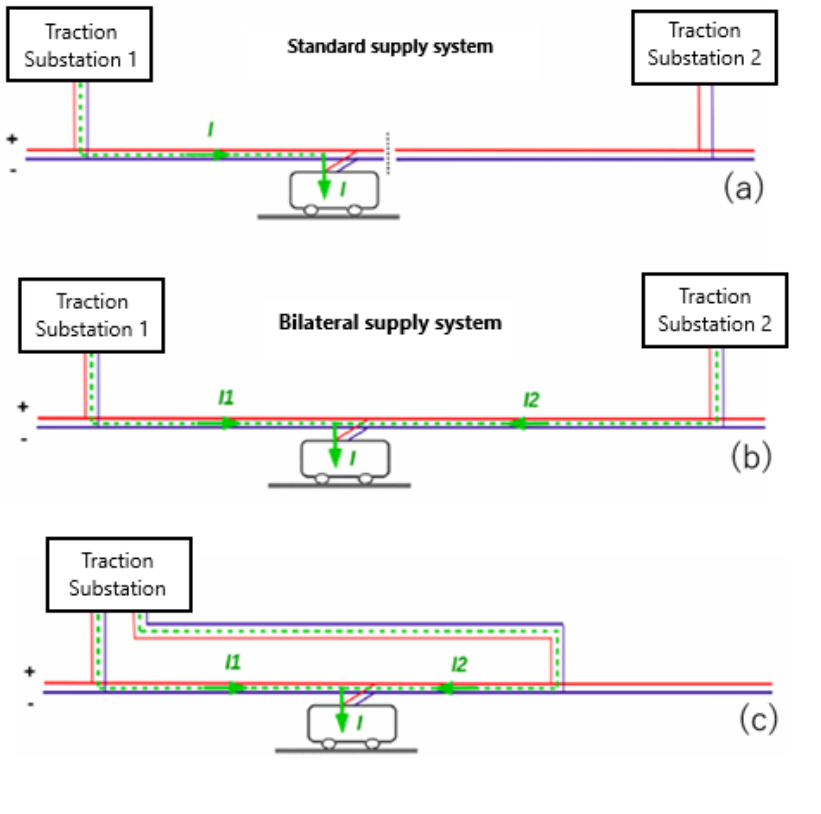

Figure 1.6: Comparison of vehicle current distribution between different supply traction substations. In (a) a standard unilateral supply system, in (b) a bilateral supply system with two substations, in (c) bilateral supply system with one substation [9]

The characteristics of the substations and of the supply system adopted in a traction grid have a strong impact on the energy consumption and the power flow within the system. The type of substations,

their dimension and their number and distribution in the grid can vary considerably for different trolleybus traction grids. The spatial structure of the overhead line has a significant impact on the energy consumption of the system, affecting transmission losses and determining the usage of the regenerative braking [17]. In [19], Mikołaj Bartłomiejczyk and Marcin Połom make a distinction between three different structures of the power supply systems: central power supply, unilateral decentralized power supply and bilateral decentralized power supply. A central system is characterised by large substations, which cover large supply areas, while a decentralized system has smaller substations densely arranged and located in proximity of the overhead line supply points. Central power supply structures, characterised by large substations supplying large areas, incur in large transmission losses. From a point of view of the recuperation of braking energy though, having the vast supply areas of the central supply system creates better conditions for the re-use of braking energy ensuring the largest number of potential consumers on the line. Decentralized power supply systems are preferable when aiming to minimize transmission losses since distances and cable lengths are significantly reduced and with it also the costs of maintaining the cable network. A solution proposed from the authors is to have bilateral supply for overhead lines, which allows to enlarge the area where the recovered energy can flow by connecting the supply areas, keeping the small distances between substations and reduced cable lengths. This is the distinction between unilateral and bilateral decentralized power supply systems. In Figure 1.7 and 1.8 two examples are provided to show the different characteristics of a centralised and decentralised supply. In Figure 1.9, an example of the inclusion of bilateral supply for a decentralised system is given.

1.3 What does PV and Storage Integration in a Trolleygrid mean?

The integration of Photovoltaic (PV) modules in traction grids is a possible solution to supplying a fraction of the load of the grid through emission-free sources. However, the potential of introducing PV may vary in relation to where the grid is located and its characteristics. But what do we mean by potential of PV systems integration in trolleygrids? And, how are PV and storage systems integrated in the grid? Before investigating the possible causes of the variation of the feasibility of the application, we want to understand how to measure the success of integrating PV and how the PV system is connected to a trolleybus grid.

When speaking about PV system integration potential, the intention is to investigate the effectiveness of the PV generation in supplying the load. This is measured investigating both how much of the PV energy is used by the trolleybus system and how much load is covered by the PV generated energy. These two elements provide an overview of how well the PV systems can perform in relation to the traction grid operation.

The integration of storage is studied as a variable affecting the potential of PV integrated in traction grids. For this reason in particular, the storage is coupled with the PV system in order to maximise the PV utilization while minimising the transmission losses between the two systems. As a matter of fact, the high variability of the load and of the generation, especially on short-term scale, limits the possibility of using all the generated energy [12]. For this reason, the potential of PV integration when the system is equipped with a battery energy storage system is measured in the same way. This means that the success in the PV system integration is studied based on the effectiveness in using the PV energy. The utilization of the battery system is also analysed to size the system appropriately.

Photovoltaic (PV) and storage systems can be connected to a trolleygrid with the same or separate connection points and they can be connected at substation level, on the AC or on the DC side, or directly to the traction network [12, 15]. Each point of connection of PV and storage systems has different advantages and disadvantages which are discussed further in Chapter 2. Since PV and storage will be studied as an integrated system, with the same connection point to the trolleybus grid, three configurations are possible: PV and storage connected to the AC side of the substations, represented in Figure 1.10, PV and storage connected to the DC busbar of the substation, shown in Figure 1.11, or PV and storage directly connected to the overhead lines, as in Figure 1.12. For the purpose of this Master thesis project, it is decided to study the potential of integrating PV (and PV coupled with storage) on

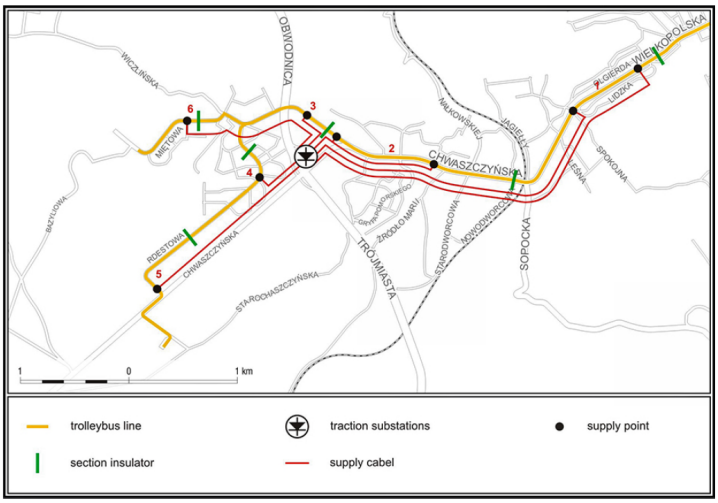

Figure 1.7: Example of centralized supply system [19]

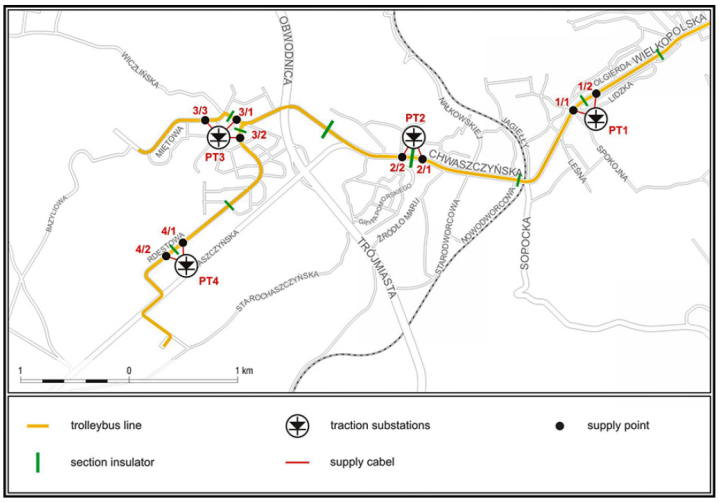

Figure 1.8: Example of decentralized supply system, one-side supply [19]

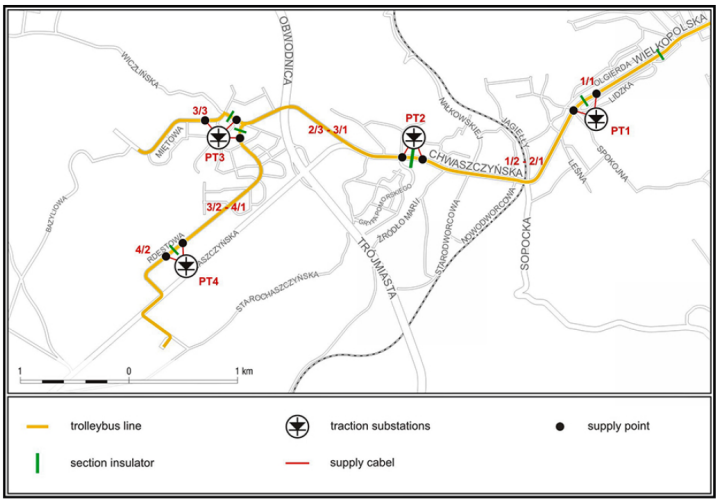

Figure 1.9: Example of decentralized supply system with bilateral supply [19]

the AC side of the substations. In Figure 1.13 and Figure 1.10, the schematics of the system with PV only and with PV and storage integrated are found.

The main reasons why this configuration is picked are here explained. Connecting the PV system on the AC side reduces the efficiency of the connection, since the generated energy has to be converted from DC to AC and to AC and DC again, increasing like this the losses. DC-to-AC conversion (and vice versa) cannot be performed without losses. The output energy of an inverter (AC) is lower than the input (DC). The efficiency of the inverter generally varies within 95% and 98%. The efficiency can change based on the DC input power and voltage [42]. AC-to-DC conversion is highly dependant on the power and voltage levels required, and it can range from 60-95%. However, high efficiency conversion is assumed for this study with rectifier efficiencies of 95% [53]. Installing PV on the DC side would reduce the losses by 5-10%, however, it would not allow to send the energy in excess back to the MVAC and would introduce strong voltage fluctuations in the traction grid due to the intermittent power generation. The short-term variability of the PV output can present power fluctuations of 45-90% of the rated power of the system. The location of the grid and the installed PV capacity have an impact on the magnitude of the voltage fluctuations [22]. For this reason, a power control system based on the measurement of the voltage levels across the networks should be implemented to limit the variation of the busbars voltages to the minimum, introducing multiple complications also in the modelling of the system which are outside the scope of this project [12]. The other reason, is that substations in trolleygrids are usually unidirectional, which means they are characterised by unidirectional diode rectifiers which do not allow to send energy back to the medium voltage grid [51, 64]. This not only has an impact on the transmission losses, due to the higher rates of dissipation of regenerated braking energy which is not used, but also on the potential integration of photovoltaic (PV) systems in the grid. If PV systems were to be placed on the DC side of unidirectional substations, all the PV generated energy which is not used by the load must be curtailed, since it cannot be sent back to the MVAC grid. Unidirectional substations could be replaced with reversible or bidirectional substations equipped with inverters that allow bidirectional operation. However, this would imply a deep modification of the trolleybus system as well.

Installing storage on the AC side also allows simpler control systems, but it does not allow to store and use regenerated braking power. The main disadvantage of installing storage systems on the AC side, besides the reduction of the utilization rate of braking energy, is that the batteries are not used for voltage regulation, and therefore present a reduction in their utilization potential [24, 36]. However, since the utilization of the PV systems and its temporal match with the load are the main focuses of this project, storage is placed on the AC side to maximise the PV generation utilization and therefore potential of integration.

1.4 Research Scope and Contributions

In order to generalise the possibility and the potential of supplying DC trolleygrids with emission-free generated energy it is necessary to understand which parameters mostly influence the energy requirements of the trolleybus grid and the potential of integrating renewable energy sources in the network. This study allows to draw some conclusions and recommendations for the application of PV and stationary storage in trolleybus grids, taking into consideration the variability of the characteristics of the grid and its location. The idea is to evaluate and quantify the differences between trolleybus systems in different cities and identify set of indicators that can be used to assess the feasibility and the potential of integrating PV systems in trolleygrids. The impact of these indicators on the grid components, load, PV and storage is studied to define the set. After this, a study on the selected indicators is performed to determine their impact on the integration of PV in the trolleybus grids of Arnhem and Gdynia. The final scope is to develop generic recommendations and a method to assess the potential of integrating PV in trolleybus grids located in different cities.

The research scope can be summarised through the following question:

What parameters affect the integration potential of PV systems in trolleybus traction grids of different cities, and how?

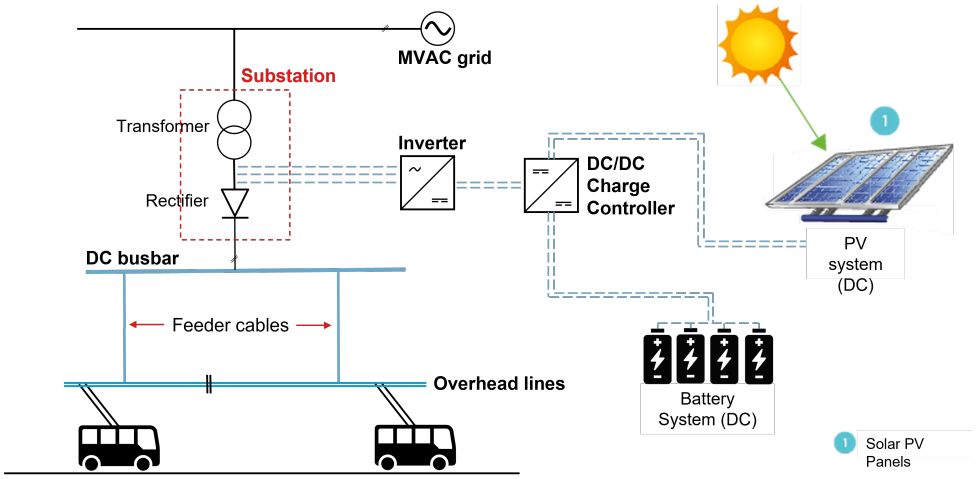

Figure 1.10: Schematics of a trolleybus traction system with integrated photovoltaic energy generation and battery energy storage system, both on the AC side of the substation - reworked from [54]

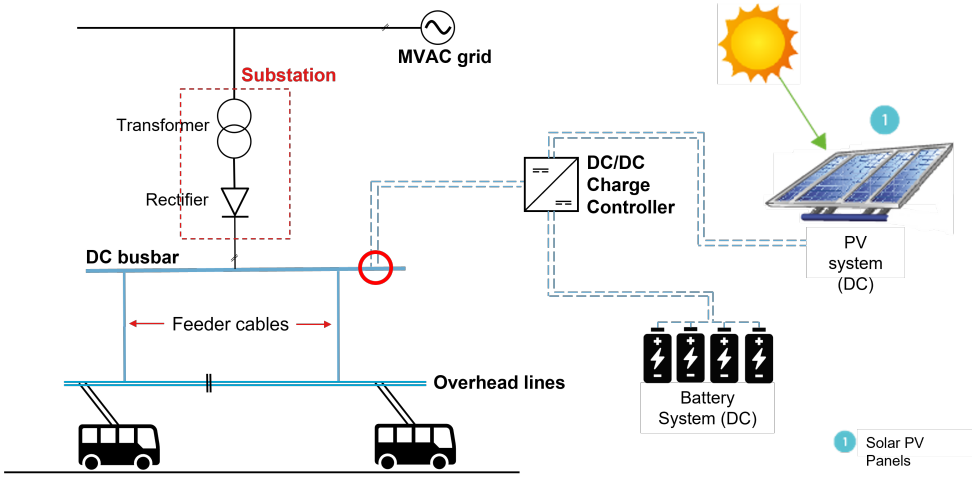

Figure 1.11: Schematics of a trolleybus traction system with integrated photovoltaic energy generation and battery energy storage system, connected to the DC busbar of the substation - reworked from [54]

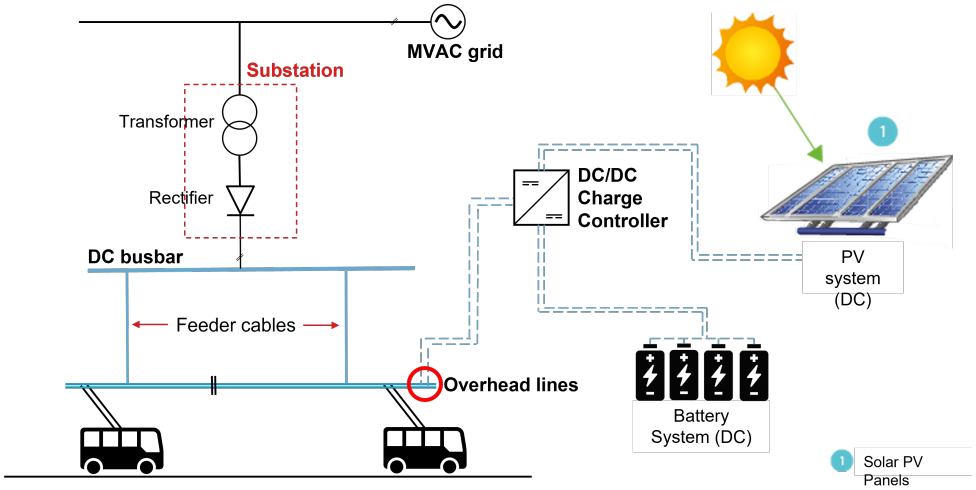

Figure 1.12: Schematics of a trolleybus traction system with integrated photovoltaic energy generation and battery energy storage system, connected to the traction network - reworked from [54]

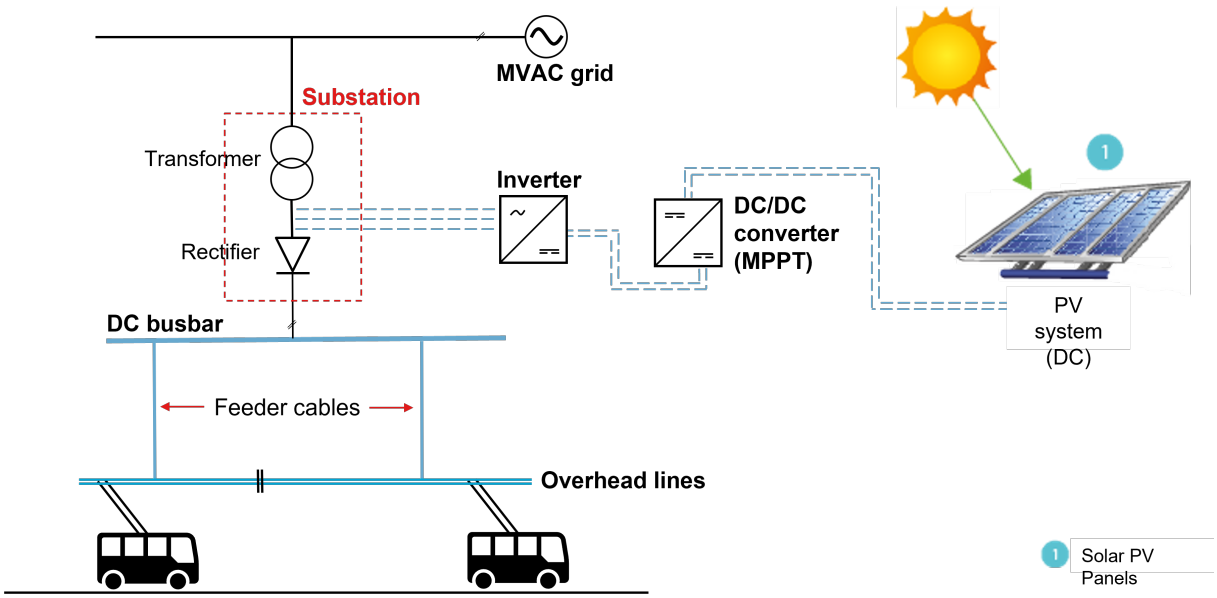

Figure 1.13: Schematics of a trolleybus traction system with integrated photovoltaic energy generation system - reworked from [54]

1.5 Research Questions and Report Structure

The research objective, namely the study of the impact of different parameters on the integration of PV in trolleygrids, is divided in 3 major research questions which give structure to the research and also will guide the reader through the report. In this section the research questions are identified and then an overview of the report structure is given.

Question 1
What parameters have an impact (qualitatively) on the components of an integrated trolleybus grid (PV, BESS, load), and to what extent?

Question 2
How does the potential of PV integration vary for different cities in respect to selected study-indicators (quantitatively)?

1. How do environmental parameters affect the potential of PV integration in trolleygrids?
2. How does the configuration of the substations (power, number and length of sections) affect the potential of PV integration in in trolleygrids?
3. How does bus traffic affect the potential of PV integration in trolleygrids ?
4. How do the HVAC requirements affect the potential of PV integration in trolleygrids?
5. How does the introduction of bilateral connections between sections affect the PV integration in trolleygrids?

Question 3
How does the introduction of stationary storage affect the feasibility of integrating PV in trolleybus grids?

In Table 1.1, an overview of the chapters where the answers to the research questions can be found is given.

Report Structure
The Report is formed by six core chapters, excluding the introduction. In Table 1.2, an overview of the content of the chapters with a small summary is provided. In the next chapter and extensive review

Table 1.1: Research questions and report chapters

	Research Question	Chapter of Interest
Key Performance Indicators	What parameters have an impact (qualitatively) on the components of an integrated trolleybus grid (PV, BESS, load), and to what extent?	Chapter 3
PV potential assessment	How does the potential of PV integration vary for different cities in respect to selected study-indicators (quantitatively)?	Chapter 5
PV potential assessment with storage integration	How does the introduction of stationary storage affect the integration of PV in trolleybus grids?	Chapter 6

of the existing literature is given, followed in Chapter 3 by an explanation of the research framework and methodology. In this same chapter the study on the indicators is reported. In the following section of the report, Chapter 4, the models used to simulate the operation of the two trolleybus grids are discussed. The structure of the models, the main equations and assumptions can here be found. Finally, Chapter 5 and Chapter 5, are used to provide the results of the simulations and to analyse the impacts of the previously studied indicators on the potential of integrating PV and storage in the two trolleygrids. In particular, the former focuses on the study performed on PV integration, while the latter contains a review of the results of integrating PV coupled with Storage. The last chapter is used to draw the conclusions of the research and draw some recommendations for the integration of PV in trolleygrids and for future work.

Every chapter ends with a section dedicated to a short summary of the content and to the main takeaways of the chapter.

Table 1.2: Report structure and content of the chapters

	Content	Title
Chapter 1	Trolleybus system brief description, with a short explanation of how PV and storage are connected. Definition of research motivation, scope and questions.	**Introduction**
Chapter 2	Review of existing literature. Two main topic blocks: electric vehicles energy demand and PV and storage integration in traction grids.	**Literature Review**
Chapter 3	Research framework and methods are presented. Data collection and analysis, identification and study of the parameters and introduction to the modelling part.	**Methodology**
Chapter 4	Presentation of the models developed and used to perform the research project: PV model, bus models, storage model and grid models.	**Models**
Chapter 5	Results obtained for the operation of Gdynia and Arnhem trolleybus grids. Analysis of the impact of selected study-parameters (from Chapter 3) on the potential of integrating PV systems in trolleygrids.	**Results: Grid operation and PV integration**
Chapter 6	Results obtained when introducing battery storage systems coupled with PV and analysis of the PV system performance. Feasibility analysis.	**Results: PV and storage coupled integration**
Chapter 7	Conclusions and recommendations for PV integration in trolleybus grids, with and without including storage. Recommendations for future work and possible improvements and next steps.	**Conclusions and Future Work**

2 LITERATURE REVIEW

The aim of this chapter is to provide an overview of the existing research and to discuss relevant literature upon which this research is built. The additional goal is to identify the research gap which this Master thesis project aims to fill.

*At the end of each section a **Summary** of what is discussed in the respective paragraphs is provided.*

2.1 Energy consumption in trolleybus grids

The electricity consumption of electric vehicles (and therefore trolleybuses) varies in relation to many external factors. In [16], Mikołaj Bartłomiejczyk and Robert Kołacz analyse and quantify the energy consumption of trolleybuses. The energy supplied to the electric vehicles from the relative power source (which can be a traction network, an autonomous generator or a traction battery) is intended for traction and non-traction needs, which can be divided in non-traction requirements during movement (actual energy used to grant comfort on-board to passengers) and non-traction requirements during stops. The energy consumption distribution for different purposes is shown in the flow diagram in Figure 2.1. The aim of this section is to understand what parameters affect the energy demand of electric vehicles, and to what extent. The existing research on this topic is taken into consideration when defining the indicators that will be used to assess the PV potential integration.

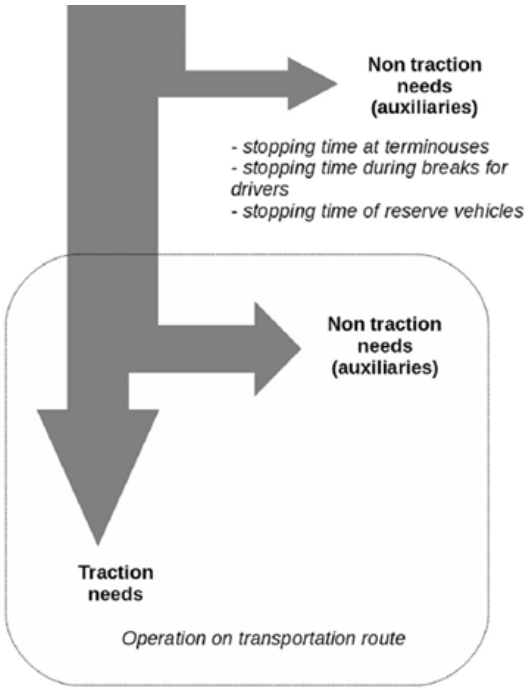

Figure 2.1: Distribution of electric energy consumed by vehicles between traction and non-traction needs [16]

Non-traction energy requirements can account for up to almost 50% of total energy consumption, reaching peaks of 70% during winter [16]. The magnitude and the variation of the non-traction energy needs depend on the location where the EV (electric vehicle) is used, since they are strongly connected

to the weather conditions and temperature levels. For this reason, existing research on the effects of environmental conditions on electric vehicles demand is discussed.

The characteristics and topography of the city, are what affects the traction requirements of the electric buses the most. In particular, city-dependant parameters as traffic, stops and road gradients are researched upon, together with individual and unpredictable parameters as the driving behaviour.

2.1.1 Ambient conditions and environmental effects

Many studies on the integration of PV in traction systems grids, do not consider the impact that environmental-related factors may have. However, these are demonstrated to have a significant effect on electric vehicles energy demand, in particular on the auxiliary loads [47]. Most of the research in this direction is done on electric cars, not specifically on trolleybuses. However, similar conclusions can be drawn for the trolleybus energy consumption.

In [47], Kai Liu et al. explore the "Interactive effect of ambient temperature on auxiliary loads" and try to improve the accuracy in estimating the energy consumption of the vehicles based on sparse real-world observations. The observed temperature during the trips analysed in the paper ranged from 5.5 to 36.6°C. In Figure 2.2, the distribution of the collected data showing the relationship between the energy efficiency of the vehicle and the ambient temperature. As one can see, the energy consumption per kilometre varies consistently with temperature, and outside the range from 10 to 30°C the variances exhibited were larger. The third-order polynomial used for fitting the asymmetrical "U" distribution, in red, is the one that gave the best fit. The authors built different models to have an estimation of the temperature dependence of energy consumption and found that the heater impact in the consumption is not always higher than the AC. As a matter of fact, from the results it appears that the heater may consume less energy than the air conditioner for specific temperature ranges. Another finding of the study is that there is a considerable amount of losses coming from an 'inappropriate' use of the AC and heating systems, namely AC remaining in operation at low temperature, heater during high ambient temperatures or situations in which both air conditioner and heater were in operation at the same time. Eradicating this unreasonable use of the vehicle auxiliary loads would save on average 9.66% of the electricity used per kilometre.

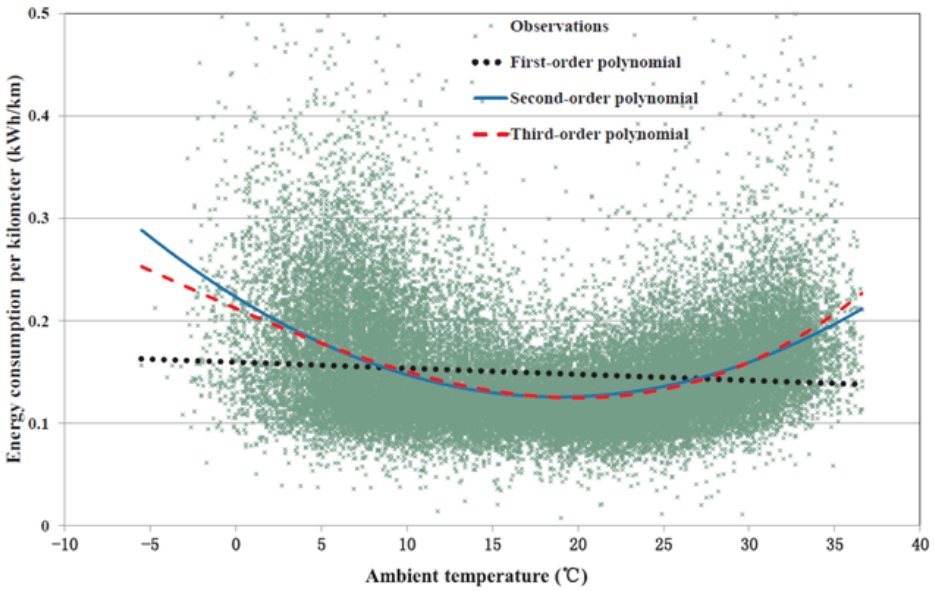

Figure 2.2: Energy consumption per kilometre as a function of ambient temperature, observations and fitted polynomial [47]

The research done by Mikołaj Bartłomiejczyk and Robert Kołacz on the auxiliary power demand of electrical buses [16], also demonstrates the impact of air temperature on the vehicle energy consumption. In the article three aspects are presented: the influence of ambient and the influence of traffic

congestion on the energy demand of auxiliaries (which will be further discussed in one of the next paragraphs) and the statistical aspect of auxiliary loads. Based on real-world measurements from vehicle data loggers' systems it is shown that energy consumption for non-traction needs has a strong influence on the total energy consumption of the system. The collected data allowed to quantify the dependence of the external temperature on the energy consumption. In Figure 2.3 the average total consumption per kilometre of a trolleybus is presented as a function of the difference between inside and outside temperatures. From this graph, it is possible to conclude that limiting the difference in temperature between the surroundings and inside of the vehicle would reduce energy consumption for non-traction purposes.

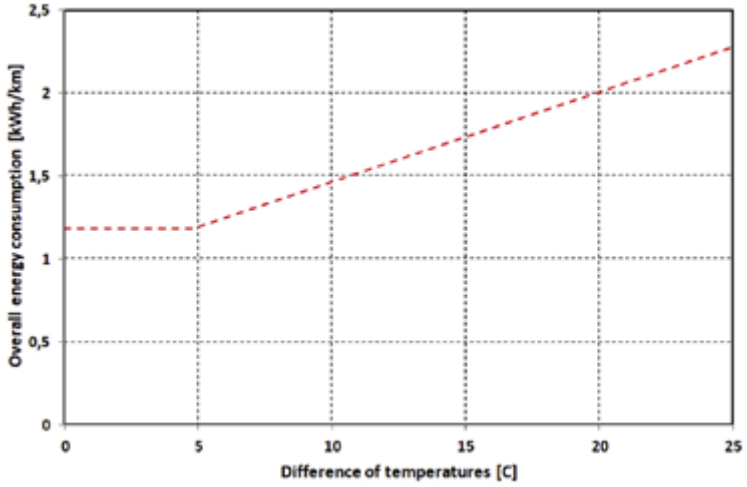

Figure 2.3: Overall vehicle power consumption as a function of the difference between ambient temperature and internal temperature, trend of the data [16]

In Figure 2.4 the energy consumption and daily average ambient temperature during a year are plotted. The relationship between energy consumption for non-traction purposes and outside temperature is evident. What is also clear from the graph, is the lack of dependency of energy consumption for traction needs on outside temperature.

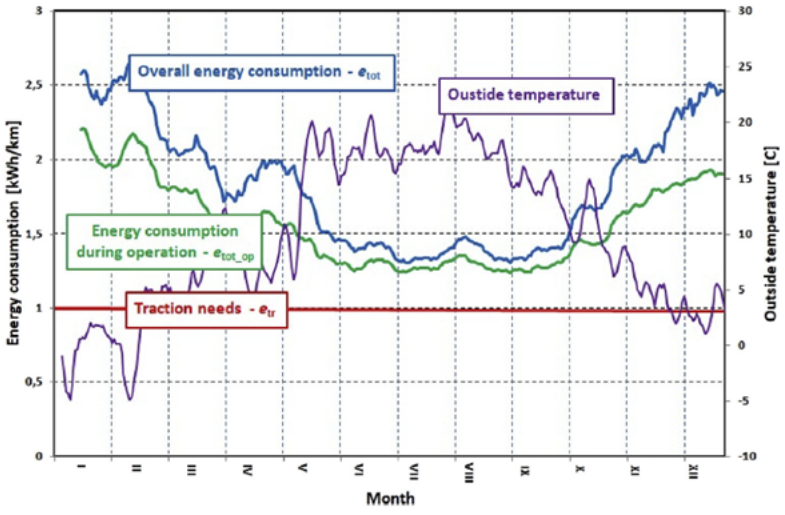

Figure 2.4: Average energy consumption and daily average outside temperature as a function of the time of the year [16]

In [39], Kiran Kambly and Thomas H. Bradley, present a study on the climate effect on the range of electric vehicles, showing the dependence of energy requirements of EVs on regional and temporal differences. Although for this study the EV ranges are less interesting, the focus on cabin thermal conditioning energy requirements of the article is a relevant topic. The variables given as input in the model (coming from the National Solar Resource Database) include Ambient Temperature, Relative

Humidity and Solar Irradiation. The model simulates the dynamics of thermal comfort within the vehicle evaluating the power requirements of air conditioning and heaters to maintain the passenger's thermal comfort. This requires the modelling of the climate at different locations and times (of the day and of the year), the thermal response of the vehicle and its HVAC system, and the energy consumption of the vehicle. The results show that both outside ambient conditions and the thermal comfort conditions within the vehicle cabin strongly affect the energy consumption of the HVAC system of the vehicle and therefore have a strong impact on the total energy consumption and in the case of EVs on the fluctuations of the available range. The authors found that the EV range varies considerably in relation to the moment of the trip and the location of the city. The reduction of the range is most pronounced in the middle portion of the day when temperatures and solar load are highest. The EV range variation from a maximum of 128 km to a minimum of 95 km, varying the moment and the location of the trip, demonstrates the strong impact that environmental conditions have on electric vehicles energy consumption.

From these studies it is possible to conclude that the trolleybus grid load varies considerably throughout the year, due to the weather variations. The energy demand of a traction grid is expected to be strongly dependant on its location and the respective environmental data.

2.1.2 Road gradients

Distances, driving patterns and driving conditions affect the energy consumption of electric vehicles. Within all the factors which affect the driving conditions, road gradients are considered as one of the most significant factors influencing the vehicle energy consumption [48, 68].

In [68], the authors develop a model to analyse how different rode slopes affect the EV's electricity consumption, considering also different traffic conditions. The developed model takes into consideration how the gravitational forces influence the vehicle and which impact this has on uphill and downhill roads on the driving behaviour. In Figure 2.5, the effects of the gravitational force on the vehicle driving behavior on the uphill/downhill road are shown. In the illustration, θ is the tilt angle, g is the gravitational acceleration and m is the vehicle mass. Driving up- and down-hill will respectively increase and reduce the power demand by a factor $mg \sin\theta$. The numerical results obtained show that the energy consumption of EVs vary with road gradients: the demand of the vehicles increases with the increase of the tilt angle on uphill roads, it decreases with the increase of the tilt angle on downhill roads and it always increases with the length of the uphill section. Through the recovery of braking energy downhill roads the energy consumption is reduced even further.

In [48], the researchers want to investigate the effect of the gradient of the roads on the vehicles energy consumption in Aichi prefecture in Japan, using GPS tracking data and digital elevation map (DEM) data for the analysed roads. A trip-base model is used due to relatively sparse data and the continuously varying slope of the streets is assigned to 12 categories of road steepness. The percentage of each total trip distance in each category describes the variation of the gradient of each trip. The results of the simulations demonstrate that the impact of road gradient on energy consumption increases almost linearly with the absolute value of the gradient and that thanks to the possibility of regenerating

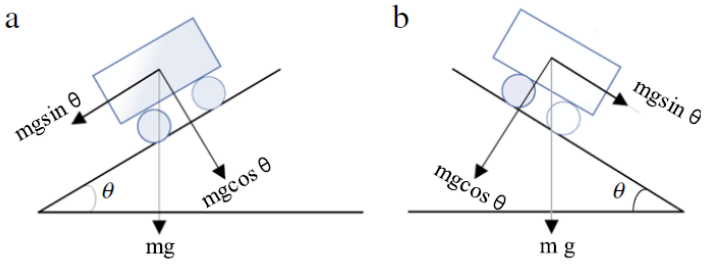

Figure 2.5: Illustrations of the electric vehicle's gravitational force on uphill (a) and downhill (b) [68]

braking energy EVs are more efficient than fuel vehicles, especially in hilly/mountainous areas where regenerating plays a central role in energy consumption.

2.1.3 Bus type and bus traffic

The system's characteristics have an impact on the total energy consumption expected. This aspect is very relevant for this study, since when modelling and researching different networks in different cities it is important to take into consideration how the systems differ in terms of bus types and bus schedules. Therefore, some previously performed studies are here discussed, in relation to the effect on the grids energy consumption of the types of buses and of the frequency of the bus rides.

In the analysis of Marc Gallet et al. on the energy demand of electric buses for public transport networks [31], the authors take into consideration the 3 different types of electric buses covering the routes in Singapore: single-decker, double-decker and articulated buses. The median value of the total energy demand for a terminus-to-terminus journey ranges from 28.7 kWh to 45.0 kWh, depending on the bus type. The median values of the specific energy demand obtained by the model based on the collected data are 1.6 kWh/km, 2.3 kWh/km and 2,5 kWh/km, for single-decker, double-decker and articulated buses respectively. In Figure 2.6 the reader can see how the specific energy demand is distributed based on the vehicle type (with SD=single-decker, DD=double-decker and AB=articulated bus). Although the article [31] does not deal specifically with trolleybuses, these results are valuable also for our research, not only because the consumption of electric buses is comparable to that of trolleybuses due to the fact that their mobility characteristics are very similar [13], but also because this analysis allows us to have a feeling of order of magnitude of the energy consumed by the vehicles based on the bus type and passenger capacity.

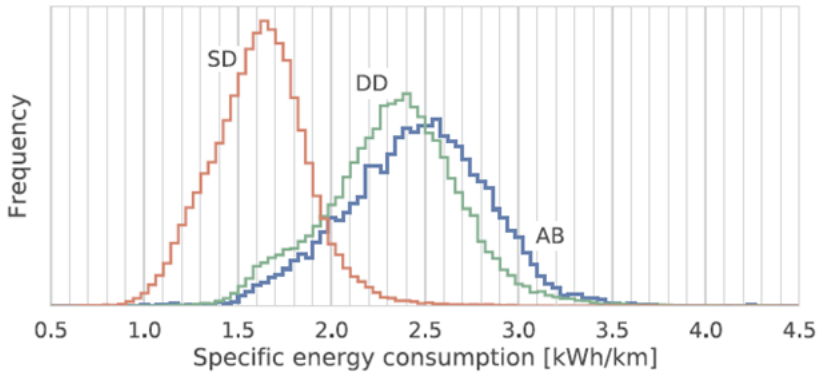

Figure 2.6: Distribution of the specific energy demand averaged over a journey per bus type [31]

In [54], the average values of the energy consumption of the Arnhem trolleybuses along each line are organised in a bar chart. This is shown in Figure 2.7. The data used to create the chart are also the ones available for this master thesis project. As one can see the values are distributed around a value of 2 kWh/km.

Another aspect affecting the energy consumption, is the number of trolleybuses running and their frequency. This has an impact on the number of buses in the grid and the overall power requirements of the trolleybus substations throughout the year. When considering regenerated energy from braking, trolleybus traffic has a significant impact on the utilization rate of this energy [18]. As a matter of fact, part of the recouped energy is re-fed back to the power grid and if no consumer is found in the supply area the energy must be dissipated as heat in the braking resistors (unless storage is available). Therefore, the degree of utilization of regenerated energy from braking is strongly connected to the average number of trolleybuses that can be found in a supply area. In [18] the authors show that during weekdays when trolleybus traffic intensity (meant as the average number of buses on a power supply area) is higher 70% of the recovered energy is absorbed, while during off-work days when the bus frequency is decreased by 50%, the ability of the network to re-use the energy is reduced by 40%-60% (in the case studied this energy is not dissipated but stored in a supercapacitor). In Figure 2.8, one can

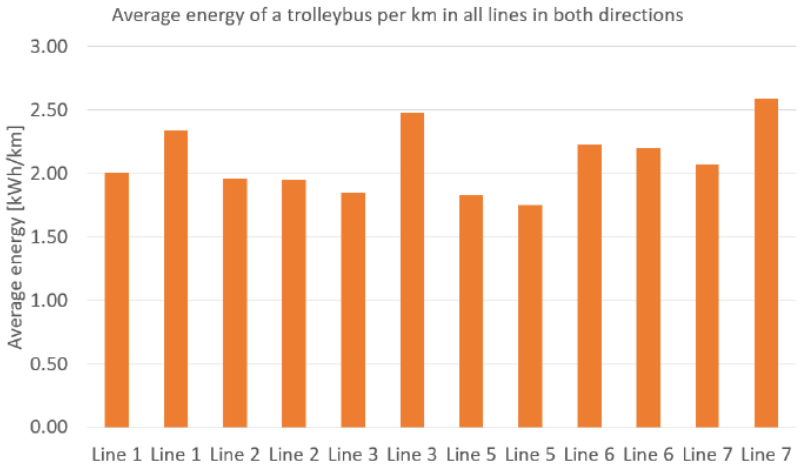

Figure 2.7: Energy demand for the Arnhem bus type, for each direction of each line of the trolleybus system [54]

see the effectiveness of recuperation as a function of the trolleybus average number in the supply area of the substation.

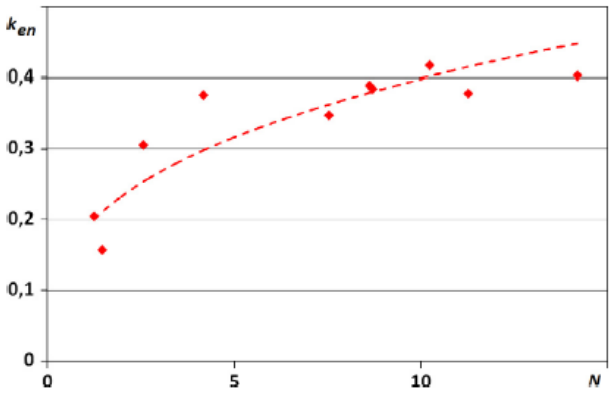

Figure 2.8: Recuperation effectiveness k_{en} plotted as a function of the average number of vehicles in the supply area N [18]

2.1.4 Traffic, stops and "Eco-driving"

Traffic, stops and driving conditions have impacts on different components of the network. Analysing and studying previous research projects, one can notice how the variability in speed of the vehicle and the continuous starts and stops affect the energy consumption for traction purposes of the trolley/electric buses. However, these parameters also have an influence on other aspects as non-traction and auxiliary energy consumption of the vehicles, transmission losses, utilization of regenerative braking, utilization of integrated PV systems and finally also on storage and in motion charging. In this paragraph an overview of the ongoing discussion and research on the topic is given.

Traffic and Stops

In [16], Mikołaj Bartłomiejczyk and Robert Kołacz estimate the influence that traffic congestion can have on the energy demand of auxiliaries. The congestion of road traffic affects both traction and non-traction energy needs. For traction needs the energy consumption is strictly related to the vehicle velocity and its variation. An increase in speed implies an increase in the traction requirements. On the other hand, speed reduction and traffic congestion have a negative impact on the non-traction energy needs of the vehicles. The authors analyse the dependence of energy consumption on commercial speed and on the adherence to the timetable (quantifying the delays caused by the congestion of road traffic along the trolleybus lines). Figure 2.9a and 2.9b, from the paper, demonstrate that commercial

speed has a strong impact on energy consumption for non-traction purposes (especially in winter) and show how this affects the total consumption of the vehicle. The effect of the delay on the energy consumption of the vehicle is shown in Figure 2.10. The conclusion drawn from the authors based on the result is that improving the traffic flow and reducing road congestion would lead not only to an increase in the attractiveness of the transport service but also to a reduction of the energy consumption of the vehicles. For this reason, they recommend introducing separate dedicated lanes for public transport vehicles.

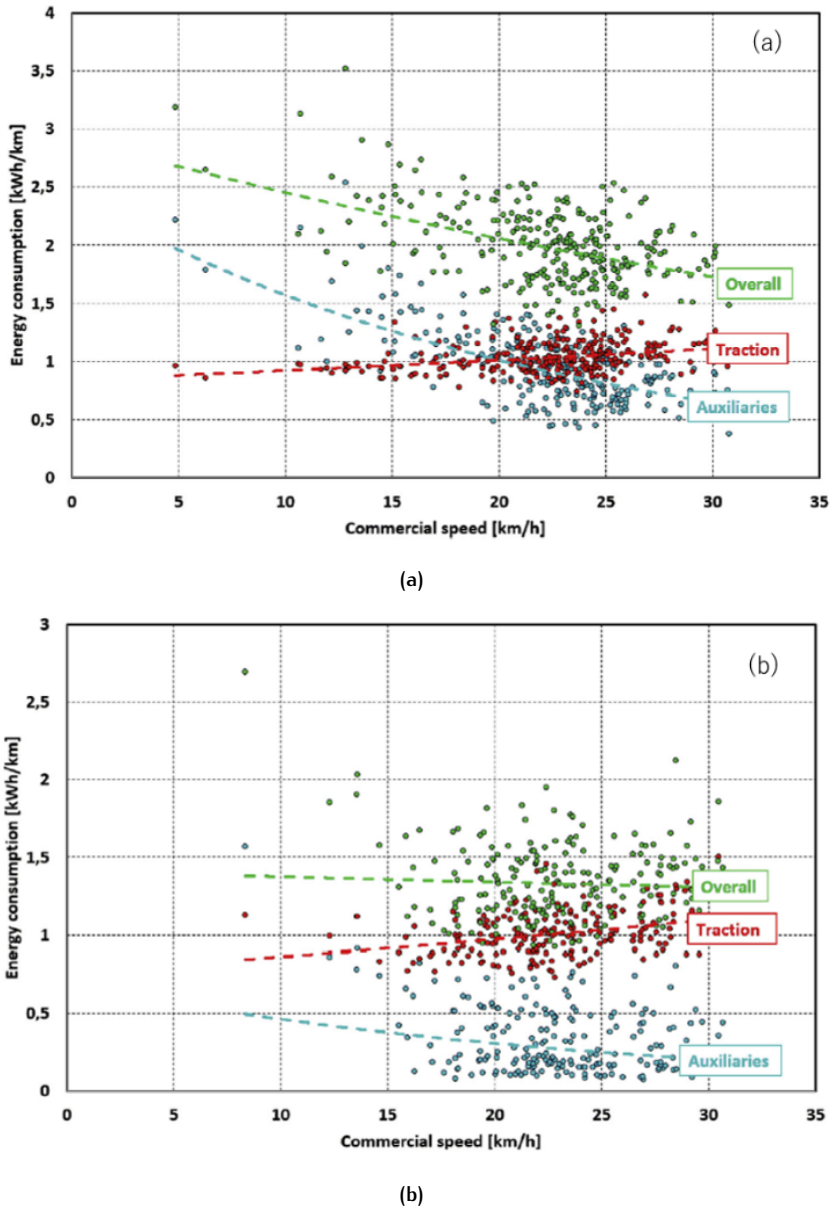

Figure 2.9: Scatter plot of the average energy consumption measured as a function of commercial speed for (a) winter and (b) spring season (the discontinuous lines are trend lines for the measured data points) [16]

Traffic has a negative effect also on the transmission losses in the network. As demonstrated in the study of Mikołaj Bartłomiejczyk et al. [17], high traffic intensity sections have higher transmission losses due to the higher power requirement of the sections. The increase in power demand leads to the increase in the current flowing through the cables and therefore causes higher transmission losses which are directly proportional to the resistance and to the square of the current. High traffic intensity sections present losses of almost double the grid average value. As a matter of fact, in some high traffic sections transmission losses of 15.3% and 13.6% are found, which should be compared to the trolleybus grid average of 8.5%. High traffic intensity, however, improves the use of recuperation energy. In fact,

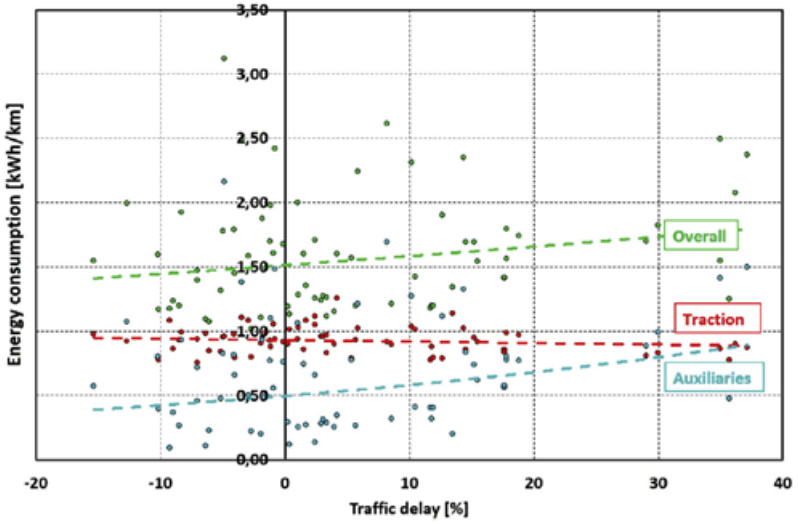

Figure 2.10: Scatter plot of the average energy consumption measured as a function of the traffic delays in the summer season [16]

the conducted analysis demonstrates that the parts of the supply system with low traffic intensity generate poor conditions for regenerative braking usage.

In [12], the author explores the potential of PV integration in the trolleybus grid of Gdynia in Poland. The analysis conducted is based on a simulation done implementing the Monte Carlo method to include the uncertainty of the PV generation and the variability of the load. In this context, traffic is also taken into consideration as a variable, and the effects that the intensity of traffic in different sections of the grids has on the utilization of the PV generated energy. In the study 3 variants are proposed in which PV system size, connection type and traffic conditions of the supplied areas change. In Table 2.1 an overview of the 6 cases explored by the author can be found. The variability of the load limits the possibility to fully utilize the PV generated energy. However, the increase of traffic intensity and the increase of the supplied area generate better conditions for PV utilization, since they increase the regularity of the load. The conclusion drawn from the simulation results is that the increase of the substation load caused by traffic intensity allows to have a higher PV generated energy utilization. In Figure 2.13, the utilization of the PV capacity installed for the 6 cases presented in Table 2.1 is shown. For cases IA and IB, which represent high traffic intensity sections, the PV energy used is always higher.

Table 2.1: Six case studies from paper [12] - PV integration in the Gdynia trolleybus grid

Label	PV system size	PV connection to the supply system	Supply area characteristics	Supply system characteristics
IA	500 kW	Substation busbars	High traffic intensity and heavy load	Unilateral
IB	500 kW	Substation busbars	High traffic intensity and heavy load	Bilateral
IIA	50 kW	Substation busbars	Small supply area and lower load	Unilateral
IIB	50 kW	Substation busbars	Small supply area and lower load	Bilateral
IIIA	50 kW	Traction network (in weak point of network)	Single supply section, small supply area with limited energy recuperation	Unilateral
IIIB	50 kW	Traction network (in weak point of network)	Single supply section, small supply area with limited energy recuperation	Bilateral

As discussed above, traffic has an influence on trolleybuses total energy consumption. This also means that if the buses are equipped with traction batteries for catenary free operation, the size and the charging/discharging cycles of the battery will be influenced by the traffic trends in the city. The analysis of

accurate energy demand profiles is necessary to determine battery capacity, to design optimal charging strategies and to define the charging infrastructure characteristics and requirements for the functioning of trolley- and electric buses [31]. In [49], the authors propose a method to size and determine an electric bus powertrain powered by hybrid energy storage, which establishes accurate energy requirements based on GPS data to characterize local traffic conditions. The research demonstrates how the implementation of accurate traffic parameters allows to prevent inaccuracies on the estimation of energy needs, which is crucial when sizing a traction battery for autonomous running of vehicles.

In [10], a case study of the practical application of In Motion Charging (IMC) in Gdynia trolleybus grid is presented. The author aims to provide some guidelines for boundary conditions in the designing of an In Motion Charging system. In the discussion of the results of the case study also traffic is included in the analysis. The presence of traffic can strongly influence the charging and discharging cycles of the on-board traction battery. In particular, traffic could lead to an increase in energy consumption above nominal values, which in a situation of catenary free operation could cause issues if the batteries are not charged enough or if the terminals are not equipped with systems that allow for charging of traction batteries.

After looking into the effects of traffic, it is possible for us to conclude that also the stopping frequency will have an impact on the buses' energy consumption and on most of the things mentioned above. High stopping frequency means: high frequency of acceleration and deceleration phases with high power peaks, low velocity and more traffic. As a matter of fact, the study done by Marc Gallet et al. [31] also demonstrated how the number of stops per km affects the average speed and the total energy consumption of the buses. A route with a high number of stops causes a higher energy consumption not only due to the reduction in speed and the increase of idle/reduced speed time which increases the auxiliary power demand, but also due to the increased frequency of high energy-intensive acceleration phases. What is also highlighted is the effect of overall traffic: not only congestion of road traffic causes the energy demand to increase, but also passenger traffic plays an important role affecting the weight and the energy needed for non-traction purposes.

Driving behaviour and "Eco-driving"
The impact of traffic on energy consumption profiles of trolleybuses has been discussed above, however not only external driving conditions influence the energy requirements. Studies demonstrate that also driving behaviour and the management of driving conditions have an effect on the energy demand of electric buses, and that the optimization of driving cycles can improve the energy efficiency of traction systems.

The impact on energy demand of EVs of driving characteristics is studied in [20]. The authors analyse the effect of the driving behaviour and style on total energy consumption, SOC utilization and range of electric vehicles. A common driving cycle is used to show the substantial energy savings that can be obtained when consciously reducing the amount of acceleration and deceleration throughout the travel. It is demonstrated that a different driving-style can have up to 30% impact on the energy consumption (between a moderate and an aggressive driving mode) over the driving duty considered for the case study. Allowing the driver to minimise periods of frequent acceleration and deceleration and allowing longer periods of steady-speed motion can bring to meaningful energy savings.

In [46], Kai Liu et al. propose new models to estimate the actual efficiency of electric vehicles, analysing the impact that heterogeneity in driving behaviour and traffic conditions have on energy efficiency, based on long-term daily trip-based data. The objective is to demonstrate to what extent the variability of energy demand is dependent on variations of traffic conditions and driving habits. The heterogeneity at the driver level was found to have a considerable effect on energy consumption and to contribute meaningfully to the variability of the consumption of the vehicles per km.

Including this factor in the analysis is not easy but moderate driving behaviour can lead to have a more regular load and therefore could have an effect on the utilization rate of PV generated energy and on the sizing of integrated storage.

2.1.5 Summary - EVs energy demand

The electricity consumption of electric vehicles (trolleybuses) varies in relation to many **external factors** and this should be taken into consideration when modelling and analysing the network energy demand. In this section different causes of energy consumption increase are analysed: **external environment conditions, road gradients, bus type and bus traffic, traffic congestion, stops and eco-driving**.

Ambient temperature is the first element to be analysed, many studies demonstrate the **strong impact** of this variable on the **auxiliaries load**. The energy consumption of the HVAC system of the vehicles is affected by temperature and relative humidity variations of the surroundings [39]. The relation between energy consumption for non-traction purposes and outside temperature is demonstrated from previous research. It is also concluded in some papers that since energy demand for auxiliaries accounts for up to almost **50% of total energy consumption**, reaching peaks of 70% during winter [16], the main way to reduce consumption in transport is to reduce the auxiliary loads. Therefore, environmental conditions cannot be excluded from the analysis on energy consumption of electric trolleybuses.

It is shown that the demand of the vehicles increases with the increase of the **tilt angle** on uphill roads and decreases with the increase of the tilt angle on downhill roads. The energy demand increases also with the **length of the uphill** section [68]. The effect of road gradients on energy consumption and regenerated energy is discussed further, and is it also demonstrated that the impact of road gradient on energy consumption increases almost linearly with the absolute value of the gradient and that thanks to the possibility of **regenerating braking energy** EVs are more efficient than fuel vehicles, especially in hilly/mountainous areas where regenerate energy plays a central role in energy consumption [48].

Other two important aspects that have an impact on the energy consumption of a trolleygrid are the **types of buses** used and the **frequency of runs**. The consumption of energy varies with the bus type, with its weight, dimensions and passenger capacity [31] and with the number of trolleybuses running simultaneously in the grid [18]. Trolleybus traffic has a significant impact on the **utilization rate of regenerated energy** and on the effectiveness of recuperation.

Finally, **traffic, stops and eco-driving** solutions impact on the grid requirements is questioned and discussed. Traffic is found to have a **negative impact** on the energy demand for non-traction needs, on the **power peaks** due to continuous stops and on the transmission losses [16, 17]. On the other hand, traffic congestion is demonstrated to increase the **use of regenerated energy** and the PV utilization. In sections with more intensive traffic conditions the two latter elements are performing better [12]. A route with a high number of stops causes a higher energy consumption not only due to the reduction in speed and the increase of idle/reduced speed time which increases the **auxiliary power demand** [16], but also due to the increased frequency of high energy-intensive acceleration phases. Eco-driving solution is proposed by multiple studies to **reduce the energy requirements**, since the heterogeneity at the driver level is found to have a considerable effect on energy consumption and to contribute meaningfully to the variability of the consumption of the vehicles per km.

To conclude, all the factors discussed in this section are found to have a significant impact on the power/energy requirements of the electric vehicles, therefore of the trolleybuses, and of the traction grid. Some of these parameters seem to be inducing variations also in the utilization of PV energy when integrated. **To what extent can these parameters affect how successfully PV systems are integrated in the trolleybus traction grids?**

2.2 PV and storage integration in traction systems

In the context of sustainable development and of electrification of the transport sector, renewable energy and storage systems both have a central role. The renovation of the urban transport system towards solutions which allow a reduction of GHG emissions, led to the exploration of possibilities of integrating renewable technologies and storage devices in traction grids, which are proven to be one of the most effective options to supply electricity to the urban transport network [19]. In this section, different solutions for the integration of PV and storage systems are discussed. First, we will look into PV integration in the traction grids, then into storage and finally into the combination of the two. As one will notice, not all the results lead to the same conclusions.

2.2.1 PV systems integration

The integration of photovoltaic systems to supply public traction systems is being explored. Its worldwide availability, urban friendly and sustainable characteristics together with the forecast cost price reduction of the technology [3], make this solution worth exploring. Literature show that different solutions have been explored in various countries, not only for trolleybus but also railway and tramway systems.

In [33], the authors research the potential of introducing PV systems on the roofs of the railway stations and analyse the issues encountered. The first problem they take into consideration is the influence of the surrounding buildings' shadows on the generation. Especially during winter season, long shadows from southern direction reduce eminently the PV generation. 20% shadow on the panel results in 60% decrease of the output. The influence of building shadows is shown for June 22^{nd} and December 11^{th} in Figure 2.11. When introducing PV systems in urban areas this issue should be taken into consideration.

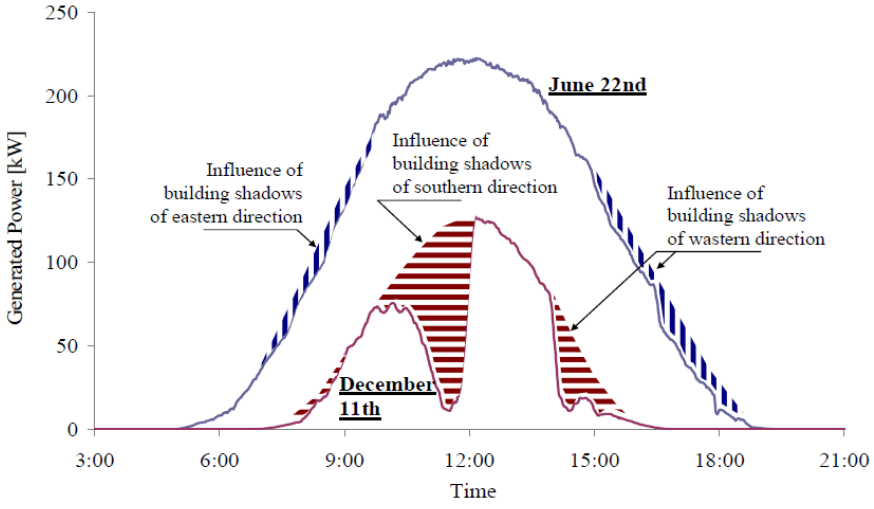

Figure 2.11: Effect of shadows on PV generation [33]

Another problem tackled by the authors in [33], is related to spatial and temporal mismatch between generation and consumption. On one hand, introducing PV systems along the railroad track continuously is not effective due to the fact that consumption happens in stations which are located discretely. Therefore, there is an issue related to the spatial distribution of generation and load. In terms of temporal mismatch, the observation is that the loads of the stations are heavy and maximum during peak hours, which happen in the morning and in the evening, while the PV generation peaks during midday. An average day load and generation curves are plotted in Figure 2.12. This causes a temporal mismatch between generation and load that should be covered either by transferring the residual energy to other stations or storing the excess. In this study, a storage solution with Lithium batteries is discussed, which will be further analysed in one of the next subsections.

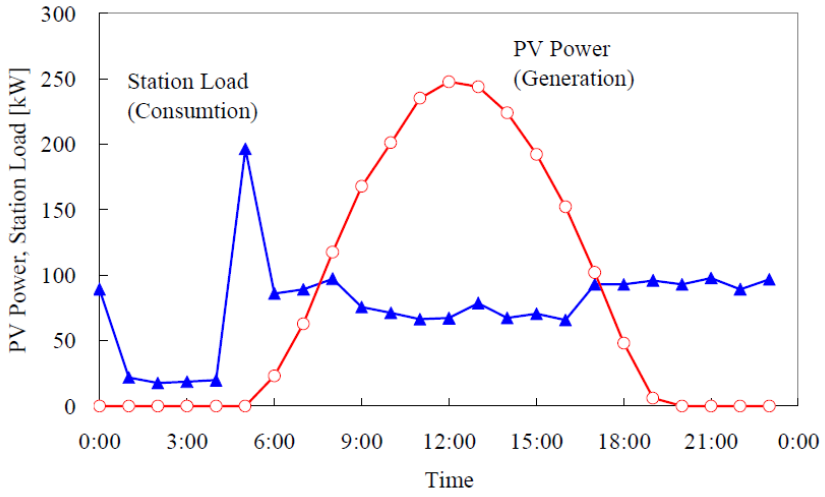

Figure 2.12: Temporal mismatch between PV generation and load [33]

In [12], Mikołaj Bartłomiejczyk presents a stochastic analysis, based on the Monte Carlo method, of the potential of PV systems supplying the trolleybus grid in Gdynia. Through the stochastic simulation, the author takes into consideration both the random nature of the load and the uncertainty of solar generation. The study proves that it is possible to reach 80% of PV utilization in the trolleybus grid under certain conditions, despite the variability of the energy demand. Moreover, the author concludes that the PV utilization is highly dependent on the substation's load and that the former increases with the latter. Another finding which is worth mentioning, is the influence of the upper limit of the generated voltage, which allows better use when it is higher. Finally, the results also show how bilateral connections always improve the ability of the system to use the solar energy, but, in particular, how this strongly impacts the sections with lower load. The author suggests some values of installed PV power in relation to the dimension of the supplied substation and to the type of connection (to the substation busbars or to the network directly). In Table 2.1, the summary of the 6 studied cases for PV integration are reported. In Figure 2.13, the reader can find a bar chart showing the PV generation use in the 6 cases. As one can see, the solution 'B' for all cases, which introduces bilateral connections, always has a better performance. Also, case I (both A and B scenarios) is presenting always better performances.

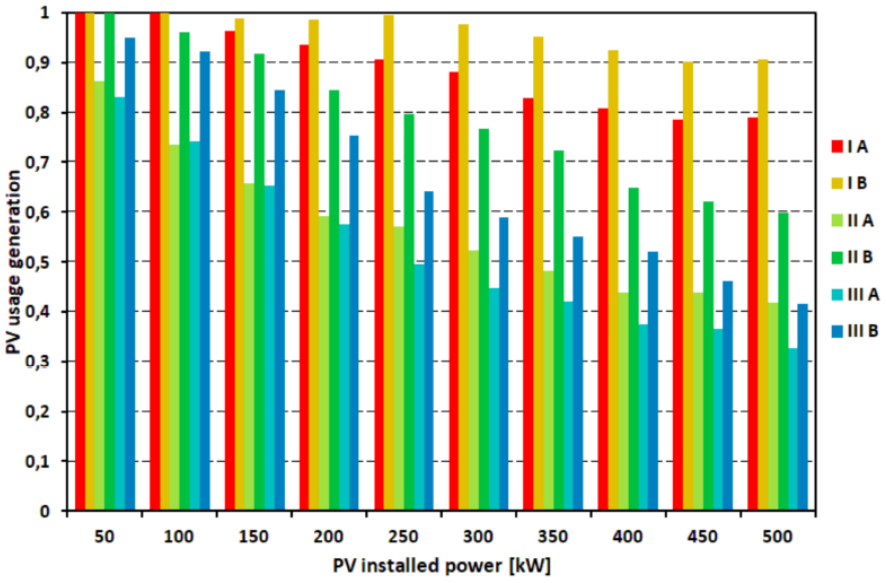

Figure 2.13: Utilization of the PV generated energy as a function of the installed PV capacity for the six cases [12]

The study presented by M. Wazifehdust, D. Baumeister et al. [64], propose two methods to determine the optimal placement and sizing of PV systems and electric vehicle charging stations in the Solingen

LVDC trolleybus grid. As in common trolleybus systems, all substations are operated unidirectional. In relation to the PV integration, the authors study different methods to determine the the zone of influence of the PV generation, based on length of the overhead fed, on voltage differences along the lines and maximum losses. The nodes (all interconnection points) to which the PV systems should be connected to have optimal performance are selected based on the zones of influence identified, the simulated nodes' feed in potential and the size of the system. The results of this study show that the nodes chosen as optimal locations for PV integration are on the heavily travelled routes and therefore have a higher energy demand. Moreover, all the selected nodes are characterised by the largest feed-in potential.

In [54], a study on the effects of integrating PV systems in the Arnhem trolleygrid is performed. Some interesting takeaways are found and here reported. The first one confirms the limitation in the application of PV systems in trolleygrids due to the temporal mismatch between load and generation. As a matter of fact, in Figure 2.14 the reader can find the ideal fraction of load covered with PV for all the substations in Arnhem grid. The bar chart shows the fraction of time in which a power requirement is simultaneous to PV generation, regardless of the magnitude of the two. As one can see, there is a physical limit, which is due to the seasonal mismatch between demand and generation caused by the increase in demand and the significant reduction of generation in winter.

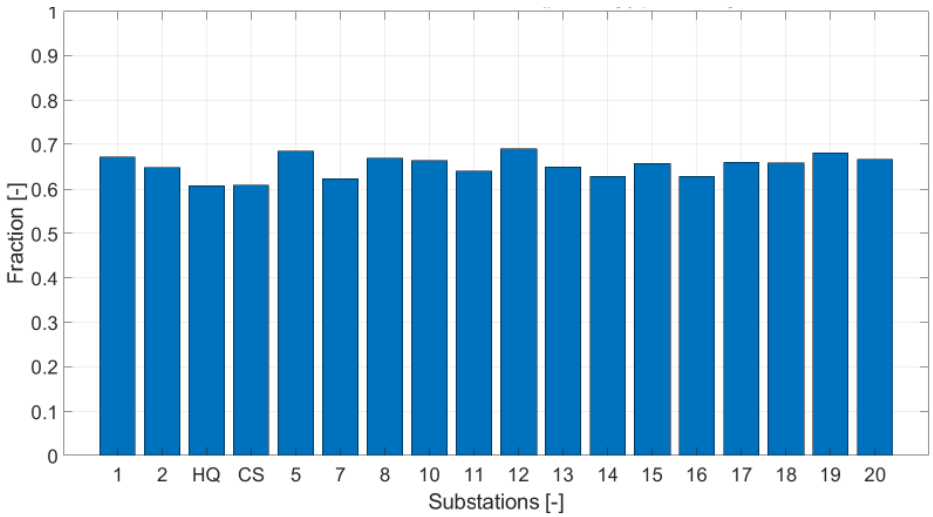

Figure 2.14: Fraction of time in which a bus can be at least partially supplied by PV generated energy

In the same report, it is concluded that the increase in traffic conditions (in terms of fraction of time in which PV and bus are matching in time) induces an increase in the PV capacity that can be installed at the substation level and of its performance. The increase in traffic causes the variation in load coverage between 5% to 15% between different substations and of utilization of PV generated energy between 55% and 65%. The analysis does not quantify the impact of traffic, however it compares the effectiveness of integrating PV in substations with different traffic conditions, showing how this has an impact on the potential of integrating PV.

2.2.2 Summary - PV integration

PV systems integration in traction grids has been partly studied, and the main issues and key findings are here reported:

- The utilization of PV generation is strongly dependant on the type of connection to the trolleybus grid and on the **location of the connection** [12].
- The utilization of PV generation is strongly affected by the section-substation supplied characteristics: **traffic, bus frequency, power demand** [12, 64].

- The **temporal and spatial mismatch** between load and generation has an impact on the utilization of the PV systems and this can be improved by the introduction of bilateral connections, as shown in [12], and of storage devices as commented in [33] and further discussed in the next paragraphs.

To conclude, this section offers some interesting food for thought. The characteristics of the power supply areas seem to have a **strong influence on the integration of PV** in traction grids. The traffic intensity in the sections, the power requirements of the substations and the bus traffic all seem to increase the PV performance. Are there specific values for which the increase of these parameters induces a better PV use? Is it possible to identify a range for these parameters in which the **PV performance** is improved?

2.2.3 Storage systems integration

Integrating energy storage systems could be beneficial to increase the utilization of the recovered braking energy, as demonstrated in [18, 34, 41]. Storage systems can be used also to reduce the voltage fluctuations, decreasing the voltage drops caused by consecutive accelerations and stabilizing the network voltage [24]. Finally, energy storage systems can effectively increase the utilization of PV generated energy, as shown in [24, 33, 52]. This last function will be further discussed in the next subsection. In this subsection different studies related to the introduction of storage systems in urban transport traction systems are discussed to have an overview of existing literature on the topic.

The studies on the integration of storage in traction transport grids vary in terms of type of technology implemented and type of connection to the grid. As a matter of facts, super-capacitors (SCs) and batteries have been widely studied in two different applications: on-board or off-board. This means that the storage system can either be installed on the vehicles or in one or more points of the network, typically connected to or close to a substation, these solutions are respectively named on-board and stationary storage [23]. The use of super-capacitors for storage applications is frequently studied beside battery systems. The reason behind this choice related to the power characteristics of super-capacitors, which allow to have a fast response to high peak power requirements, to the high efficiency and long lifetime. Moreover the implementation of these devices is easier, since the state of charge of the SCs can be determined just by measuring the voltage difference at the terminals [8].

On one side, mobile applications of storage units are used for peak power demand shaving during the acceleration of vehicles and allow catenary-free operation. The peak shaving feature of on-board storage has beneficial effects on the network in terms of reduction of transmission losses in the lines, of limitation of voltage drops due to high power requirements and of improvement of the utilization of recovered braking energy. The regenerated energy from braking can be stored without incurring in transmission losses to reach stationary storage, introducing like this an increase in energy efficiency of the vehicle. However, mobile storage has the disadvantage of the weight and the space it requires on the vehicles [8]. Through on-board storage higher efficiencies of the trolleygrid system can be reached, but more capacity has to be installed due to the modularity required. On the other hand, stationary storage systems are more effective in supporting the contact lines when installed on the DC side of the substations. The increase in size of the networks, in frequency and passenger capacitance of the buses, can have a damaging effect on the lines and the power quality, due to overloading of the lines. Stationary storage connected to the traction grid, can support it and improve the supply lines performance [24]. The advantage of stationary storage when compared to on-board is that it has no real restrictions in terms of weight and space requirements and that it can recover energy from several braking vehicles at a time. However, due to the voltage boundaries of the contact line, not all the braking energy can be stored. As a matter of fact, if a vehicle is too far from the storage system it will not be able to store all the energy because of the losses in the lines. The reduction of line losses will also remain unvaried, due to the fact that contrary to the on-board storage situation, the current in the lines will be similar as in the no-storage case [8]. On-board storage allows to supply locally the buses without requiring power from the catenary. In Table 2.2, the comparison of the results of the paper comparing on-board and stationary storage are provided. A range of energy savings is provided in the tables since two scenarios are provided in the research.

Table 2.2: Comparison of stationary (DC connected) versus on-board Energy storage systems (ESS) [8]

	Stationary storage	On-board storage
Number of ESS needed	6	55 (5/vehicle, 11 vehicles)
ESS usable energy capacity [kWh]	4.53	1.46
Total energy capacity needed [kWh]	27.18	80.3
Energy savings [%] - high traffic	11.7 - 16.1	19.6 - 26.3
Energy savings [%] - moderate traffic	17.1 - 22.3	22.8 - 29.3
Energy savings [%] - low traffic	25.7 - 33.4	29.3 - 35.8

In particular, R Barrero et al. in [8] simulated 2 scenarios: one with high (optimistic scenario) and one with low (base scenario) efficiency of vehicle components. The authors propose a model based on quasi-static method, to simulate power flow in a metro grid including unidirectional substations, vehicles and stationary energy storage systems on- and off-board. In the base scenario, during the night energy savings reached 29.5%, while they achieved only 29.9% at peak times. In the optimistic scenario, under low traffic conditions, 36.3% of energy savings are achieved. When simulating the off-board storage, not only the size but also the distribution and connection points have to be optimised. For this reason, the simulation consisted in a sensitivity analysis to find the optimal stationary storage system which would allow to have a reduction in energy consumption which was globally comparable to that of on-board storage. Also in this case both scenarios (base and optimistic) and traffic conditions are simulated. It is interesting to notice, that for the stationary storage case higher energy savings in higher traffic intensity conditions are reached. While in the case of on-board storage, the results show that the potential introduction of mobile storage is higher in lower traffic conditions. However, the maximum energy savings in the stationary case would be lower both for the base scenario, 25.7%, and for the optimistic one, 33.4%. If on-board storage is performing better in terms of energy savings, the capacity of storage installed is considerably higher in the optimized solutions found: 27.18 kWh for stationary and 80.3 kWh for on-board.

In [41], as discussed above, Yasunori Kume et al. Study the effects of introducing Li-ion batteries in a railway system to temporarily store the regenerative power. The results show that the connection of the storage energy system to the substation reduces the energy consumption by storing and re-using regenerated energy. Comparing the yearly power consumption before and after the installation if is found that the power consumption was reduced of 12.8%.

In [23], the authors study the effect of the introduction of storage systems in a tramway network and provide a comparison in terms of energy and cost efficiency between storage technologies and their connection to the traction system. The variants on which the analysis is based are the following: stationary lithium batteries or stationary supercapacitors, on-board lithium batteries or on-board supercapacitors. For simplicity, this study uses the same dimensions for on-board and off-board storage, to give a clear indication of the weaknesses and strengths of the options. The introduction of storage in the system has the purpose of increasing the utilization of regenerated braking energy. The results of the study show that energy savings can be increased with the introduction of storage systems. In particular, the greatest advantages are obtained if several storage systems are installed along the line, with distancing between them based on the effective reach of the energy storage device. Also from the cost/benefit point of view stationary systems represented the best solution. Finally, batteries are picked as preferred technology due to the equivalence in performance and to being more competitive in terms of investments. Battery stationary energy storage systems are, therefore, the storage option selected for this study. The investment effectiveness found in this paper and the forecast reduction in prices that the technology will undergo [36] make it the most interesting and competitive option.

In [11], Mikołaj Bartłomiejczyk shows the impact of installing a supercapacitor connected to a substation in Gdynia trolleybus grid. The characteristics of the area supplied by the substation in question, namely the hilly terrain and the reduced size of the supply area, caused high amounts of recuperation energy and insufficient number of vehicles which could receive this energy. This led to the decision of installing a supercapacitor connected to the substation, to store the excess regenerated energy and re-use it when needed. The collected data and results of the study demonstrated that introducing a supercapacitor system into service in a specific substation resulted in a decrease of about 12% of the total energy demand. This number is relatively small due to the fact that the running vehicles did not

have a recuperation system, the author expects the energy savings to reach 25% energy savings resulting from accumulation in the energy storage system if all the exploited vehicles would be equipped with regenerative braking systems.

2.2.4 Summary - Storage integration

Storage integration in the grid has been demonstrated to have high potential in terms of energy savings, especially when combined with systems which allow the re-use of regenerative energy from braking. On-board and off-board solutions both lead to a **reduction in the energy consumption** and to an increase in **stability of the grid**. The trade-off is connected to the availability of space and weight on the vehicle, to the available funds, to the storage capacity required and to the functions of the storage system. As discussed, off-board can reach similar energy savings with lower capacities, but for instance does not allow catenary-free operation and high utilization of regenerative braking.

To conclude, battery stationary energy storage systems are the storage option selected for this study. The higher cost-effectiveness found and the limited interest in energy recuperation for this research, together with the forecast reduction in prices for the Li-ion battery technology [36] make it the most interesting and competitive option. In the next section, some former studies on combined PV and storage integration in traction grids are discussed.

2.2.5 PV and storage integration

In this Master thesis project, the introduction of storage in the grid is functional to the implementation of PV systems. The aim is to study how the inclusion of storage affects the potential of supplying trolleygrids with PV generated energy. For this reason, previous literature on the combined integration of photovoltaic and storage is now reviewed. PV integration has been studied less than storage, also due to the reduced number of options in the integration compared to storage devices. Research on combined PV and storage in traction grids is very limited.

In [33], Hitoshi Hayashiya *et al.* propose a study on the potentials, peculiarities and prospects of introducing solar power generation systems in a railway network. As previously discussed, the results of the research demonstrated the existence of a temporal and spatial mismatch between PV generated energy and the load (temporal mismatch effects are shown in Figure 2.12). The authors introduce the topic of storage systems as a solution to limit the mismatch between generation and load by storing and re-using the energy when required. This type of implementation of storage systems is what is interesting for this research. Understanding the effects of including storage and the feasibility of this application are the main goal. In [33], a combined system of 78 kW of PV capacity and 240 kWh of Lithium-ion battery capacity are installed connected to a station of the railway. The measurements show that this system allows to reduce the energy draw from the grid and that on many days the station is able to operate without emissions, which means that all the energy required from the grid was supplied from the combined PV and storage system. PV plus battery system was overall able to cover the station demand completely for 128 days out of 277, demonstrating like this that large energy savings can be achieved combining these two technologies. In Figure 2.15, the concept of having a 'zero-emission' station is illustrated. The energy generated by the PV modules which is not directly used by the load, is stored and used when the PV generation is not enough to cover the load demand (for instance during night time). This increases the potential of PV integration both in terms of utilization of the PV generated energy and in terms of load covered with the renewable output (directly or indirectly).

Research on the integration of PV and storage in traction grids is ongoing in Solingen, Germany. In [52], M. Salih, D. Baumeister et al. deal with the challenges and the impact that the integration of battery assisted trolleybuses, PV units and EV charging stations would have on the LVDC trolleybus grid. When realising the vehicle power profile, both bus and environment characteristics (traffic, number of passengers, topography, etc.) are considered. The storage system studied in this research is formed by on-board traction batteries that charge directly from the overhead lines. Therefore, a different

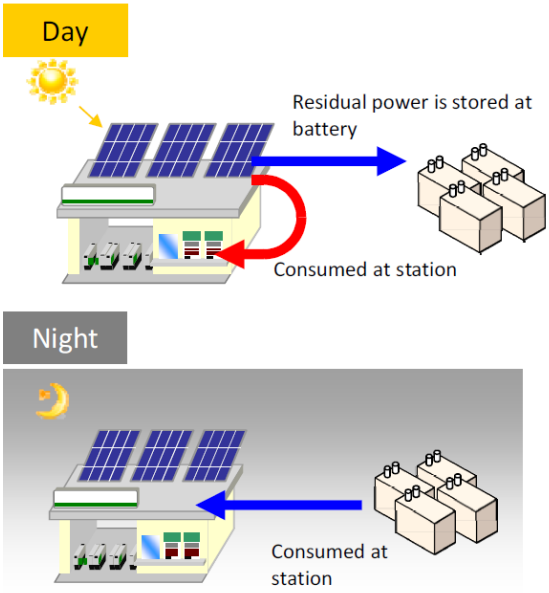

Figure 2.15: 'Zero-emission' station supplied by direct and indirect PV generation [33]

application of storage is proposed, which causes the focus of the research to be on the effect of the increase in the load of the grid due to the charging of the batteries from the overhead lines. The PV system is modelled as an ideal source with random cloud reduction factors to make the simulation more realistic. The simulation results show that the grid seems capable of handling the operation of battery assisted trolleybuses without impacting the grid infrastructure. However, the simulation is done for only one bus, and the increase in number of trolleybuses equipped with traction batteries could destructively influence grid stability. No major insights or results are provided in relation to the effects of PV integration. Therefore, one can conclude that this research is still incomplete when speaking about combined PV and storage integration.

In [24], Flavio Ciccarelli *et al.* analyse the impact of the integration of a photovoltaic system and a stationary super-capacitor in the tramway network in Naples. Their study proposes an optimization method based on the minimization of a cost function to optimize size and utilization of PV and storage. The aim of the paper is to determine feasibility of integrating PV and storage. To do this the size, distribution and utilization of the PV systems are optimised. Together with this, also the optimal size of the energy storage system, the time needed to charge the super-capacitors and the reduction of the losses are found. The results of the optimization process shoe that an optimal solution can be found, which demonstrates the technical feasibility of integrating PV and storage in a railway traction system.

A simulation of PV and storage combined integration in a railway network is performed in [40]. A model of the metro line in Istanbul is proposed to study the feasibility of using a PV system to supply the interior lighting of urban rail vehicles. The simulation involves the use of solar panels on the vehicles' roof and an on-board battery system. This allows us to see how this application is different from what is studied in this thesis project, due to the limited load that has to be supplied and the on-board characteristics of storage. The introduction of the battery bank allows to increase the utilization of regenerative energy from braking, obtaining like this additional energy savings. According to the results, the designed PV and battery system can supply the daily power demand and bring to a reduction of power consumption up to 50% when LED lights are used. A payback time of 7.5 years is found based on some rough estimations of the systems costs, which allow to define the solution as cost-effective if a 20-year lifetime is assumed.

2.2.6 Summary - PV and storage integration

In [24] show that the introduction of PV and storage at the station of a railway network, allow to have 128 days out of 277 with zero-emissions. The station was supplied completely by the direct and

indirect use of PV generation for more than 46% of the days of operation. In [32] and [40], simulations of PV and storage systems integration in traction networks are proposed. In both cases the **technical feasibility** was demonstrated.

The combined effect of PV and storage has been only partially studied and for different type of applications. The results of the research are not complete and leave a lot of space for further studies. Although multiple studies demonstrate the feasibility of the application of PV and storage [24, 33, 40], these all **differ in type of application**. As a matter of fact, on-board and stationary storage are both considered and on-board PV is also considered in the case presented in [40].

2.3 Research Gap

Research has been done on the integration of storage and of PV systems in traction systems, however the potential of this application has not been studied in relation to the characteristics and the location of the trolleygrids. In the previous sections of the chapter, the reader finds an extensive review of the existing literature. When speaking about integration of PV and storage systems multiple studies have been conducted. Although multiple studies demonstrate the feasibility of the application of PV and storage [24, 33, 40], these all differ in type of application. In this thesis project the focus is set only on trolleybus traction grids and on the integration of PV and storage in this type of systems. Literature is very limited in terms of justification and assessment of the performance of the PV systems in traction grids. Research is especially very limited for trolleybus grids. The analysis of the discussed studies allows us to have some results that guarantee the possibility in terms of costs and the positive effects of this solution. This makes this option an interesting topic to research more upon, since it seems to be inducing a reduction of the energy drawn from the MVAC grid and therefore to an increase in the share of renewable energy in the transport sector and a reduction of the GHG emissions. What are the elements that cause the variation in the potential of integrating PV systems in trolleygrids?

The aim of this study is to examine, define and select city-/location-/trolleygrid-related parameters that are expected to have an impact on the different components of the trolleybus system under analysis: load, PV and storage. The effect of these parameters on the integration of PV in the trolleybus system is then studied and assessed, by comparing per each of the selected parameters the results obtained for grids of different cities. In particular this projects uses Arnhem and Gdynia grids as case studies. The research will develop further by investigating the potential of PV integration when stationary storage systems are also introduced in the trolley-grid system.

2.4 Summary and takeaway points of the chapter

In this chapter the reader finds an extensive review of the existing literature. In particular, this can be divided in two main thematic groups: **Electric vehicles energy demand** and **PV and Storage integration** in traction grids. Each section of the literature review is concluded with a summary of the key points of each topic group to which the reader can refer. The aim of the chapter is to understand what can cause the load to vary and to discover the feasibility and interest in PV and storage integration in traction grids.

Through the discussion of existing literature, the gap in research is identified. Many variables are found to have an impact on the energy demand of electric vehicles: traffic, road gradients, environmental characteristics, etc.. PV integration, with and without storage, appears to be a feasible solution to reduce the emissions of trolleybus grids, but why is the performance of PV systems integrated in different traction grids different? **What are the elements** that cause the variation in the potential of integrating PV systems in trolleygrids of different cities? And, **what is their effect** on the performance of PV?

3 METHODOLOGY

In this chapter the methodology and the research approach are briefly presented, followed by an overview of how data collection and analysis is performed. The last part of the chapter is dedicated to the study of the Key Performance Indicators (KPIs), the impact that these have on the trolleybus systems with integrated PV and storage, and the selection of the parameters to use in this research project. All these elements, together with the existing relevant literature, constitute the basis required to start the simulations. In the next chapter, the discussion on the methods used is completed with the details of the models used for the simulation of the operation of the trolleybus grids.

3.1 Methodology and Research Approach

Figure 3.1 represents the flow chart of the research approach. PV integration in trolleygrids is defined as starting point, since through the study of existing literature its feasibility and interest is established. The content enclosed in the green square is the thesis core, with Literature and Data as inputs to the research project. The analysis of the characteristics of the trolleybus grids and their location lead to the definition of the Key performance indicators (KPIs) which will be used to interpret the simulation results and draw recommendations on the PV potential integration. On the other side, storage integration is investigated in terms of effects on the PV system performance in the trolleygrids. Models and assumptions are used to simulate the operation of the grids, of the PV systems and the Energy storage systems.

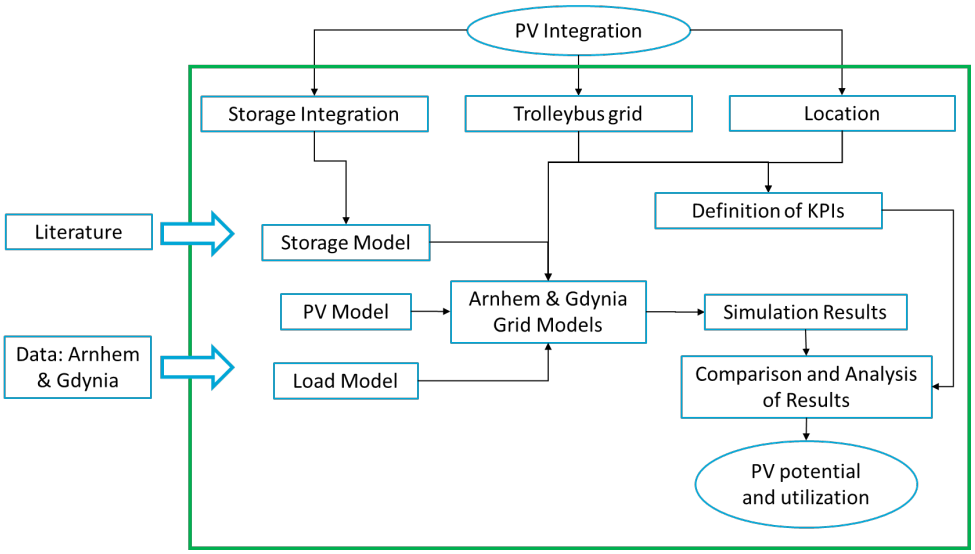

Figure 3.1: Methodology flow diagram step by step from PV integration to the analysis on how PV potential varies in different grids - own work

The interest in photovoltaic integration in traction grids, specifically in trolleybus grids, is described in the Introduction chapter (1) and in the Literature Review Chapter (2), where the research gap is also identified. This project is focused on understanding the impact that the characteristics of the trolley-grids and of their location have, together with the presence of energy storage systems, on the potential of PV integration. Literature related to trolleybuses and traction grids, electric vehicles energy

consumption and the integration of storage and photovoltaic in traction grids is firstly studied. The literature review allows to have a solid theoretical and experimental base to start with.

The second step in the methodology is also related to inputs: data collection and data analysis. The data for Gdynia and Arnhem are gathered, sorted, analysed and organised as inputs for the models. Due to the large amount of data required this process is time demanding. For the two cities data related to the environment, the location, the trolleygrid and the trolleybuses are gathered and organised. The next section goes more into depth on the methods used to gather, organize and analyse the data for the two cities.

The identification of the KPIs uses of the data in input: existing literature and the collected data on the two grids. Therefore, this can be defined as the third step in the research framework and it is discussed in the last section of the chapter. This step consists of a research on the parameters which have an impact on the functioning of trolleybus grid systems with PV ans storage integrated. The aim is to define a set of indicators that can be used to assess the potential of integrating PV systems in trolleygrids.

The final step before the analysis of the results is the modelling of the grid operation. The models created and used are a Bus Load model, including HVAC model and bus velocities, grid model, to simulate the whole year operation, PV generation model and Storage model. In Chapter 4, an extensive description of all the models used and created is provided, together with a brief validation of the outputs of the new codes.

In Figure 3.2 the methodology flow chart is divided into the four blocks identified in the previous paragraphs, namely: *Existing Literature, Data Collection and Data Analysis, KPIs selection and study* and *Models*, which are the 4 steps that are necessary to obtain the tools and the outputs to analyse the potential of integrating PV and storage in trolleybus grids.

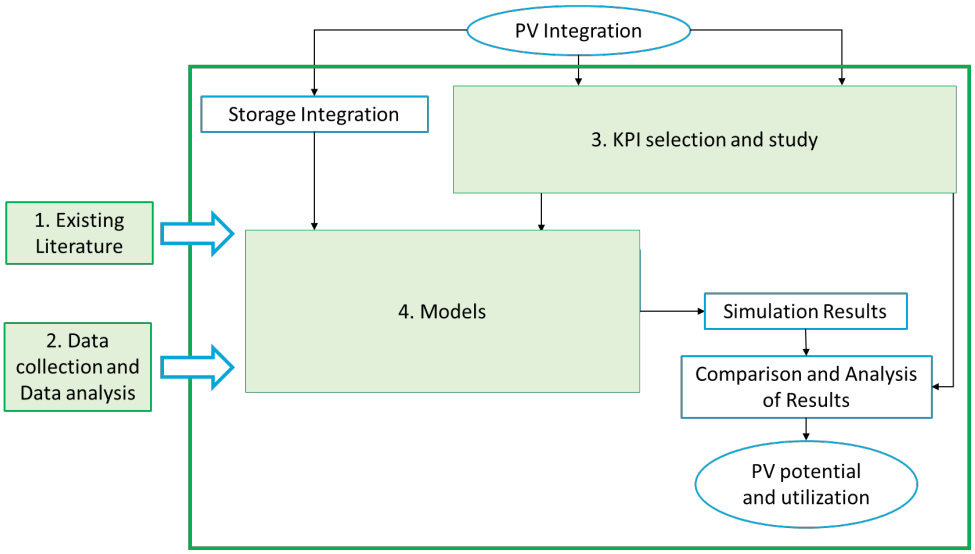

Figure 3.2: Methodology flow diagram: identification of 4 main steps of the research to get to the results - own work

3.2 Data Collection and Data Analysis - Arnhem and Gdynia

Data collection is a process consisting of gathering observations, measurements and details of the systems that will be studied. The aim of the research, the type of data required and the methods and procedures to collect, store and process the data have to be considered before starting the data collection. In Chapter 1 and Chapter 2, the scope of the research project are identified. Based on the research questions, it is possible to conclude that the aim is to gain insights on the reasons of the *variation* of the potential of integrating PV in trolley grids and *measure* these variations. The data to be collected is quantitative data which can be expressed in numbers and graphs and be analysed.

When speaking about PV system integration potential, the intention is to investigate the effectiveness of the PV generation in supplying the load. This is measured investigating both how much of the PV energy is used by the trolleybus system and how much load is covered by the PV generated energy. These two elements provide an overview of how well the PV systems can perform in relation to the traction grid operation.

The first part of the data collection process can be defined as 'Secondary data collection'. Existing datasets that have previously been gathered from other sources are found. The sources used can be classified as: existing literature, university research groups, researchers working on the same topics and private/government companies. The collected data through this process is:

- Weather data for the cities of Arnhem, Gdynia, Szeged and Athens
- Technical data of the trolleygrids of Arnhem and Gdynia:
  - Power system parameters (grid configuration, number of substations and sections, section division, number of buses used in the grids, energy requirements)
  - Substation and section parameters (Voltage levels, cable types, capacity of substations)
  - Bus characteristics (volume, weight, electrical motor characteristics, presence of on-board batteries)
- Measurements of the buses operation in the Arnhem grid:
  - Power and velocity profiles measurements in Arnhem grid (2 per direction of each bus line)
  - Voltage and current measurements at bus connection point to the overhead lines for the same runs
  - Bus operation signals measured during the same runs (pedal signals, HVAC on/off signals, time, etc.)
- Maps of the trolleybus lines and of the division into sections of the two trolleygrids, Arnhem and Gdynia

The second part of the data collection process is more 'experimental'. Unfortunately, a limited amount of data is found on the cities and on how the traction grid is integrated in them. In particular the following elements are missing:

- Bus Stops positions
- Distances travelled by the buses (full bus lines and between bus stops)
- Location of traffic lights in the cities
- Road gradients of the streets travelled by the buses
- Bus stops timetables
- Length of the sections in which the overhead lines are divided
- Supply points of each section (feed in points from substations)

The first five items are necessary to simulate the bus operation in the grid and the travelling of the buses in the two different cities.

In order to gather these data, Google Maps and OpenStreetMap websites are used. The distance between two following bus stops is measured for all the bus stops in the two grids through Google Maps. After identifying the location of the traffic lights through OpenStreetMap, their position along each line is measured on Google maps. In parallel, by looking at the travelling distances on foot on

Google maps, the gradients of the roads are registered. This process is very time demanding, due to the necessity of performing it for 6 bus lines in Arnhem and for 12 bus lines in Gdynia. Finally, the schedule of the buses is retrieved from the bus transport companies of the two cities (respectively Breng and ZKM, in Arnhem and Gdynia).

These data are then organised in tables and prepared to be used as inputs for the simulations. In Appendix D an example of the tables made to store the data on the bus positions, section lengths, traffic light positions and timetables can be found. Together with this, a brief explanation of the process to store the data is provided.

To conclude, in Table 3.1 an overview and comparison of the main data collected for the two trolleygrids in Arnhem and in Gdynia is provided. In this table synthetic information is provided for the reader to have an overview of the two systems being studied and the differences between them. In Figure 3.3 and 3.4, the maps of the section division of the two trolleygrids are provided. The different colours in the grid identify different sections. For the Arnhem grid map, sections are colour coded based on the substation that is supplying them. For the Gdynia grid map, the substation are shown and indicated on the map with the connection to the supply points in the sections.

Table 3.1: General characteristics of the trolleygrids of the two cities - comparison

Gdynia (Pl)		Arnhem (Nl)
12	**Number of Bus Lines**	6
84	**Number of buses**	54
30	**Number of sections**	43
10	**Number of Substations**	18
3	**Section/Substation ratio**	2.4
2.8	**Bus/Section ratio**	1.0
8.4	**Bus/Substation ratio**	2.3
600-1800	**Substation Ratings [kW]**	800-1000
675-704	**Substation Voltage [V]**	630-720
1.3	**Length of sections - average [km]**	1.1
2 (4)	**Parallel Lines**	2
Multiple	**Bus Type**	Multiple
1225	**Average Yearly Irradiance [kWh/m²]**	1165
4.4	**Average daily sunshine duration [h]**	4

3.3 KPIs definition and study

In this section the Key Performance Indicators (KPIs) which are used to assess the potential variation of PV integration in the trolleygrids are discussed. In particular, these parameters are here explained and analysed based on the impact that they are expected to have on the trolleybus systems. The identification of the parameters is done considering their relation to city and location of the grid and the impact that they have on the integration of PV and Energy Storage systems in the trolleybus grids. After defining the KPIs, some recommendations on how to use them to assess the PV integration potential are given. Together with this, some indicators are selected and prioritised for this study. As a matter of fact, not all the indicators are used in this study to compare the results obtained for the grid models of the two cities. In the dedicated subsection, the reader will find more information on the selected study-parameters.

3.3.1 KPIs Definition and Evaluation

The Key Performance Indicators can be grouped into 3 categories: environmental-related parameters, city-related parameters and trolleybus system-related parameters, which can be subdivided further into grid- and bus-parameters. The reader finds here the list, definition and explanation of each parameter. KPIs are given in order based on the category they are part of.

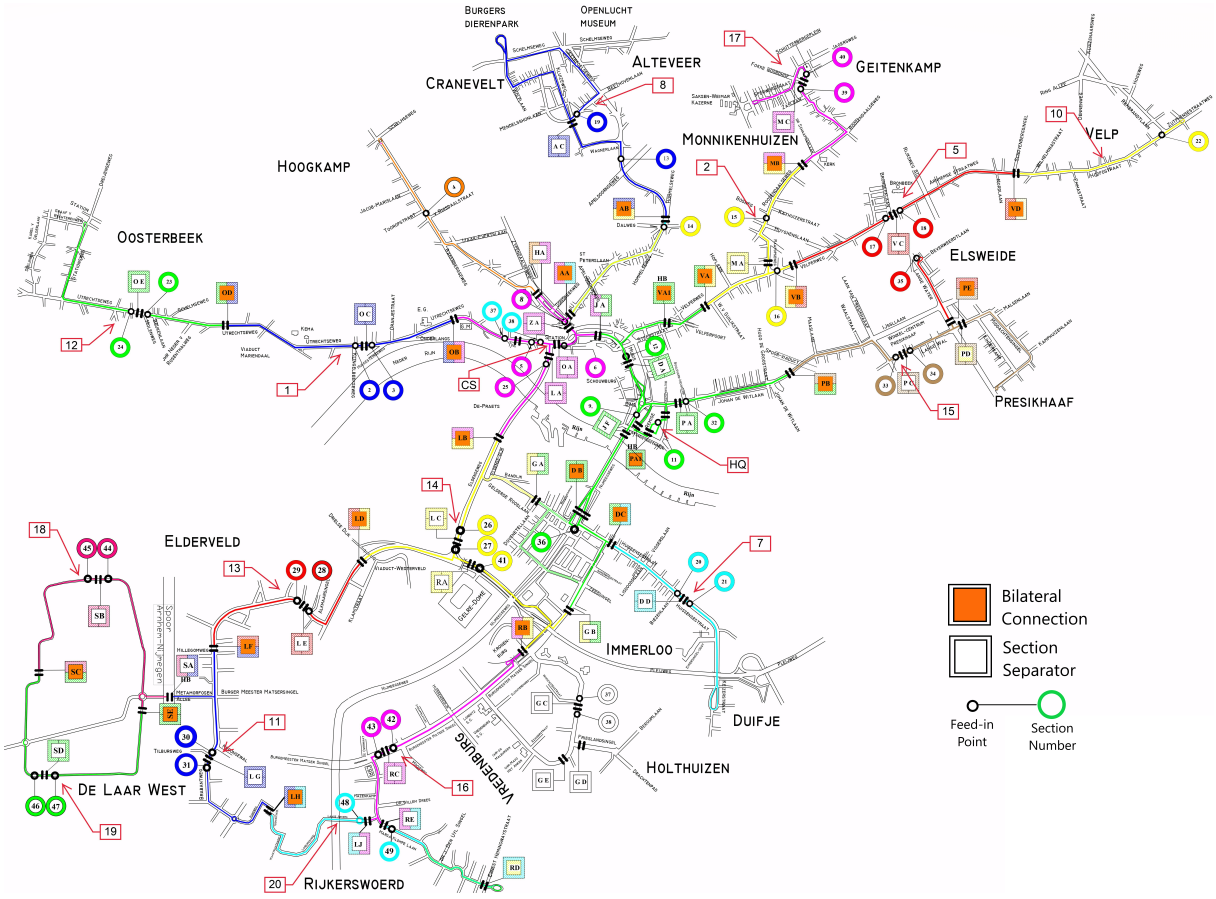

Figure 3.3: Arnhem trolleygrid structure: map of the division in sections - Connexxion

Environmental-related parameters

- Yearly Irradiance
  The yearly irradiance as a KPI represents the average yearly radiation at a specific location. It is an expression of the irradiation received on a horizontal plane at a certain location on average during one year time. The insolation decreases with the latitude (in absolute values) to reach its maximum in equatorial territories. It can be expressed in power or energy terms. The average yearly irradiance as expressed in Table 3.1, indicates the annual solar irradiation at for the optimally tilted modules. This value can be used for basic PV system sizing to calculate the equivalent sun hours at a location, namely the hours in which there is a solar irradiance of 1000 W/m². In the next chapter, in the PV modelling section, the calculation of the irradiance on a solar module and its effects on the modules performance is given. This indicator is used to assess the impact of the weather on the potential of a PV system integrated in the trolleygrids. The indicator will be expressed as power per unit area (W/m²).

- Sunshine Duration
  This KPI defines the absolute or percentage value of hours, in which the sun is actually illuminating the surface of the earth. The World Meteorological Organization defines the sunshine duration as "the number of hours for which the direct solar irradiance is above 120 W/m²". This data is influenced not only by the sunrise and sunset times, but also by the cloudiness. The variation of cloudiness and of cloud types causes the variation of the irradiance intensity, which affects the sunshine duration [67]. The physical quantity used to measure the sunshine duration (SD) is time and the units are seconds, minutes or hours. Relative and percentage quantities can also be used in specific cases [62]. In this study the SD is expressed in "hours per day" or in "daily sunshine hours". This parameter has an impact on the PV installed capacity and on the time in the day during which the load is able to see and use the PV generated energy. Therefore, it determines the long term temporal mismatch between load and generation in the grid, which causes the need of energy storage options to cover it. Thus, this indicator can also affect the

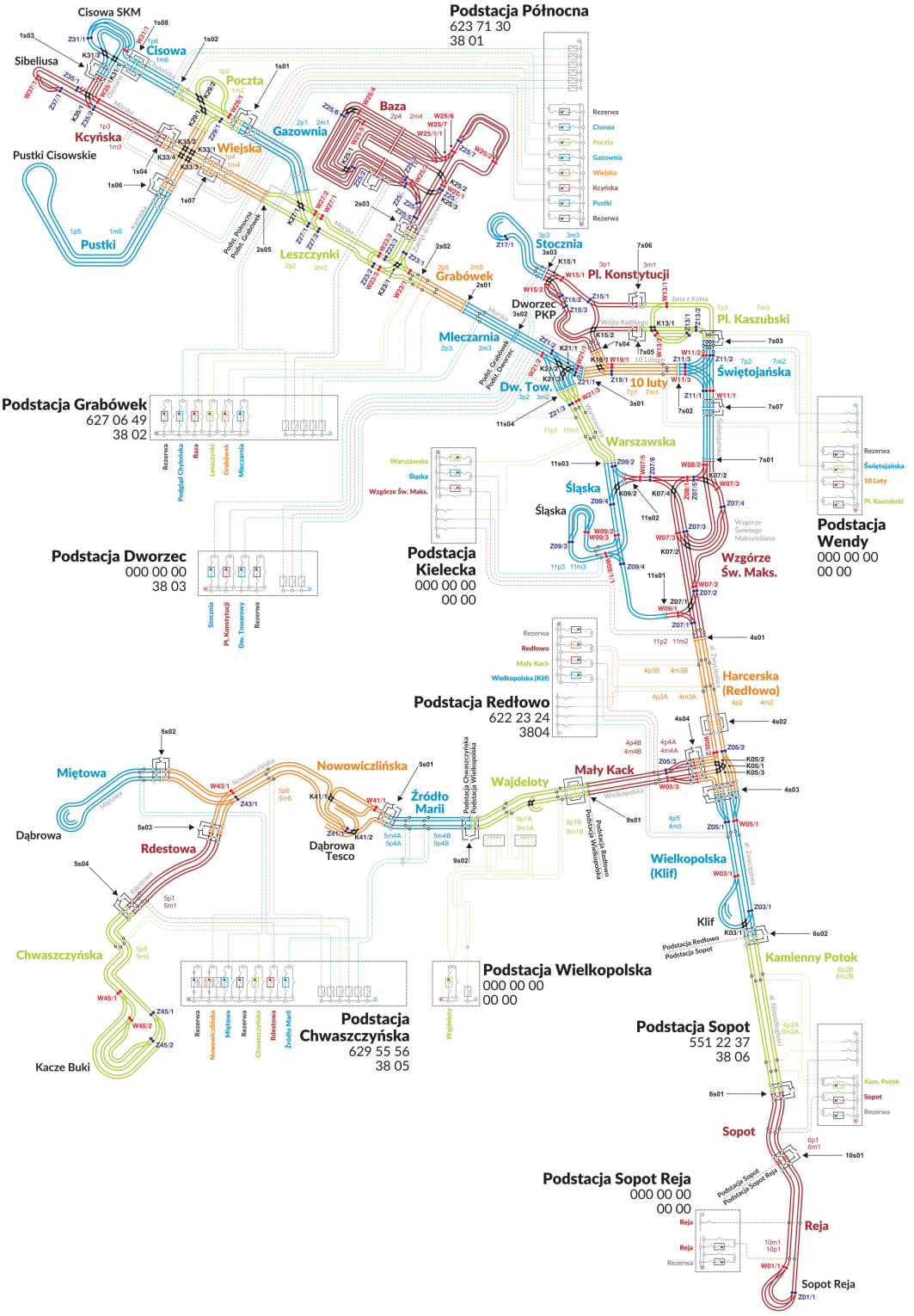

Figure 3.4: Gdynia trolleygrid structure: map of the division in sections - PKT

storage capacity requirements and the type of storage required. Together with the average yearly irradiance it can be useful to categorise the locations' potential for PV integration.

- Ambient Temperature
  As discussed in Chapter 2, ambient temperature strongly affects the energy consumption of electric vehicles due to the variation of HVAC power requirements that temperature variations cause. Not only the energy demand of the traction grid is affected by this parameter. As a matter of facts, the ambient air temperature has an impact also on the PV efficiency and on the battery lifetime. With the increase of ambient temperature, the output voltage of the solar panels decreases and the short circuit current slightly increases, causing a reduction in the power output [27]. Therefore, the location can affect the performance of the PV system and depending on the location and on the weather conditions different PV modules might be more suitable for different applications. In [3], the effect of temperature on the modules is analysed as well and the authors underline the importance of considering this parameter when sizing and simulating the performance of a PV system. Another important variable affected by ambient temperature is the battery lifetime. In the case of high temperatures operation, although the performances of the battery are increased the total lifetime of the battery is decreased and therefore the number of cycles is reduced. The interest in this KPIs can be related to its strong connection to the change in location and the effects that different climates can have on the integration of PV and storage in the trolleybus grids.

City-related parameters

- Road Gradient
  Road gradients are included in the bus demand model since they have a significant impact on the load variability and on the power peaks. As discussed thoroughly in the literature review chapter, the influence of gradients on energy consumption is not negligible. Uphill and downhill roads significantly affect the energy demand and the mismatch between PV generation and energy demand. Sections with downhill roads prevalence will require different PV/Storage ratios compared to section with uphill roads, due to the very diverse demand profiles that they generate. Also in terms of regenerative braking road with different gradients have different acceleration/deceleration profiles which cause different necessity of storage for energy recuperation from braking and to cover power peaks caused by the acceleration phases. In terms of different cities, this parameter can highlight how the structure of a city impacts the potential of PV integration in traction grids, but it can also provide some recommendations on where it is best to place PV or to build a trolleygrid in relation to the hilliness of the city.

- Traffic Intensity and presence of dedicated lanes
  Road traffic congestion strongly affects the energy demand of buses both in terms of traction and of non-traction (HVAC) energy needs. The presence of traffic, as discussed in Chapter 2, has a significant impact on the HVAC requirements. In [16], the relation between commercial speed and delay and the auxiliary energy requirements is shown (this characteristics can also be found in Figure 2.10). The traffic intensity affects the bus energy demand but has a strong impact also on the integration of the new sustainable technologies in the grid. The increase in traffic in supply sections that are fed by PV can increase noticeably the utilization of the solar generated energy. As a matter of facts, the increase in traffic congestion causes a reduction in travel speed and therefore an increase in the time that the vehicle spends in the area supplied by the PV system and/or by the stationary energy storage system. Moreover, the continuous phases of acceleration and deceleration cause peaks in power demand and increases in regenerated energy and this affects the integration of storage technologies to smoothen the power demand curve.

  Proposed as possible solution to traffic congestion in multiple studies discussed in Chapter 2, the presence of dedicated lanes can have a strong impact on the traffic conditions experienced by the bus and therefore on the energy requirements and on the travel time of buses in supply areas that are fed by PV and/or stationary storage. The impact of Dedicated Lanes can be explained as elimination of the effects of traffic on the system: reduction of time spent in certain sections and therefore effects on the PV utilization and on the storage to increase self-consumption, reduction in frequency of acceleration/deceleration phases and therefore of storage requirements to cover peaks in power and regenerative energy waste.

- Number of stops
  The number of stops of a bus affect the power and energy requirements. Continuous and frequent stops cause continuous and frequent peaks in power and braking energy recuperation. This not only affects the load variability and the stability of the grid, but also has an effect on the storage in terms of peak shaving requirements and on the PV utilization due to the reduction of the regularity of the load. The increase in time spent in a section fed by PV generated energy due to continuous stops, would increase the PV utilization especially in the case in which on-board storage is included and the charging of the batteries is done through the catenary line.

- Number of passengers and passenger flow
  The number of passengers on- and off-boarding influences the weight and the energy demand of the buses in terms of traction and non-traction (HVAC) energy requirements. This variable also has an impact on the number of buses and on the overall load of the system, due to passenger flow peaks during the day, and consequently the inclusion of additional lines and the increase in bus traffic. This affects the efficacy of the PV and storage integration due to daily and seasonal fluctuations of passenger numbers. Another important variable to consider in relation to passenger traffic is the extremes of this interval: high variations in passenger traffic during the day cause high variations of energy demand (peak and night figures have very different trends during the day). This could strongly affect the PV utilization and also the installed PV capacity.

- Eco-driving solutions
  Different driving modes can be defined based on the acceleration and deceleration trends. It is demonstrated that aggressive driving behaviour, characterized by continuous acceleration and deceleration moments, has a significant impact on the energy consumption of an electric vehicle and that the energy savings obtainable by limiting the frequency of acceleration and deceleration throughout a driving cycle are noticeable. In [20], it is shown that the energy consumption difference between a 'moderate' and an 'aggressive' driving mode can reach 30%. The effect of aggressive driving behaviour will be taken into consideration as increased number of power peaks in the demand and will be considered in relation to the structure of the system in the various cities. This parameter can strongly affect the sizing and the utilization of PV and storage in the grid and the installed capacity ratio between the two, due to the reduction of load stability that it causes which decrease the PV utilization and due to the storage requirements to cover peaks in power and to store the regenerated energy.

Trolleybus system-related parameters

- Substation Voltage
  The substation voltage has strong impacts on the power flow in the grid. As a matter of fact the substation voltage affects transmission losses, regenerative braking and bilateral connections. The different voltage levels in the grids determine the current requirements to cover the power demand of a bus in a certain position of the section, the voltage requirements to send power back to the overhead lines and have power exchange between buses and also the distribution of power between two sections which are bilaterally connected. The substation voltage sets regulates the voltage on the sections that are supplied. Very small variations of voltages can change the power flow in the grid. Therefore, the analysis which could be conducted on substation voltage is a sensitivity analysis to understand what impact every small variation of the system has on integrating PV. The comparison of the two grids, characterised both by a 30V or higher variation will provide no indication of the impact of the voltage levels on PV. In particular, the correlation between substation DC voltage setting and the operation of PV on the AC sides is negligible.

- Section Lengths and Number of sections per substation
  This indicator is more complex and actually contains 2 different parameters which give an overall indication of the substation configuration in terms of size. The size of the substation varies in relation to the power requirements, the number of section fed and the overhead km served. The effect of an increasing number of sections fed by a substation can induce an increase in the power requirements, due to the higher probability of supplying at least one section. Increasing section lengths on the other hand, namely the km of overhead lines supplied by the same feed in point, has an impact on the energy demand due to the increase in transmission losses that this can cause. However, increasing the length of a section could be beneficial in terms of utilization of

regenerated energy. This due to the fact that the probability of having multiple buses on the same section would increase with the section length. This indicator will be used to assess what impact the length of sections and their distribution under substations have on the integration of PV systems.

- Substation Load Demand
  The Substation Load Demand gives an indication of the substation size in terms of energy/power demand. The size of the substation varies in relation to the power requirements, the number of section fed and the overhead km served. The previous indicators related to the section distribution under the substations provides an indication of the size of the substation more related to the spatial distribution. This KPI can provide general information on the size of the substation in terms of demand. Together with the previous indicator, this will be used to understand the effects of the size of the substations and their distribution in the grid on the integration of PV.

- Cables Type
  The transmission of current through the power lines causes losses that cannot be neglected. The type of cable used for the overhead lines and for the feeders has a huge impact on the losses and therefore on the power requirements. In Arnhem and in Gdynia 630 mm^2 copper and aluminium wires are used as feeder cables, respectively in the two cities, and 100 mm^2 copper cables are used for the catenary. The difference between cable types is limited between the two case studies, therefore this parameter is used in the simulations but it is not used to assess the impact that the cable variation has on the potential of integrating PV systems.

- Parallel Lines
  In order to reduce transmission losses, compensatory connections between fractions of the overhead lines are introduced [14]. One of the modifications of the overhead cables included in the modernisation process of the trolleybus traction grids, is to connect certain intervals of the overhead cables for the two directions of travel in order to reduce the losses of power transmission. As a matter of fact, when supplying power to a bus in a section these connections allow to split the required current into two fractions (or more if more cables are combined between them) and therefore to reduce the losses caused by the transmission of high currents. This allows to reduce the effective resistance of the catenary (thus the transmission losses) in certain circumstances in half (if the connections are done between 2 cables). In sections with high bus traffic intensity, where multiple buses could be found in the same position, multiple lines can exist for the same travel direction. In this case the combination of multiple overhead lines could bring to a beneficial reduction of the voltage drop along the line. In the cases of Arnhem and Gdynia trolleygrids, overhead lines are connected in parallel. In both systems only 2 lines are connected in parallel most of the times. There are some exceptions in Gdynia, where the number of lines in parallel can become 4, in high traffic bus stops and in deposits.

- Bus Type
  The bus energy requirements depend on the type of bus used in the catenary of the different cities. It has been discussed, considering previous studies, that buses vary in type, weight and dimension and this can cause meaningful differences in the grid characteristics in terms of energy and voltage requirements. The integration of PV and storage in terms of size is therefore influenced by the average bus requirements in the networks.

- Bus Traffic
  As assessed in the literature review chapter, the simultaneous presence of more than one bus on the same supply section has an impact on the energy demand of the section, on the peaks in power and the voltage drops in the section. Having multiple buses in the same power supply section allows the increase in energy exchange between the buses and lower transmission losses between them, which has an effect on the load regularity, on the utilization of the regenerated braking energy, on the necessity of storage to increase regenerated energy use and on the utilization of the PV generated energy. Bus traffic influences all the individual components of the system and the integration and combination of the components in a system.

- Presence of OESS
  The presence of on-board energy storage systems strongly influences the requirement of addi-

tional stationary storage systems, the power demand of the buses (also due to the increase in weight that this causes) and the regenerative energy utilization. As a consequence, it also impacts the integration of the PV in the grid in terms of sizing and capacity, but also in terms of regularity of the load and mismatch with the demand. On-board storage can reduce power peaks and generate a more stable load which can increase PV utilization on one side but can reduce the capacity required on the other side.

- Presence of Bilateral Supply
  Bilateral supply, as explained when discussing the existing literature on the topic, can strongly influence the network operation. Bilateral connections between sections allow power flow between sections and therefore between different supply areas (of the one or two substations). This has an impact in the size, the modularity and the effectiveness of PV and stationary storage integration in the grid. The range in which the PV and stationary storage can supply buses is increased by bilateral supply, and the interruption of bilateral connection would reduce the utilization of PV generated energy and the range of influence of the storage system. On-board storage would also be affected, in particular due to the impact of bilateral supply on the power exchange between buses. The presence of bilateral supply in a system can bring to a completely different optimal point for the integration of PV and storage in the grid, in terms of sizing and location.

- HVAC requirements
  The energy consumption of the electric trolley buses, as extensively discusses in Chapter 2, is expected to vary considerably in relation to the moment of the trip and the location in which it is performed. The energy consumption of the HVAC system of the vehicles is affected by temperature and relative humidity variations of the surroundings, which is strongly connected to the place in which the vehicle operates. It is also found in some of the papers that the energy demand for auxiliaries can account for almost 50% of total energy consumption in some cases, reaching up to 70% during winter [16]. In relation to the effect of the HVAC energy requirements on the mismatch between load and generation, the seasonal variation of the HVAC power requirements has an impact on the seasonal mismatch. As a matter of fact, PV generation is characterised by a reverse U-shape trhoughout the year, with high generation in summer months and lower generation during the winter months. Therefore, in very hot climates, with very high Air Conditioning and Ventilation requirements during the summer, the seasonal match between generation and load is improved by the HVAC requirements. On the other hand, cold climates are expected to have higher mismatch between generation and load due to the steep increase in demand during winter months when high heating requirements happen.

- Regenerative energy dissipated
  High dissipation rates of regenerated energy imply that energy storage could be used to store the recouped energy in order to supply it later to the grid (either to the same bus or to another bus when it reaches the supply section). This parameter is influencing therefore the size and the type of storage which should be integrated in the grid. If the regenerative energy is stored and reused the utilization of PV could be reduced.

The indicators are also classified based on the impact they are expected to have on the different components of the system that is being analysed. The parameters are therefore evaluated and analysed changing the component(s) of the system on which they are expected to have an impact on. The different components of the system on which the impact of the parameters is studied are:

- Effect on the photovoltaic generation and efficiency (**PV**)
- Effect on the Stationary Energy Storage System size and efficiency (**SESS**)
- Effect on the load, namely on the bus energy consumption (**BUS**)
- Effect on the PV utilization and on the load seeing the PV, when the load actually receives and uses the PV generated energy (**PV** $\cap$ **BUS**)
- Effect on the PV and storage combination and optimization, how the parameters affect the storage of PV energy and the variation of PV self-consumption (**PV** $\cap$ **SESS**)

- Effect on the storage utilization and on the load seeing, when the load sees and uses the storage system to provide energy, to cover power peaks (**SESS** ∩ **BUS**)
- Effect on the integration of PV and SESS in combination with the load, cumulative effect on the whole system (**PV** ∩ **SESS** ∩ **BUS**)

As one can see, not only the expected effect of the KPIs on the individual system components is analysed, but also how the indicators are expected to affect the integration between subsystems is researched upon.

The table shown in Figure 3.6 highlights the differences in the expected impacts of the different parameters on the subsystems and system components. The colours in the table range between green, yellow and red, on a scale going from 1 to 5, in which red identifies the highest impact (5/5) and green the lowest (1/5), as per Figure 3.5.

Figure 3.5: Colour coding (1-5) of KPIs Table in Figure 3.6 (How to read the table)

The table is colour-coded to convey and highlight the fact that each parameter has a different influence on the system and that some parameters are expected to affect more (or less) some parts of the system with respect to others. Also, what one can notice by just having a look at the table is that almost all the parameters affect the load, namely the buses' energy requirements throughout the year. Another observation that can be done is that few of the identified KPIs have an impact on the PV and only one on the storage element, however it is important to notice that most parameters affect PV and storage in combination with the load and therefore the overall performance of the system.

3.3.2 KPIs selection criteria and comparison strategies

Once the Key Performance Indicators are identified and explained, a range of parameters is selected for this study. It is decided to select only a limited number of parameters for multiple reasons: availability of data, type of analysis performed and time constraints. The first element is the data that are in our disposal. As mentioned previously, retrieving data for the traction grids of the two cities was a long process and not all the data were found. For instance the information on traffic, dedicated lanes, passenger flow and power profiles are insufficient for both cities. For this reason, some indicators are excluded on one side and on the other side it was necessary to reproduce velocity profiles for the grids in order to simulate the bus operation. The second point is the type of analysis done on the KPIs. In this study the focus is to obtain some indications of the impact of the indicators on the potential of PV for different trolleygrids of different cities. To do this the operation and configuration of the grid in Arnhem and Gdynia are compared. The two systems are analysed based on their characteristics, their analogies and differences to establish the impact of the selected indicators on them. Some of the parameters identified though are more suitable for sensitivity analysis rather than to be used to compare the performance of the two grids. This because either they are found to not vary significantly or because it would be possible to find a trend only when varying the parameter a considerable amount of times. Here is where the last element, time constraints, becomes relevant. Simulating the yearly operation of the two grids repeatedly is not possible due to their high time consumption. Finally, the attention was placed also on having a balance within the study on the effects that the indicators have on load, PV and mismatch. Therefore, the aim is to try to select the KPIs also to have an overview of the effects on these three elements.

In Figure 3.7 the type of comparison and the difficulty elements for each parameter are described. Highlighted in green are the KPIs selected for this thesis research.

3.4 Summary and takeaway points of the chapter

The research is developed in four blocks:

1. **Literature Review**
2. **Data collection and organization**
3. **Definition of Key Performance Indicators (KPIs)**
4. **Models and simulations**

After this, the **analysis of the effects of the KPIs** on the integration of PV in trolleygrids is performed, based on the results obtained from the simulations.

The first two elements of the list form the **inputs to the research project**: the existing literature study and the data and measurements required, based on the research questions defined in Chapter 1. In this chapter in the second section the reader can find an explanation of the data collection and organization process. This can be divided into two main parts 'Secondary' and 'Experimental' data collection. The required input data can be considered quantitative. In Appendix D, the reader can find an example of the tables generated to organise the data for the trolleygrid of Arnhem and Gdynia.

After collecting data for the Gdynia and the Arnhem grid, used as case-studies for this research, and analysing it, a **set of Key Performance Indicators (KPIs)** is identified. The aim is to generate a system which allows to **assess the potential of integrating PV systems** in trolleygrids through the evaluation of the KPIs. A qualitative study on the impacts of the KPIs on the trolleybus system is also provided. The parameters are classified based on their type, **environmental-, city- and trolleybus system-related parameters**, and also based on the **impact on the system**. In Figure 3.6, the reader can find a colour-coded table with an overview of the KPIs and their qualitative impact on the components of a trolleybus system with integrated PV and stationary storage. In Figure 3.7, the type of analysis performed and the selection of KPIs is summarised.

In the next chapter, the modelling part is dealt with in detail, from an overview of the structure to the equations, the physical and mathematical models implemented and the assumptions made.

KPI	PV	SESS	BUS	PV ∩ BUS	PV ∩ SESS	SESS ∩ BUS	PV ∩ Bus ∩ ESS
Environmental-related							
Yearly irradiance	PV generation			Load covered with PV	PV self-consumption		
Sunshine duration	PV generation			When BUS sees PV	PV self-consumption		
Ambient Temperature	Cell Efficiency	Battery performances & lifetime	Energy demand (HVAC)				
City-related							
Road Gradient			Energy demand, regenerative braking & power peaks	Spatial and temporal mismatch	Regenerative braking & spatial mismatch	When BUS uses SESS	
Traffic intensity / delays (Dedicated Lanes)			Energy demand (traction & HVAC) & power peaks	When BUS sees PV	Power peaks & PV self-consumption	When BUS uses SESS & power peaks	
Number of stops			Traction demand & power peaks	When BUS sees PV	Power peaks & PV self-consumption	When BUS uses SESS & power peaks	
Number of passengers (Variation in number)			Energy demand (HVAC & Bus weight)	Load regularity & PV utilization	PV self-consumption		
ECO-driving solution			Energy demand & power peaks	Load regularity & PV utilization	Power peaks	When BUS uses SESS & power peaks	
Trolleybus system-related							
Substation Voltage			Transmission losses & regenerative braking			When BUS uses SESS & regen. braking	
Sections (Length/Number)			Section load & losses	When BUS sees PV	Spatial mismatch	When BUS uses SESS	
Substation Load Demand			Transmission losses & regenerative braking	Load covered with PV	Temporal mismatch	When BUS uses SESS	
Cables type			Transmission losses	Load covered with PV			
Parallel lines (number/distance)			Transmission losses	Load covered with PV			
Bus Type			Energy demand			When BUS uses SESS	
Number of buses per section			Section load, voltage stability & regenerative braking	Load regularity & PV utilization	Regenerative braking	When BUS uses SESS	
Presence of OESS			Energy/Power demand (Bus weight & HVAC)	Load regularity & PV utilization	PV self-consumption	When BUS uses SESS	
Presence of Bilateral Supply			Section load & regenerative braking	When BUS sees PV	Spatial mismatch	When BUS uses SESS	
HVAC requirements			Energy demand (HVAC) & power peaks	Load regularity & PV utilization	Seasonal mismatch	When BUS uses SESS & power peaks	
Regenerative energy dissipated			Energy demand & efficiency		PV/SESS ratio	When BUS uses SESS	

Figure 3.6: KPI effect on PV, Storage and load and their integration in the system based on the relations between the components - colour-coded table

KPI	Included in study	Comparison	Notes
Environmental-related			
Yearly irradiance	Yes	Comparison of the PV potential based on the environmental characteristics of the location. No variation in the load.	The environmental parameters can provide an assessment a priori of the potential of integrating PV for any traction load, based only on the weather data.
Sunshine duration	Yes		
Ambient Temperature	Yes		
City-related			
Road Gradient	No	Compare the effect of different road gradients on the PV potential.	Only average values can be used, per section of the grid. This does not allow a full analysis and comparison considering the available data.
Traffic intensity / delays (Dedicated Lanes)	No		Difficult to take into consideration because a very small amount of data is available, for both cities.
Number of stops	No	Compare the effect of the number of stops in every section of the substations.	The number of stops is variable with the velocity profiles and the type of traffic. This is difficult to take into account due to the limited amount of data available on traffic conditions in the two cities.
Number of passengers (Variation in number)	No		Difficult to take into consideration because a very small amount of data is available.
ECO-driving solution	No	Compare the effect of reducing the frequency of acceleration and deceleration phases in the driving cycles.	Create different velocity profiles, with different characteristics and simulate the grids' operation.
Trolleybus system-related			
Substation Voltage	No	A sensitivity analysis on this KPI should be performed (future study).	The available data is not accurately measured and has not been confirmed by the suppliers.
Sections (Length/Number)	Yes	Effect on the integration of PV a of substation size and configuration (section number and length).	These indicators can be used to provide information on the effect of the distribution of substation and sections in the grids.
Substation Load Demand	Yes	Effect on the integration of PV of substation size in terms of energy and power demand.	
Cables type	No	A sensitivity analysis on this KPI could be performed (future study).	All the substations present similar characteristics, the analysis on the available data would not generate results.
Parallel lines (number/distance)	No	Compare the effect of varying the number or the distance of connection of parallel lines based on the differences between the cities. A sensitivity analysis on this KPI could be performed (future study).	This study is based on the data of Gdynia and Arnhem, no big difference is found in this parameter between the two grids.
Bus Type	No	Comparison between the buses used in the grids of different cities and the impact (average bus dimensions and weight considered).	Effects on multiple parameters of the bus energy consumption: traction and non-traction energy requirements.
Number of buses per section	Yes	Effect of the average an da maximum bus traffic under a substation on PV potential.	The bus traffic is expected to have an impact on the integration of PV systems, and can cover for missing information on traffic intensity.
Presence of OESS	No	Comparison between different storage solutions.	Low percentage of buses with OESS, difficult to isolate and to compare. Should be studied separately in comparison with the potential of stationary storage.
Presence of Bilateral Supply	Yes	Effects of introducing Bilateral Supply on the involved substations.	Limited analysis due to time constraints and modelling, but also because of non confirmed data of most substation voltage levels.
HVAC requirements	Yes	Effects of removing HVAC requirements on PV potential.	Interesting due to the high share of load demand HVAC covers.
Regenerative energy dissipated	No	Effects of different levels of regeneration and rates of utilization of the regenerated energy on the PV system integration.	Difficult to analyse with the simulated power profiles due to the assumptions made and the errors introduced simulating the bus movements (velocity and power profiles).

Figure 3.7: KPIs comparison methods and notes on data availability and further study interests (highlighted in green the selected KPIs)

4 MODELS

In this chapter, the reader will find a detailed explanation of the models used to perform the simulations of the two trolleygrids of Arnhem and Gdynia. In Figure 4.1, the reader can find a diagram explaining the modelling process and illustrating the different components of the model. The simulation of the grid yearly operation is obtainable only through previous modelling of the other elements. The model is built with bottom-up approach, starting from the bus components to the modelling of the substation and grid operation. The results obtained from the simulations are analysed in the next chapter. The reader in the next section will find in order the description of the following models: PV generation, HVAC, Velocity and power profiles, Storage and Grid operation. In the last section of the chapter an analysis of the errors introduced in the simulations due to parallel lines approximations is made.

4.1 PV Model

In this section the explanation and derivation of the PV model used to compute the PV generation in the different cities is given. The aim of the section is in first place to give an overview of the inputs to the model and then to illustrate how the PV model was built, what the outputs of the model are and which assumptions are made. Through this model it is possible to find the first recommendations for cities based on the comparison drawn between the cities in relation to the environmental KPIs defined: Yearly irradiance, Sunshine duration and Air temperature. This analysis is done in the next chapter and it supports the evaluations done on the variation of the potential of PV integration in trolleybus grids.

4.1.1 Input data and Module tilt range selection

In this subsection the input data for the model and the method to determine in which range to look for the optimal tilt angle for the modules in the different cities are explained. Observing the latitude of the locations, 52° for Arnhem (Nl) and 54.5° for Gdynia (Pl) we can expect the PV modules to be installed at slightly different tilt angles and to have very similar azimuth. As a matter of facts, the optimal tilt angle decreases with the decreasing latitude in the Northern Hemisphere and since the cities are located close to each other and both in the Northern Hemisphere it is expected that the modules will be installed facing south.

Before downloading the weather data for the modules optimal tilt and azimuth from the Meteonorm database, a first calculation is done in order to select the range of tilt and azimuth angles in which the optimal combination can be found. In the next paragraphs the equations used to find these values are given and the further steps to select the input data to feed in the PV model are illustrated. In first place, the following weather and irradiance data are retrieved from Meteonorm:

- Solar altitude (a_S)
- Solar azimuth (A_S)
- Global horizontal irradiance (GHI)
- Diffuse horizontal irradiance (DHI)

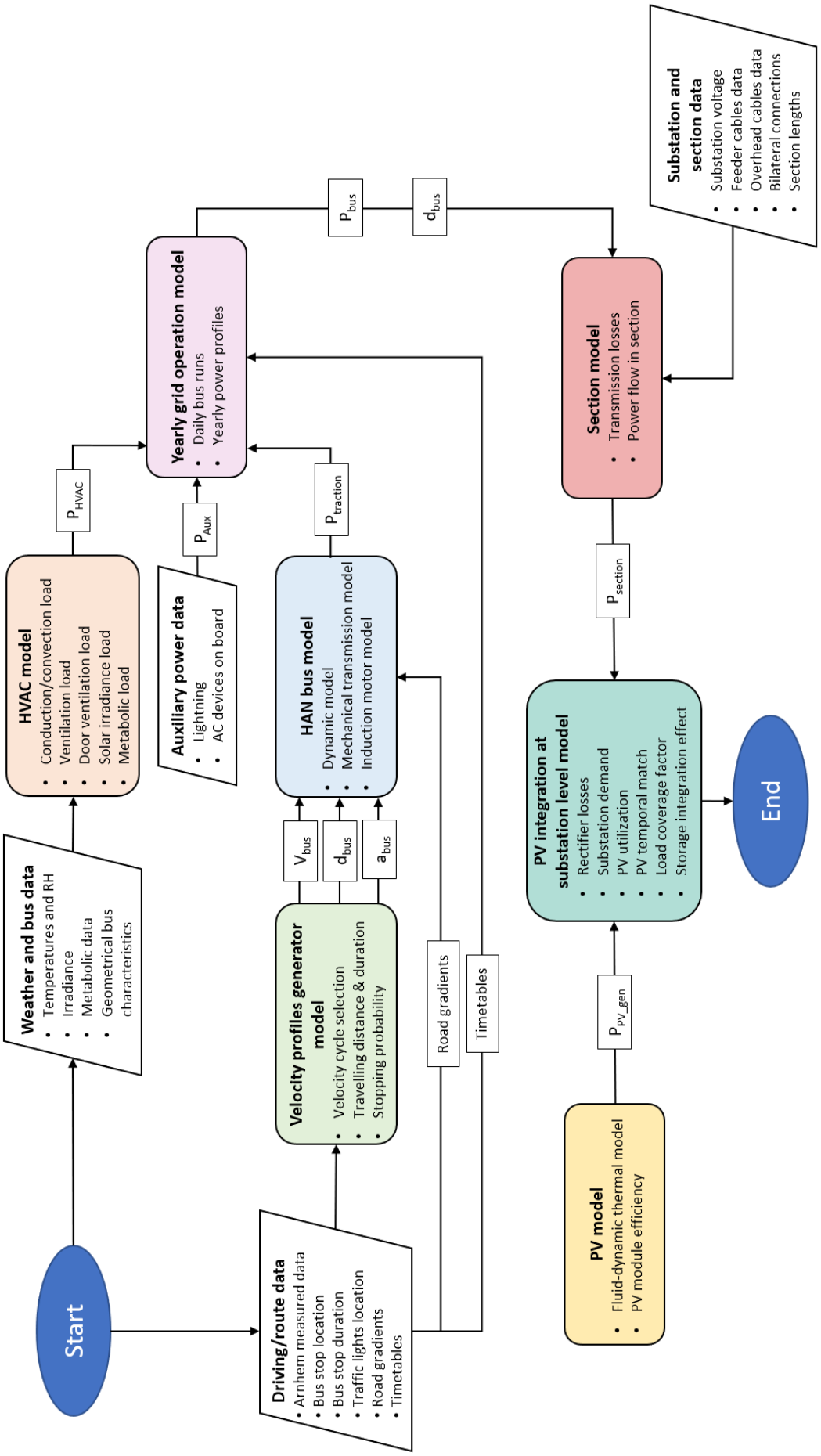

Figure 4.1: Flow diagram illustrating the connections between the different models and the overall modelling structure

From this data the DNI, SVF, AOI and all the irradiance components on the tilted modules have been calculated. Here below, the equations from [3] used to find the parameters listed above.

- Direct Normal Irradiance (DNI)

$$DNI = \frac{GHI - DHI}{cos(a_S)} \tag{4.1}$$

  In equation 4.1, DNI stands for Direct Normal Irradiance and is computed from GHI, DHI and solar altitude data from Meteonorm database.

- Sky View Factor (SVF)

$$SVF = \frac{1 + cos\theta_M}{2} \tag{4.2}$$

  with θ_M in 4.2 being the solar module tilt.

- Angle Of Incidence (AOI)

$$\begin{aligned} cos\,(\gamma) = cos\left(\frac{\pi}{2} - \theta_M\right)\ cos\,(a_S)\ cos\,(A_M - A_S) + sin\left(\frac{\pi}{2} - \theta_M\right)\ sin\,(a_S) = \\ = cos\,(a_M)\ cos\,(a_S)\ cos\,(A_M - A_S) + sin\,(a_M)\ sin\,(a_S) \end{aligned} \tag{4.3}$$

  if $cos\,(a_M)\ cos\,(a_S)\ cos\,(A_M - A_S) + sin\,(a_M)\ sin\,(a_S) > 0$
  with γ being the angle of incidence, namely the angle formed between the considered surface normal and the incident direction of the radiation [3].

- Direct irradiance on tilted module ($G_{M,dir}$)

$$G_{M,dir} = \text{DNI} \cdot AOI \tag{4.4}$$

  if $a_S > 0$ and $A_S - \frac{\pi}{2} \leq A_M \geq A_S + \frac{\pi}{2}$ otherwise $G_{M,dir} = 0$
  with DNI and AOI, Direct normal irradiance, calculated in 4.1, and angle of incidence, as in 4.3, respectively.

- Diffuse irradiance on tilted module ($G_{M,diff}$)

$$G_{M,diff} = \text{DHI} \cdot SVF \tag{4.5}$$

  with DHI and SVF, Diffuse horizontal irradiance data and Sky View Factor, as in 4.2, respectively.

- Reflected irradiance on tilted module ($G_{M,refl}$)

$$G_{M,refl} = \text{GHI} \cdot \alpha(1 - SVF) \tag{4.6}$$

  With α being the albedo of the surroundings, chosen to be 0.2 (average for city).

- Global irradiance on tilted module (G)

$$G_M = G_{M,dir} + G_{M,diff} + G_{M,refl} \tag{4.7}$$

No Shading Factor is considered, however the space required for the installation in the feasibility analysis takes into consideration the shades. This is explained further in the respective section of Chapter 6.

The optimal azimuth angle and the tilt angle range of the PV module are identified through an iteration, in which the yearly irradiance per square meter on the modules in the two locations is calculated for each combination of azimuth and tilt. The results are shown in Figure 4.2 and Figure 4.3. In this way the optimal ranges of tilt and azimuth angles are found, for which the yearly irradiance on the modules is maximised. Like this the optimal tilt is then identified by downloading the weather data for each angle and finding the maximum yearly generation.

After this, per minute data from Meteonorm are been downloaded at the optimal azimuth angle (modules facing south - 180°) for every angle in the optimum tilt angle range to find the best module

A_M [°] \ θ_M [°]	0	10	20	30	40	50	60	70	80	90
90	1016,02	1057,61	1078,20	1077,15	1054,51	1010,95	947,81	867,00	770,98	662,66
120	1016,02	1045,82	1057,20	1051,31	1029,67	994,71	949,13	895,31	830,34	751,27
150	1016,02	1054,77	1078,58	1089,18	1086,04	1066,40	1027,47	968,51	891,26	798,05
180	1016,02	1061,08	1095,18	1117,64	1119,18	1097,84	1054,27	989,80	906,38	806,56
210	1016,02	1051,59	1072,77	1080,62	1074,87	1055,91	1018,53	961,34	886,06	794,99
240	1016,02	1045,12	1055,49	1048,21	1025,14	988,64	941,80	887,55	823,91	746,54
270	1016,02	1056,40	1075,80	1073,65	1050,01	1005,59	941,75	860,42	764,08	655,66

Figure 4.2: Gdynia - optimal PV module tilt range and azimuth identification (own work)

A_M [°] \ θ_M [°]	0	10	20	30	40	50	60	70	80	90
90	988,46	1019,71	1031,74	1024,20	997,30	951,87	889,29	811,45	720,73	619,87
120	988,46	1011,10	1016,34	1005,86	980,96	943,39	895,35	839,78	775,09	698,64
150	988,46	1019,90	1037,24	1041,20	1031,37	1006,32	965,82	907,83	834,01	746,63
180	988,46	1026,87	1053,97	1068,00	1064,76	1040,94	997,26	935,04	856,19	763,08
210	988,46	1021,82	1040,15	1044,62	1035,28	1012,68	973,98	917,44	844,81	758,27
240	988,46	1014,97	1023,83	1016,18	993,20	956,87	909,82	854,75	790,42	714,16
270	988,46	1021,79	1035,84	1030,19	1005,00	961,05	899,66	822,71	732,52	631,85

Figure 4.3: Arnhem - optimal PV module tilt range and azimuth identification (own work)

inclination that maximises PV generation. In Figure 4.2 and Figure 4.3 the optimum angles and the Direct and Diffuse irradiance components on the tilted module are indicated. In relation to the azimuth of the modules, the azimuth is kept constant at 180° (modules facing south). This because, by means of the first approximation it is found that the maximum variation is of +/-1° around 180°. Moreover, the energy yield variation during the year with the application of the azimuth variation of 1° is not significant. Therefore, for simplicity, time expense and applicability this small variation is neglected for all the cities and 180° azimuth angle is used.

A_M [°]	180	
θ_M [°]	39	
$G_{M,year}$	1224,0	kWh/m²
$D_{M,year}$	524,8	kWh/m²
D_M/G_M	42,9%	

(a)

A_M [°]	180	
θ_M [°]	37	
$G_{M,year}$	1164,9	kWh/m²
$D_{M,year}$	558,3	kWh/m²
D_M/G_M	47,9%	

(b)

Figure 4.4: Optimal angles and global and diffuse PV module irradiance for (a) Gdynia and (b) Arnhem (own work)

At this point, the data that is necessary for the PV model is downloaded from Meteonorm, selecting the correct and optimal combination of tilt and azimuth angles. The input data given to the PV model is one year data of:

- Per minute global irradiance on the tilted modules
- Per minute air temperature
- Per minute wind speeds at 10m from ground level
- Per hour sky and ground temperature
- Per hour cloud cover factor

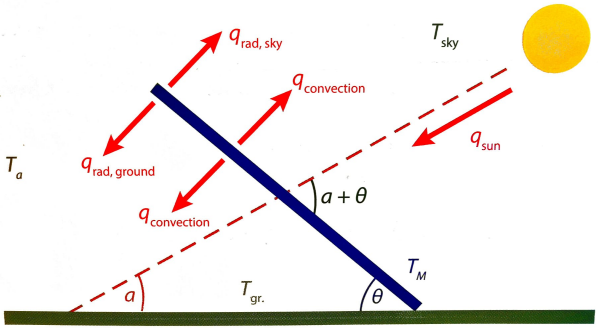

Figure 4.5: Representation of the heat exchange between the PV module surfaces and the surroundings [3]

As seen above, the main inputs of the PV generation model are meteorological data retrieved from Meteonorm, however also the modules characteristics are given as input to the model. The selected module is the 'AstroSemi 365W' mono-crystalline panels from Astroenergy. Mono-crystalline PV modules are still the best performing modules with highest efficiencies between the modules that are largely distributed. Moreover, these modules have been used in previous research, which will allow us to benchmark our research better, and have been installed in the largest Dutch solar park in Groningen . The solar modules have 365 Wp rated power and 19.7% efficiency. The PV module specification sheet can be found in Appendix A.

4.1.2 PV model: Module Temperature and Efficiency Calculation

To compute the PV module working temperature during the year the Fluid-Dynamic model is used. The module temperature is estimated as a function of meteorological parameters. This model develops through the calculation of the energy balance between the PV module and the external surroundings. The model presented is based on Appendix G of the [3] book. Three types of heat transfer are considered: conduction, convection and radiation.Considering all the heat contributions, the heat transfer balance for the PV module can be written as:

$$\alpha G_{\mathrm{M}} - h_{\mathrm{c}}\left(T_{\mathrm{M}} - T_{\mathrm{a}}\right) - \epsilon_{\mathrm{back}}\sigma\left(T_{\mathrm{M}}^4 - T_{\mathrm{ground}}^4\right) - \epsilon_{\mathrm{top}}\sigma\left(T_{\mathrm{M}}^4 - T_{\mathrm{sky}}^4\right) = 0 \tag{4.8}$$

Before explaining all the heat transfer contributions, it is important to go through the two main assumptions of the model:

- The module temperature is considered to be uniform. This assumption is not fully realistic since PV modules are constituted by different materials building the layers surrounding the solar cells. The aim is to evaluate the temperature of the solar cells, which are affected by temperature when generating. However, this assumption is justified, since the cells not only have very low thickness but also low heat capacity when compared to the other layers. Therefore the PV module is considered as one piece and the working temperature of the module to be uniform.

- The balance is set equal to zero because the module temperature is considered to be constant over each time step considered. This means that we are considering a steady state condition and that the actual exponential decay seen from the temperature is not considered.

Moving now to describing the heat transfer components considered in equation 4.8. Three types of heat transfer between the PV module and the surroundings are included in the energy balance: conduction, convection and radiation. They are illustrated in Figure 4.5 and further explained here:

- Solar Irradiance: αG_{M}
  Where α is the module absorptivity, defined as the fraction of incident radiation converted into thermal energy in the module. This value can be calculated from the Reflectivity R and Efficiency η of the module through:
  $$\alpha = (1 - R)(1 - \eta) \tag{4.9}$$

- Heat transfer due to convection from the front and rear sides of the modules, depending on the surrounding air: $h_c\,(T_M - T_a)$
  Where h_c stands for the overall convective heat transfer coefficient considering both top and back of the module and T_a denotes the air temperature.

- Radiative heat exchange between ground and rear module surface: $\epsilon_{back}\sigma\left(T_M^4 - T_{ground}^4\right)$
  Where ϵ_{top} is the emissivity of the back of the module and is assumed to be 0.89, σ is the Stephan Boltzmann constant ($5.670 \cdot 10^{-8}\frac{W}{m^2K^4}$) and T_{ground} the ground temperature.

- Radiative heat exchange between sky and upper module surface: $\epsilon_{top}\sigma\left(T_M^4 - T_{sky}^4\right)$
  Where ϵ_{top} is the emissivity of the front glass of the module and is equal to 0.84, σ is the Stephan Boltzmann constant ($5.670 \cdot 10^{-8}\frac{W}{m^2K^4}$) and T_{sky} the sky temperature.

The conductive heat exchange between the module and the mounting structure can be neglected due to the very small areas if the contact points. To solve the thermal energy balance equation, the first step is to linearize the equation considering that:

$$(a^4 - b^4) = (a^2 + b^2)(a + b)(a - b) \tag{4.10}$$

The energy balance can thus become linear with respect to the module temperature T_M by defining $h_{r,\text{sky}}$ and $h_{r,\text{ground}}$ in equations 4.11 and 4.12 respectively,

$$h_{r,\text{sky}} = \epsilon_{top}\sigma\left(T_M^2 + T_{sky}^2\right)\left(T_M + T_{sky}\right) \tag{4.11}$$

$$h_{r,\text{ground}} = \epsilon_{back}\sigma\left(T_M^2 + T_{ground}^2\right)\left(T_M + T_{ground}\right) \tag{4.12}$$

and rewriting the energy balance equation 4.8 as:

$$\alpha G_M - h_c\,(T_M - T_a) - h_{r,\text{sky}}\left(T_M - T_{sky}\right) - h_{r,\text{ground}}\left(T_M - T_{ground}\right) = 0. \tag{4.13}$$

Rearranging equation 4.13, the formula can be expressed as a function of T_M as in 4.14. However, since $h_{r,\text{sky}}$ and $h_{r,\text{ground}}$ in the formula also depend on T_M, the equation has to be solved through iterations assigning an initial module temperature and recalculating $h_{r,\text{sky}}$ and $h_{r,\text{ground}}$ at every iteration.

$$T_M = \frac{\alpha G + h_c T_a + h_{r,\text{sky}} T_{sky} + h_{r,\text{ground}} T_{ground}}{h_c + h_{r,\text{sky}} + h_{r,\text{ground}}} \tag{4.14}$$

Further explanation on the derivation of the thermal model can be found in Appendix G of the [3] book. In particular, it is possible to find more detailed information on the convective heat transfer coefficients and on how they are calculated for the top and the back surface of the PV module and on the evaluation of this model in comparison with other options. As mentioned in the section related to the inputs to the model, T_{sky} and T_{ground} are given as inputs in the model as for the measurements of the wind speeds, useful for the convective heat transfer coefficients calculation. It is important to notice that the wind speeds are measured through anemometers that are usually installed at 10m, therefore the wind speeds experienced from the PV module have to be scaled through:

$$w = w_r\left(\frac{y_M}{y_r}\right)^{\frac{1}{5}} \tag{4.15}$$

The second part of this section is dedicated to the description of how the PV module efficiency is calculated based on the module operating temperature, computed as above, and on the incident radiation on the module. Let us first have a look at the the effect of temperature of the PV module performance. On the module's data sheet provided by the manufacturers the temperature coefficients are given. These values represent the effect of the deviation of the solar cell temperature from 25°C at STC.The temperature coefficients are usually given for V_{oc}, $I_{sc} and P_{mpp}$. The Power at the maximum power point of the module at T_M and STC irradiance G_{STC} can be calculated as:

$$P_{\text{MPP}}\,(T_M, G_{\text{STC}}) = P_{\text{MPP}} + \frac{\partial P_{\text{MPP}}}{\partial T}(\text{STC})\,(T_M - T_{\text{STC}}) \tag{4.16}$$

with $\frac{\partial P_{\text{MPP}}}{\partial T}(\text{STC})$ power temperature coefficient. From this the efficiency can be calculated as:

$$\eta\left(T_{\text{M}}, G_{\text{STC}}\right) = \frac{P_{\text{mpp}}\left(T_{\text{M}}, G_{\text{STC}}\right)}{G_{\text{STC}} \text{A}_{\text{M}}} \tag{4.17}$$

where A_M is the module area. Rearranging equation 4.17, the efficiency temperature coefficient $\frac{\partial \eta}{\partial T}(\text{STC})$ can be obtained:

$$\eta\left(T_{\text{M}}, G_{\text{STC}}\right) = \eta(\text{STC}) + \frac{\partial \eta}{\partial T}(\text{STC})\left(T_{\text{M}} - 25^{\circ}\text{C}\right) \tag{4.18}$$

Quantifying the effect of irradiance variation on solar cell performance is less straightforward than for the effect of temperature. This because this data is not provided as for the temperature variation in the data sheet from the manufacturers. The Power at the maximum power point, at STC temperature and varying G_M can be computed as:

$$P_{\text{mpp}}\left(25^{\circ}C, G_{\text{M}}\right) = FF \cdot \text{V}_{\text{OC}}\left(25^{\circ}C, \text{G}_{\text{M}}\right) \text{I}_{\text{S}}\text{C}\left(25^{\circ}C, \text{G}_{\text{M}}\right) \tag{4.19}$$

in which FF stands for Fill'in factor which varies differently in relation to the type of module, for mono crystalline silicon the maximum variation of the FF for irradiance between 1 and 1000 $\frac{W}{m^2}$ is about 23%. Further derivation of these equations can be found in Chapter 20 of SOLAR ENERGY book [3].

$$\eta\left(T_{\text{STC}}, G_{\text{M}}\right) = \frac{\text{P}_{\text{mpp}}\left(25^{\circ}\text{C}, G_{\text{M}}\right)}{G_{\text{M}} \text{A}_{\text{M}}} \tag{4.20}$$

Finally, to estimate the overall module performance the following equation is used:

$$\eta\left(T_{\text{M}}, G_{\text{M}}\right) = \eta\left(25^{\circ}\text{C}, G_{\text{M}}\right)\left[1 + \kappa\left(T_{\text{M}} - 25^{\circ}\text{C}\right)\right] \tag{4.21}$$

where the first term represents the effect of irradiance and the second that of temperature, with κ computed as:

$$\kappa = \frac{1}{\eta(\text{STC})} \frac{\partial \eta}{\partial T} \tag{4.22}$$

representing the temperature effect on the performance relatively to the STC conditions efficiency.

4.2 HVAC model

The HVAC model proposed is based on a thermodynamic heat exchange model. The total heat requirements for the two buses in Arnhem and in Gdynia grid are calculated throughout the year. The HVAC power output is per second dataset of the requirements to meet the inside cabin comfort conditions for the passengers. When integrating these data in the grid operation a 5-minute duty cycle is generated. The HVAC power is fixed at a the nominal value of 36.5 kW (value obtained from Arnhem measurements), and the time in which the HVAC is on and off varies based on the amount of energy needed to meet the HVAC requirements obtained from the thermodynamic model. Here, all the modelling of the HVAC is presented. Therefore, in the section of grid operation simulations, when speaking about adding HVAC power to traction power, we have to consider the HVAC 5-minute duty cycle curve.

4.2.1 HVAC Thermodynamic Model

The total heat requirements are made up of multiple components:

- $\text{Q}_{\text{transfer}}$ - Conductive and convective heat transfer load
  This term represents the conductive and convective heat losses through the vehicle body due to the difference in temperature between the cabin and the external environment.

- $Q_{ventilation}$ - Ventilation heat load
  This term represents the heat loss due to air ventilation and air circulation, required to guarantee the correct income of fresh air and oxygen within the cabin and to maintain the correct air quality. This heat component is determined by the inside-outside temperature difference and by the difference in humidity.

- Q_{doors} - Door opening ventilation heat load
  This term is also characterised by air ventilation, in this case due to the opening of the doors for passenger transit. This heat component is determined by the inside-outside temperature difference and by the difference in humidity.

- Q_{solar} - Solar heat load
  This term represents the solar heat gain due to solar radiation: direct, diffuse and reflected radiation components are included.

- $Q_{metabolic}$ - Metabolic heat load This term represents the metabolic heat gain caused by the presence of people on the bus. This heat components depends on the number of passengers and on the characteristics of the passengers and their behaviour, some assumptions are made to include these elements.

The measured data from Meteonorm in input in the model are: relative humidity per hour during one year, global and diffuse irradiance on a horizontal plane per hour during one year, air temperature per minute during one year. Other than these, other data are given in input to calculate the different heat components. In each sub-paragraph the different heat components are calculated and explained and the data in input are reported in the respective tables. Before describing each heat load, the main HVAC design parameters and main assumptions of the model are discussed.

When calculating the heat loads thermal comfort requirements inside the bus cabin are taken into account. As discussed in [45], passengers feel thermally uncomfortable when air temperature within the bus cabin is high, solar radiation is strong through the glass windows and the air movement and circulation is low. Being public transport a service, it is necessary to take into consideration not only measures to reduce the energy requirements of heating, ventilation and air-conditioning in the buses but also to balance these measures with the passengers' satisfaction and thermal comfort when onboard. The thermal comfort requirements are addressed in terms of cabin temperature and humidity, in relation to climate and expected passenger clothing in summer and winter with people involved in a sedentary activity. The method to calculate air re-circulation is strongly affected by temperature and humidity differences. The mass flow rate is taken as constant and is not varying due to the passenger transit, since passenger number is assumed to be constant in time for the HVAC model. Considering what mentioned above and based on ASHRAE standard 62 (1999) [1] the design parameters for the HVAC have been selected and reported in Table 4.1

Table 4.1: HVAC model - Inside temperature and humidity requirements

Parameter	Value	Description
T_{winter}	21°C	Winter cabin internal temperature
T_{summer}	25°C	Summer cabin internal temperature
RH_{cab}	60%	Humidity in the cabin throughout the year

Other major assumptions are introduced in the model:

1. The vehicle is considered to be composed of 2 parts: windows and body. For the sake of simplicity, the vehicle body is considered to be equal throughout the whole bus and the windows and doors to be only one layer of glass [58]. In future research, if the model wants to be developed further, this assumption should be modified to evaluate heat loads differently based on the different characteristics of the façades of the bus.

2. The vehicle dimensions are chosen to be an average of the dimensions of the buses used in the different trolleybus grids (see Table 4.2).

3. In every city (and therefore in every trolleybus grid) multiple types of buses are used, which vary also in geometrical dimensions. In this model only one type of bus per city is used, which is chosen to be the average of the geometrical characteristics of the bus types of the city.

4. No passenger transit is considered. In the model the number of passengers on board is constant and the time in which the doors are open is fixed.

5. The proportion between glass and aluminium components on each façade is based on [58]. In the paper the author identifies the surface areas of glass and aluminium body and the same proportions are used and applied to the geometrical dimensions of the bus in question. In Table 4.2 the fraction and the surface area of each material in every façade of the bus is shown.

6. The bus speed is assumed to be constant in time and to define the velocity to use an average of the registered velocities in Arnhem and of the Braunschweig driving cycle has been used, namely 10 m/s.

7. Other smaller assumptions are made in the model and will be further explained in the respective paragraph.

Table 4.2: HVAC model - Bus surface area, composition and characteristics

	Component	Fraction[%]	Tilt[°]	τ	S [m^2] Gdynia	S [m^2] Arnhem
Front	Glass	44.0%	90°	0.76	3.64	3.93
	Body	56.0%		0	4.63	5.00
Rear	Glass	26.8%	90°	0.76	2.21	2.39
	Body	73.2%		0	6.06	6.54
Left	Glass	30.2%	90°	0.76	12.70	18.93
	Body	69.8%		0	29.42	43.83
Right	Glass	31.0%	90°	0.76	13.07	19.48
	Body	69.0%		0	29.05	43.28
Bottom/Top	Body	100.0%	0°	0	33.05	45.72
Total	Glass	18.2%	-	0.76	31.63	44.72
	Body	81.8%		0	102.20	144.37
	Total	100%		-	133.83	189.09

Q_{transfer} - Conductive and convective heat transfer load

This term represents the conductive and convective heat losses through the vehicle body due to the temperature difference between the cabin and the external environment. This difference in temperature induces heat transfer through the vehicle surfaces: heat will transfer from inside to outside during winter and from outside to inside during summer. The equation used to quantify the heat loss due to conductive and convective heat transfer is [2]:

$$Q_{\text{transfer}} = U\ S\ (T_o - T_i) \tag{4.23}$$

With S being the surface area, T_o the outside surface temperature, which is considered to be equal to the outside air temperature in this model, T_i the inside surface temperature, which is here considered the same as the inside temperature requirement and therefore 21°C in winter and 25°C in summer. Finally U is the heat transfer coefficient which includes both conductive and convective characteristics of the vehicle body. U is computed as:

$$U = \left(\frac{1}{h_o} + \frac{\lambda}{k} + \frac{1}{h_i}\right)^{-1} \tag{4.24}$$

In equation 4.24, h_o and h_i are respectively the outer and inner surface convection coefficients, λ the thickness of the element and k the conduction coefficient of the material. The convection coefficients can be found through equations 4.25, in which v is the inner and outer air velocity respectively for the inner and outer surface coefficient [58]. The air velocity varies between inside and outside space and

therefore the convective coefficients differ. The inner air speed is considered to be negligible, while the outer air speed is considered to be equal to the mean bus speed, namely 10 m/s.

$$\begin{aligned} h_i &= 9 + 3.5 {v_i}^{0.66} \\ h_o &= 9 + 3.5 {v_o}^{0.66} \end{aligned} \tag{4.25}$$

The material properties and the convective coefficients are reported in Table 4.3. The geometrical characteristics of the considered buses are tabled in Table 4.2.

The heat transfer load must be computed separately for different materials and therefore 2 components are calculated for the two bus parts considered: body and windows.

Table 4.3: HVAC model - Conductive and convective heat load parameters (from [58])

Parameter	Value	Description
$\mathbf{h_{inside}}$	9 $\frac{W}{m^2K}$	Inner surface convection coefficient
$\mathbf{h_{outside}}$	25 $\frac{W}{m^2K}$	Outer surface convection coefficient
$\mathbf{k_{glass}}$	1.05 $\frac{W}{mK}$	Glass thermal conductivity
$\mathbf{k_{body}}$	0.2 $\frac{W}{mK}$	Body thermal conductivity
$\lambda_{\mathbf{glass}}$	0.005 m	Glass thickness
$\lambda_{\mathbf{body}}$	0.0017 m	Body thickness

$Q_{ventilation}$ - Ventilation heat load

This term represents the heat loss due to air ventilation and air circulation, required to guarantee the correct income of fresh air and oxygen within the cabin and to maintain the correct air quality. For breathing, passengers consume oxygen and since the vehicle cabin volume is limited, fresh air is necessary to meet the oxygen level requirements. According to the American Society of Heating, Refrigerating, and Air Conditioning, in their "Ventilation for Acceptable Indoor Air Quality" Standard [1], the recommendation is to supply 8 L/s of fresh air per passenger. The heat load due to air exchange between the cabin volume and the outside environment is determined by the inside-outside temperature difference and by the difference in relative humidity. It can be calculated through the following equation:

$$Q_{ven} = V_{ven} \rho \, c_p \, (T_o - T_i) + V_{ven} \, (RH_o - RH_i) \, [4775 + 1.998 \, (T_o - T_i)] \tag{4.26}$$

The first term of equation 4.26 represents the sensible heat load, while the second part calculated the latent heat load. In Table 4.4 the parameters used in the above equation are reported and described.

Table 4.4: HVAC model - Ventilation heat load design parameters

Parameter	Value	Description
$\mathbf{v_{average}}$	10 m/s	Average speed of the bus (Arnhem and Braunschweig data considered)
$\mathbf{V_{average}}$	0.32 m^3/s	Average air flow at 10 m/s [1]
$\rho_{\mathbf{air}}$	1.225 kg/m^3	Air density at 15°C
c	1006 $\frac{J}{kgK}$	Air heat capacity in the temperature range considered at atmospheric pressure of 1.013 bar

Q_{doors} - Ventilation heat load due to door openings

This term is also characterised by air ventilation, in this case due to the opening of the doors for passenger transit. It represents the momentary heat flow related to the door opening at the bus stops. This heat component is determined by the inside-outside temperature difference and by the difference in humidity [1], but also depends on the number of doors opened and the time during which the doors

are open [60]. For the HVAC model the doors are considered to be open 25% of the time, estimated from the data available from Arnhem trolley-grid, and the number of doors opening is chosen as 2. The other consideration to be done is on the volumetric flow rate of the air, which is different from that of the ventilation heat component. All the necessary data is summarised Table 4.5, except for air properties which can be found in Table 4.4. Equation 4.27 is what has been used to compute this heat load component.

$$Q_{doors} = t_{door}\, n_{door}\, V_{door} \rho\, c_p\, (T_o - T_i) + V_{door}\, (RH_o - RH_i)\, [4775 + 1.998\, (T_o - T_i)] \tag{4.27}$$

Table 4.5: HVAC model - Ventilation through door openings

Parameter	Value	Description
$\mathbf{V_{door}}$	2.78 m^3/s	Average air flow through the doors when open
$\mathbf{t_{door}}$	25%	Percentage time in which the doors are open
$\mathbf{n_{door}}$	2	Number of doors opening simultaneously

Q_{solar} - Solar heat load

This term represents the solar heat gain due to solar radiation: direct, diffuse and reflected radiation components are included. The large windows on both sides of the bus cause the mean radiant temperatures in the vehicle to be high . This heat gain to irradiance contributes to the heating in winter and increases the air conditioning requirements in summer and therefore has to be considered when modelling the HVAC system. Some assumptions are made also for this component:

- Only the transmitted component of the radiation is considered. Due to the continuous movement of the bus the air flow surrounding the vehicle body is considered to absorb the absorption heat gain of the material through convection.
- The transmission factor of the glass surfaces is chosen to be 0.76 [61].
- Based on the assumption above, the aluminium body of the vehicle, considered as an opaque surface with null transmissivity, is excluded from this calculation and therefore the top and the bottom surfaces are totally excluded together with all the components which are not made out of glass.
- The direction of the bus is not varying and the four surfaces are considered to be facing south at all time. This assumption was made taking into consideration the fact that other components of the heat load have been excluded and that only transmission through glass is considered. However, this assumption might be modified in the future.

The equations used to compute the solar heat load are now shown. The total heat gain due to radiation can be computed as the sum of direct, diffuse and reflected components, which are respectively correlated to the direct, diffuse and reflected irradiance on the glass surfaces of the bus.

$$Q_{solar} = Q_{dir} + Q_{dif} + Q_{refl} \tag{4.28}$$

The direct, diffuse and reflected components of the irradiance on the surfaces are computed through equations 4.4, 4.5 and 4.6 [3] and then used to find the heat gain due to the different components of the irradiance, according to equation 4.29 [58].

$$Q_{irr} = S \tau G_{irr} \tag{4.29}$$

Where S and τ are the surface area and transmissivity, respectively and G_{irr} the relative irradiance component: direct, diffuse and reflected. When calculating the various components it is important to keep in mind that the tilted surfaces are the vehicle's body surfaces and not solar modules anymore. Therefore,the tilt angle of the surfaces considered is always 90°, since the top and bottom surfaces of the vehicle are not included in this calculation, as mentioned in the assumptions above.

$Q_{metabolic}$ - Metabolic heat load

This term represents the heat gain due to the presence of passengers on the bus. Metabolic activities occurring inside the human body create heat and humidity which is constantly released to the cabin air through the body tissues. This heat generated from the body depends on the characteristics of the passengers and their behaviour. As previously mentioned no passenger flow is considered for this model (since data are scarce), therefore the number of passengers in the bus cabin is assumed to be constant. The selected amount is of 40 passengers, which is the average mid-capacity of the considered buses, including both seated and standing available spots. For this reason the metabolic heat production rate of the passengers is taken as average between that of standing and of sitting, namely 65 W/m2. The passenger metabolic rate differs from the driver's, which is an average made between the rate of a car driver and the one of a heavy vehicle driver resulting in 120 W/m2 [2]. In Table 4.6, the reader can find the overview of the so far explained data.

Table 4.6: HVAC model - Conductive and convective heat load parameters [58]

Parameter	Value	Description
$\mathbf{n_{passenger}}$	40	Number of passengers on the bus on average between seated and standing
$\mathbf{M_{passenger}}$	$65\ W/m^2$	Average metabolic heat per passenger's surface (average between seated and standing)
$\mathbf{M_{driver}}$	$120\ W/m^2$	Average metabolic heat per driver's surface

The total metabolic heat load can then be computed as:

$$Q_{\text{metabolic}} = Q_{\text{driver}} + \text{n}_{\text{passengers}}\ Q_{\text{passenger}} \tag{4.30}$$

The metabolic load of a person, without considering the behaviour which has been already taken into account, depends on their weight and height according to the following equation [28]:

$$Q_{\text{person}} = \text{M}_{\text{person}}\ \text{A}_{\text{DU}} \tag{4.31}$$

With M_{person} being the metabolic rate of the person and A_{DU} the DuBois area which is used to estimate the surface area of a person from ones weight and height. The equation used to compute the DuBois area is here shown [28]:

$$\text{A}_{\text{DU}} = 0.202 \cdot \text{Weight}^{0.425}\text{Height}^{0.725} \tag{4.32}$$

Due to the fact that the number of passengers is fixed, also weight and height of the passengers on-board is not varying in time. Nevertheless, country statistics are taken into account to compute the metabolic heat gain on the bus in the different countries. Average men and women weight and height are found and the fraction of the country population is accounted for as the gender fraction on the bus. In Table 4.7 these values can be retrieved.

Table 4.7: HVAC model - Dutch and Polish demographic data

Parameter	Netherlands		Poland		Description
	Women	Men	Women	Men	
Height [26]	1.7 m	1.84 m	1.65 m	1.8 m	Average population height per sex
Weight [26]	73.2 kg	87.9 kg	71.5 kg	89 kg	Average population weight per sex
Population %	50.20% [4]	49.80% [6]	51.54% [5]	48.46% [7]	Female and male population %

Output

The proposed thermodynamic model gives as output the HVAC power requirements curve for the two cities throughout the year. In Figure 4.6, the HVAC demand for Arnhem and Gdynia is plotted, in orange and blue respectively. The curves follow a similar U-trend, with high power requirements in the winter and lower requirements in the summer. If the temperature and irradiance trends characterising the two cities are checked, in **??**, it is then possible to understand the reasons for this shape. In both

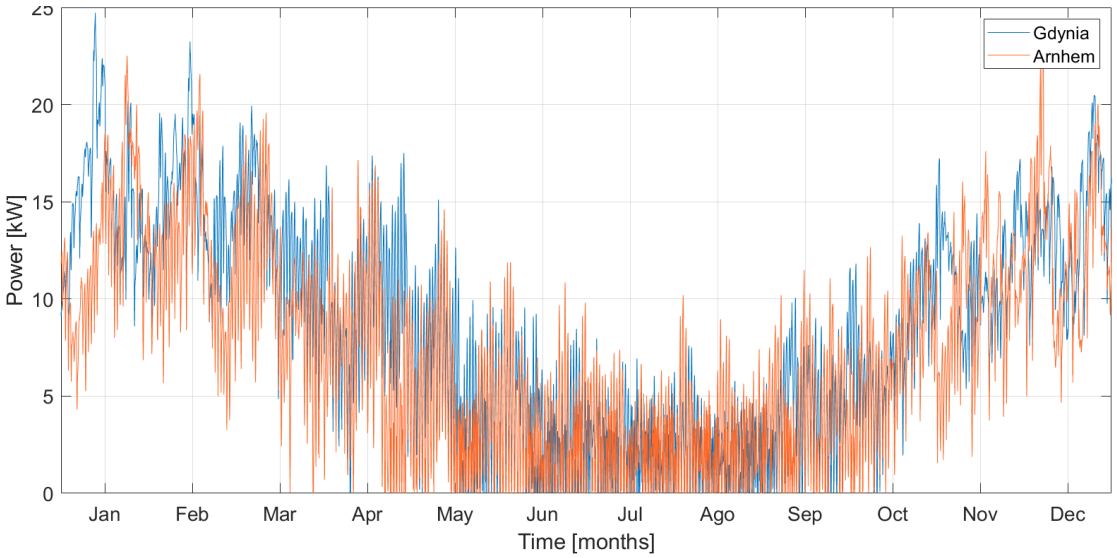

Figure 4.6: Per second HVAC power requirement during one year in Gdynia and Arnhem - simulation output

cities the low winter temperatures induce a substantial heating load during the winter, on the other hand, the mild summer climate with temperatures that fluctuate around an average of 25°C.

It is important to consider that the operating temperatures of the HVAC system, set at 21°C and 25°C, respectively in summer and winter, are standard temperatures which could vary based on the comfort requirements and expectations of each country and population. This means that if the inside cabin temperatures are reduced the curves would flatten slightly with an increase in power demand during the summer to reach lower temperatures inside and decrease in winter since the difference in temperature between outside and inside would be reduced.

4.2.2 5-minute duty cycle generation

The analysis of the measured data coming from the Arnhem grid bus operation, reveals the existence of the HVAC power duty cycle. As a matter of fact, when checking the HVAC current requirements this on/off cycle is detected. For this reason, this behaviour of the HVAC system is re-proposed in the simulations. The HVAC demand is adapted to the cycle found and the new yearly requirements are obtained based on the thermodynamic power demand and on the duty cycle.

The duty cycle time, t_{cycle}, is 300 seconds, or 5 minutes. The on time, t_{on}, of the HVAC system for each cycle is calculated based on the average power requirements of the bus in the cycle period. It is calculated as:

$$t_{on} = t_{cycle} \frac{\overline{P_{HVAC}}}{P_{rated}} \tag{4.33}$$

where $\overline{P_{HVAC}}$ is the average power requirement in the 5 minutes and P_{rated} is the nominal HVAC power, namely 36.5 kW.

4.2.3 Validation of the HVAC model output

The auxiliaries power demand can reach shares of 50-70% of the total power demand of the buses throughout the year, of which more than 80% is consumed by the HVAC system [16]. These data are found also in this model, with HVAC consuming up to 40% of the overall substation loads throughout the year. Since this is a newly built component of the model, it is necessary to validate the outputs of the simulations comparing them to the measured data available.

For Arnhem trolleybus grid operation, data are available on the power consumption of the substations throughout the years. In order to understand the impact that the HVAC has on the load demand and the variations that it causes throughout the year a comparison is made between the energy requirements registered in January and in May. In the two plots, in Figure 4.7 and 4.8, the per unit values of the energy demand for the Arnhem grid are reported. In the former, the measured data for Arnhem substations during 4 years is plotted. On the y-axis the January requirements and on the x-axis the May requirements are found. As one can see January's demand is on average 1.55 times the demand registered in May. In Figure 4.8, the simulation results are plotted for 2020 for all the sections of the grid. The same graph is provided, with January and May per unit values of energy demand on the y- and on the x-axis respectively. What can be seen is that the outputs of the simulations present a very similar trend and that the January demand is 1.36 times the May one. The difference between the measured and the simulated data is of 12%, which is reasonable, especially when considering that 2020 is taken into consideration for the simulations which has been a warmer year compared to 2019, 2018 and 2017 and which presents lower trends only with respect to 2016. However, as one can see from Figure 4.9, January presented higher temperatures in 2020 also in comparison to 2016 [29].

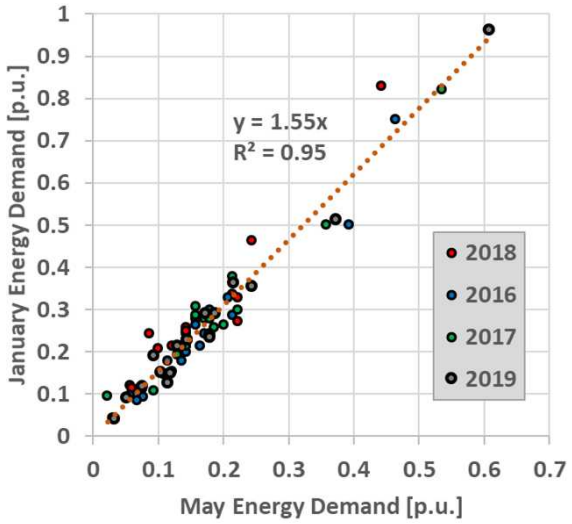

Figure 4.7: Comparison between January and May data - HVAC demand effect, measured data

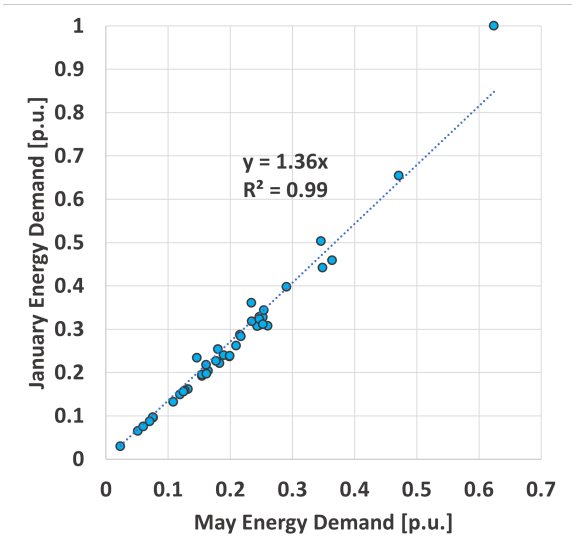

Figure 4.8: Comparison between January and May data - HVAC demand effect, simulated data (2020)

It is decided to plot the comparison between these two months in order to evaluate the impact of the HVAC on the energy requirements of the grid. As a matter of fact, these two months present the same timetables and schedules, except for possible holidays, but different weather characteristics. In fact, comparing January with one of the summer month would not be fair, due to the reduced number of runs that summer timetables present.

4.2.4 HVAC on-off switching analysis

Another finding coming from the analysis of the measurements conducted in Arnhem trolleygrid is related to the on/off switching of the HVAC happening during the on time of the duty cycle, as can be seen in the plot in Figure 4.10. The HVAC current is plotted against the expected HVAC duty cycle current, and what can be noticed is that in some instants in time the conditioning system is turned off during the on-time of the duty cycle. The measurements are not registered per second, for this reason in Figure 4.10, the current is plotted against the time in which the data is measured, however to avoid confusion the time is not indicated. The measured data is registered every ΔT, with ΔT being a varying fraction of one second.

A study is conducted on the possible reasons and triggers of the HVAC system and some conclusions are drawn. However, the limited knowledge on the signals used to perform this analysis caused by imprecise explanations received by who performed the measurements do not allow us to complete it

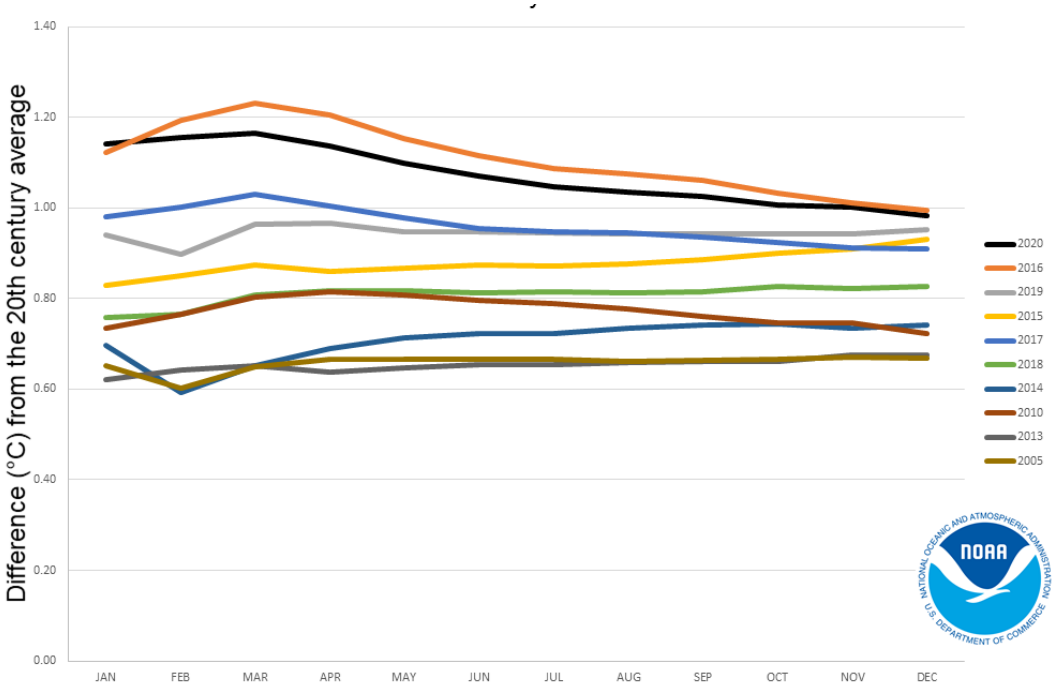

Figure 4.9: Average temperature increase per month for each year, with respect to the 20_{th} century average values [29]

and draw final conclusions. The impact of the HVAC system and auxiliaries on the energy demand of vehicles is substantial, reaching peaks in which it covers 70% of the demanded bus power. For this reason, it is strongly suggested to further research on the reasons and the signals that are inducing the switching off of the HVAC during the on-time of the duty cycle.

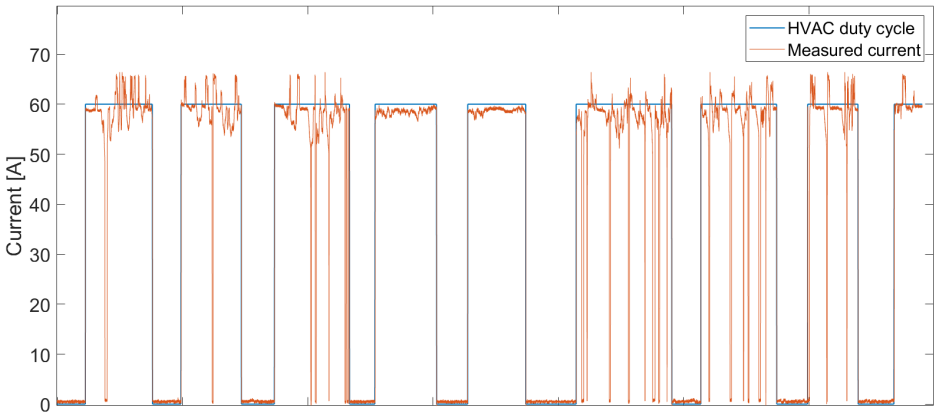

Figure 4.10: HVAC measured current compared to the expected duty cycle operation

The conclusions and findings so far are here provided, followed by a description of how this is then implemented in the simulations.

1. The switching off of the HVAC system happens only if the bus is moving
   The turning off of the HVAC system during the on-time of the duty cycle occurs only in times in which the vehicle is moving. In Figure 4.11, it is possible to see that when the velocity of the vehicle is zero then there are no instants in which the current is dropping to zero.

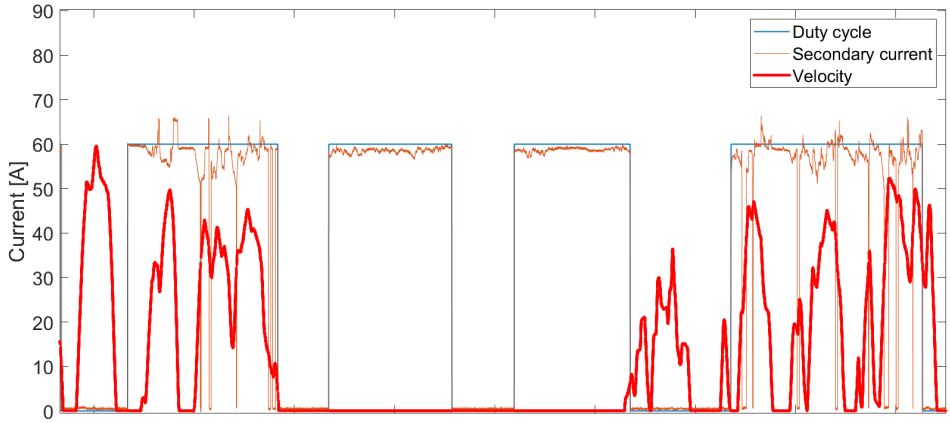

Figure 4.11: HVAC measured current compared to the expected duty cycle operation, plotted together with bus velocity profile

2. The switching off of the HVAC system can be related to the regeneration of braking power Figure 4.12 shows the HVAC signal and a signal called REKEA. It is possible to notice from this plot that in multiple occasions the turning off of the HVAC power during the on-time, is connected to the REKEA signal going to zero. REKEA, for what is known, is a 1/0 signal which is on in the times in which it is possible to regenerate braking power. In the plot this signal is multiplied by 100 for visualization purposes. The auxiliaries, namely HVAC, lightning, ticket machines and all the system components which have a power requirement which is not related to the movement of the bus, are likely to be the first receivers of regenerated power.

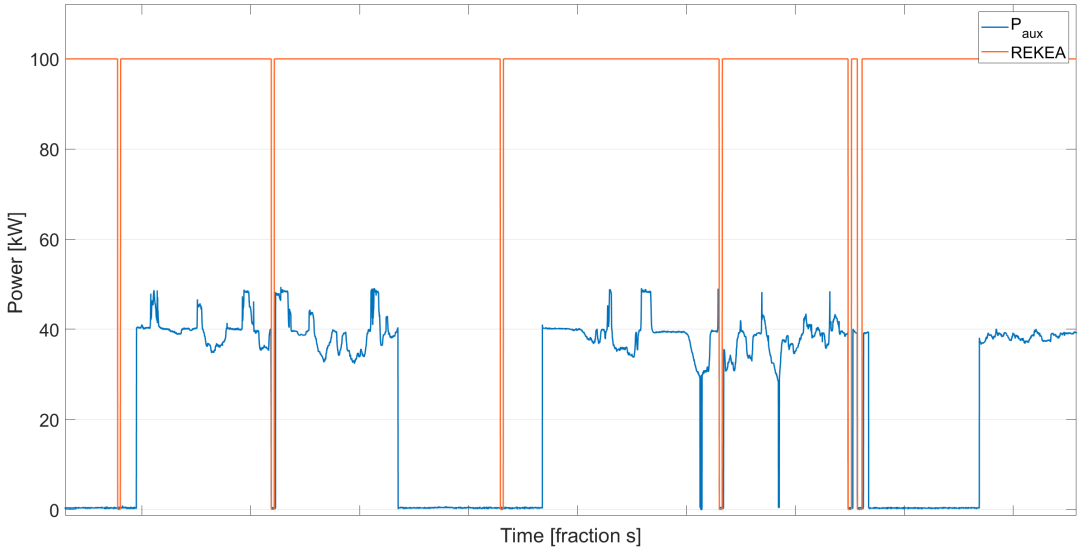

Figure 4.12: HVAC measured current plotted with the REKEA signal - relation between the HVAC operation and regenerative braking

In Figure 4.13, the same plot as in Figure 4.12, is provided but now also the actual bus power requirements and the braking power are plotted. In the moments in which regeneration is not possible, so when REKEA signal goes to zero, the HVAC system seems to be turned off if the bus is braking. The REKEA signal probably represents a limit for the bus and not for the overhead lines. When REKEA is off, the bus cannot use the regenerated power, therefore this is entirely sent to the DC grid instead of being used by the bus.

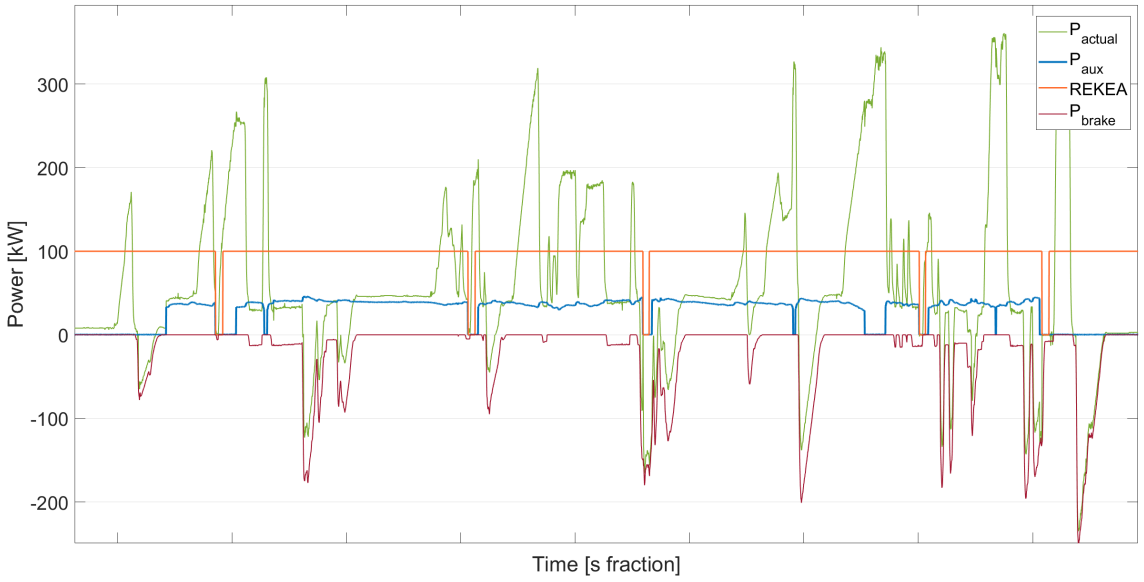

Figure 4.13: HVAC measured current relation with regenerative braking and REKEA signal - analysis of braking power use

3. The switching off of the HVAC system can be connected to 2 variables predicting the available catenary power and the desired bus power
   One other condition that seem to be closely matching the switching off of the heating and ventilation system of the buses is when the *desired traction power* is higher than the *available traction power*. In all the moments in which this condition is verified, the HVAC system turns off, in order to reduce the *desired* power. This is shown in Figure 4.14, where the two variables are plotted together with the auxiliaries power requirements. However, these two variables, the *desired traction power* and the *available traction power*, cannot be reproduced with the available measured data. Different options are tested including velocity and power derivatives, voltage and current levels and overhead signals. The two variables have the appearance of simulated or predicted values, however no indication on how they are obtained is provided and it was not possible to model them

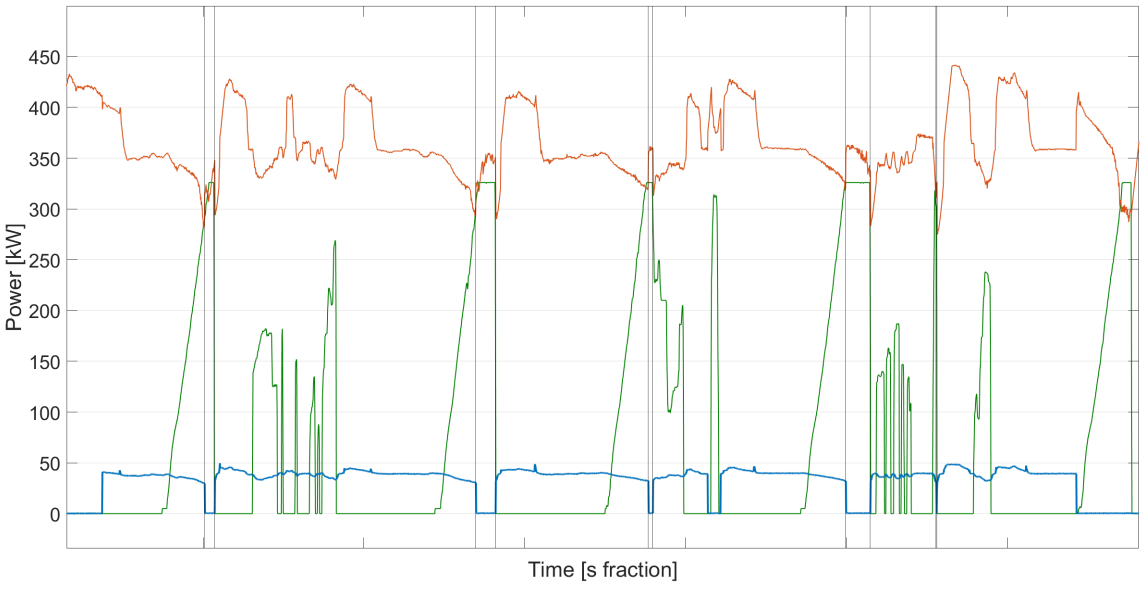

Figure 4.14: HVAC measured current relation with predicted available and desired traction power

Since it is not possible to reproduce the signals mentioned above without having more information on them, the on/off switching of the HVAC system is reproduced imposing a cap on the power require-

ments. At every simulated second, if having the HVAC power on causes the demand to exceed the power limit then it is switched off and turned on only when, always according to the duty cycle, the total power (traction + HVAC) is below the threshold. This is selected based on the specifics of the electric motors installed in the two buses in Arnhem and Gdynia.

4.3 Velocity and Power Profiles Generation

In this section, it is possible to find a description of the model used to generate velocity profiles for the different lines of the two cities. It became necessary to build this model, once it was clear that the available data would not be enough to simulate properly the operation of the two trolleygrids. As a matter of facts, the available velocity measurements are 2 for each line in each direction for the Arnhem trolleybus system only. This means that for each line in each direction the velocity profile is repeated throughout the whole year and that for the trolleygrid in Gdynia no measurement is available. This model, used to simulate the driving cycle of the buses, is necessary to cover for the missing data and to allow us to compare the operation of the two trolleygrids, with similar velocity cycles in terms of acceleration/deceleration phases along the different lines.

4.3.1 Input data to the model

In order to recreate velocity profiles for the buses on the lines of the two cities a lot of data is needed in input. In first place, the existing measurements from Arnhem and the Braunschweig driving cycle data are imported in the model and used to generate a set of single velocity cycles, a single cycle from 0 m/s to 0 m/s, in Figure 4.15 the complete Braunschweig driving cycle placed side by side to the set of single velocity cycles generated from this set of data (in Figure 4.16. The measurements for the Arnhem grid are registered not per second but per varying fraction of second. For this reason, before splitting the various velocity cycles coming from the measurements on each line, all the data have been transformed in per second data. Only after this, all the driving cycles for both directions and all lines (therefore in total 12 driving cycles for 'Arnhem minimum' measurements and 12 for 'Arnhem Maximum') have been put in a single vector and then divided into isolated velocity cycles from 0 to 0m/s. In appendix Appendix B the reader can find in Figure B.1, Figure B.3 and Figure B.2 the plots of the three datasets including all the isolated velocity cycles generated from the Braunschweig driving cycles, the 'Arnhem minimum' data and the 'Arnhem maximum' data.The measured data from Arnhem and the Braunschweig data form the base data-set which is used to create full profiles for the different bus lines in Gdynia and Arnhem. In the next subsection the steps to generate the velocity profile for each line are given, but first the other input data are explained.

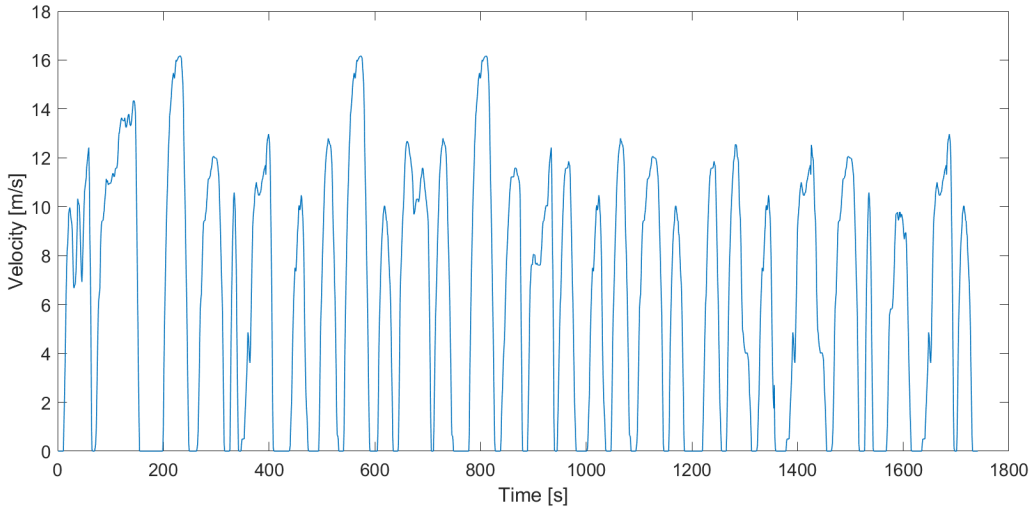

Figure 4.15: The complete Braunschweig driving cycle

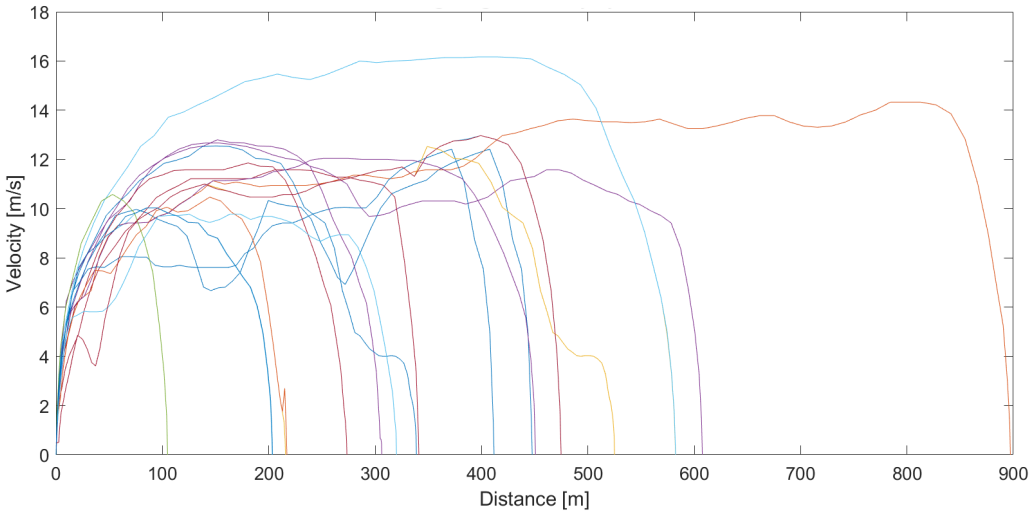

Figure 4.16: The Braunschweig data-set divided in single velocity cycles from 0 m/s to 0 m/s plotted against the travelled distance

Once the 3 data-sets of isolated velocity cycles are created (Braunschweig, Arnhem minimum, Arnhem maximum), the distance travelled is calculated for every cycle and then all the additional required data to cover the other inputs needed from the velocity profile generator model is gathered. In particular, the missing inputs to the model for each line are:

1. The three timetables: Weekdays, Saturday and Sunday Holidays (which will also be used to simulate the whole grid operation)

2. The distance between subsequent bus stops
   For reference, find an example of Arnhem Line 1 (Oosterbeek to Velp) bus stops positions along the line in Figure 4.17.

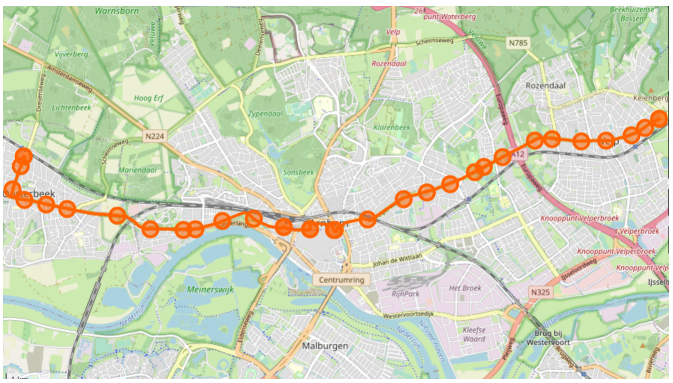

Figure 4.17: Arnhem Line 1 (Oosterbeek to Velp) bus stop positions along the line

3. The position of the traffic lights along the line
   For reference, find an example of Arnhem Line 1 (Oosterbeek to Velp) traffic light positions along the line in Figure 4.18

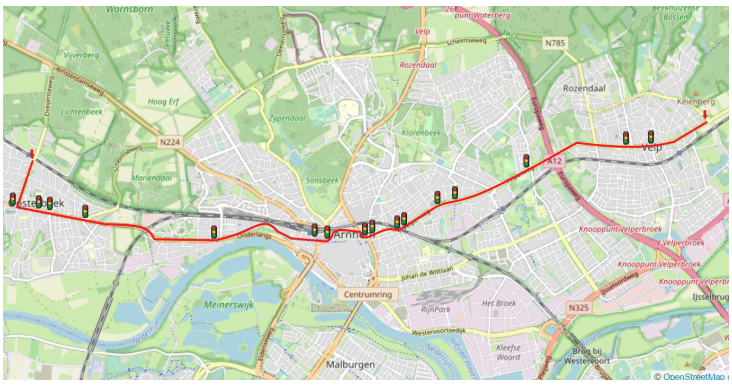

Figure 4.18: Arnhem Line 1 (Oosterbeek to Velp) traffic lights positions along the line

After gathering all this information for each line of Gdynia and Arnhem grids, all the inputs to the model are ready.

4.3.2 Velocity profiles generation model

In the previous subsection, the inputs required for this model are discussed. Here, the reader will find all the necessary steps to obtain the velocity profile of a bus line.

Step 1
The bus stops and the traffic lights positions are ordered in one vector. This allows the model to identify all the possible stops that the bus could have during this run.

Step 2
The stops are associated to their duration. The traffic lights are considered to be zero-duration stops. This because all the stops between to subsequent official bus stops have to fit in the scheduled duration of the travelling from the previous to the following bus stop. This means that a vector is generated with zeros corresponding to a traffic light stop and the duration of the bus stops from the timetables corresponding to the official bus stops.

Step 3
Not all stops happen at each run: a traffic light might be green and a bus stop might have now on/off-boarding passengers. For this reason in this step the actual stops for the run are identified in relation to three probability scenarios of stopping. In Table 4.8, one can find the parameters that define these three scenarios: Weekday, Saturday, Holiday. For each line at the last bus stop, the bus always has 100% probability of stopping. In some lines other additional bus stops are set to have 100% stopping probability, as for example Arnhem Central station for Arnhem bus lines.

Table 4.8: Velocity Profiles - Three scenarios with different stopping probabilities

Traffic Scenario	Probability of stopping at a traffic light	Probability of stopping at a bus stop
High Traffic	60%	70%
Medium Traffic	40%	60%
Low Traffic	40%	50%

Step 4
The duration is re-calculated based on the actual stops that the bus is making. If the bus skips one stop the time it has to reach the following stop becomes the sum of the duration of the two subsequent stops. Namely, if bus leaves from A and stops directly at C, skipping bus stop B, the duration of the travel from A to C will be the sum of the duration between A and B and B and C.At this point we have the actual stops and the available time to perform these stops and for the bus run.

Step 5
At this point, the identified single velocity cycles from the data-sets previously generated have to be associated to the stops that the bus is making along the line. This is done by associating the velocity cycle that best matches the analysed bus stop in terms of distance travelled. The duration is also taken into account, but at a second stage. In Figure 4.19, one can find the flow diagram representing the algorithm used to select and match the velocity cycle to the bus stop. The diagram represents the selection of velocity cycles for one stop of the bus (valid both for traffic lights and bus stops). This is repeated for every actual stop (as found in Step 3) along the line.

As previously stated, there are three data-sets of single velocity cycles, these will be used to generate different profiles along the same line. In particular, one can see which data-set is used to simulate which velocity profile in the outputs subsection in Table 4.9. This means that the velocity profile is generated using the single velocity cycles from the indicated database and that 4 velocity profiles are generated in total for each direction of each line. It is important to mention that one extra cycle is generated compared to the scenarios using the Braunschweig data-set to compare the results obtained from two different types of data with no difference in terms of probability of stopping and schedule.

Step 6
Once a velocity cycle (or a combination of two velocity cycles) is selected for each stop made from the bus the full velocity profile is created by stacking each cycle after the other. Finally, the position of the bus is calculated at every second for the whole velocity profile.

These six steps are repeated for every direction of every line in Arnhem and Gdynia (for a total of 18 lines). As previously mentioned for each direction of each line 4 velocity profiles are created. In the next subsection the outputs of the model are briefly discussed.

4.3.3 Velocity Profiles - Outputs

The velocity profile generator model is used to recreate the driving cycles of the buses during the year in the grids along all the possible routes travelled. The outputs of the model reflect these needs, but also take into consideration the fact that simulating a different velocity profile for every run would cause a noticeable increase in the code running time. This increase in memory requirements and code running time is not justified, considering that no big change would be found in the velocity and power profiles also if they were to change at every bus run. For this reason a limited number of velocity profile is produced to simulate each line. Overall 4 velocity profiles are obtained for each direction of every line using the different scenarios. In order to avoid repeating the same one along the year, the 3 different scenarios (weekday, Saturday and holiday) are used to simulate different profiles. The change in scenario represents a variation of road and passenger traffic conditions, namely a variation of the probability that the bus has of stopping at a traffic light and at a bus stop. In Table 4.8 the reader can find the stopping probabilities used for each scenario respectively. In Table 4.9 the summary of the characteristics of the 4 velocity profiles obtained for each direction of every line are given.

Table 4.9: Velocity Profiles - outputs characteristics

Output Velocity Profile	Traffic Scenario	Velocity cycles data-set used	Timetable used
Weekday	High traffic	Arnhem minimum	Weekdays
Saturday	Medium traffic	Arnhem maximum	Saturday
Holiday	Low traffic	Arnhem minimum	Holiday
Braunschweig	High traffic	Braunschweig	Holiday

Finally, in Figure 4.20 an example of velocity profile output is provided. The simulated velocity profiles is compared to the measured one of the same line. As one can see the two profiles differ in number of stops, moments of peaks in velocity and of breaks, but present similar trends.

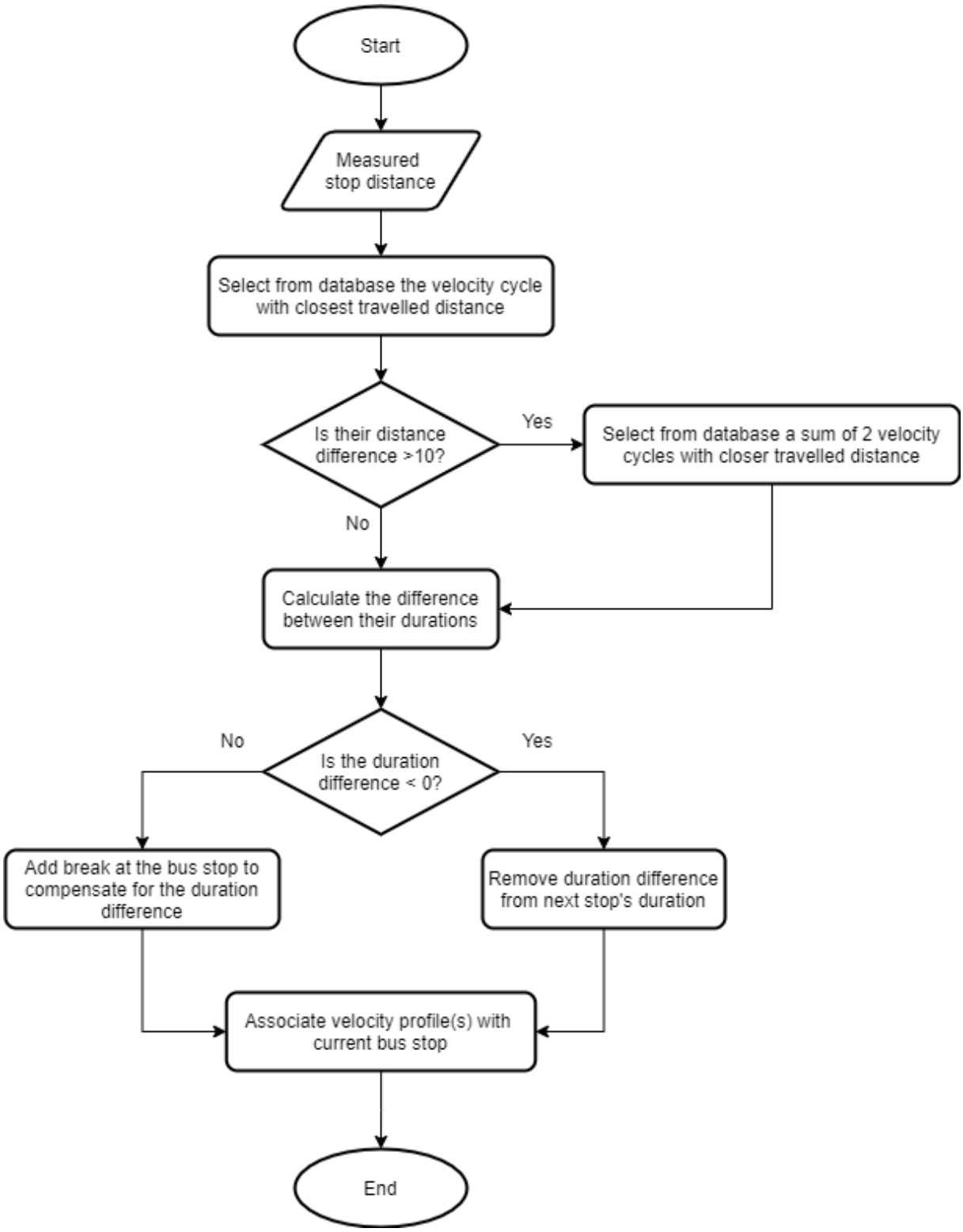

Figure 4.19: Flow diagram explaining the process to associate a velocity cycle to a bus stop (own work)

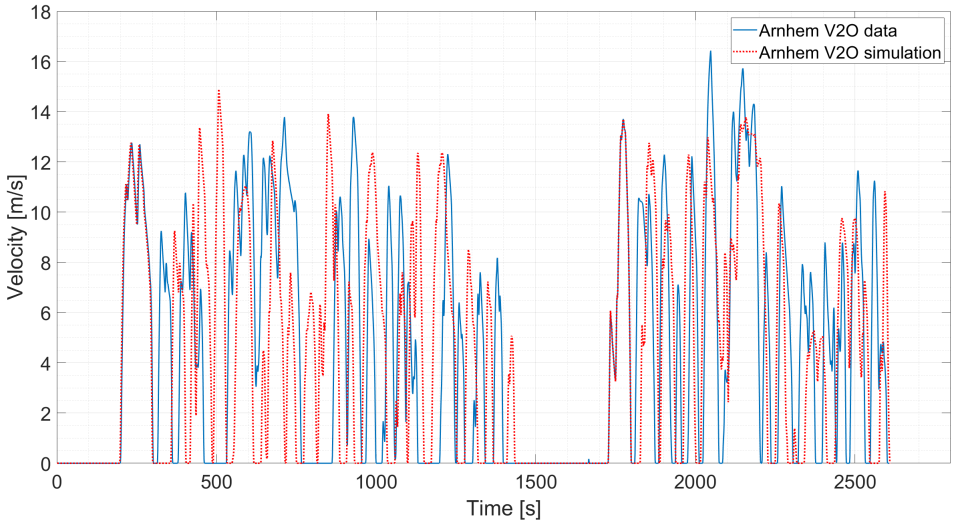

Figure 4.20: Comparison between Arnhem V2O data measured and simulated

Validation of the velocity profiles

In this section, the outputs of the generated velocity profiles are briefly analysed in comparison to the measurements performed in Arnhem. The model is created to increase the variability and use profiles that differ between them in time for the simulation of the grid operation. Therefore, the performance of the velocity profiles generation model is measured in relation to the characteristics of the profiles and not comparing how they develop in time. The purpose as mentioned is not to reproduce the same profiles as the measured ones, but to have multiple velocity profiles with similar characteristics but variable in terms of number of stops (based on the traffic for instance), distribution of the velocity cycles in time, position in time. In Table 4.10, the overview of the average values for the Arnhem velocity profiles are reported both for measured and simulated outputs.

Table 4.10: Average values obtained from velocity profiles simulations compared to the actual measurements of the bus drives

	Simulation	**Measurement**
Peak speed [km/h]	58.1	56,3
Average speed [km/h] (without stops)	25,8	26,4
Average speed [km/h] (with stops)	19.7	18,4
Peak acceleration $[m/s^2]$	1.5	1.5
Peak deceleration $[m/s^2]$	-1.9	-2.0
Number of stops	26	23

On average, the peak speed and the average speed of the simulated profiles is higher. However, when looking at the average speed without considering the time in which the bus is not moving (v=0 km/h), it is possible to see that on average the speed is higher for the measured data. This can be related also to the number of stops. The increased number of stops of the simulated profiles induces more acceleration moments and shorter breaks at the stops. When skipping stops the bus must stop for more time in order to conform to the timetable. The peaks in acceleration and deceleration are very similar.

If we plot the distribution of the average and maximum velocity characteristics for each line in Arnhem, we obtain what is shown in Figure 4.21. It can be observed from the plots that the simulation and measured values fall in the same range of values along the different lines of the trolleygrid. However, for the maximum speeds for directions AC2DLW and HD2BZ for example, the simulated velocity profiles are all characterised by higher maximum speeds with respect to the measured data. For line DLW2HAN instead all the simulations present lower maximum speeds. It is difficult to assess if this is due to the fact that the measurements dataset is formed only by two velocity profiles per line, and

therefore it does not allow to see how the velocity profiles change with varying traffic conditions and passenger traffic. As a matter of fact, on average the simulated profiles present more widely distributed characteristics. This is a positive outcome since the aim was to increase the variability of the data. However, sticking to the three lines used as examples, the fact that the simulated profiles all present higher or lower maximum (or average) speeds compared to the measured data could also be related to the fact that the assembling of the velocity profiles is independent from the characteristics of the road in terms of slopes and location. This can cause some errors if very hilly or very central streets are crossed from the buses along the line.

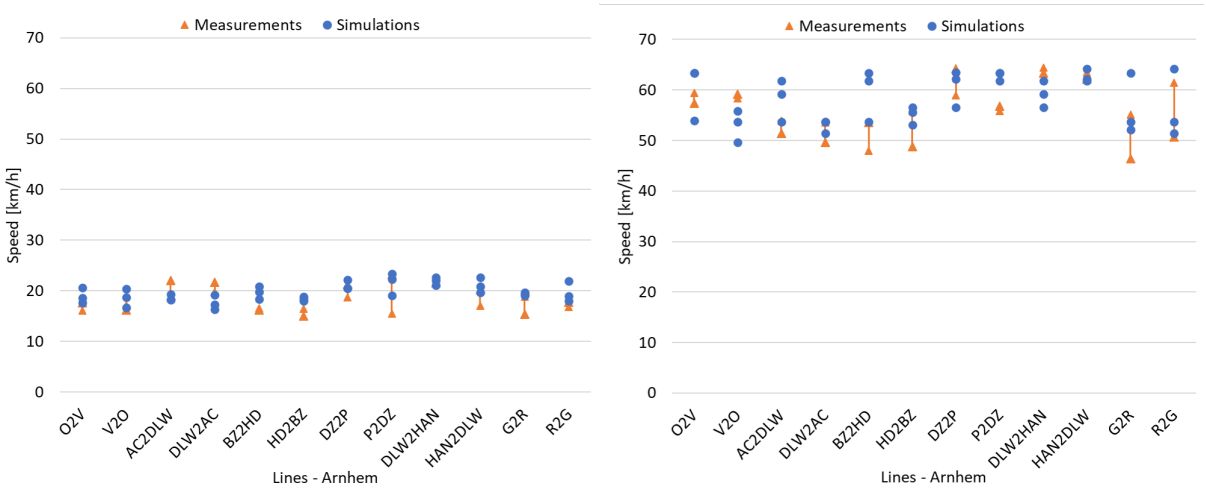

Figure 4.21: Distribution of average (left) and maximum (right) speed data for simulated and measured velocity profiles in Arnhem

4.3.4 Power Profiles Generation

In order to simulate the operation of the two trolley-grids for one year, it is necessary to reproduce the power profiles of the buses. The main input to the generation of the power profiles are the previously generated and explained velocity profiles, the accelerating and braking pedal signals to introduce torque limits, the road gradients of the streets travelled from the buses of the different lines and the characteristics of the trolleybuses used. In the next subparagraph the reader finds the details of how the braking and accelerating pedal signals are recreated. The following subparagraph gives an overview of the model created from HAN University that has been used to simulate the power profiles from speed measurements. In this case, the model is used with inputs that are also simulated instead of measurements. The road gradient data are collected through google maps and the bus characteristics can be found in [15], page 28. The bus characteristics are used from HAN university researchers to build the power model, therefore they are kept constant when simulating the buses in Arnhem. For Gdynia instead, a different bus type is used, with different physical/geometrical characteristics but also different electric motor. Although multiple bus types are used in both grids, especially in Gdynia, not all are simulated due to the unnecessary and extensive increase of the modelling time that this would require. The characteristics used are the ones of the most common trolleybus type in the two grids. The different characteristics of the electric motors are presented when discussing the model created by HAN university.

Braking and Accelerating Pedal Signals Analysis and Generation

In order to check the status of the bus and to regulate the motor torque accordingly, researchers from HAN University use the braking an accelerating pedal signals measured during the bus rides. Since all the data used in this simulation has been modelled and not measured, the available measurements from Arnhem trolleygrid can be used, but only as reference to build new ones from the simulated velocity profiles.

The measured signals of braking and accelerating pedals from bus rides in Arnhem are analysed together with the measured power and velocity profiles to find a trend in the data. The objective of the data analysis is to associate the on/off pedal signals respectively to accelerating and braking moments, in order to recognise braking and accelerating moments in velocity profiles and rebuild the pedal signals for the simulated data. The idea is to understand the characteristics of the velocity profile when the pedal signals are activated. To do this the derivative of the velocity of the bus is calculated.

In Figure 4.22 and Figure 4.23, the histograms of the distribution of the velocity derivatives are given. The first one, represents the probability that a certain positive velocity derivative is associated to a power requirement. This allows us to define what is the minimum positive velocity derivative to have 70% probability that in that moment the bus is accelerating due to the pressing of the acceleration pedal, and not because of other causes (as downhill streets). In the second figure, the same thing is done with the reduction of speed. Namely, the negative derivative limit is defined, below which there is 70% probability that the reduction in velocity is caused by the activation of the braking pedal and not due to other causes (as uphill streets).

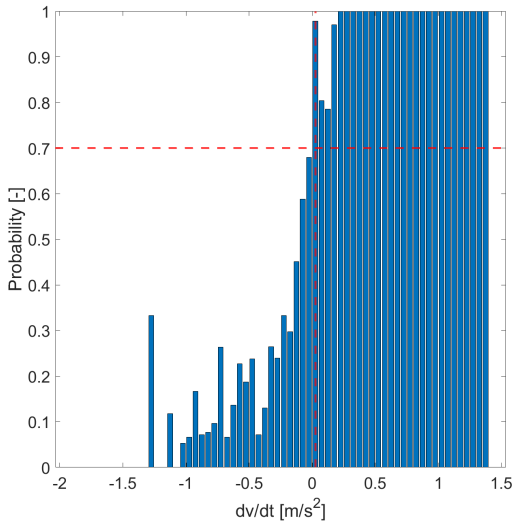

Figure 4.22: Positive velocity derivative associated to a power requirement, probability higher than 70% marked in red

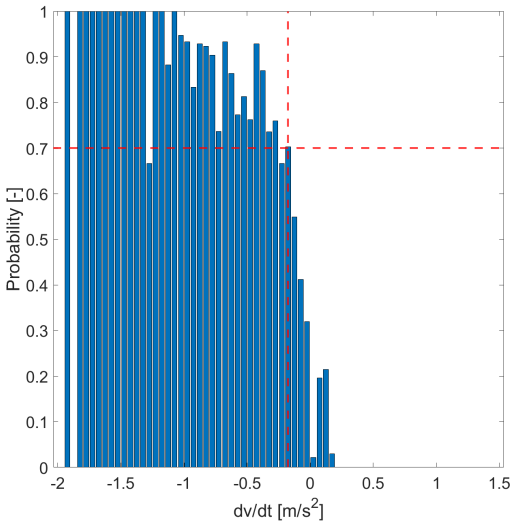

Figure 4.23: Negative velocity derivative associated to regenerated power, probability higher than 70% marked in red

Once these two limits are defined, the pedal signals are recreated with the condition that if the derivative of the velocity is above the positive threshold at instant t and is still positive at instant t+1, then the accelerating pedal signal should be ON. On the other side, id the derivative of the velocity is below the negative threshold at instant t and is still negative at instant t+1, then the braking pedal signal should be ON. In Figure 4.24 and Figure 4.25, the reader can find the comparisons between the measured pedal signals and the recreated data. One can notice that the modelled acceleration pedal signal is matching well the measured data and that the braking pedal signal simulation seems to be performing less well. However, when looking back to the derivative histograms in Figure 4.22 and Figure 4.23, one can notice how the probability of being mistaken for the braking pedal is higher than for the other one. Taking 70% of probability of having power regenerated means that there is still 30% chance that it is not the case. For the accelerating signal the probability shoots to one soon after the set limit, while this does not happen for the braking pedal. This accuracy is more than enough for the use of these data in the model, as a matter of facts it is tested that increasing the probability to 90% does not make a difference in terms of the output obtained from the power profile model.

Power model - HAN University

In this section the model that is used to reproduce the power demand profiles of the buses from the velocity profiles is discussed. In the previous sections the required inputs are discussed. To simulate the power requirements of the buses, a control curve is used, characterised by a region in

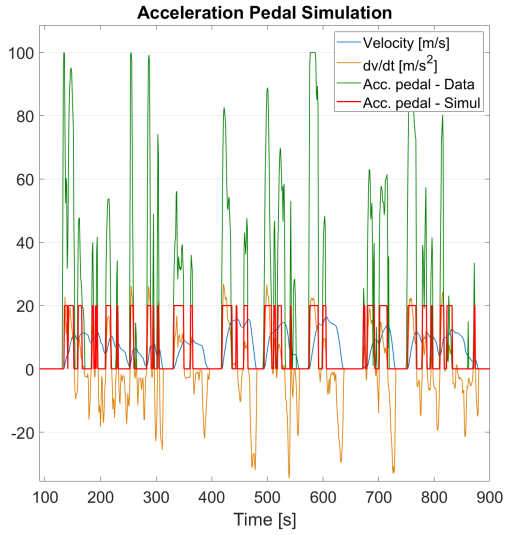

Figure 4.24: Validation of the simulated acceleration pedal signal, comparison between measurement and simulation

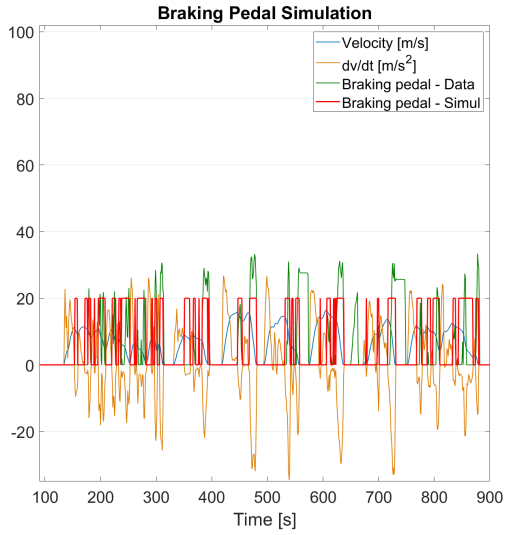

Figure 4.25: Validation of the simulated braking pedal signal, comparison between measurement and simulation

which constant torque is imposed, while maximising the power and a region in which the torque is maximised at constant rated power. Therefore, these regions can be defined as partial and full load regions respectively. In Figure 4.26 and 4.27, the plots of the torque and power curves are provided for the Arnhem and Gdynia bus, respectively on the left and on the right side. It is possible to see that the rated bus power for Arnhem and Gdynia buses are different and that also the rotational speed limits differ. This is because the two electric motors installed in the buses have different specifics, as can be seen from their datasheet included in Appendix B.

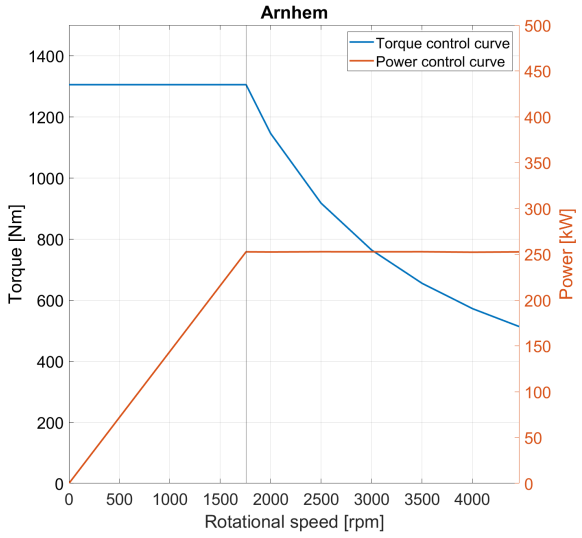

Figure 4.26: Torque and power control curves for Arnhem buses - power profiles model

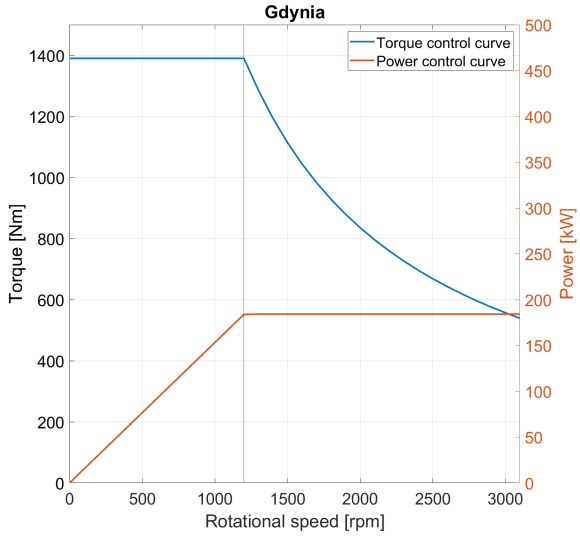

Figure 4.27: Torque and power control curves for Gdynia buses - power profiles model

The model is based on the calculation of the traction power obtained as

$$P_{\text{mechanical}} = T_{\text{motor}} \cdot \omega_{\text{motor}} \tag{4.34}$$

where T_{motor} and ω_{motor} are respectively the electric motor torque and rotational speed at all times. The motor torque is calculated as the sum of the wheel, friction and inertia torque components and the rotational speed as the wheel rotational speed multiplied by the gear ratio. In Appendix B the equations can be found.

Once the motor torque is calculated it is controlled through the curves previously mentioned: constant torque and constant power, based on the rotational speed of the motor. Finally, once the values of the mechanical power are obtained they are added to the braking power regenerated by the system. This last component is calculated through a transfer function characterised by experimental coefficients found by HAN University.

4.4 Storage Model

The integration of an energy storage system is used to study its effects on the potential integration of PV at substation level. Therefore, the model created simulates the operation of a Stationary Battery Energy Storage System (BESS) connected on the AC side of the substations, coupled with the PV system. The BESS is seen from the DC side as an AC source of electricity together with PV and the grid. The feed in point of the three generation units is the same. The integration of storage is meant to increase the self consumption and therefore the PV utilization and reduce both the grid power requirements and the PV generated power dump into the AC grid.

As mentioned in Chapter 2, one of the drawbacks of installing stationary storage compared to on-board storage is the reduction of the possibilities of recouping braking energy. In this case, with stationary storage installed on the AC side, there is no possibility of recovering and storing braking energy due to the unidirectional operation of the inverter. In the simulation all the power that is not exchanged between buses on the same section or on sections of the same substation is burnt in the braking resistors. The effectiveness of the BESS is therefore only associated to the PV component and has no impact on the reduction of energy consumption due to energy recuperation.

In Figure 4.28, the reader can find a flow chart representing the algorithm behind the storage model. The model is simply simulating the operation of a battery system, considering its depth of discharge, its charging and discharging efficiency and the power and capacity ratings of the system. For these parameters, Tesla Powerpack characteristics have been used as reference. Powerpack is chosen as reference since it is battery storage systems designed for commercial and utility scale, and because of its high performance and scalable design. In Table 4.11 the battery specifics which are considered useful for our simulation are reported [59]. The depth of discharge is limited to the range 5% to 95% to increase the lifetime of the battery, and propose a conservative scenario of battery use, although this is not a limitation imposed by Tesla on the product (the indicated DoD is 100%).

Table 4.11: Tesla Powerpack system specifications [59]

Parameter	Datasheet value
Maximum power	130kW (AC)
Energy Capacity	232 kWh (AC)
System Efficiency (round-trip efficiency - 4h system)	89.5% (AC)
Depth of Discharge	100%

The initial State of Charge (SOC) of the battery is 50%. Due to the fact that the starting point of the simulation is the beginning of the year, the battery will be used as source of energy rather than as storage since the PV generation level will be low. Starting from higher SOC increases the use of the battery on the first day when it is completely discharged in any case. Therefore, the halfway value of 50% has been picked as initial SOC point. The BESS model simulates the operation of the system by checking the available capacity within the battery. If in discharge mode the model checks whether drawing a certain amount of energy from the battery allows it to keep the SOC level higher than 5%, while in charge mode the check will be on the available storage capacity, namely on the possibility of storing a certain amount of energy without bypassing the limit of 95% SOC. Once these checks are performed, the battery will supply (in case of discharge) or store (in case of charge) either the total amount of energy or a fraction of it. The remaining part of the load that is not covered by the PV or the battery system will be supplied by the AC grid, while the PV excess which cannot be stored will be dumped in the AC grid. Before checking the SOC of the BESS the system defines the charge/discharge status computing the difference between total load and generation.

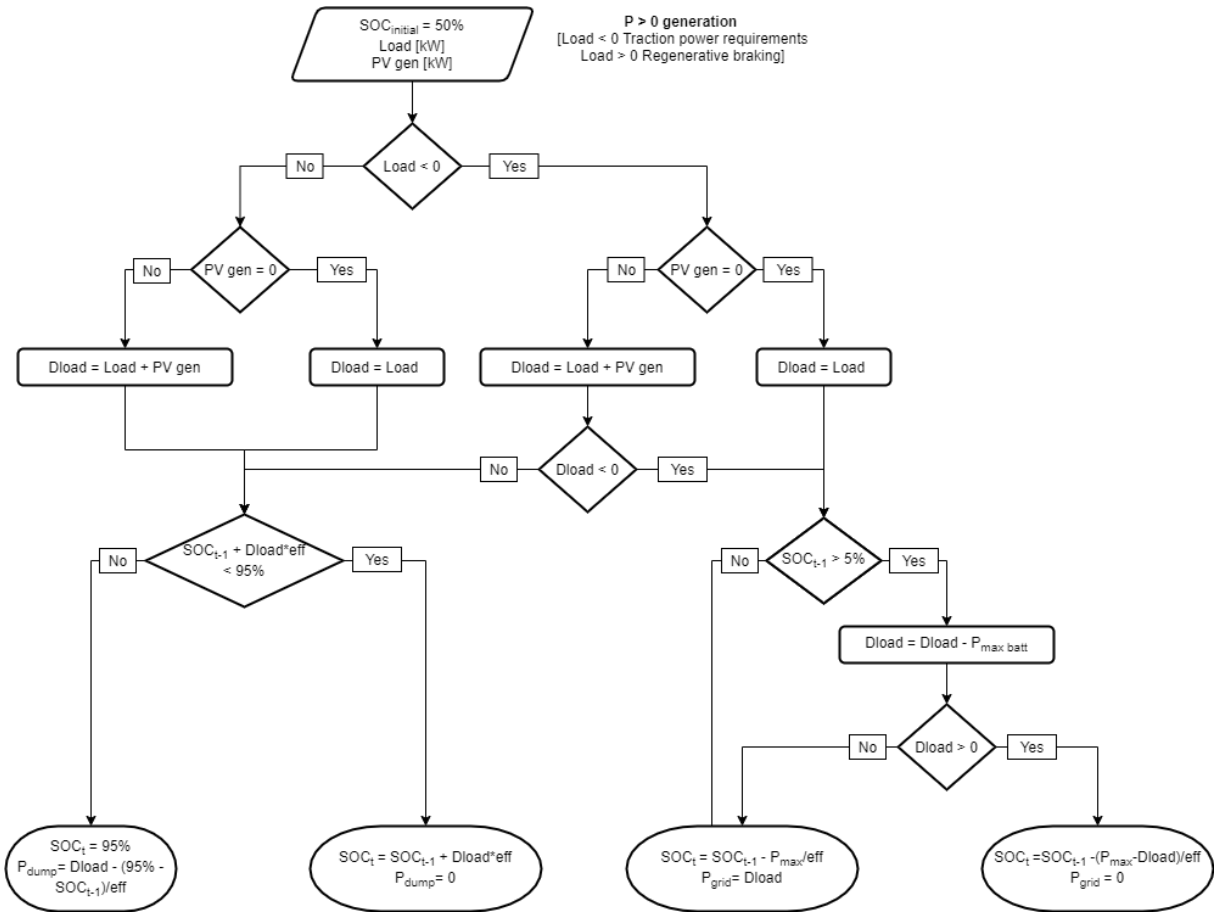

Figure 4.28: Flow diagram of the mismatch power management and of the storage operation (own work)

To summarise, the load is covered in order of priority by direct PV, stored PV or AC grid energy and the PV energy is, again in order of priority, directly used to supply the demand of the trolleygrid, stored in the BESS or sent to the AC grid. The ideal situation would involve having no participation of the AC grid and being able to supply directly and indirectly the load with PV and storage. However, due to the big temporal mismatch, both on the long and on the short term, between load and PV generation, this is not possible without installing a huge capacity of storage, which not only would make the system extremely expensive but would also reduce the battery utilization without improving considerably the PV utilization which can reach very high values also with reasonable BESS dimensions. The analysis on the storage performance coupled with PV is given in **??**.

4.5 Grid Models

In this section, the overall grid operation modelling is explained. This section can divided in 3 main parts. As one can see also from the diagram in Figure 4.1, once the power profiles are obtained and the HVAC yearly requirements are simulated, first the yearly operation of the grid is modelled, and then the operation at section and substation level is modelled. Therefore, first the yearly operation model and then the two section models for Arnhem and Gdynia respectively are here described.

4.5.1 Yearly Operation of the grid

In order to obtain the yearly power and energy requirements of each substation, it is necessary to simulate the operation of the grids in the two cities for the whole year and the energy requirements at section level. In order to find the yearly power profiles of the buses travelling attached to the overhead lines, the operation of the buses along each line is modelled following the timetable of the specific line

for the day of the year in question. Therefore, it is necessary to have as input the timetables of the different types of days for Gdynia and Arnhem and the calendar of the year, to know which timetable to use on every day. The modelled year is 2020, leap year, therefore composed of 366 days. It is decided to model this year for a matter of comparison with previous models and simulations ran in other studies. In relation to the timetables, in Arnhem for each line 6 different types of timetables are identified, while in Gdynia only 3 different types are given. In Table 4.12, the possible types of days during the year are listed. For each day type, a corresponding timetable for each line is available.

Table 4.12: Types of days and of timetables for Arnhem and Gdynia trolleybus grids

Arnhem Timetables	Gdynia Timetables
”Regular weekday”	”Regular weekday”
”Summer weekday”	
”School Holiday weekday”	
”Regular Saturday”	”Regular Saturday”
”Summer Saturday”	
”Sunday and holidays”	”Sunday and holidays”

The total number of trolleybuses operating in Arnhem and in Gdynia are found to be 54 and 84, respectively.

The steps to obtain the yearly power profiles for two grids are equal and here listed and explained.

Step 1
The first step is to gather all the timetables for the lines of the different grids in both directions and organise them in runs. In other terms, the bus schedules are analysed to select which runs can be subsequent and covered by the same bus. As an example, if a bus leaves from Oosterbeek Station (terminus at one end of line 1 in Arnhem) at 8:16 in the morning and arrives at Velp Beekhuizenseweg (terminus at the other end of the same line) at 9:00, it will not cover the 8:56 run, but the 9:26 run. The timetable is reconstructed to follow one bus. The output of this step is 54 timetables for the 54 buses that are necessary to cover the scheduled runs in Arnhem and 84 timetables for the 84 buses that are required to cover all the runs in the Gdynia trolleygrid.

Step 2
Once the timetables per bus are generated, a matrix indicating the line and the direction of the bus next run and one containing the instant in the day in which it will happen are created, in order to import this information in Matlab. Using these matrices the model can define the location of the buses in the grid both in space and in time and can identify the section providing the demanded power at all times.

Step 3
The code takes as inputs the number and type of day, and all the information generated so far. Based on the day the bus schedule is defined (as previously mentioned there are 6 different schedules in Arnhem and 3 in Gdynia) and based on the time in the day the HVAC requirements are identified. It is important to define the HVAC requirements in relation to the time of the year due to the non-negligible variations during the year. At this point the duty-cycle of the HVAC is created and the HVAC power demand profile is available.

Step 4
At this point the daily power requirements for each bus used during the day are created. A power profile between high, medium and low traffic (see Figure 4.2.4) is selected based on the type of the day and associated to each run of the buses. The power profiles obtained from the Braunschweig velocity cycle are never used. The HVAC and additional auxiliaries power is then added to the power profile of each run. In the case in which the bus is not moving for more than 10 minutes, the HVAC power demand will automatically be set to zero. While the bus moves within the DC traction grid, its power is supplied by different substations. Knowing the direction of the run and the moment in which the run starts through the velocity profiles the position in time of the buses is found. This allows the model also to detect the section in which the bus is at all times and therefore the substation feeding the bus.

Steps 3 and 4 are repeated for every day of the year to generate the power demand of each bus running in the grid throughout the whole year.

Step 5
The power profiles, the auxiliaries power profiles, the velocity profiles, the positions of the buses and the corresponding section of the grid are all saved in different matrices for each day. Every matrix has the number of columns equal to the number of buses in the grid (which is 54 and 84 for Arnhem and Gdynia respectively) and rows being the second in the day in which there is the specific power demand. The matrices are saved for each day, therefore 366 files are saved containing the information for each day.

These data points are saved to further analyse the demand not in terms of buses but at section and substation level. In this way it is possible to test and study the potential of integrating PV at substation level and the effects of the different parameters on it.

In the next subsections the two section models used for Arnhem and Gdynia, in order, are discussed.

4.5.2 Arnhem Power Flow Section Model

In Arnhem trolleygrid, two types of sections can be found: linear sections and "fork" sections. If the first type is easy to simulate, since at every moment there can be only one bus at a certain distance from the supply, the second type is characterised by a more complex structure which involves multiple branches being connected to each other to form a single power supply section. In Figure 4.29 and 4.30 the schematic of the two sections is proposed. Moreover, some sections of the trolleygrid are connected between each other through bilateral connections. This implies that these sections have to be simulated together if bilateral connections are introduced, since the two feed in points of the two sections feed both the buses on one and the other section based on the bus position and on the potential difference between the feed in point voltage levels. In some situations, the connection between two sections generates a non-linear structure, generating a "fork" configuration. Therefore, when simulating sections which are bilaterally connected two other cases are introduced: linear bilateral sections, in Figure 4.31, and "fork" bilateral sections 4.32. Overall, to simulate the Arnhem grid four power flow models are required to simulate the four cases presented: linear sections without bilateral connections, "fork" sections without bilateral connections, sections bilaterally connected that form a linear structure, sections bilaterally connected that form a "fork" configuration.

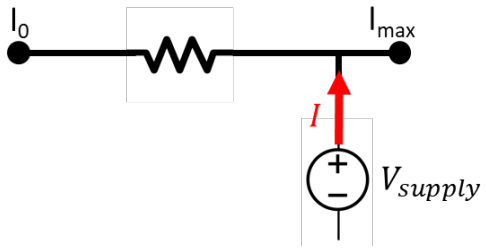

Figure 4.29: Electrical schematic of a linear section - power flow section model Arnhem

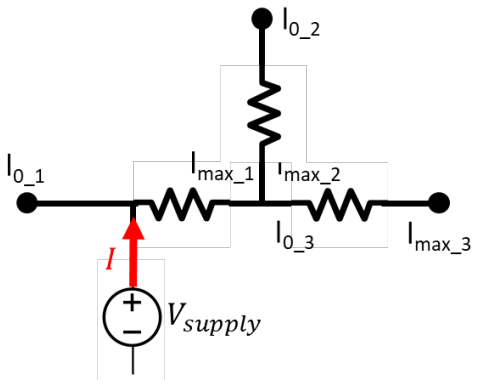

Figure 4.30: Electrical schematic of a "fork" section - power flow section model Arnhem

"Fork" sections are not simulated making use of power flow calculations, due to the limited amount of time the simulation of these sections was not finalised and the model is still presenting many points without a proper solutions throughout the year. For this reason, for these sections (which account for 7/44 sections of the grid) an assumption is made and they are simulated as the sections of Gdynia grid, with fixed transmission losses. The losses selected are chosen as an average between the losses of the sections they are connected to, since no literature is found on section transmission losses in Arnhem. All previous research introduces extreme assumptions (as no feeder cables) which would introduce a higher error than the average value that is picked. An improvement to the work proposed is simulating the operation of the grid with the complete fork section model.

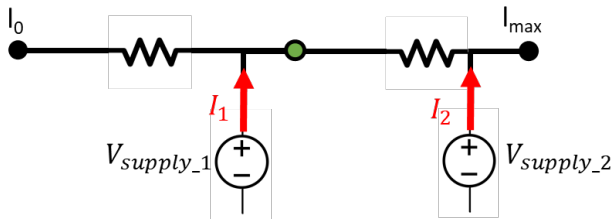

Figure 4.31: Electrical schematic of two sections bilaterally connected, forming a linear structure

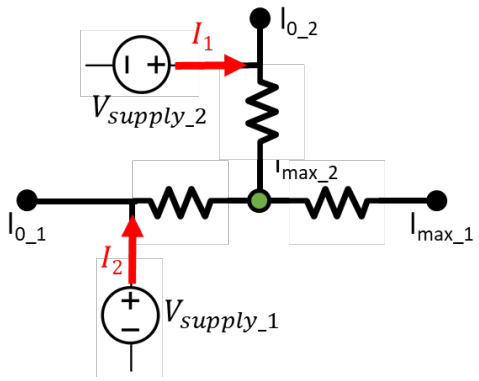

Figure 4.32: Electrical schematic of two sections bilaterally connected, forming a "fork" structure

Some sections are bilaterally connected to two other sections. This is the case for sections 13+14+8 and for 12+16+17 (refer to section map in Figure 3.3). For these two cases some extra assumptions are made. In Figure 4.33a and 4.33b the actual schematic and the schematic of how the sections are modelled are proposed respectively in the top and bottom figure. As the reader can see from the schematic representation, the modelling of this specific case is split into two simulations. One of the sections, in the figure section n3, characterised by lower voltage levels and higher power requirements with respect to the neighbouring section, is simulated bilaterally connected to the neighbouring section without any traffic on it. Therefore, section n2 is seen as an extra feed in point for section n3. Then, sections n1 and n2 are simulated with their respective bus traffic, connected in parallel. The total power requirements of section n2 will be computed as the sum of the requirements obtained from the two simulations.

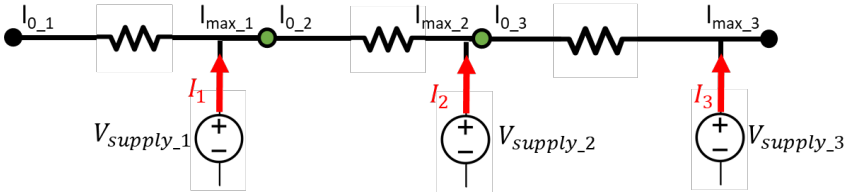

(a) Schematic of section connected bilaterally to two other sections

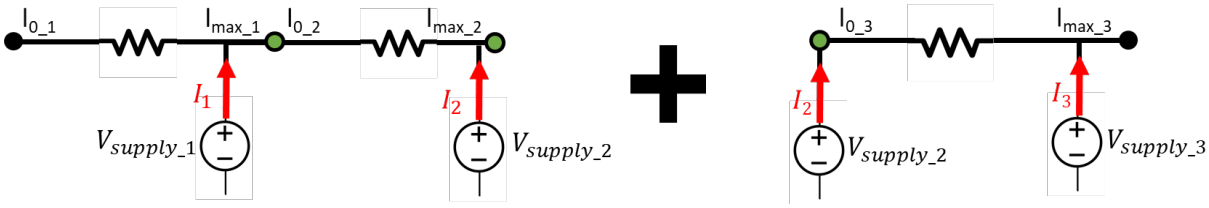

(b) Schematic of modelling method for a section connected bilaterally to two other

Figure 4.33: Electrical schematic of 3 sections connected bilaterally

Power Flow Calculations

The underlying theory of the models of all types of sections is related to the calculation of voltages and currents in all the points in which there is a power requirement or supply along the section. The substation voltage, fixes the voltage level of the section at the supply point. At every second the buses on the section are found and their power requirements and positions are stored in two vectors. Based on the power required (or produced in case of regenerative braking power) and on the position of the bus the voltage drop along the line and the current are computed. The resistance of the overhead cables is calculated using the *Total distance approximation* assumption for the parallel lines, explained in **??**. Along all the catenary only 2 lines are connected in parallel. However sections 6 and 19 do not have parallel connections and therefore for these sections the voltage drop along the lines will be doubles. The calculation of the voltage and current in all the points in which there is a power flow is done

through an iteration, since multiple buses can be found at the same time under the section, inducing a multi-point optimization problem. This is done for every second of the year for every section of the trolleygrid. As a matter of fact, bus power and position are variable in time and the voltage of the catenary will vary based on these two elements.

The simulation of bilaterally connected sections works in the same way, however this time the optimization sees two supply points. This means that the voltage levels now are determined by two different points: the two feed in point of the different sections. The iteration to find a solution takes longer then in this case since the current sent from each substation is optimised based on the voltage drop occurring in both sections. These simulations can take up to 60 times more than the simulations of a single section, increasing the computational time from 15min simulation per section to 3h per section. For this reason, not all sections are also simulated when bilaterally connected. Some sections are picked to study the effects of bilateral connections on the simulation outputs and on the PV integration performance.

4.5.3 Gdynia Transmission Losses Section Model

The amount data related to the location of the substations, to the feeder cable lengths and characteristics and to the location of the feed in points along each section, for the Gdynia trolleygrid is very limited. Therefore, it is not possible to use the power flow model for the Gdynia section simulations. In [14], the authors propose a study on a method to calculate the transmission losses for a trolleybus traction grid. One of the grids used to perform the study is Gdynia grid. The method used by the researchers in the paper consist of measuring the voltage drop between the substation DC output and the bus connection point to the catenary. The voltage is measured in time at the two points and together also current and position of the bus are registered. In this way the power lost in transmission is estimated in time, and the location of the bus is used to estimate the section in which there is a power requirement.

The data found in this paper related to the transmission losses in each section of the grid is used to simulate the operation of each section. Power exchange is allowed within one section but section of the same substations are not exchanging power between them. Therefore the regenerated braking power which is not used in the section is considered to be burnt in the braking resistors. The same assumption is made in Arnhem grid. In Table 4.13 the values for the transmission losses calculated for every section of the grid are reported. The introduction of a fixed transmission loss factor reduces the precision of the model since there is now simulation of the power flow in the grid. On average though, this assumption allows to have a good estimation of the substation requirements. Using the power flow model to calculate the section power demand would introduce in the simulations even more assumptions and errors, since there is a lot of information missing on the structure of the grid in Gdynia. Due to the fact that the data on the losses is provided per section and has been measured and previously researched upon allows us to consider it as a good estimation of the losses to expect in each section. Moreover, installing the PV systems on the AC side of the substations allows us to have the same amount of results for Gdynia as for Arnhem, since the power requirements of the substation is what is relevant for the research. The voltage levels and the power flow increase the accuracy of the simulation and the results, however are not relevant for this study, if not in terms of losses that they induce.

The section numbers identify the substation (with the first digit) and the section (second digit) numbers. In red the worst sections are highlighted. High transmission losses are expected in these three sections. 1/6 is a very long section and 2/3 and 3/2 are high traffic sections. The other sections present lower transmission losses, spread around an average of 7.5%.

4.5.4 Validation of the Grid Model Outputs

In the next paragraphs an overview of the model outputs is provided and compared to the available data. First, Arnhem grid operation simulation outputs are analysed, followed by the data for Gdynia trolleygrid.

Table 4.13: Transmission losses per section in Gdynia grid

Substation/Section Number	Section losses [%]
1/1	4.90
1/2	9.80
1/3	3.40
1/4	9.10
1/5	7.80
1/6	14.00
2/1	6.00
2/2	5.00
2/3	15.30
3/1	8.20
3/2	13.60
3/3	2.80
4/1	5.70
4/2	9.50
4/3	5.50
5/1	8.70
5/2	2.50
5/3	4.80
6/1	7.70
6/2	11.70
6/3	7.80
7/1	5.70
7/2	9.50
8/1	4.10
9/1	7.20
10/1	10.90
10/2	8.40
10/3	6.10
10/4	7.20
10/5	9.50

Arnhem Trolleygrid

The simulation outputs for Arnhem grid are compared to measurements of the yearly energy requirements of each substation during three different years: 2019, 2018 and 2017. In Table 4.14, the overview of the data found is provided and in Figure 4.34 the simulation output for each substation is plotted in a bar chart together with the measurements performed. In the plot, some substation numbers are circled in blue. These represent the substation that present lower matches between simulated and measured values, namely the ones in which the modelled value differs from all the three measurements. As a matter of fact, the measurements in some cases also noticeably differ between them, introducing in the validation an extra difficulty.

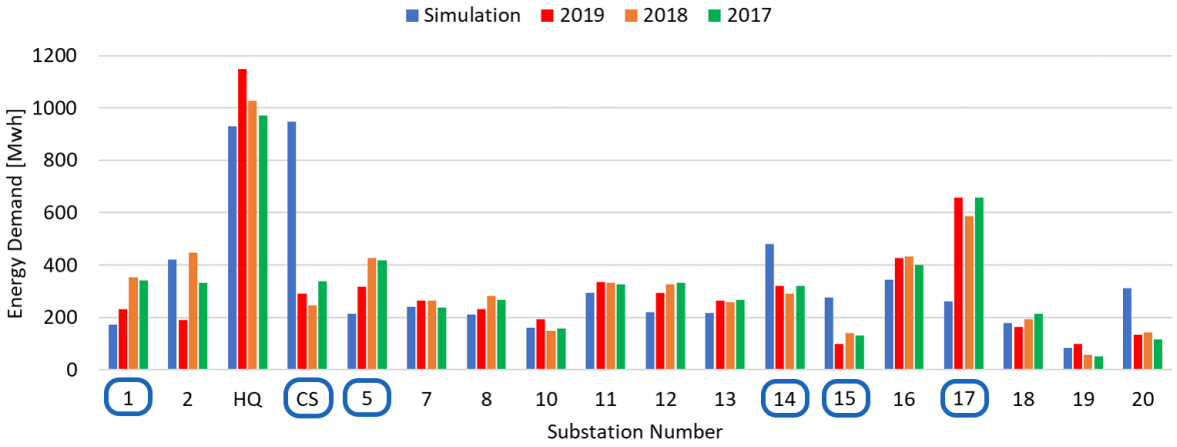

Figure 4.34: Bar chart - comparison between simulated and measured energy demand values for each substation in Arnhem grid

However, analysing the substations which are found to be differing the most it is possible to notice by looking at the difference between the measured values, that these substations present variations in the energy consumption through the different years. The model used so far, does not include the possibility of connecting bilaterally some of the sections of different substations and does not allow power exchange between the sections of the same substation. All the substations that have been circled in Figure 4.34 are actually substation under which multiple sections are connected in parallel with sections of other substations or with high traffic, in the case of Central Station. In Figure 3.3 the map of the sections of Arnhem trolleybus grid is provided, in which also substations and bilateral connections are shown. Some of the substations which present big differences are here analysed to understand what the reasons of this offset could be.

- **Substation 1** is formed by two sections which are connected bilaterally with substation 12 and CS. Substation 1 is probably providing to CS an amount of yearly energy that can cover for some of the excess found for that substation. Moreover, if substation 12 is feeding a part of substation 1 it will probably increase the coverage of substation CS that 1 has even more.

- **Substation CS** is a high traffic substation, with multiple sections fed by it. Therefore, allowing also power exchange between the sections under the same substation can reduce the energy requirements of the substation. However, Central Station is formed by 3 different substations number 4, 9 and 21. The connection and dependence between the three substations is not clear. For this reason assuming power exchange between all the sections would be a strong assumption. If the three substations have 3 different DC busbars the power exchange will not be possible. These three substations are all characterised by low voltage levels, which allow us to assume that when bilateral connections are active CS substation will be heavily supported by the neighbouring substations.

- **Substation 14** is formed by 3 sections which are ache connected bilaterally to a section of a different substation: 13, 16 and CS. Substations 13 and 16 are probably partly contributing to the energy demand of substation 14 and this would explain the lower value presented in these two substations.

- **Substation 15** is characterised by a very long section which is partially fed from another section bilaterally. Not considering bilateral connections increases considerably the voltage loss and the losses along the catenary of that section.

- **Substation 17** is feeding also a section of substation 2, which partially can explain also the dip in the data registered in 2019 for substation 2 if the connection was introduced in that year. Moreover, section 40 (supplied by this substation) is characterised by very hilly roads, this might be the cause of the underestimation, since the road gradient data is not gathered with high precision but retrieved from Google Maps and since the velocity profiles are not adapted to the road gradients.

Table 4.14: Arnhem grid simulation outputs compared to measured data (bilateral connections are not included in the simulations)

Substation Number	Simulation [MWh] (no bilateral conn.)	Measured [MWh] (2019)	Difference (2019)
1	171.8	231.6	-25.8%
2	420.6	190.7	120.5%
HQ	930.9	1149.2	-19.0%
CS	947.4	289.8	226.9%
5	212.9	317.6	-33.0%
7	241.1	265.5	-9.2%
8	212.4	232.6	-8.7%
10	160.7	194.3	-17.3%
11	292.5	335.9	-12.9%
12	220.2	294.9	-25.3%
13	216.6	265.3	-18.4%
14	479.3	320.4	49.6%
15	276.0	99.0	178.8%
16	344.6	426.9	-19.3%
17	261.9	657.8	-60.2%
18	178.9	164.3	8.9%
19	82.6	97.2	-15.0%
20	312.6	133.7	133.8%
Total	**5962.9**	**5666.7**	**5.2%**

Due to the time limitation and to the complicated structure of some of the sections, the bilateral connection modelling will be limited to certain sections. This will allow us to verify the assumptions made on bilateral connections and to assess its effects.

Introduction of bilateral connections

Three groups of sections are simulated with bilateral connections. The modelled sections are all in Arnhem trolleygrid and all linear, they all present a simple structure (no 'fork'). In Figure 4.35, the reader can find a bar chart presenting the variations in energy demand with the application of the bilateral connections in (a) and the voltage levels of the substations feeding the respective sections.

The first set of sections is formed by sections 2 and 23. In Figure 4.36, the map of the two sections is shown. When sections are bilaterally connected the section insulator is indicated by an orange box, while if they are not connected it is indicated by a white box. As one can see, the section 2 and 23 are connected between them and not with the other neighbouring sections. Indicated with a circle and the number of the section is the supply point of the section. It is possible to see that the feed-in points are located at the opposite ends. This is the reason why when connecting bilaterally the two sections the overall energy consumption is considerably reduced. The sum of the energy demand of the two sections goes from 160 MWh to 110 MWh. This means that the application of the bilateral connections induces the reduction of losses by 50 MWh. Section 2 is still supplying more power than 23 since the substation voltage is considerably higher.

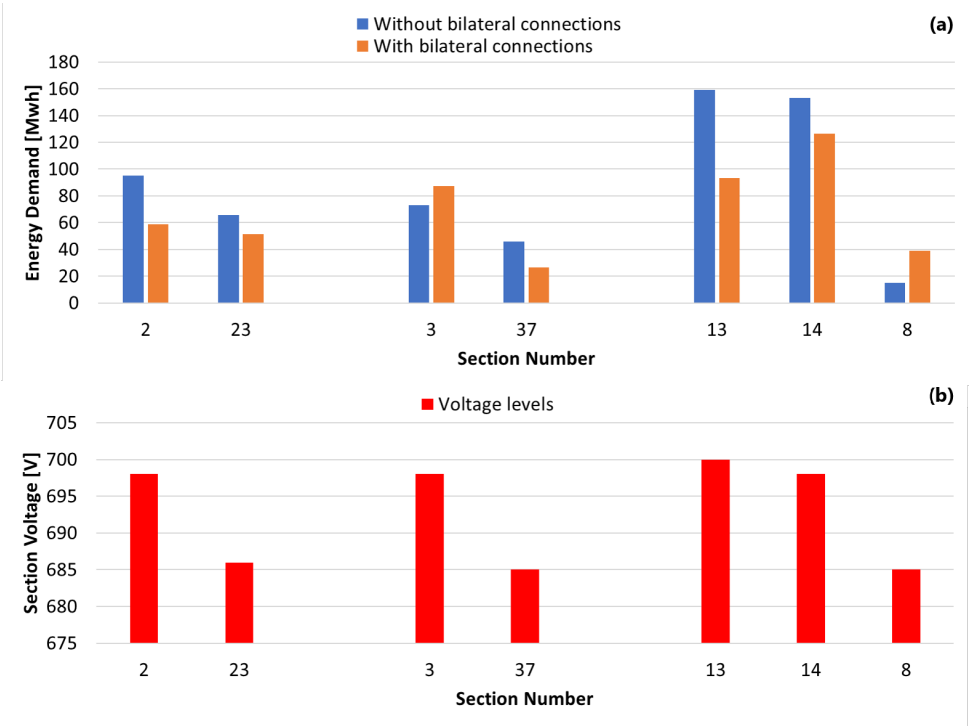

Figure 4.35: Effect of bilateral connections on 3 groups of sections in terms of energy demand (a) and voltage levels of the sections (b)

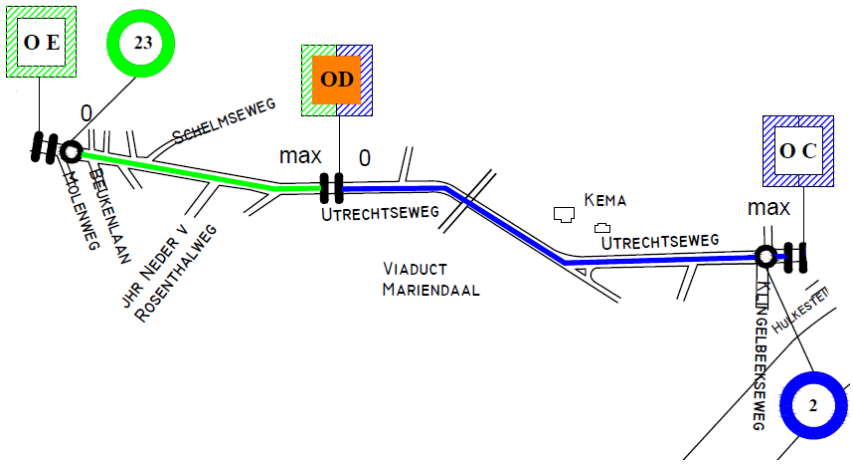

Figure 4.36: Map of sections 2 and 23 in Arnhem grid

The second group is defined by the connection between section 3 and section 37. In Figure 4.38, the map of the two sections is shown. A similar situation as the one presented above is found in this case. The two sections are connected bilaterally between them and insulated with the other neighbouring sections. Also, the supply points are found at the two opposite ends of the sections with respect to the connection between the two. Also in this case the total energy demand is reduced by 10 MWh. The reduction in this case is lower since the total length of the two sections combined is lower, 1470 m compared to 2150 of the previous set. Finally, the demand of section 3 is noticeably increasing and the opposite trend is found for section 37. This is due to the voltage levels. Section 3 is supporting section 37 supplying the buses on the latter section.

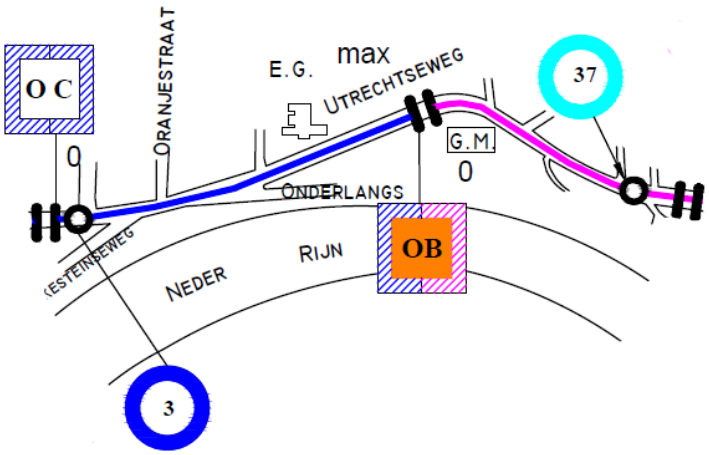

Figure 4.37: Map of sections 3 and 37 in Arnhem grid

The last set of sections studied is the combination of section 13, 14 and 8. In this case the simulation is split in 2 due to the fact that the three sections are connected between them, namely section 14 is connected bilaterally both with section 13 and section 8. What can be seen is that the overall energy consumption is reduced, from 330 MWh to 260 MWh and that the share of supply is also rearranged. The supply point of section 14 is at the beginning of the section, close to the connection with section 13. For this reason, since section 13 is 1670 m long, section 14 is partially supplying its load. On the other side, section 8, although with lower voltage level, can support section 14. As a matter of fact, section 8 presents very low traffic conditions and a total length of 100 m. For this reason it can supply the buses on section 14 which are close to section 8 reducing the transmission losses.

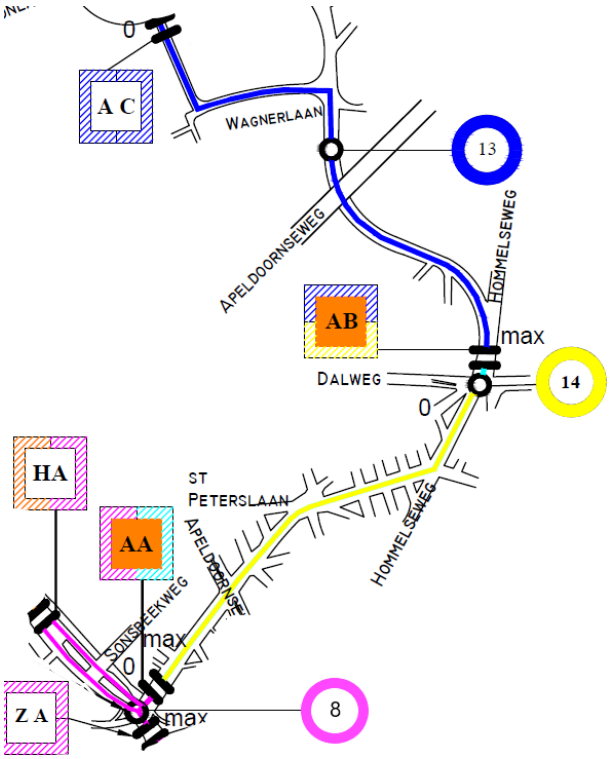

Figure 4.38: Map of sections 13, 14 and 8 in Arnhem grid

Gdynia Trolleygrid

The validation of the outputs of the grid simulation for Gdynia trolleygrid is more complicated due to a lower availability of measurements and data, as previously mentioned. The validation is performed top down, comparing the obtained results with previous studies conducted on the same DC traction grid. The copious availability of previous research allows to benchmark the results, even if in a fragmented way. The comparison is done with different papers and in Table 4.15 below the results are reported. The simulations proposed in this study are compared to data coming mainly from 2011 and 2014. This not only to attribute to the fact that most of the available measurements to benchmark the results were registered during those years, but also to have a fair comparison. As a result of the very scarce data to use for the simulations and to reduce the number of assumptions made when modelling, the reference scenario for the Gdynia trolleygrid is with 0% vehicles with on-board batteries, 0% lines with IMC and a total of 12 lines. During the years, following the progress in research on traction systems, IMC and on-board batteries have been implemented and trolleybus new lines are served from the LVDC traction grid. Therefore, to compare the results of this model, we will refer to the same scenario in time and not to the latest status of the grid.

Table 4.15: Verification of the model output Gdynia

Parameter	Simulation	Available data	Average data	Difference [%]
Number of buses	84	85	85	-1.2%
Energy consumption [kWh/km]	1.72	1.90	1.86	-8.3%
		1.2 - 2.5		
		1.45		
		1.98 - 2.15		
Average mileage [km/veh] 10^3	51.67	56.26	56.26	-8.2%
Total vehicle km [km] 10^6	4.34	4.96	4.96	-12.5%
Average speed [km/h]	19.0	15.5	15.9	19.5%
		14-18		

What can be seen from the comparison, is that although the number of buses in use in the simulation seem to be consistent with the number of running buses, 84 against the existing 85 [66], the simulated bus energy consumption appears to be lower than the measured one, 1.7kWh/km versus 1.9kWh/km [10, 65, 66]. The simulation performed in this study excludes the possibility of operation without catenary for the buses and of charging/discharging on-board batteries. In motion charging appears to be an option in 4 different lines in the Gdynia grid and the presence of on-board batteries would cause an increase of the energy consumption. Another assumption introduced in the models is that only one type of bus is used in the Gdynia trolleygrid. However, this is not the case and also larger buses (18m instead of 12m) are being used, increasing like this the average bus consumption. Finally, the assumptions made for the HVAC energy demand model could be a cause of the reduction of the consumption, since less strict inside temperature conditions are considered in the model. This is also confirmed when we look at the distribution of the energy demand of substation 2 in Gdynia.

When comparing more specific data as the consumption throughout the year of one substation, Substation 2, we find very similar results, with a percentage difference on average in the year of approximately 10% and a total yearly consumption that is 5% different from the measured data. In Figure 4.39a, the plot of the comparison of the energy consumption in the different months of the year measured [12] and simulated is shown. What can be seen, is that the discrepancy increases in the summer months. This might be related to the assumptions made to simulate the HVAC operation, on the irradiance effect on the bus heating (refer to Section 4.2 for the details and assumptions made for this model). However, the measured data must also be questioned, since it is an unexpected result to have higher energy consumption during the summer months than in the spring/autumn months. This result could be related to multiple causes. The first cause could be identified in the inside-cabin temperature requirements which might be set during summer at the same level as in spring and autumn, this would cause a noticeable increase in the AC requirements due to the higher temperatures (in Appendix A the reader can find the temperature characteristics in Gdynia throughout the year). Another possibility is that the measurements presented in [12] and plotted in Figure 4.39a have been taken in 2016. As a matter of facts, between the 29^{th} June and the 1^{st} July 2016 to cover the shortage of buses during the

Open'er Festival, trolleybuses were equipped with high-capacity lithium-ion batteries to serve extra routes in Gdynia and Sopot [10]. The vehicles covered using auxiliary drive long sections of the routes without catenary. The occurrence of the festival not only caused the number of buses to increase but also introduced routes without catenary, which imply that the buses would then charge while covering routes with overhead lines. A combination of these two elements, would explain the increase in the error of the model in the months that go from June to August, as can be seen in Figure 4.39b.

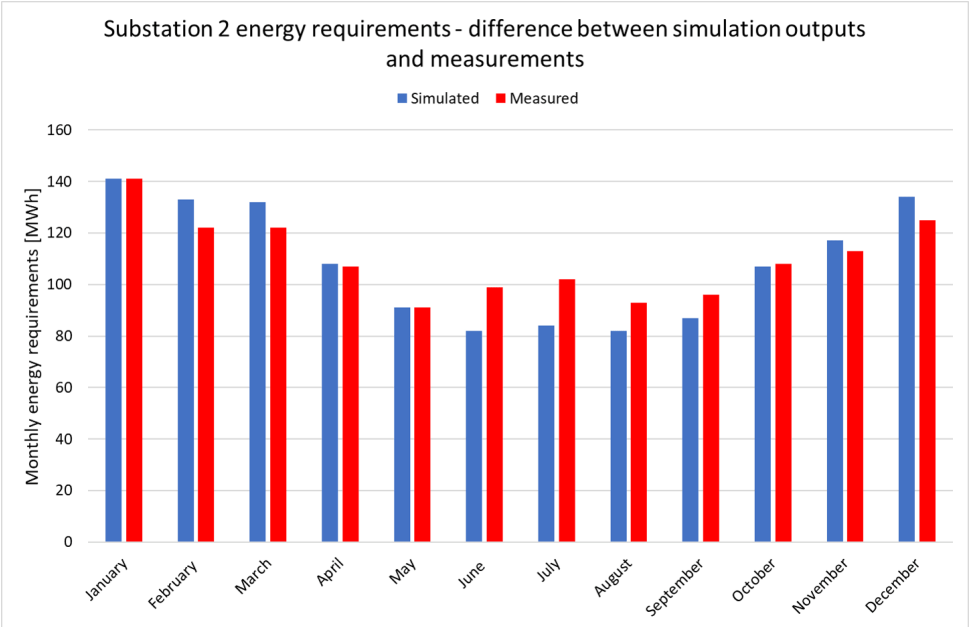

(a) Comparison between simulated and measured monthly energy requirements for Substation 2 in Gdynia

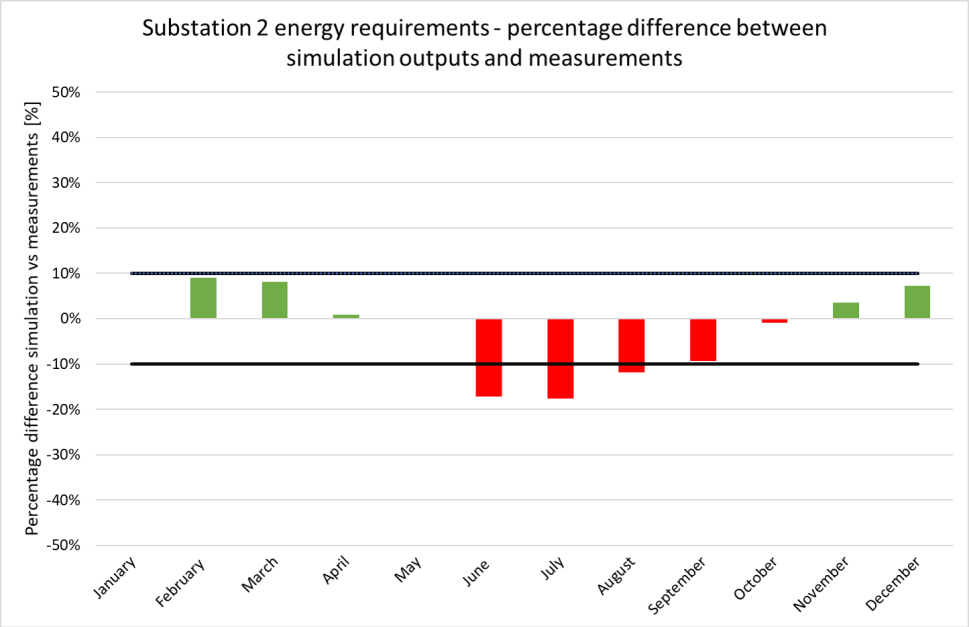

(b) Comparison between simulated and measured monthly energy requirements for Substation 2 in Gdynia - percentage error

Figure 4.39: Gdynia grid-validation of the model outputs: Substation 2 energy requirements

One final point of comparison is related to the average speed during the different days of the week. Although these data are also reported, from [66], these are coming from 2013. At this point no dedicated lanes were present for the trolleybus rides, while they have been implemented in the following years. Therefore, although a noticeable difference in the average speed is found between the simulation and these measurements, it is the only data that are found in literature, and have not been confirmed in any other paper, and still the values found are within 20% difference from these.

4.6 Parallel lines approximation analysis

In this section, the reader finds a study on the approximation used in the simulations to compute the voltage drop along the overhead lines, in a section. In particular, this subsection discusses the percentage error caused by the approximation used to calculate the voltage drop when the bus is moving along the catenary in one section (one supply point), in presence of connections between parallel lines of the catenary. In order to reduce transmission losses, compensatory connections between fractions of the overhead lines are introduced [14]. One of the modifications of the overhead cables included in the modernisation process of the trolleybus traction grids, is to connect certain intervals of the overhead cables for the two directions of travel in order to reduce the losses of power transmission. As a matter of fact, when supplying power to a bus in a section these connections allow to split the required current into two fractions (or more if more cables are combined between them) and therefore to reduce the losses caused by the transmission of high currents. This allows to reduce the effective resistance of the catenary (thus the transmission losses) in certain circumstances in half (if the connections are done between 2 cables). In sections with high bus traffic intensity, where multiple buses could be found in the same position, multiple lines can exist for the same travel direction. In this case the combination of multiple overhead lines could bring to a beneficial reduction of the voltage drop along the line. Before starting with the analysis of the approximation used in the models, in the next paragraphs a brief analysis of the effect of parallel connections is given starting from the voltage drop problems in the traction grid.

4.6.1 Voltage drops along the line with and without parallel connections

While moving along the catenary the bus is supplied with power from a substation. If we focus on a single section supplied in one point from one of the substations, with one bus moving along the overhead line section (no bilateral connections are here considered) we can represent its equivalent circuit as shown in Figure 4.40. As one can see, the lines are modelled as resistive components, this is an assumption which can be introduced since the impedences along the overhead cables are negligible in comparison to the resistances. The resistance of the line increases with the distance of the bus from the supply point of the section according to 4.35

$$R_{line} = \rho \frac{l}{A} \tag{4.35}$$

Where ρ is the resistivity of the cable in Ohm/m, l the length and A the cross-section area of the wires, respectively in m and m^2.

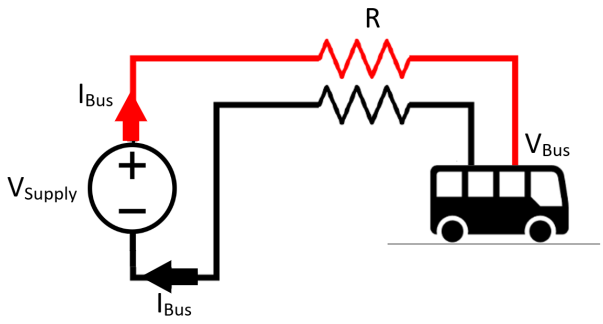

Figure 4.40: Equivalent electrical circuit of one supply section with one bus

Through Kirchhoff's Voltage Law and Ohm's Law, the voltage drop across the bus can be found though equations 4.36 and 4.37. In 4.36 Kirchhoff's law applied to the equivalent circuit of the section and in 4.37 the equation rearranged to find the voltage across the bus and replacing V_R according to Ohm's law and equation 4.35.

$$V_{Supply} - 2V_R - V_{Bus} = 0 \tag{4.36}$$

$$V_{Bus} = V_{Supply} - 2I_{Bus}\rho\frac{l}{A} \tag{4.37}$$

From these last equations, it can be concluded that the voltage drop along the line, which is also the difference between the supply and the bus voltages, once the cables are selected is only affected by the distance of the bus from the supply and the power requirements of the bus. As a matter of fact the electric power demand of the bus can be computed as:

$$P_{Bus} = V_{Bus} * I_{Bus} \tag{4.38}$$

In Figure 4.41, the voltage drop is plotted for different powers (from 0 to 300kW with steps of 20kW) and as a function of the distance from the supply point. The supply voltage is 700V in this example. This image graphically shows and confirms what discussed so far: the voltage drop along the line increases with increasing power and with increasing distance from the supply point due to the increase in current and in distance travelled by the current respectively.

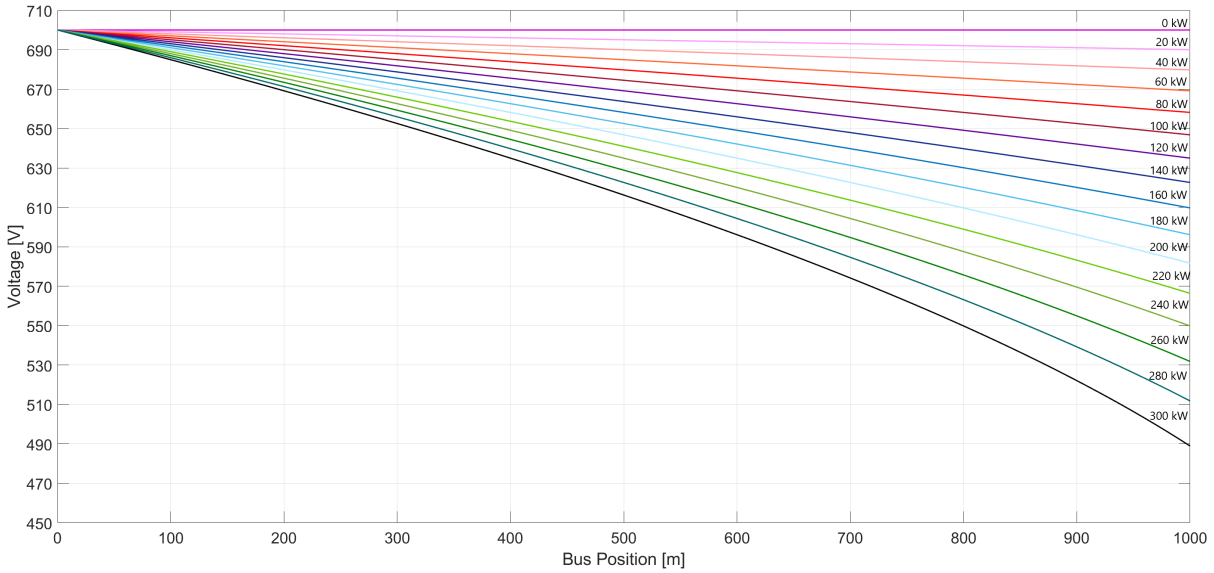

Figure 4.41: Voltage drop along one supply section due to the travelling of one bus as a function of bus power and distance from the supply point (0m)

The introduction of connections between the overhead lines of the two driving directions can sensibly reduce the losses along the lines, thus the voltage drop, due to the decrease in current carried by the cables. In Figure 4.42 one can find the equivalent circuit of one section with the overhead lines of the two direction combined. For simplicity, the return wire is omitted (or considered to be behind the other cables, for both driving directions).

Using this figure as reference, the equation to compute the bus voltage when compensatory connections are introduced is now derived. In Figure 4.42 and in the equations that will follow abbreviations and symbols are used, the reader can always refer to the Nomenclature for the list of symbols and abbreviations used, however, here the useful nomenclature for the next calculations is explained:

- V_{supply} - supply point voltage
- V_{bus} - bus voltage (voltage drop across the bus)
- R - resistance of one line (does not account for the return)
- l_s - distance between two subsequent parallel connections
- l_{total} - total distance of the bus from the supply point
- l_{single} - distance of the bus from the last parallel connection before its position (with respect to the supply point)

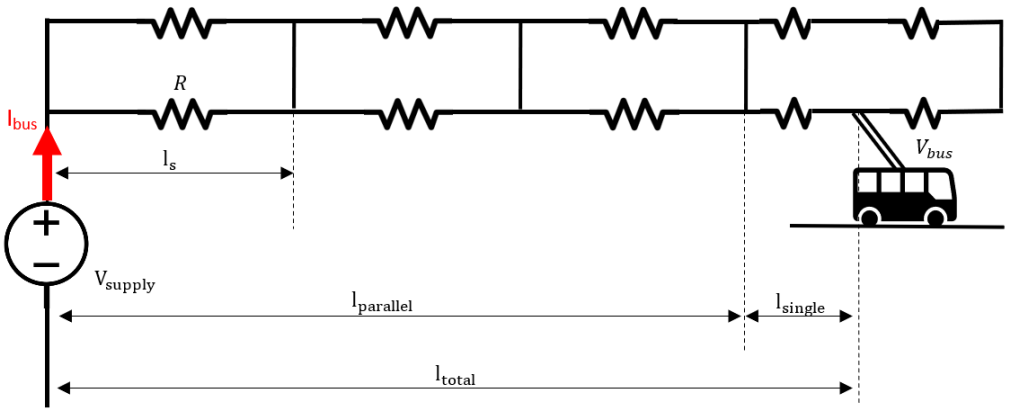

Figure 4.42: Electrical representation of the two traveling directions lines connected in parallel in one supply section of the grid, with one bus travelling on it (own work)

- $l_{parallel} = l_{total} - l_{single}$ - length of the line connected in parallel between the bus and the supply point

Making use of equation 4.35, Kirchhoff's current and voltage laws and Ohm's law the following equation is obtained for the calculation of the bus voltage when the two lines are combined and both are used to supply the current to the bus:

$$V_{bus} = V_{supply} - 2 * \frac{R}{2} * l_{parallel} * I - 2 * R * l_{single} * I * (1 - \frac{l_{single}}{2 * l_s}) \tag{4.39}$$

This equation can be re-written as in 4.40 to highlight the quadratic dependence of the bus power on voltage, when the power is calculated as a function of resistance and voltage only.

$$V_{bus} = \frac{V_{supply} + \sqrt{V_{supply}^2 - 4 * (2 * P_{bus} * R * (\frac{l_{parallel}}{2} + l_{single} - \frac{l_{single}^2}{2 * l_s}))}}{2} \tag{4.40}$$

In equations 4.39 and 4.40 the resistance along the line is multiplied by 2 since also the resistance and the voltage drop across the return line have to be considered when applying Kirchhoff's voltage law.

The difference between equations 4.37 and 4.39 is that in the second one the parallel connections are considered and used to send current to the bus with reduced losses. As a matter of fact, in equation 4.39, with parallel connections, only half of the current is transmitted through each of the two cables until $l < l_{parallel}$ and then in the last fraction of the section where the bus is located the current splits in the two wires differently, based on the distance between the connections l_s and the position of the bus between the twol_{single}. The transmission losses along the line are calculated as:

$$P_{loss} = I_{bus}^2 * R \tag{4.41}$$

Therefore, the reduction of the current through the cables induces a quadratic reduction of the power lost in transmission.

In Figure 4.43, the voltage drop across the line with varying electric power demand and distance from the supply point (at 0m) is shown for the scenario without parallel connections, represented by solid lines, and with parallel connections every 300m, in dashed lines. The presented example, considers to have a total section length of 1000m (max distance from the supply point reached) and a supply voltage of 700V. This supply voltage is chosen since all the substation voltages of the two cities fall around this value.

In Figure 4.44, the same scenario is shown but this time with a lower distance between two subsequent compensatory connections, namely of 100m. In order to visualize more clearly the impact of the voltage drop on the distance between two parallel connections, the same situation as for the previous two cases is shown in Figure 4.45, but representing only the parallel connection option with 100m or 300m distance between two connectors, in solid and dashed lines respectively.

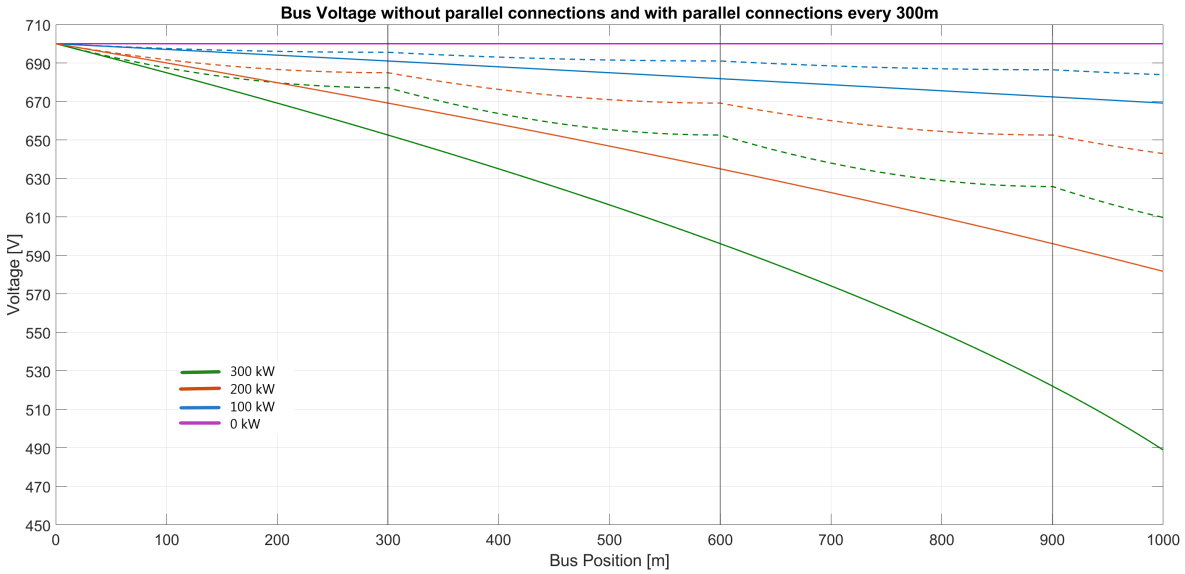

Figure 4.43: Voltage drop along a power supply section in function of bus power and distance from the supply point (0m) with and without parallel connections every 300m, in dashed and solid lines respectively

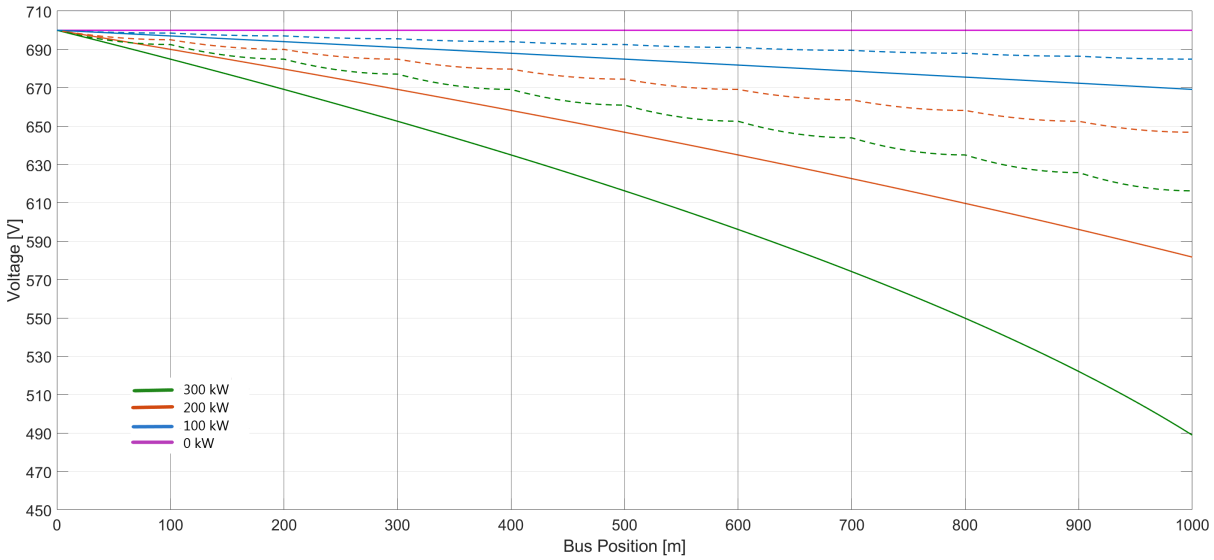

Figure 4.44: Voltage drop along a power supply section in function of bus power and distance from the supply point (0m) with and without parallel connections every 100m, in dashed and solid lines respectively

By looking at the figures, it is evident how the voltage drop along the lines is strongly affected by the presence of these connectors through the overhead grid. This is true especially for high powers and long distances, where in percentage the voltage drop is reduced up to 26% at 1000m distance from the supply and 300kW power demand, in this scenario (1000m section length and 700V). If the voltage is reduced to 680V for instance the voltage increase is of 32.5% at 1000m distance from the supply. At 1150m distance from the supply point and 700V supply voltage, the difference between the two bus voltages reaches 45.5%! This also means that the section length can be increased if lines are connected between them.

Another thing that can be observed by looking at Figure 4.45, that the reduction of the distance between subsequent contacts reduces the voltage drop even further. This is due to the fact that with an increase of the space between two connections, the bus distance from a connection is on average higher. For instance, if lines are connected every 100m the bus would find its self at 50m max from one of the connections. While if lines are connected every 300m the bus can arrive to be up to 150m away from one of the connections. The proximity of two subsequent connections increases the benefit of this

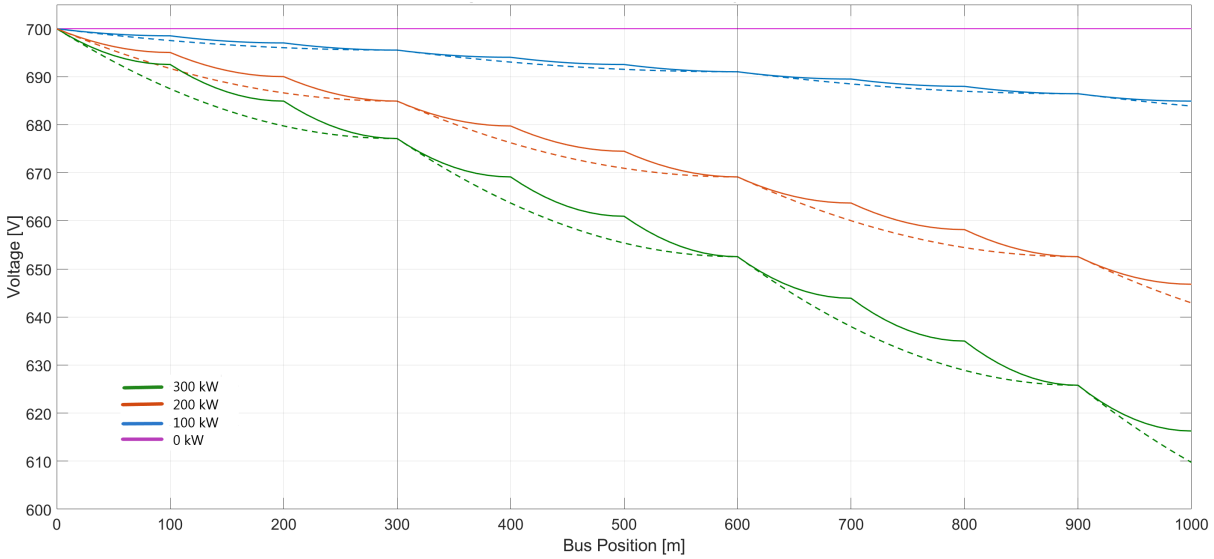

Figure 4.45: Voltage drop along a power supply section in function of bus power and distance from the supply point (0m) with parallel connections every 100-300m, in solid and dashed lines respectively

application, allowing a larger fraction of l_{total} to be in parallel. The higher is the ratio between $l_{parallel}$ and l_{total} the lower the transmission losses will be.

4.6.2 Approximation used in the simulation and consequent error

After understanding the reason why parallel lines are introduced and the benefit that they have on the system, the analysis on the error committed due to the approximation used to compute the bus voltage is discussed. Two different approximation methods are tested: Total distance approximation and Total current approximation. Both have the goal to simplify the calculations and reduce the simulation time and both introduce additional assumptions on the part of the section where the bus can be found, namely on the current passing through l_{single}.

Total distance approximation

In this approximation the bus is considered to be at distance l_{total} from the supply point and $l_{parallel}$ is considered to be equal to l_{total}. If we look at equation 4.37, the third term containing l_{single} is neglected and in the second term $l_{parallel}$ becomes now l_{total}. This means that no distinction is made between the sections in which the lines carry the same amount of current (half of the total if 2 lines are connected in parallel) and the last fraction in which the bus is, between two connections. In Figure 4.46, a representation of how the equivalent circuit looks like for this case is given.

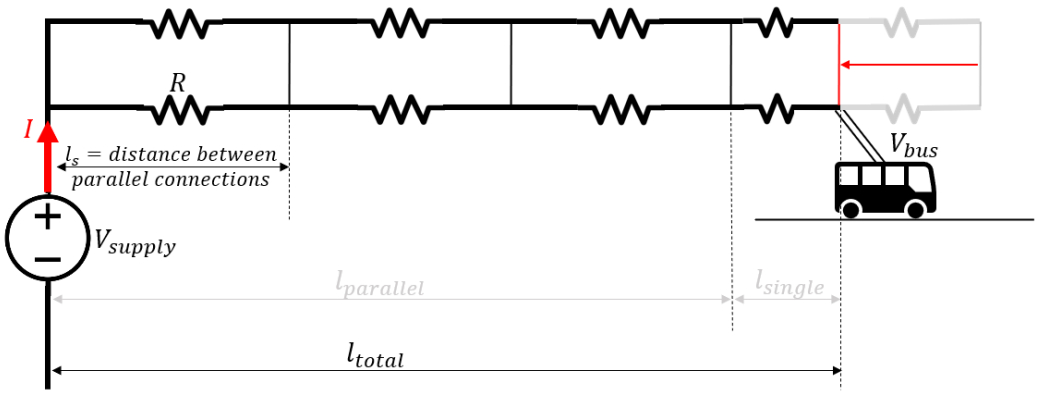

Figure 4.46: Electrical representation of the Total distance approximation method (own work)

Making use of the same equations used to derive the actual bus voltage, this model be re-derived. In equation 4.42 the voltage from Kirchhoff's voltage law to find the bus voltage approximation, and in 4.43 the same expression but in function of bus power instead of bus current.

$$V_{bus} = V_{supply} - 2 * \frac{R}{2} * l_{total} * I \tag{4.42}$$

$$V_{bus} = \frac{V_{supply} + \sqrt{V_{supply}^2 - 4 * P_{bus} * R * l_{total}}}{2} \tag{4.43}$$

Total current approximation

In this approximation the bus is considered to be at distance l_{total} from the supply point and $l_{parallel}$ and l_{single} are still present and defined. However, the third term of equation 4.37 is modified, because the current is assumed to be passing all through l_{single} and not through the upper line as well. A representation of this situation can be found in Figure 4.47.

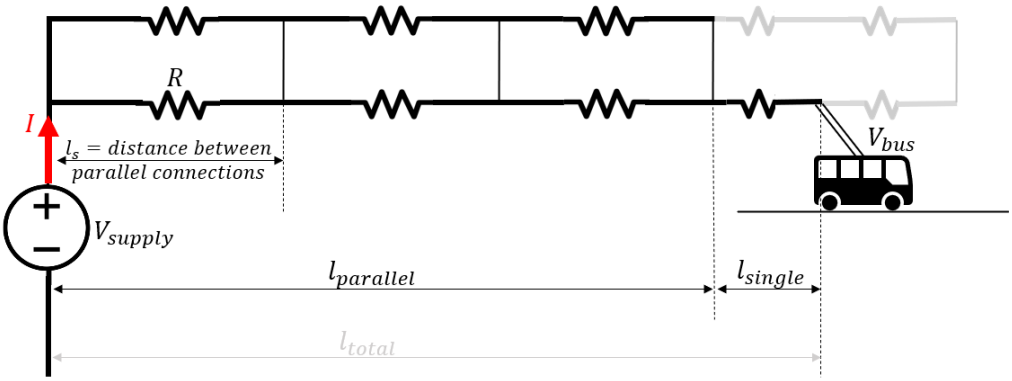

Figure 4.47: Electrical representation of the Total current approximation method (own work)

Again, using the same methods, the bus voltage can be derived and in 4.44 the voltage from Kirchhoff's voltage law in 4.45 the same expression but in function of bus power can be found respectively.

$$V_{bus} = V_{supply} - 2 * \frac{R}{2} * l_{parallel} * I - 2 * R * l_{single} * I \tag{4.44}$$

$$V_{bus} = \frac{V_{supply} + \sqrt{V_{supply}^2 - 4 * P_{bus} * R(l_{parallel} + 2l_{single})}}{2} \tag{4.45}$$

When simulating the grid operations some assumptions are made in order to reduce the running time of the code. However, when including approximations and assumptions, it is good practice to know the effect that these have on the results. For this reason, in this subsection the error introduced when approximating the calculation of the bus voltage along the line is analysed. Different grids have different supply voltages, section lengths and different distances between parallel lines connections. Moreover, the bus power and the bus distance from the supply points are continuously changing. These elements are taken into consideration to have a general overview of the effects that the approximation on the voltage has on the results. In particular the voltage drop will be analysed with varying bus power, bus position along a section and the distance between two subsequent connections following the intervals indicated in Table 4.16 (in which EoS stands for End of Section). Section length and supply voltage are also variable, but are fixed prior simulation.

As seen in the previous paragraphs the bus voltage is what is calculated differently, the equations used to compute the actual bus voltage and the total distance approximation bus voltage are 4.40 and 4.43 respectively. From these two equations the error is computed as:

$$Error[\%] = \frac{V_{bus} - V_{bus-aprx}}{V_{bus}} * 100 \tag{4.46}$$

Table 4.16: Parameters involved in the parallel lines approximation analysis and their variation range

Parameter	Variation Range
P_{bus} = Bus Power	[0:20:300] kW
l_{total} = Bus Position	[0:10:EoS] m
Distance between //	[100:50:300] m

We will now go through the results obtained and analyse the impacts of the parameters variation on the error. The simulated section is a section in Arnhem grid, with substation voltage of 716V and 1300m long. This section has been chosen because of its length. The supply point in very long sections is usually placed in the middle in order to reduce transmission losses and voltage drops. The supply voltage effect on the error is also assessed at the end of this subsection the reader can find the results for the total distance approximation.

When looking at the maximum errors committed with the two approximations analysed, shown inn Figure 4.48, it is possible to see that the Total distance method is a better approximation to use. It performs almost 5 times better than the Total current method and therefore, the analysis on the Total distance approximation and its error are only discussed. This method of calculating the voltage drop when parallel connections are introduced is also the one that is used in the grid models. In Appendix C, the reader can find some plots showing the results of the other approximation.

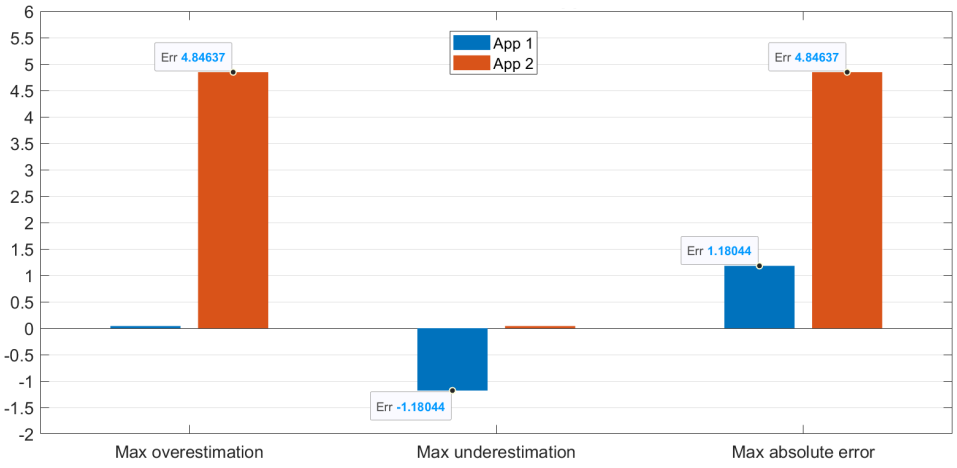

Figure 4.48: Maximum errors introduced when simulating the operation of one bus moving along a section with parallel connections. Both approximations are shown

Although only the *Total distance* approximation is analysed, in Figure 4.49 the voltage drop as a function of the distance from the supply point and with different bus power requirements is plotted also for the *Total current* method. One can compare the results obtained with the two approximations:

- Both approximations have a linear variation of the voltage in relation to the position of the bus
- Total distance approximation varies linearly only with the total distance of the bus and is not affected by the variation of the position of the parallel connections
- Total current approximation varies linearly with the distance of the bus with respect to the position of the connection between the lines that immediately precedes the bus and with respect to the total distance from the supply point
- No approximation takes into consideration the connection that is following the bus position, which is considered in the actual bus voltage calculation

Total distance approximation error analysis

Starting from the first parameter in Table 4.16, the effect of increasing bus power on the error of the approximation is assessed. In Figure 4.50 the error of the approximation is plotted against the distance of the bus from the supply point. Each of the represented curves have different bus power requirements

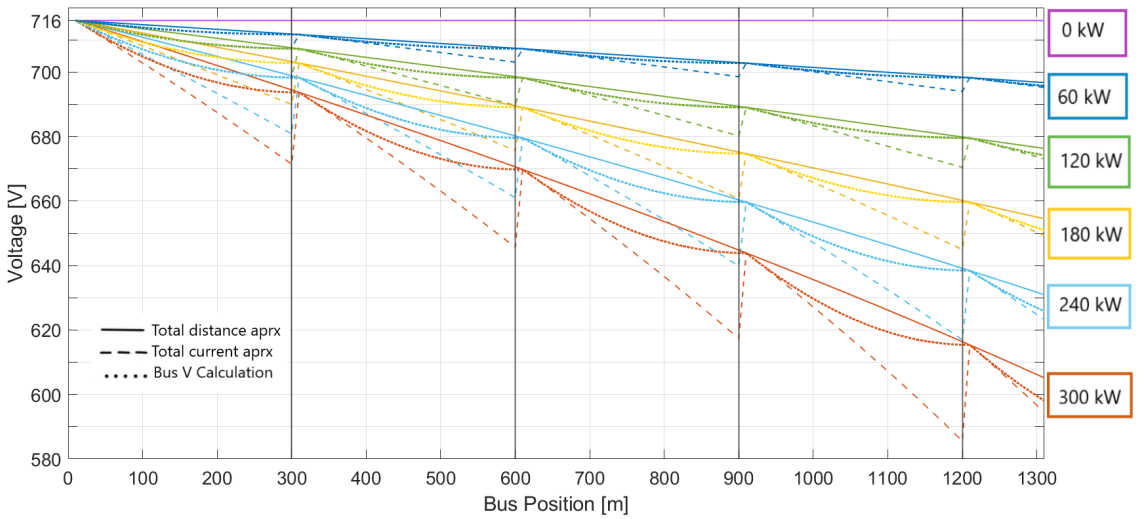

Figure 4.49: Voltage drop along a power supply section in function of bus power and distance from the supply point with parallel connection every 300m. Actual voltage drop in dotted line, total distance approximation of the bus voltage in solid and total current approximation in dashed.

ranging from 0 to 300kW as indicated in Table 4.16. The plotted curves are all referred to the scenario in which the connections between the lines are located at 300m one from the other. This scenario is represented because the variation in the error is more visible than in the other conditions and since the error here reaches its maximum. However, in Appendix C the reader can find the plots of the power variation effect also for the other tested distances between the parallel connections.

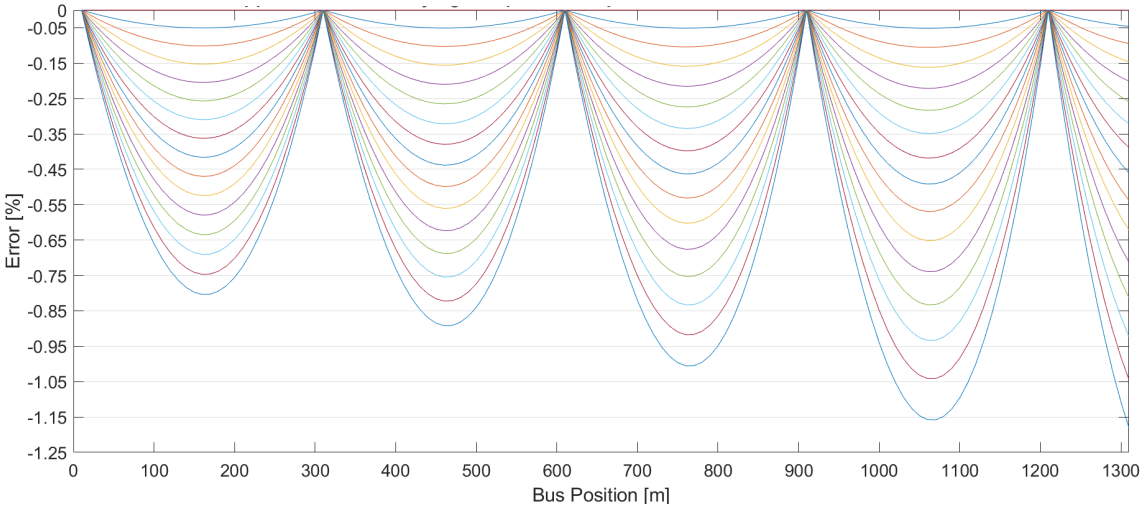

Figure 4.50: Error introduced using the total distance approximation of the bus voltage, plotted as a function of the distance from the supply point (0m), with parallel connections every 300m. Increasing power requirements are shown, with every curve representing a power demand

It is possible to see from Figure 4.50 that the error in the approximation is increasing with the increasing voltage drop. The Total distance model approximates better the actual bus voltage when the bus power is limited and when the bus is positioned close to the supply point. With increasing distance from the supply and electric power requirements, the voltage drop and the transmission losses increase (as previously discussed and as shown in Figure 4.41), and the approximation also performs worse.

We have discussed that with increasing distance from the supply point the error committed by introducing the approximation increases. However, as one can notice from Figure 4.50, there are points along the line in which the approximation method has 0% error and matches with the actual bus voltage calculation. These points are where the compensatory connections between the lines are located: in this example this happens every 300m. By looking at Figure 4.51, one can see how the error goes to zero when the bus position is equal to the location of one of the parallel connections. This is visible

also when looking at the voltages in figure Figure 4.49. This result is expected from this approximation, since the total distance model considers that at every point the bus is fed by perfectly connected in parallel cables. This means that according to this model, at every point of the line the bus is finding a compensatory connection with the other traveling direction cable, which in reality it is only true every 100-300m.

It can be already concluded, by what discussed so far and by the graphs analysed, that this approximation **always underestimates** the voltage drop.

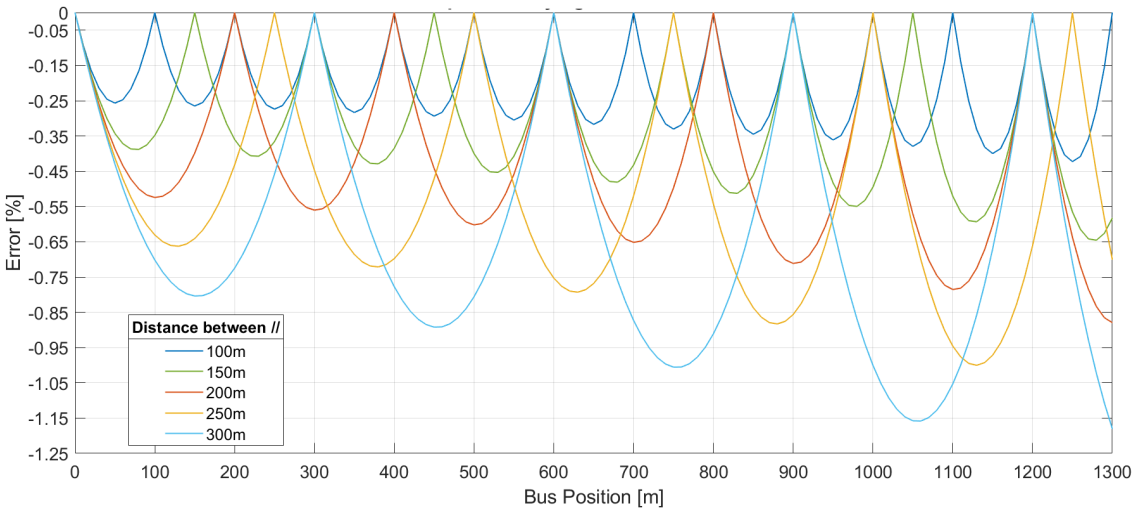

Figure 4.51: Error introduced using the total distance approximation of the bus, plotted as a function of bus distance from the supply point (0 m) and of varying distance between parallel connections - at 300 kW power requirements

Focusing on the distance between parallel connections, referring to Figure 4.51, the error is increasing with increasing distance between the lines. Again, the higher the voltage drop the higher the error. Finally, by picking a random point in the supply section, it is possible to demonstrate that not only the absolute position of the bus plays a role but also its relative position within each fraction of line between to subsequent connections. Although the error is higher overall if the distance between the parallel connections is longer, based on the relative position of the bus within two connections it can happen that this is not the case. As an example, 700m distance from the supply point is taken. In Figure 4.52a and 4.52b one can see where this point is located along the 1300m supply section and where is is relatively located within two parallel connections. When the bus is at 700m distance from the supply, the error in the approximation is lower for the case in which parallel connections are at 250m one from the other rather than in the case in which they are at 200m from each other, as shown in Figure 4.52c.

To conclude this analysis, a research on the effects of varying the supply voltage is performed. The reduction of the line voltage causes the overall increase in current for the same power requirements of the bus and therefore and increase in transmission losses and in the voltage drop. Moreover, if the same voltage difference between the approximation and the actual value is found at lower voltage levels, this will have in percentage a higher error. Therefore, it is expected that at lower voltages the error in the approximation will increase. This is confirmed by the simulations and is represented in Figure 4.53

4.7 Summary and takeaway points of the chapter

In Figure 4.1, the model structure is presented. A lot of **data is necessary as input** to the models, and it is summarised in the white parallelograms. In the flow diagram the model components are presented and the connections between them are shown. Three main modelling groups can be identified:

- **Load model**
  Formed by:
  - Bus load model: HVAC model, velocity generator model and power profile generator model (HAN University model)
  - Yearly grid operation model
  - Section power model
- **PV generation model**
- **PV and storage integration model**

The modelling of storage is functional to the analysis of the integration of PV in the trolleygrid. For this reason, this model is considered to be part of the third component and does not represent a model itself. Moreover, the storage element is simulated (storage model flow diagram in Figure 4.28) without going into detail in the internal electrochemical processes, while the PV model proposed accurately **estimates the PV** module temperature through a **fluid-dynamic thermal model** and its generation through an **efficiency model**, both function of meteorological data.

In order to study the integration of PV in trolleygrids, it is necessary also to derive the power profile of the substations **throughout the year**. This is done by **simulating the bus operation** in the grid and on **every section** of the catenary in the grid. In order to simulate the yearly grid operation, the bus power profiles are generated through a combination of three models: velocity profiles generation, traction power profile generation and HVAC demand.

Velocity and power profiles are created for the two directions of all the lines of Arnhem and Gdynia system. In Figure 4.19 the flow chart explaining the process to associate the velocity cycles to the stops. Once the traction power is obtained from the velocity profiles and the HAN University power model, the yearly operation of the grid is simulated based on the scheduled runs. The HVAC demand is added based on the time of the year in which the bus is running. This is formed by a duty-cycle with varying duration based on the HVAC requirements. These are simulated through an energy balance model.

The last steps are the creation of **section yearly power profiles** and the integration of PV and storage model. The former is done through the generation of section schedules, so based on the movements of buses under the specific section. The **PV and Storage integration** model is the combination of the previous models, integrated together based on the substation of interest.

In the last section of the chapter, an analysis of the error introduced in the model due to the approximation of the voltage drops in presence of **parallel connections** along the overhead lines is provided.

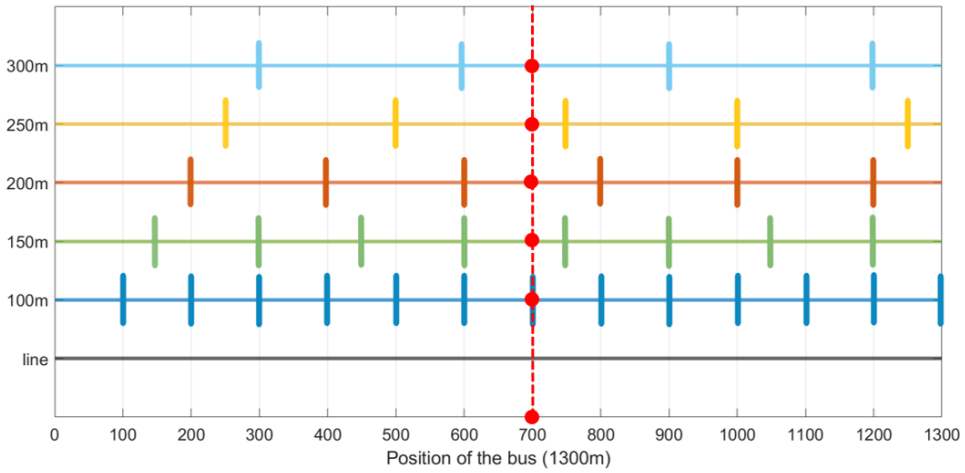

(a) Characteristics of the position based on the distance between parallel connections along the line

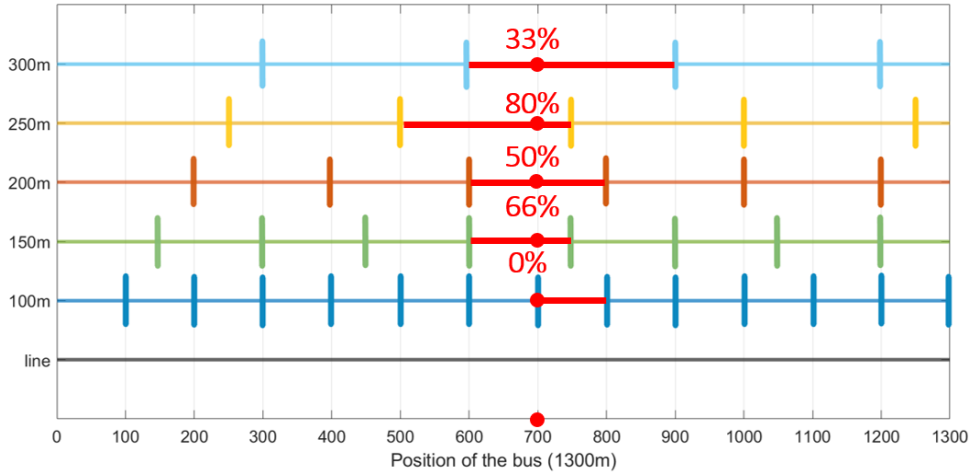

(b) Fraction of section between two subsequent parallel connections travelled by the bus

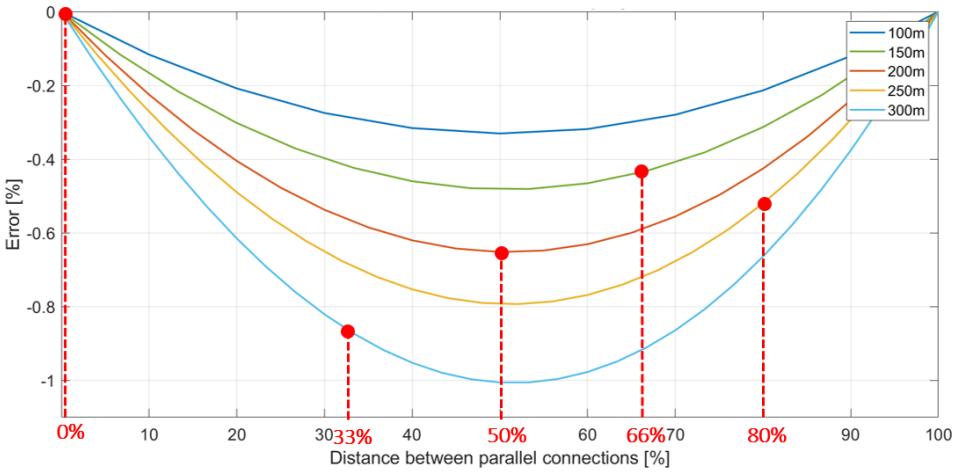

(c) Error variation in relation to the position of the bus between two subsequent parallel connections

Figure 4.52: Error introduced using the total distance approximation of the bus voltage, varying in relation to the position between two subsequent parallel connections. Example: bus at 700m from the supply point.

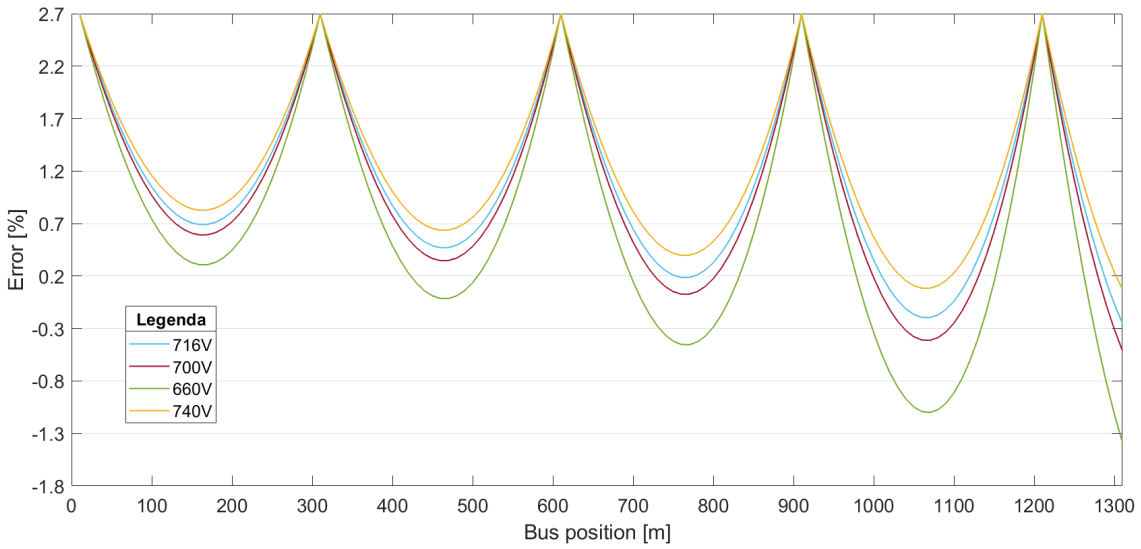

Figure 4.53: Error introduced using the total distance approximation of the bus voltage as a function of bus distance from the supply point (0 m) and supply voltage, at 300 kW power requirement and with parallel connections every 300m

5 RESULTS: GRID OPERATION AND PV INTEGRATION POTENTIAL

In this chapter the results of the simulations are analysed and discussed. Before analysing the impact of the KPIs (selected in Chapter 3) on the results obtained for PV integration in the two trolley grids (Gdynia and Arnhem), the results of the yearly operation of the two systems are compared. The effect of the Indicators on the PV potential is then analysed and some examples are proposed.

5.1 Substations of Arnhem and Gdynia: Yearly operation results

Before discussing the results found on the potential of integrating PV in the two grids, an overview of the structure of the two grids and of the results obtained from the simulation of the yearly operation of the two systems is given. In the previous chapters, the traction grids have already been described based on the data available for the two (see Table 3.1 and the relative section in Chapter 3). However, the aim of this section is to provide the reader with the data obtained from the simulations and with the required information on the substation to evaluate the performance of PV integration. The information on the grid that can be found in the paragraphs below is related toç

- Energy and power demand
- Bus traffic
- Section number and section length
- Transmission losses
- General grid configuration

A summarising table with a comparison between the grids and their substation configuration is given at the end of the section in Table 5.3.

Arnhem DC trolleygrid
Arnhem trolleygrid is formed by 18 substations, feeding 1 to 5 sections each, for a total of 43 sections. From the simulations, 42 buses are found to be necessary to cover all the bus runs in the grid. These data are summarised in Table 5.3. Due to their position in the city and to the distribution of the traffic the sections are characterised by different power and energy requirements. As a consequence, the substations vary in size based on the location and traffic conditions of the sections they supply. In Table 5.1, the outputs of the model for the substations of the Arnhem trolleygrid are summarised. The total energy demand of the grid is 5.8 GWh and is distributed in 18 substations, with an average yearly energy demand of 324 MWh. Arnhem substations present an average of 6.5% transmission losses, lower than the average value found for trolleybus grids of 10% [54]. The distribution of the load in smaller substations placed closer to the sections that they are supplying allows to reduce the transmission losses, due to the proximity of the substations to the feed-in points on the catenary. The overhead lines are covering in total almost 50km with only 42 buses. This leads to a spread of the bus traffic in the grid and to low traffic levels in the different sections. The average number of buses simultaneously having a power requirement under the same substation is 1. Also, 50km are covered by 44 sections, which gives an average of 1.1km length for each section. These characteristics contribute to the low transmission losses: low traffic levels induce low currents, while short sections offer low resistance paths. Having low traffic levels, though, causes low utilization of regenerated braking energy, due to the absence of other buses on the same section, which therefore must be burnt in braking resistors. For this study

buses are considered to be exchanging power only within the section and not with all the buses in the sections supplied by the same substation. This is an assumption made due to the uncertain values of the substation voltages and must be kept in consideration at all times.

Table 5.1: Substation simulation outputs and characteristics - Arnhem

Substation Number	Supplied Sections []	Energy [MWh/year]	Substation Losses [%]	Yearly Av. # of buses	Max # of buses	Av. Supplied Section length [km]	Total Substation km covered
1	2	168	6.19	0.5	3	1090	2180
2	3	412	6	1.2	6	1113	3340
HQ (3,6)	4	912	7.51	2.8	10	1113	4450
CS (4,9,21)	5	928	3.51	4.6	14	468	2340
5	3	209	5.7	0.6	4	993	2980
7	2	236	5.46	0.8	2	1330	2660
8	2	208	6.71	1	3	2255	4510
10	1	157	7.41	0.5	3	1590	1590
11	2	287	6.08	1.3	5	1175	2350
12	2	216	5.03	0.7	3	1125	2250
13	2	212	5.22	0.5	3	1035	2070
14	3	470	6.16	1.1	5	1203	3610
15	2	270	7.52	0.8	3	1545	3090
16	2	338	4.22	1.1	4	985	1970
17	2	257	4.47	1	3	1050	2100
18	2	81	5.71	0.2	1	1155	2310
19	2	175	7.25	0.8	2	1325	2650
20	2	306	7.42	1.1	5	1595	3190

Gdynia DC trolleygrid

Gdynia trolleygrid is formed by 10 substations, feeding 1 to 6 sections each, for a total of 30 sections. From the simulations, 84 buses are found to be necessary to cover all the bus runs. Due to the positioning and the characteristics of the sections around the city, as for Arnhem, different sections and different substations are characterised by traffic levels and different power and energy demand. An overview of the outputs of the yearly operation model is given in Table 5.2 for each substation in terms of power and energy requirements, number of sections supplied, average and maximum number of buses simultaneously under the substation, and the km covered by the overhead lines at section and substation level. The total energy demand of the grid, 7.5 GWh, is subdivided over 10 substations which, on average, have a yearly load of 745 MWh. Just by looking at this data, it is possible to conclude that the decentralization characterizing Arnhem grid is not found in this traction system also. Although the total energy requirement of Gdynia grid is by 30% higher than that of Arnhem system, at substation level the average load is actually double of that found in Arnhem. The higher number of buses, consequence of the higher number of bus lines (12 against 6) and bus runs, together with the lower number of substations cause the traffic levels of the Polish grid to be noticeably higher with an average of 3 buses simultaneously operating under the same substation. The higher traffic levels and the more centralised structure of the grid, cause the transmission losses to increase, with an average of 8.5% at grid level, higher than in Arnhem by 2 percentage points. Also, the number of sections in which the overhead lines are divided into is lower, 30 compared to 43 in Arnhem. Although the total amount of km is lower in Gdynia, 40km, the section lengths on average are found to be 1.3km, and therefore higher than for Arnhem. However, the increase in traffic levels and section lengths could be a positive feature when considering the energy braking recovering rates, due to the higher probabilities of finding buses on the sections.

Based on the review of existing literature on DC traction grids and based on the results obtained, some conclusions can be drawn in relation to the performance of the grids and some predictions can be made on the potential of PV integration in the systems of the two cities. The higher traffic levels coupled with the lower level of decentralization in the Gdynia trolley grid cause higher transmission losses but also could allow the increase in regenerative power utilization. The same factors are expected to have a positive effect also in terms of PV utilization. As concluded in [12], higher traffic and enlarged supply areas are increasing the chance of the buses to be located under substations supplied by PV generated energy. In the next section the results of this study related to PV integration in the grid are discussed

Table 5.2: Substation simulation outputs and characteristics - Gdynia

Substation Number	Supplied Sections []	Energy [MWh/year]	Substation Losses [%]	Yearly Av. # of buses	Max # of buses	Av. Supplied Section length [km]	Total Substation km covered
1	6	905	9.1	3.3	9	1423	8540
2	3	1298	8.9	6.6	18	1150	3450
3	3	616	9.3	2.7	11	1007	3020
4	3	867	7	3.4	12	900	2700
5	3	686	6	3.2	10	793	2380
6	3	1301	9.1	4.7	14	1717	5150
7	2	268	8	0.9	5	2100	4200
8	1	54	4.1	0.5	3	1100	1100
9	1	310	7.2	1	6	1370	1370
10	5	1136	9.2	4.3	12	1393	6965

further. These results will allow to quantify the impact of traffic, section length and centralization on the PV integration and its feasibility.

Table 5.3: Comparison of the data outputs for the two grids - simulation results

Parameter	Gdynia (Pl)	Arnhem (Nl)
Number of Bus Lines	12	6
Number of buses	84	54
Number of sections	30	43
Number of Substations	10	18
Section/Substation ratio	3	2.4
Bus/Section ratio	2.8	1.0
Bus/Substation ratio	8.4	2.3
Average bus traffic per substation	3.1	1.1
Total Energy demand [GWh]	7.5	5.8
Average substation energy demand [MWh]	745	324
Average substation transmission losses [%]	8.5	6.56
Length of the grid [km]	39	49
Length of sections - average [km]	1.3	1.1

5.2 PV integration in trolleygrids - the effect of the KPIs

The aim of this section is to provide the reader with the results related to the integration of PV in the trolleygrids. The PV systems are placed on the AC side of the substations in order to allow the excess PV generation to be sent back to the AC grid without curtailing. 'Curtailment' refers to the action of restricting or denying the flow of generated energy, resulting in the decrease of a plant's output. This would be necessary if the PV system is installed on the DC side. In fact, substations in trolleygrids are usually unidirectional, which means they are characterised by unidirectional diode rectifiers that do not allow to send energy back to the medium voltage grid [51,64], as discussed in Chapter 2. Therefore, placing the system on the DC side would not allow to send the excess back to the MVAC grid. An analysis is performed on every substation of the two traction grids, Arnhem and Gdynia, to find their performance in terms of PV Utilization and Load coverage. This will be further explained in the following subsection while discussing also how the PV sizing is done. After this the effects of the KPIs (identified and selected in Section 3.3 of Chapter 3) is studied. Finally, three illustrative comparisons between different substations are presented followed by an overall evaluation of the performance of the two grids.

5.2.1 PV Utilization, Load Coverage and PV system sizing

The indicators identified and used to analyse the variation of the potential of integrating a PV system in a specific substation are:

1. PV Utilization
   This factor represents the percentage of solar power which is directly used to cover the load of the trolleygrid (5.1), and can be computed as:

$$PVU = \frac{\int_t P_{\text{load}} - P_{\text{grid}}\, dt}{\int_t P_{\text{PV}}\, dt} = \frac{\text{Load Covered with PV}}{\text{Yearly PV Energy}} \tag{5.1}$$

   with P_{load} the total load power demand, P_{grid} the AC grid power demand and P_{PV} the PV generated power.

2. Load Coverage
   This factor is the fraction of the load that can be supplied by the direct output of the PV system, and it can be calculated with through the following equation:

$$LC = \frac{\int_t P_{\text{load}} - P_{\text{grid}}\, dt}{\int_t P_{\text{load}}\, dt} = \frac{\text{Load Covered with PV}}{\text{Yearly Load}} \tag{5.2}$$

   with with P_{load} the total load power demand and P_{grid} the AC grid power demand.

These two factors are used to give an indication the effectiveness of PV integration, both in using the PV generated power and in covering the load. They are both computed for all the substations of the two grids while varying the PV capacity installed between 50kWp and 800kWp. These limits are introduced to have a range in which the installation would be realistic and feasible. Installing less than 50 kWp, would mean that a very small fraction of the load is covered, as will be demonstrated by looking at the next plots and as seen in [54]. Installing more than 800kWp would not be feasible in terms of space requirements, but also would drastically reduce the utilization of the PV generated energy. In Figure 5.1a and Figure 5.1b, the PVU and the LC for 2 substations are shown. Substation 2 and 9 of the Gdynia grid, plotted in the two figures, differ by size, number of bus runs and schedules, number and length of the supplied sections, road gradients, temporal match between load and generation, etc.. These elements may all play a different role on the effectiveness of integrating PV and should be isolated and analysed separately. Substation 2 and 9 of the Gdynia grid exemplify the typical PVU and LC curves for large and small substations.

Another parameter used to assess the potential of the PV system integration, is the fraction of time in which the PV generated power is able to cover the load. This parameter is proposed in terms of total and partial (20%) coverage of the load. This will be used mainly to compare the performance of PV installed in different substations and the overall potential of PV integration in Arnhem and Gdynia grid. The fraction of time in which the PV generation covers the load is computed as:

$$F_{\text{PV}\rightarrow\text{Bus}} = \frac{t(P_{\text{PV}} >= P_{\text{load}})}{3600 \cdot 24 \cdot \text{Days in a year}} \tag{5.3}$$

This indicator represents the time in the year in which there is a load and this load can be partially or totally covered by PV generated energy. The fraction is computed over the total year length. It combines the fraction of time in which there is a load and the fraction of time in which the load is covered in one unique indicator.

In order to proceed with the analysis, the PV systems have to be sized for each substation. The sizing can be done either based on power or on energy requirements. The energy yield sizing method is excluded for this study, due to the fact that using this method the temporal mismatch between generation and load is completely neglected. Accounting only for yearly yields means comparing the yearly energy generation and demand, without accounting for any temporal distribution of the two. Therefore, it could be possible that the power requirement is very low and constant throughout the year or very high in some months and very low in others, and this would not be taken into account. The

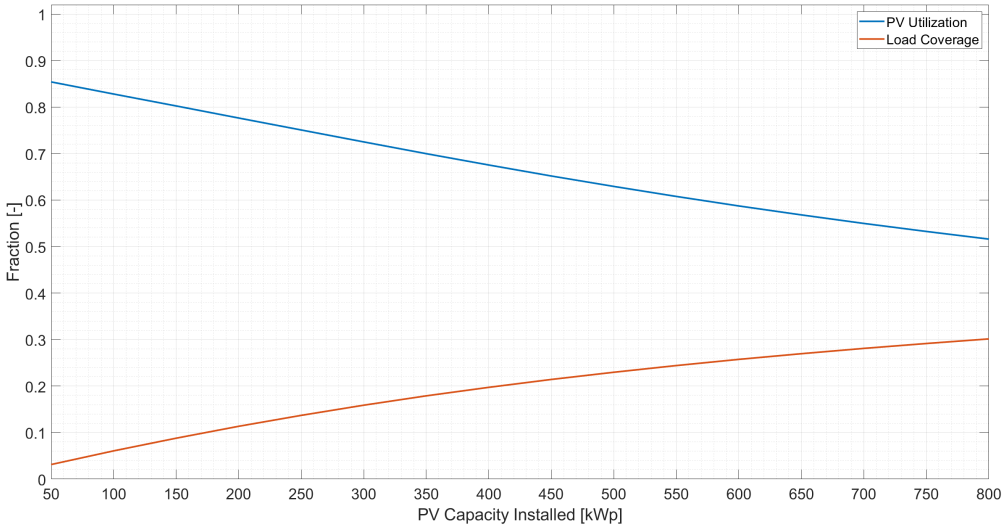

(a) PVU and LC curves for Substation 2 in Gdynia grid (Yearly demand 1298 MWh)

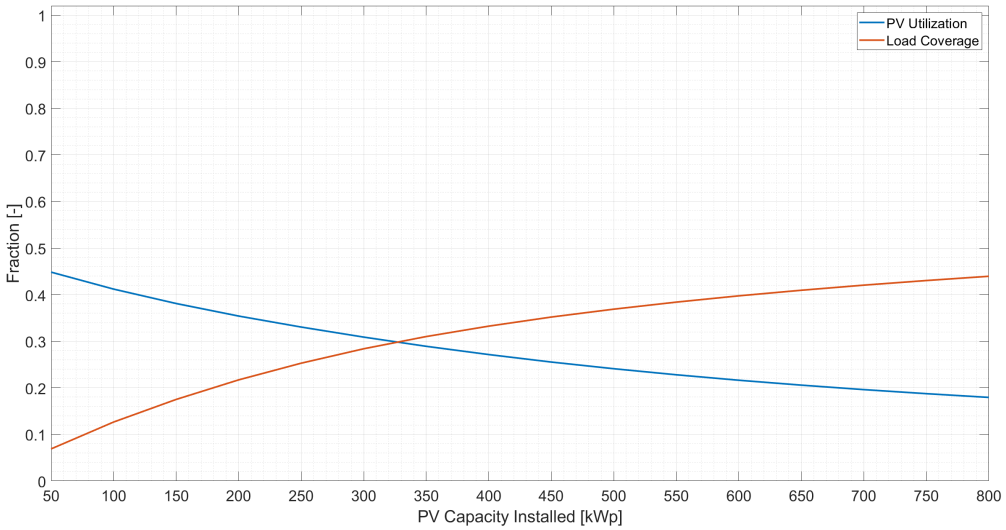

(b) PVU and LC curves for Substation 9 in Gdynia grid (Yearly demand 310 MWh)

Figure 5.1: Comparison between PV Utilization (PVU) and Load Coverage (LC) in substations of different sizes

same for the PV generation. Since PV generation and load vary considerably during the year because of the variance in irradiance and temperature levels, it is imprecise to compare them in terms of yearly energy. The sizing of the PV systems for each substation is done based on the power demand and the installed PV capacity is calculated as:

$$P_{\text{PV}} = \frac{\overline{P_{\text{load}}}}{0.25} = \frac{\text{Yearly Average Power}}{\text{Capacity Factor}} \tag{5.4}$$

Where 0.25 represents the average capacity factor for utility scale PV systems around the world [21]. In this paper, an analysis of the capacity factor for utility scale installation is proposed. The capacity factor varies in relation to the location, the size of the system and the DC to AC inverter ratio. This value of 25% is taken as an average of the values proposed in [21]. Once the sizes of the PV systems are identified for every substation, the PV utilization and the Load Coverage for the given installed PV capacity are found from the curves previously generated. In Table 5.4 the data can be found for all the substations of both grids. The size and PVU and LC found are used to evaluate the effects of certain parameters on the effectiveness and feasibility of applying PV to supply the traction substations. These

parameters are the Key performance Indicators identified and selected in Chapter 3. In the previous paragraphs, the explanation of how the sizing is done for all the substations is provided together with the outputs: PV capacity, PVU and LC for each substation. Now, these data are used to study the impact of the KPIs on the PVU and on the LC. Does the KPI impact the PVU? Does it impact the LC? What effect does the KPI have on PVU and LC?

Table 5.4: PV size for all the substations (Arnhem indicated in green and Gdynia in red) with the respective values of PV Utilization (PVU) and Load Coverage (LC)

Substation Number	PV capacity [kWp]	PVU [-]	LC [-]
8	25 (< 50)	-	-
18	38 (< 50)	-	-
10	73	0.318	0.1243
1	78	0.3022	0.1195
19	82	0.3526	0.1398
8	97	0.3778	0.1533
5	97	0.3298	0.1338
13	99	0.2801	0.1145
12	100	0.3852	0.1564
7	110	0.3992	0.1616
17	119	0.4194	0.1686
7	122	0.4231	0.1799
15	126	0.3981	0.1611
11	133	0.4524	0.182
20	142	0.4252	0.1721
9	141	0.3871	0.1653
16	157	0.4139	0.1686
2	192	0.4686	0.1915
14	218	0.4596	0.1872
3	280	0.5077	0.2175
5	312	0.55	0.2363
4	395	0.5761	0.248
1	412	0.5749	0.2473
HQ (3,6)	424	0.6071	0.2486
CS (4,9,21)	432	0.6248	0.2561
10	517	0.6296	0.2709
2	591	0.5914	0.2547
6	592	0.6327	0.2725

The analysis is organized in subsections based on the KPI that is being studied, to follow the order of the sub-questions of research question number 2, identified in Chapter 1. Therefore, the impact of environmental parameters is studied first. Then the effects that the substation configuration in terms of section number, length and power requirements is assessed, followed by the analysis of the impact of bus traffic, HVAC requirements and presence of bilateral supply on the potential integration of PV in trolleygrids.

5.2.2 KPIs Study: Environmental-related parameters

In order to assess the impact that the climate has on the potential of PV integration in the trolleygrid of a city, an analysis is conducted on the effects of relocating the grids in a city with a different climate. The idea is to keep the load constant and change the generation to see the effects that this has on the PV Utilization and on the Load coverage. To do this, the traction power is used, in this way the load is completely independent from the environmental parameters. The HVAC is set to zero and the grid operation is simulated neglecting the heating, ventilation and air conditioning loads, but including extra auxiliaries as lighting, screens and ticket validation machines. Therefore, the demand side does not depend on the environmental data. Four different sets of environmental data are used, based on

the weather data of cities in which trolleygrids can be found. The cities used in this study are: Gdynia, Arnhem, Szeged and Athens.

To compare the results of PV integration when varying the location of the grid, the PV size has to be fixed based on the load only, therefore, the size of the solar system is found based on power requirements rather than on energy requirements, as per Equation 5.4. In this way, the size of the PV system installed is kept constant in all the cities with different climates and the outputs of this system are compared in relation to the effectiveness in supplying the traction load. The PV capacity installed is calculated based on the traction power instead of the total power demand for this analysis. The idea is to relocate the grid, ans therefore maintain the same characteristics in terms of city and trolley-system and move them in a different location, characterised by different daily sun hours and different irradiance levels. Keeping constant all the other KPIs, therefore all the variables that can affect the load and its matching level with PV generation, the impact of the environmental-related KPIs can be assessed.

The results analysed here are the ones coming from the simulations of the Gdynia trolleygrid. Due to the close similarity of results in terms of environmental analysis, Arnhem is only briefly shown at the end of the analysis. The study performed and the conclusions drawn are valid for both cities and are based on the observation of both.

In Figure 5.2, the curves of PV utilization and load coverage for a substation in Gdynia (number 2) are plotted for varying environmental data. In solid line the simulation with Gdynia weather data, dashed Arnhem data, dotted Athens data and dot-dash line Szeged. From the plot, the different variation rate between the PVU and the LC can be seen. The load coverage is very similar between Gdynia and Arnhem, however it presents large variations when moving the traction system to Athens or Szeged. The PVU on the other side, presents narrow variations for all the cities.

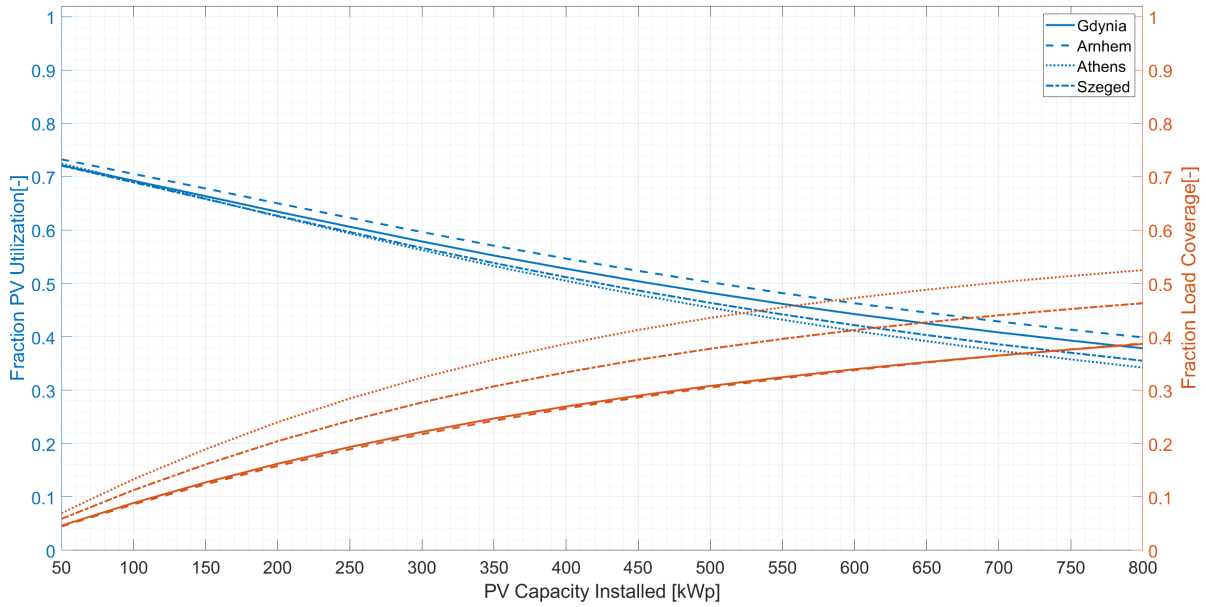

Figure 5.2: PV Utilization and Load Coverage variation with varying environmental data and PV generation (Substation 2 of the Gdynia grid, environmental data of: Gdynia, Arnhem, Athens and Szeged)

In order to analyse the impact that the weather has on the potential of PV integration in traction grids, the variation of PVU and LC is analysed for a fixed PV capacity when varying the city. In Figure 5.3 and 5.4, the PV utilization and the load coverage are plotted as function of the average yearly radiation $[W/m^2]$ and the average daily sun duration. The dimension of the bubbles in the graph quantifies the median value of PVU and LC for all the substations in Gdynia. It is possible two notice that the PVU median value is not affected noticeably by the variation of environmental data. On the other hand the LC varies by more than 10 percentage points. Also, the utilization of PV energy is reduced while increasing average sunshine duration and radiation while the load coverage increases.

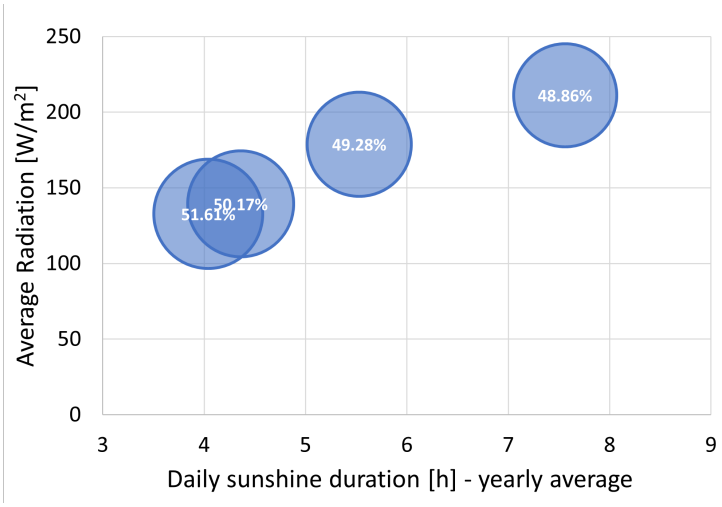

Figure 5.3: PV Utilization median values for Gdynia substations plotted as a function of Average Radiation and Sunshine duration

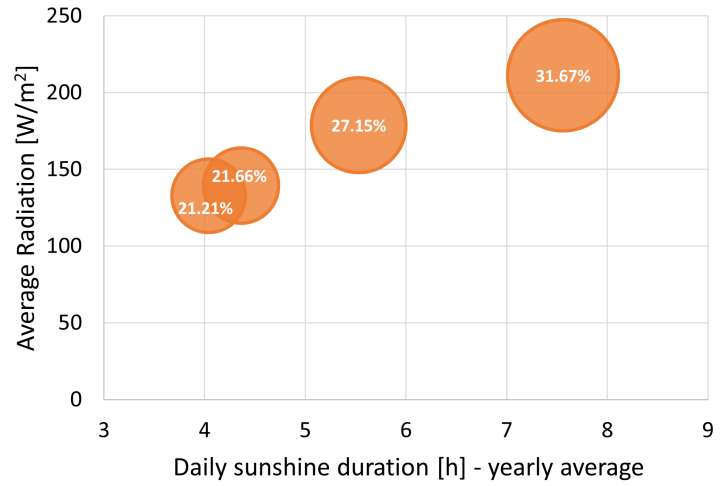

Figure 5.4: Load Coverage median values for Gdynia substations plotted as a function of Average Radiation and Sunshine duration

To understand why the load coverage is increasing significantly while the PV utilization is slightly decreasing, in Figure 5.5, 4 weeks of Gdynia traction load and PV generation in Gdynia and Arnhem are plotted. Gdynia is characterised by 4.36 sun-h/day with an average 139.35 W/m^2 radiation. Athens is characterised by 7.56 sun-h/day with an average 211.24 W/m^2 radiation. Relocating the grid in Athens from Gdynia causes a PV utilization reduction of 1.31 percentage points (from 50.17% to 48.86%), and a load coverage increase by 10.01 percentage points (from 21.66% to 31.67%). What are the reasons behind the different trend?

When looking at the four weeks in the year, it is possible to see that the utilization of the PV generated energy is not visibly increased. The energy generated by PV is exceeding the load more frequently in Athens. The increase in generation is followed by an increase of the PV energy that is dumped in the grid. Therefore, a slight reduction in the utilization is expected. Due to the increase in the total energy generated and used by the load (since the load coverage is increasing) the fraction of PV used decreases, but not significantly. On the other hand, as mentioned, the increase in PV generation causes the load covered to be much higher when the traction grid is simulated in Athens. As one can see in Figure 5.5, the load area (in light blue in the week plots) has a higher fraction covered by the "PV Athens" line than by the "PV Gdynia" yellow area. As a matter of fact, in the winter months when there is a bigger difference between the generation curves, the load is also higher and therefore able to use all the PV energy. In the summer the difference between the generation curves is reduced and a similar fraction of the load is covered.

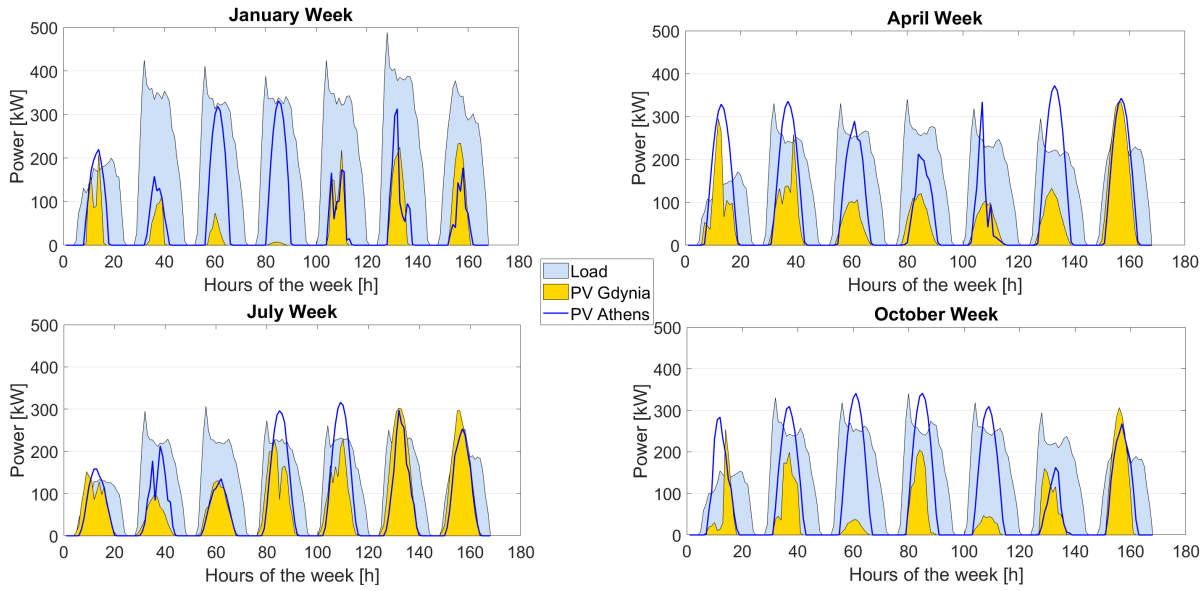

Figure 5.5: Load coverage with changing environmental data: weeks of the year load vs generation in Gdynia and Athens

Both the effect of the Sun Duration and Radiation Level are considered when observing the week plots. The increase in sun duration allows to cover more hours, so extends the load coverage 'horizontally', while the increase in radiation levels causes the increase in the peak and a 'vertical' extension of the load area covered by PV generated energy. In winter the difference between the generation in the two cities is noticeable both in terms of sunshine duration (horizontal extension) and in terms of radiation intensity (vertical).

To draw some conclusions on the environmental KPIs: sun duration and yearly radiation (or yearly irradiance) have an impact on the potential integration of PV in terms of how much load is possible to supply through the PV generated energy. The PV utilization though presents minimal reduction when increasing the sunshine duration and the irradiance due to the higher rates of energy dump. However, this reduction is limited. Integrating PV systems in the same grid located in a different city can induce a different potential and feasibility. As a matter of fact, this could reduce the size of PV installed and obtain similar results. The integration of storage in combination with PV could increase even more the feasibility of supplying traction grids in cities characterised by specific environmental parameters.

In Figure **??**, the values obtained for Arnhem grid are shown. The PVU and the LC present lower values, but similar trends as analysed in the previous paragraphs.

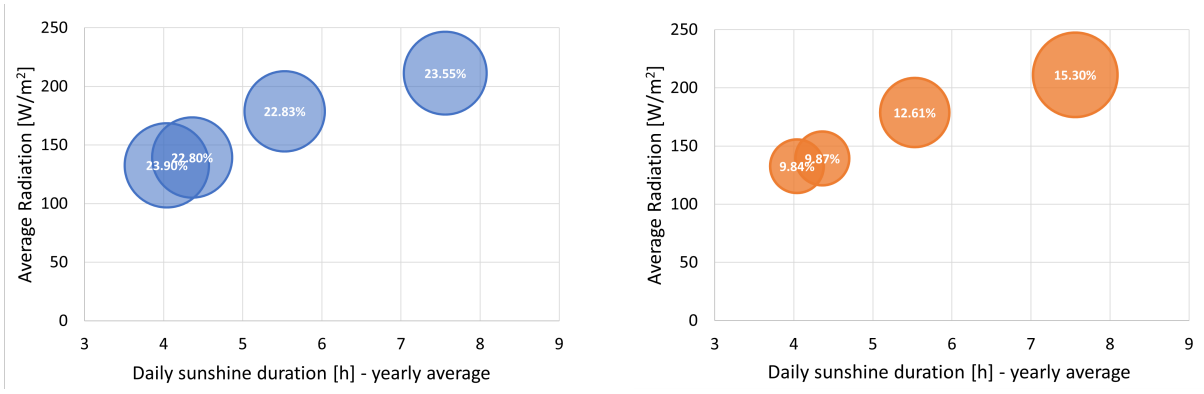

(a) PV Utilization median values for Arnhem substations

(b) Load Coverage median values for Arnhem substations

Figure 5.6: PVU (a) and LC (b) variations due to the change of environmental data - sunshine duration and irradiance

5.2.3 KPIs Study: Substation configuration effect (section number, section length and power requirements)

The first elements investigated related to the trolleygrid system are the section number and total section length covered by one substation. The PV Utilization and the Load Coverage are plotted against the number of sections Figure 5.7 and the average length of the sections found under the substation in Figure 5.8. It can be seen that the increasing number of sections causes a parabolic increase of the PV Utilization and of the Load coverage. The variation of PV utilization and load coverage induced by the increase in average length of the sections found under one substation does not present a proper trend. In both cases, the number of sections and the average section length, the PVU and LC variations follow similar trends, however, the former presents higher variations. The PVU has a higher variation range than the Load Coverage. Due to the seasonal mismatch between load and generation there is a physical limitation in the amount of load that can actually be covered by PV generated energy. The proposed fitting for the data is parabolic, second degree polynomial, in the case of the analysis on the effect of the number of sections 5.7.

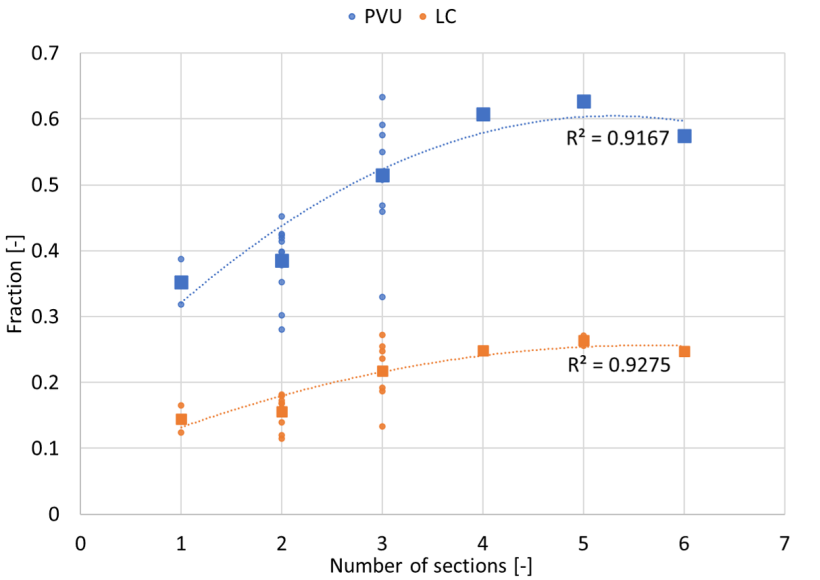

Figure 5.7: PV Utilization and load coverage variation when varying number of sections supplied by the substation

The average length of the sections (5.8) supplied by one substation is not presenting a clear trend in the data. The expectations on this parameter were that the increase in km causes the increase in probability of finding a bus and supplying power to it and the increase in transmission losses which would both enhance the PV utilization. When observing the plots though, not only this trend is not found, but also both LC and PVU seem to be slightly decreasing when the average section length is increased. This can be explained by considering the effect of the parameter on regenerated energy utilization. The increase in the section length does actually cause the increase in probability of having more buses to supply on the section, however this higher chance of having buses on the same section induces an increase in the utilization of regenerated energy and therefore a lower energy requirement at substation level. Therefore, analysing the section length alone does not provide any trend, since the variation in PVU and LC are affected also by the traffic on the sections and the possibility of using regenerated power.

The PV utilization and Load coverage are also plotted as a function of the total kilometers of overhead lines supplied by the substations. The plot, in Figure 5.9, confirms that increasing the number of sections covered has a strong impact on the potential of PV. As a matter of fact, when plotting PVU and LC against the total km covered by the substation, which is a parameter that includes both the number of sections and the section lengths, the values of PVU and LC, although not properly fitted by a regression model, are marginally increasing with the increasing number of km. This is due to the fact that increasing the km by increasing the number of sections instead of their lengths allows the PV generation to be used by more buses without increasing the possibility of power exchange between

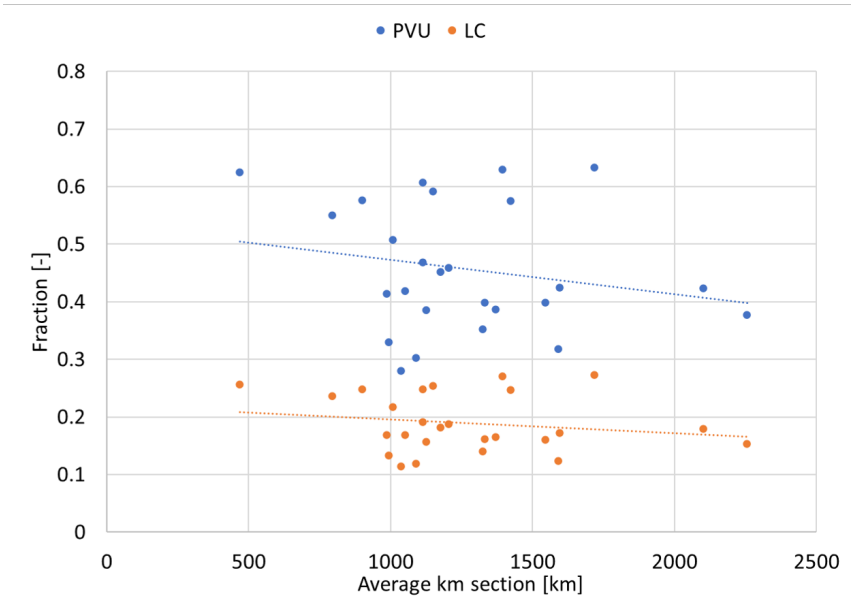

Figure 5.8: PV Utilization and load coverage variation when varying average section length supplied by the substation - No trend

buses. More buses are found under the same substations simultaneously although they are not in the same section and therefore are not exchanging power. One of the assumptions made until this point is that regenerative power is exchanged between buses only if in they are connected to the same section of overhead line.

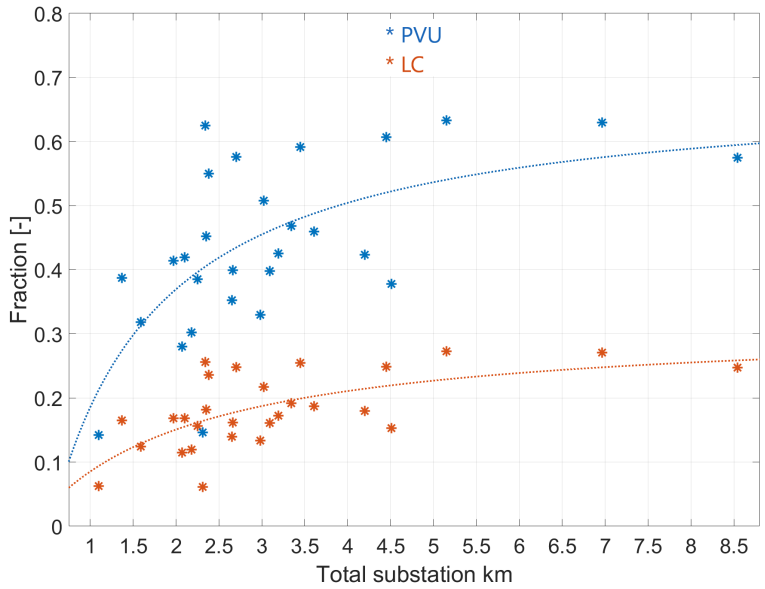

Figure 5.9: PV Utilization and load coverage variation when varying the amount of the total number of km covered by the substation

In Figure 5.1, two substations with large and small power and energy demand are shown. Although the curves are following similar trends for the two, the performance of the PV systems (varying the capacity) appears to be weaker for the substation with lower yearly yield (Figure 5.1b). A study on the impact of substation size on the potential of integrating PV is proposed to verify the veracity of this observation. In Figure 5.10 and 5.11 the reader can find the plots with both PVU and LC variations for varying energy and power requirements of the substation.

The results for both energy and power requirements effects on the PV performance are fitted with a exponential regression model. The R^2 values found are always higher than 0.9, indicating a good fit of the regression model. However, also in this case, it is possible to notice that the data seem to be

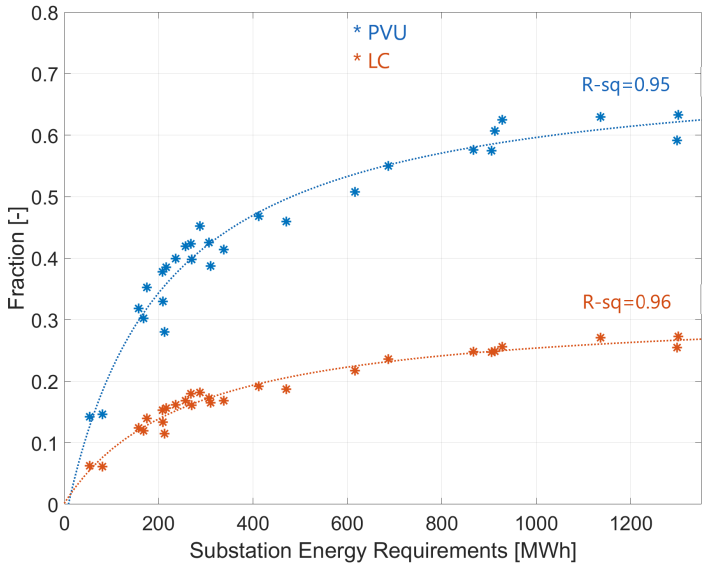

Figure 5.10: PV Utilization and Load coverage variation with varying energy requirements of the substation

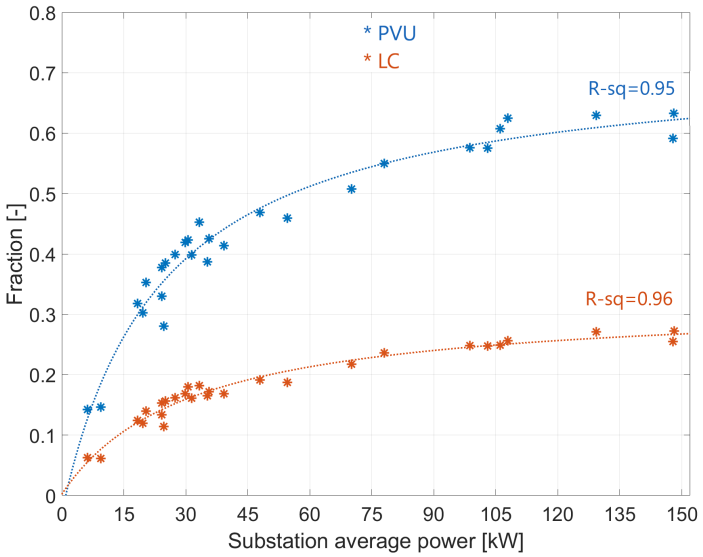

Figure 5.11: PV Utilization and Load coverage variation with varying power requirements of the substation

reaching a plateau of approximately 0.6 when the energy requirements are equal or higher than 900 MWh (or the power requirements are equal or higher than 100 kW on average). The distribution of the values shows that for small substation the performance of PV integration is strongly affected also by limited variations in the size of the substation. On the other hand, for large substation with energy requirements that are higher than 600 MWh/year the PV performance is not strongly affected by variations in the load.

To conclude the study on the impact of the size and configuration of the substation on the PV utilization, the effects of the power and total km are studied together. An overall coefficient representing the substation dimension is defined as the product of the substation average power requirements and the total km of overhead lines supplied by the substation. This will be defined as "Substation Service Coefficient". In Figure 5.12 the PVU data are plotted against the product of power and km of the substation. The PVU and the LC rapidly increase with substation service variations when the size is lower than 250 kWkm, and reach a plateau after that. Again the regression model proposed, rational second degree function, fits the data properly. To verify whether the space or power size of the substation have a stronger impact on the performance of the PV systems, the power and km sizes are also plotted against each other to see the effects of one and the other on the PV utilization.

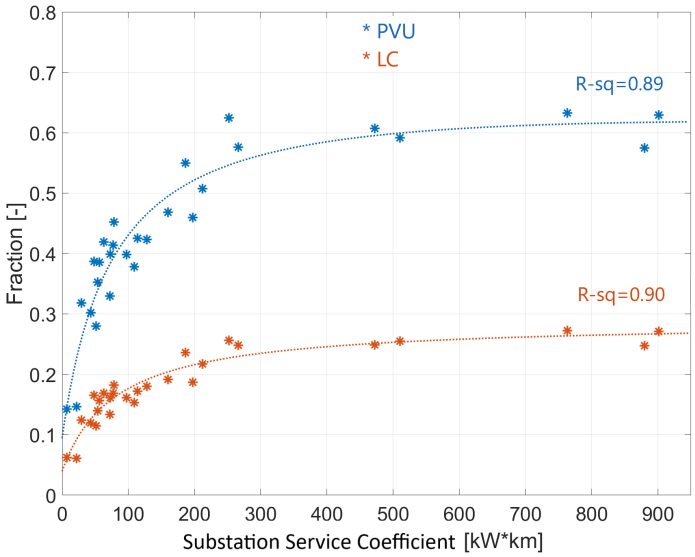

Figure 5.12: PV Utilization variation with varying *substation service coefficient*: power and km size

In the bubble plot presented in Figure 5.13 the bubble size represents the PVU fraction and on the y- and x-axis the total km and average power requirements are found respectively. It is possible to establish, by observing the variation in the PV utilization levels, that the variable that has a stronger effect is the average power requirement of the substation. Therefore, the impact of increasing the radius of influence of the PV system in terms of km seems to be affecting less the PV potential than actually increasing the number of sections fed and the power size of the substation, which is expected due to what has been seen in the previously presented plots.

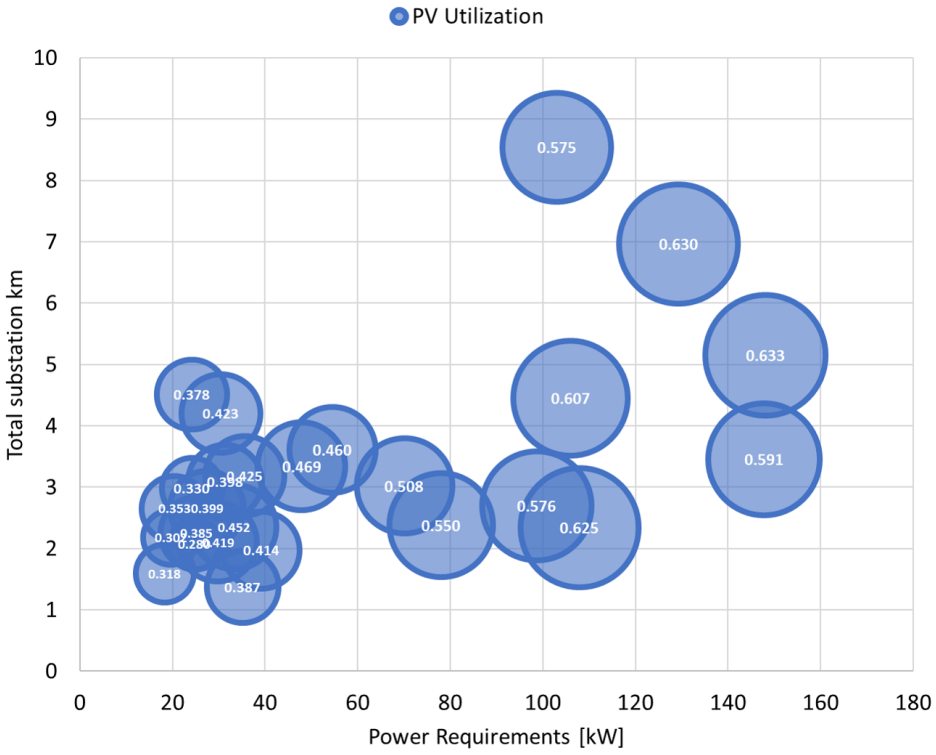

Figure 5.13: PV Utilization variation with varying substation dimension: power and km size in contrast

5.2.4 KPI Study: Substation bus traffic effect (Number of buses simultaneously powered by the substation at any moment)

The study of the effects of the varying number of buses simultaneously powered by one substation is also performed, to understand the effects that bus traffic has on the PV potential. In the previous paragraphs, it is concluded that increasing the section length does not really affect the performance of PV, due to the balanced effect of increasing the load, the transmission losses and the regenerative braking use. The increase in the numbers of buses seemed to be playing a neutral role increasing the load but also the regenerative energy utilization. To asses the impact of bus traffic the PV Utilization and the Load Coverage are plotted as functions of the average number of buses found under the substations during the year. In Figure 5.14, the plot is shown.

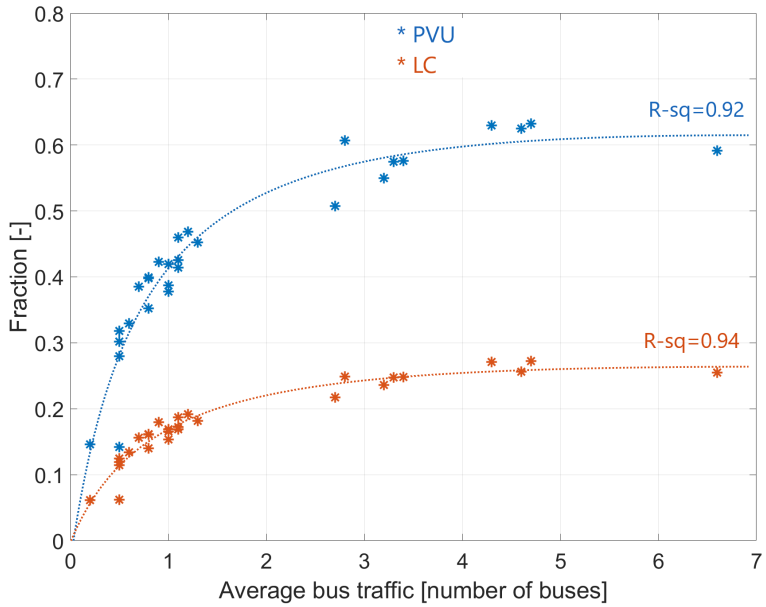

Figure 5.14: PV Utilization and Load Coverage variation with varying substation bus traffic, yearly average number of bus simultaneously connected to the catenary supplied by the substation

It is possible to observe how the values of PV utilization and load coverage follow similar trends between them and how again PVU presents a larger variation range than LC. The proposed regression model, rational function, performs well with both datasets fitting the regression with $R^2 > 0.9$. Also in this case the curve presents stronger variations for lower bus traffic and reaches a 'saturation' point in which the PVU and LC do not increase anymore when the average number of buses under the section is higher than 3.

To conclude this section, it is interesting to understand the relation between the size of the substation and the traffic and the effects that the two have on the PV performance. In Figure 5.15, a 3D scatter plot is shown with the PV utilization plotted as a function of both indicators. The values of the PV utilization can be classified in levels based on the number of sections under the substations and the average traffic is increasing with the increasing number of sections. This is expected considering the fact that a higher number of sections corresponds to a higher probability of having a bus being supplied by the substation. From the plot though it is possible to see the trend identified in Figure 5.14. The increase in the average bus traffic causes an increase in the PV Utilization for all the substations, with an intensified effect on the smaller substation with lower number of sections. It is possible to confirm also from this chart, that once the average number of buses reaches values that are higher than 3 no big variation in PVU is registered.

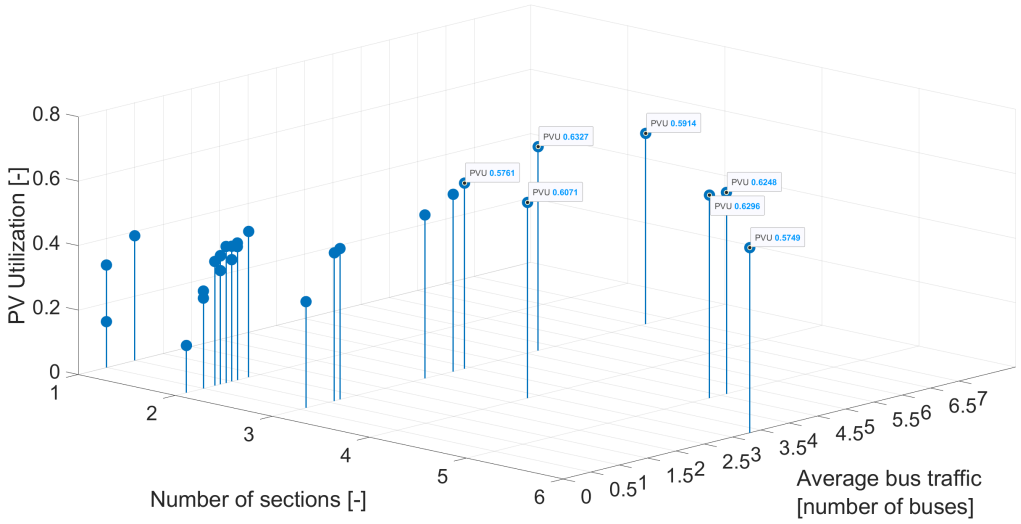

Figure 5.15: PV Utilization variation with varying section number and bus traffic

5.2.5 KPIs Study: HVAC requirements effect

The heating, ventilation and air conditioning system energy requirements can strongly vary throughout the year. Moreover, as seen in the literature review, the HVAC share of the total power demand can reach values 50-70% in some periods of the year [16]. In Arnhem and in Gdynia, the HVAC energy requirements are especially high in the winter months due to the low temperatures found in the two cities and the consequent high heating load. In Figure 4.6, the HVAC power demand throughout the year for a bus in Gdynia and in Arnhem is shown. It is possible to notice how, for these two cities, the demand curve is significantly higher in winter than in summer and that the curves are characterised by a U-shape throughout the year.

Different substations can be characterised by different HVAC demands based on the bus traffic, based on the number of sections fed by the substations and on the amount of time in which a bus can be found under a substation. However, although the HVAC may be scaled differently for each substation, the shape of the demand of the system throughout the year is the same. In Figure 5.16, the HVAC demand of one bus (before the implementation of the duty cycle) and the PV generation (per unit surface) curves are plotted for Arnhem (the same plot is found for Gdynia). The two curves present inverted U-shapes. If on one side the HVAC shows the peaks at the extremes of the year, the PV generation has the opposite distribution peaking in the summer months.

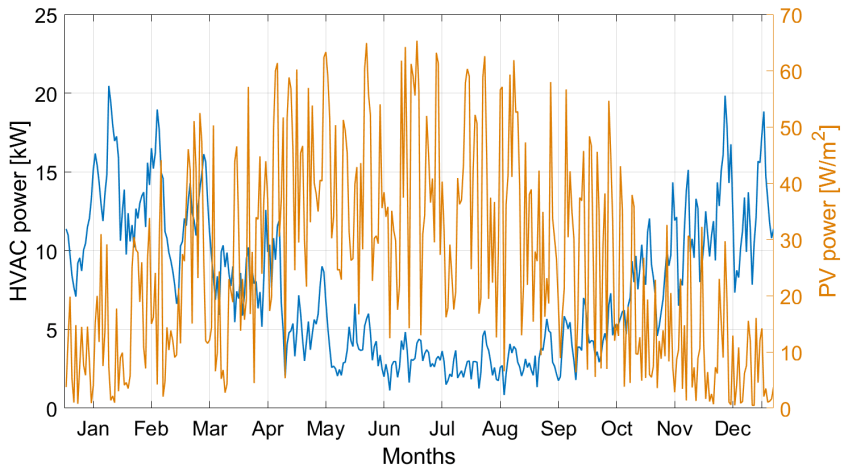

Figure 5.16: HVAC power demand and PV power generation throughout one year (Arnhem characteristics)

When we look at the power requirements of the substations throughout the year, we can observe a similar trend. In Figure 6.10, the substation power demand is plotted against the PV generation. The seasonal mismatch between generation and load is characterised by high load and low generation in winter and high generation and low load in summer.

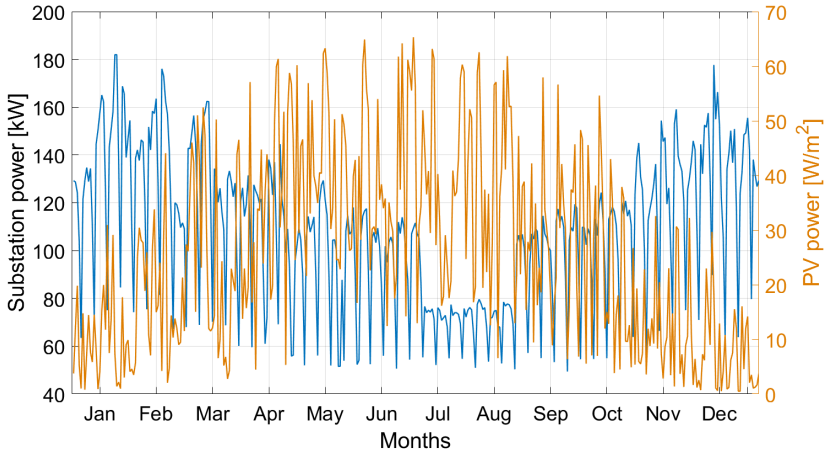

Figure 5.17: Substation power demand and PV power generation throughout one year (Arnhem characteristics)

Removing the HVAC power requirements from the substation load, gives us the profile of the traction power throughout the year. The traction power is independent from the seasonal variation of temperature and irradiance. The only possible variation in the load throughout the year is related to the modification of the bus schedules during the different periods of the year. The traction power is plotted against the PV generation in Figure 5.18. The traction power is found to be almost constant through the year, with a fixed decrease in the summer months due to the implementation of a different timetable which reduces the bus runs. Both in the total and the traction power profiles, it is possible to some dips in the power demand which represent the Sunday traffic.

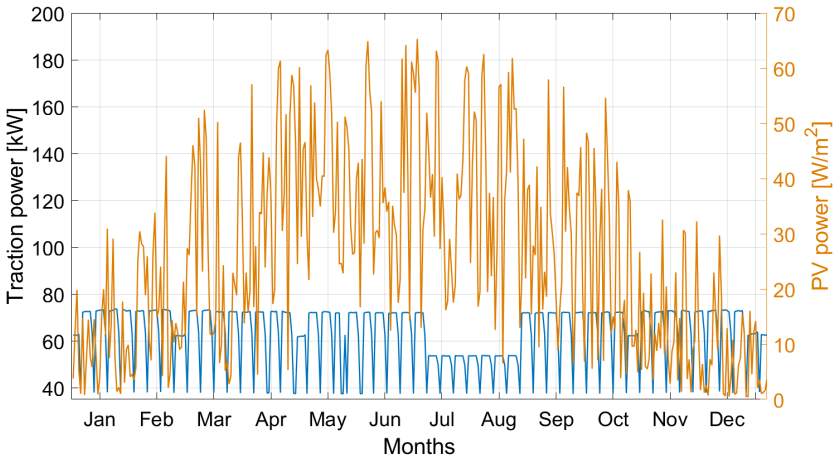

Figure 5.18: Substation traction power demand (no HVAC) and PV power generation throughout one year (Arnhem characteristics)

By looking at the power profiles in the figures above, with and without HVAC requirements, it is expected that removing the HVAC power demand would have a positive effect on the potential of integrating PV. The effects of removing the HVAC demand on the integration of PV are studied to define whether it would be bring any improvement to the PV potential to supply the HVAC differently.

For this analysis, as for one on the environmental data, the PV system for each substation is sized based on the traction power demand. The obtained PV Utilization and Load coverage values are compared to the ones obtained for the total demand of the substation to draw some conclusions on the effects of removing the HVAC power demand. In Figure 5.19 and 5.20 the PVU and LC variations when removing the HVAC power demand are shown. The size of the bubbles in the the two charts represents

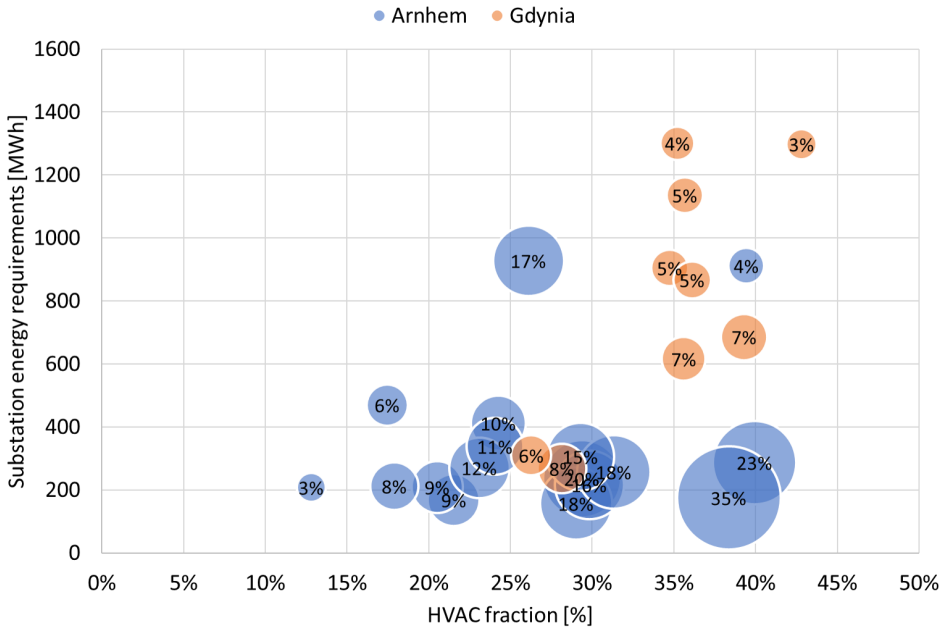

Figure 5.19: Reduction of the PV Utilization (PVU) due to the removal of the HVAC load from the substation power requirements

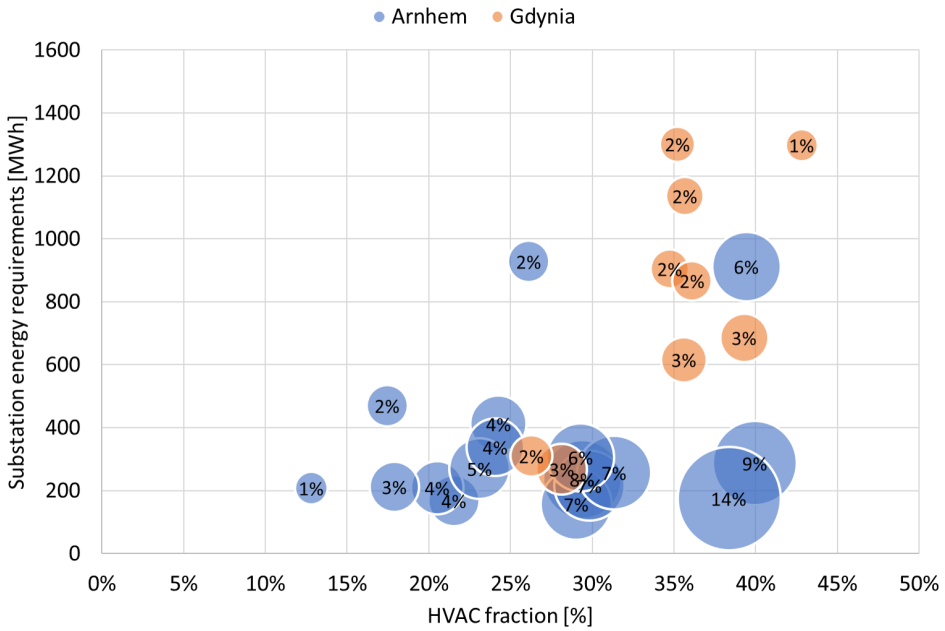

Figure 5.20: Reduction of the Load Coverage (LC) due to the removal of the HVAC load from the substation power requirements

the decrease in PV utilization and Load coverage found when removing the HVAC requirements from the substation load. The bubbles are distributed in the graph based on the substation total energy requirements (with HVAC) and the fraction that the HVAC covers (in percentage).

The results show that for no substation removing the HVAC has a positive effect on the PV performance. As one can read from the figures, the reduction in PV Utilization for the different substations can go from a minimum of 3 percentage points to a maximum of 35 percentage points in the worst case. The load coverage is also reduced by 1 percentage points to 14 percentage points. This result is unexpected but can be explained. Removing the HVAC power demand induces the reduction of the load and the increase in regenerated power, which can both strongly affect the PV Utilization. In Figure 5.11 the effects of the reduction of the power requirements of a substation on the PV integration are shown. The elimination of the HVAC can cause a reduction of the demand of up to 40%. As can be seen in the

plots in Figure 5.19 and 5.20, the HVAC can account for 13-43% of the total power demand. Secondly, removing the HVAC means having more regenerated power in the LVDC grid, since the first used of regenerated power is removed. As a matter of fact, the bus auxiliaries (HVAC+others) are the first consumers of the recouped braking energy. This means that, removing the HVAC, more power will be sent to the overhead lines and therefore shared between buses, reducing the substation load even more.

Some last observations can be done on Figure 5.19 and 5.20. The different colours of the bubbles represent the two cities, Arnhem in blue and Gdynia in orange. What can be seen is that smaller substations are affected more by the removal of HVAC. This is expected since the reduction in size seen by these substations moves them along the steeper part of the line in Figure 5.10, where small variations of power demand cause higher differences in PVU and LC. Finally, it is possible to observe how the overall performance of the substations in Gdynia is found to be better. Also smaller substations, due to their better characteristics in terms of km, number of section and traffic perform better than those in Arnhem.

5.2.6 KPIs Study: Bilateral Connections effect

The simulation of bilaterally connected sections is only partial. This is due to the fact that the model was not completed yet. As mentioned in Chapter 4, multiple types of sections and interconnections between sections exist and therefore multiple models have to be made. The progress in the models is not enough to simulate all the sections and especially to simulate all the sections with the appropriate bilateral connections. The limited amount of outputs is mainly caused by the high computational time required to run the model for bilaterally connected sections, which can take up to 6-7 hours, and by the limited precision of the outputs for more complicated sections. These simulation started in the last month of the research and therefore the time constraints had a strong impact on the amount of obtainable outputs.

The model has been run for 4 bilaterally connected sections. The outputs of these simulations allow us to see the effect of the connections for 3 different substations. In Figure 5.21, the PVU and LC values of the substations after the bilateral connections are activated are shown. The previous values are indicated by a red cross, while the new data points are represented by a green square. The red arrows represent the shift between the two points.

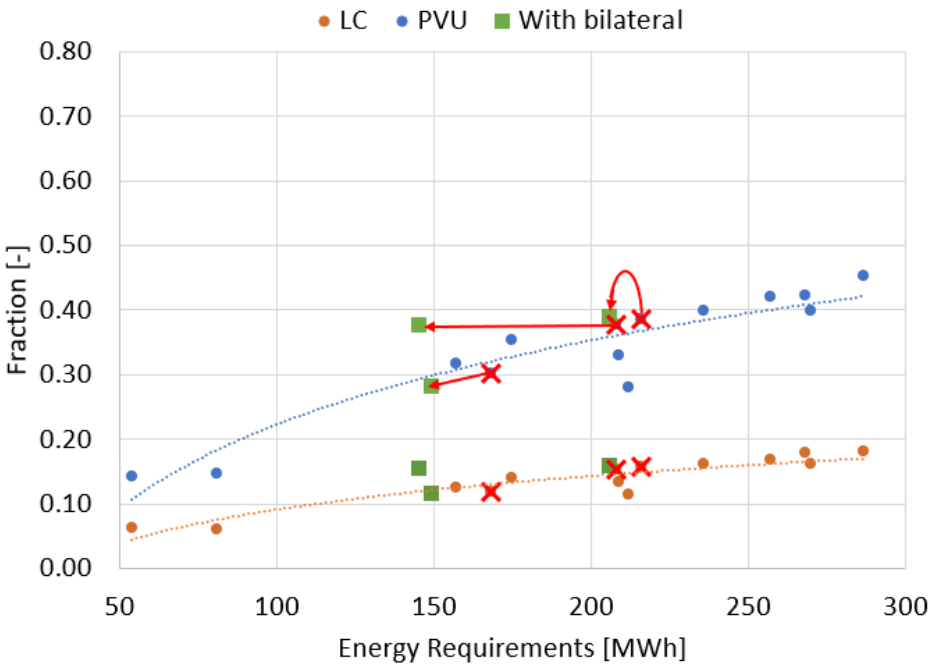

Figure 5.21: Effect of bilateral connections on the PV utilization (PVU) and load coverage (LC)

It is difficult to draw conclusions based on these three values only. However, some observations can be made. In first place, one can notice that the introduction of bilateral connections between sections of different substations always causes a reduction of the demand of the substation. This decrease in the energy requirements is caused for all the sections by the minimization of the transmission losses. The activation of the bilateral connections allows to supply buses through 2 substations instead of one, minimizing the losses due to the balanced division in power between the substations based on the location of the bus and its distance from each of them. The split of power between the two feed in points is also connected to the voltage levels of the two substations. A higher supply voltage will induce a higher power share of the substation. When observing the plot in Figure 5.21, it is possible to see that one substation has a higher drop in energy consumption. This is related to the fact that one or more sections of the substation are fed by the bilaterally connected section. This of course generates an increase in the power requirements of the substation that is feeding an increased number of buses. In the plot the substation in question is not represented, due to the fact that not all the sections supplied by the substation have been simulated. In Chapter 4, the results obtained when introducing bilateral connections are further discussed.

The second, and last, observation that can be made is that the reduction in energy demand induced by the bilateral connections is not necessarily causing a drop in the PV performance. The new values obtained for PVU and LC of the newly simulated substations actually are placed very close to the regression curve or above. From the data it could be seem that a new curve could be drawn with slightly higher PV performance. This might be caused by the fact that allowing power exchange between sections generates a more constant and distributed load. The fact that the two sections feed simultaneously buses on both sections increases the average bus traffic found under the section and the the number of sections fed by the same substation. We have seen that both elements have a positive effect when speaking about integrating PV in traction substations.

Although some minor observations are made, the analysis of the effect of connecting sections between them in the whole grid is far from complete. This will be one of the main recommendations for future related work.

5.2.7 Comparison between substations: overall effect of the studied KPIs

The aim of this section is to compare the results obtained for PV integration for some substations to verify the effect of the studied Key Performance Indicators on the integration of PV in different substations.

Comparison between substation 2 and 6 in Gdynia - large substations

The first comparison proposed is between two substations in Gdynia trolleygrid, specifically numbers 2 and 6. These two substations are both characterised by high energy requirements. They have very similar size in terms of energy and of power requirements and the same number of sections supplied. They present different bus traffic and section lengths. In particular, substation 2 has higher bus traffic with an average of 6.6 buses compared to the 4.7 of substation 6, but lower km covered 3450 km against 5150 km. Another factor that is relevant for this analysis, is the 'service' coefficient, obtained by multiplying the average substation power and the total km. Substation 2 and 6 present the same average power requirement of 148kW. Multiplying the total km and power we obtain, respectively for 2 and 6, 510 kWkm and 763 kWkm. All these data are summarised in Table 5.5, together with the PV capacity installed the PVU and LC.

Table 5.5: Substation 2 Gdynia and 6 Gdynia comparison between PV performance

Substation number	Energy [MWh]	Number of sections	Total subs. km	Average bus traffic	Service coeff. [kWkm]	PV cap [kWp]	PVU [-]	LC [-]
2 - Gdynia	1298	3	3.45	6.6	510	591	0.5914	0.2547
6 - Gdynia	1301	3	5.15	4.7	763	592	0.6327	0.2725

In Figure 5.22, the PV Utilization and the Load Coverage curves for the two substations are plotted. Substation 6 performs better both in terms of PV utilization and Load coverage for all PV Capacities. If the PV system is sized as per Equation 5.4, the PVU of substation 6 is found to be by 4 percentage points higher and the LC by almost 2 percentage points than substation 2, as can be seen from the data reported in Table 5.5.

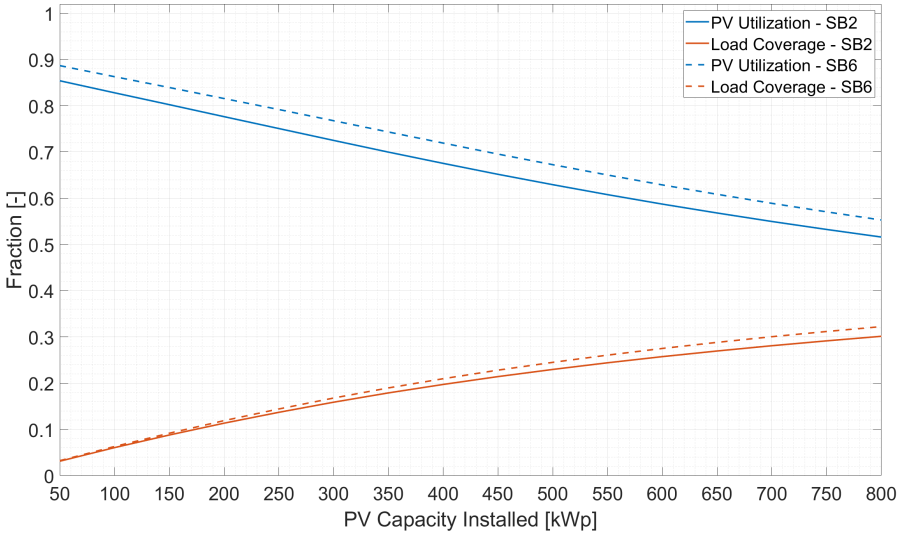

Figure 5.22: Comparison between PV Utilization and Load Coverage of substations 2 and 6 in Gdynia trolleygrid when varying PV size

When looking at the plots of the effects of average bus traffic and of the Service coefficient, it is possible to see that the shift from 6.6 average buses to 4.7 induces lower variations in the PV performance than the shift from 763 kWkm to 510 kWkm. Moreover, the difference found between the PVU and LC is limited due to the similarity found between the two substations: energy and power requirements and number of sections. The PVU an LC range in which the substation are found is very similar. To compare specific substations it is interesting also to check the temporal distribution of the load. In Figure 5.23 the fraction of time in which the load is in each period of time through the day is plotted. The daytime is subdivided in 4 time periods:

- 4-8 : in this time period the presence of sun light is variable throughout the year depending on the season. 4AM is the earliest sunrise time and 8AM the latest in Gdynia.
- 8-15 : in this time period there is always sun light. The variability of PV depends only on the weather conditions.
- 15-21: this time period is also characterised by variable sunlight. At 15 the earliest sunset happens on the shortest day and at 21 the latest.
- 21-4: during these hours there is never sunlight throughout the year.

Another factor that may influence the better performance of substation 6 compared to substation 2 in Gdynia, is how the bus runs under the substation are happening. As a matter of fact, substation 6, in orange in Figure 5.23, is characterised by more runs in the period 8-15 and less in the period 21-4. These two time ranges are the ones in which the PV systems operate at best and at worst throughout the year, respectively.

Comparison between substation 1 and 16 in Arnhem - small substations of different sizes (lower than cap)

The second comparison proposed is between two substations characterised by different energy requirements, but which are both in the region in which the regression model proposed for the PVU and LC presents a steep slope. The energy requirements of substations 1 and 16 of Arnhem grid, are both lower

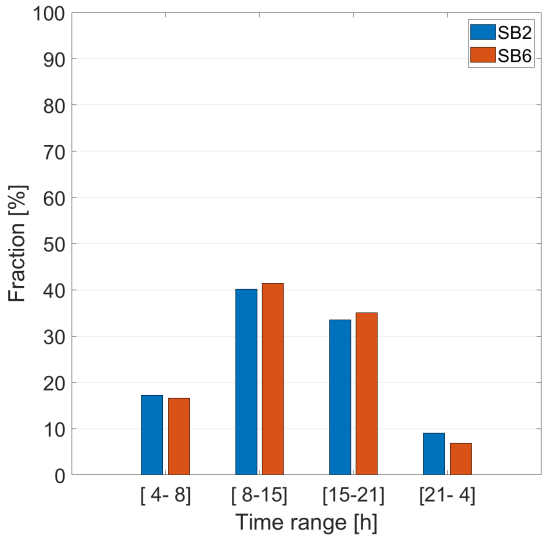

Figure 5.23: Comparison between the distribution in time of the load of substation 2 and 6 in Gdynia

than 400 MWh/year. By referring to the plot in Figure 5.10, one can see where the two substations are placed. In Table 5.6, the details of the two substations are provided. They present the same number of sections and similar total overhead cable length supplied, however substation 16 has double energy requirements and bus traffic. These two factors have a strong effect on the PV performance and as a result we see that the PVU and LC of the larger station are noticeably higher. The PV utilization presents a value by 11 percentage points higher and the load coverage by 5 percentage points.

Table 5.6: Substation 1 Arnhem and 16 Arnhem comparison between PV performance

Substation number	Energy [MWh]	Number of sections	Total subs. km	Average bus traffic	Service coeff. [kWkm]	PV cap [kWp]	PVU [-]	LC [-]
1 - Arnhem	168	2	2.18	0.5	43	78	0.3022	0.1195
16 - Arnhem	338	2	1.97	1.1	77	157	0.4139	0.1686

When observing the variation of PVU and LC for the two substations in Figure 5.24, one can see that the load coverage at the same PV capacity installed is always higher for the smaller substation. Reducing the load does cause an increase in load coverage and intuitively this makes sense, since a fraction of the load that is not supplied is basically removed. However, the PV systems are sized according to the power requirements of the substation. Therefore, if in substation 1 a PV capacity of 160 kWp (as in substation 16) is installed, the LC would actually be higher reaching a value around 20%, but the PV utilization would not be optimised and present values of 22% approximately.

Comparison between substation 7 and 9 in Gdynia - small substation with different section number and load distribution in time and space

The last comparison presented is between the two smallest substations of Gdynia grid, numbers 7 and 9. This example is provided to show the effect of the number of substation and the total length of the catenary fed by the substations on the PV system performance. The effects of the temporal distribution of the load throughout the day are also analysed for this case. Although no trend is found when plotting the data of all the substation as a function of their distribution in time, for some substations a correlation between the performance of PV and the bus timetables can be seen.

In Table 5.7, the overall details of the to stations can be found. Substation 7 presents lower energy demand, but higher number of sections and length of catenary supplied. As a matter of fact, the overall Service coefficient of this substation is higher than the one of substation 9. The potential of integrating PV in substation 9 in Gdynia is lower than in substation 7. The PVU is 4 percentage points

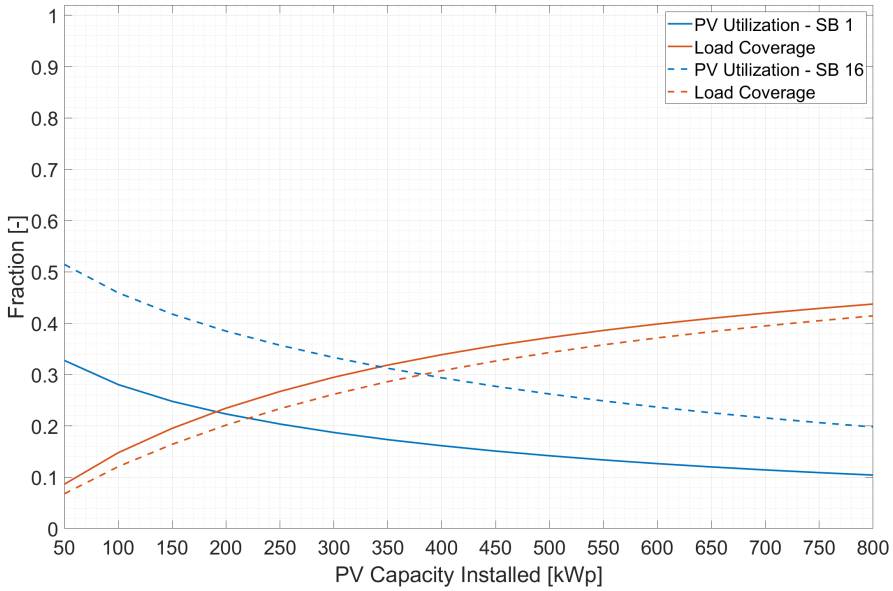

Figure 5.24: Comparison between PV Utilization and Load Coverage of substations 1 and 16 in Arnhem trolleygrid when varying PV size

Table 5.7: Substation 7 and 9 in Gdynia grid comparison between PV performance

Substation number	Energy [MWh]	Number of sections	Total subs. km	Average bus traffic	Service coeff. [kWkm]	PV cap [kWp]	PVU [-]	LC [-]
7 - Gdynia	268	2	4.20	0.9	128	122	0.4231	0.1799
9 - Gdynia	310	1	1.37	1	48	141	0.3871	0.1653

and the Load coverage 1.5 percentage points higher for the latter substation. The increase in the spatial distribution of the load causes the improvement of the performance of the PV system installed in the smaller substation. Another interesting point of comparison between the two is the daily temporal distribution of the load. This is plotted in Figure 5.25. Substation 7 timetables are characterised by runs that happen by approximately 55% of the time in the period going from 8 to 15, which is the time range in which there is always sunlight throughout the year. On the other hand, substation 9 has 53% of its runs happening in the variable time periods, so either between 4 and 8 or between 15 and 21. This has a strong impact on the variability of the match between generation and load. In Figure 5.26, the match between PV generation and load in time throughout the year is plotted.The effect of having higher share in variable periods of time during the day is evident from this bar chart. In the summer months, when the sunrise is at its earliest hour and the sunset at its latest substation 9 has higher match between load and PV generation, while in the other months substation 7 performs better.

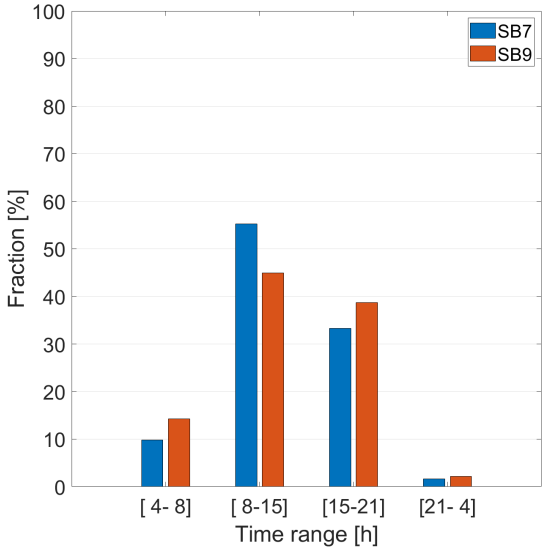

Figure 5.25: Comparison between the distribution in time of the load of substation 7 and 9 in Gdynia

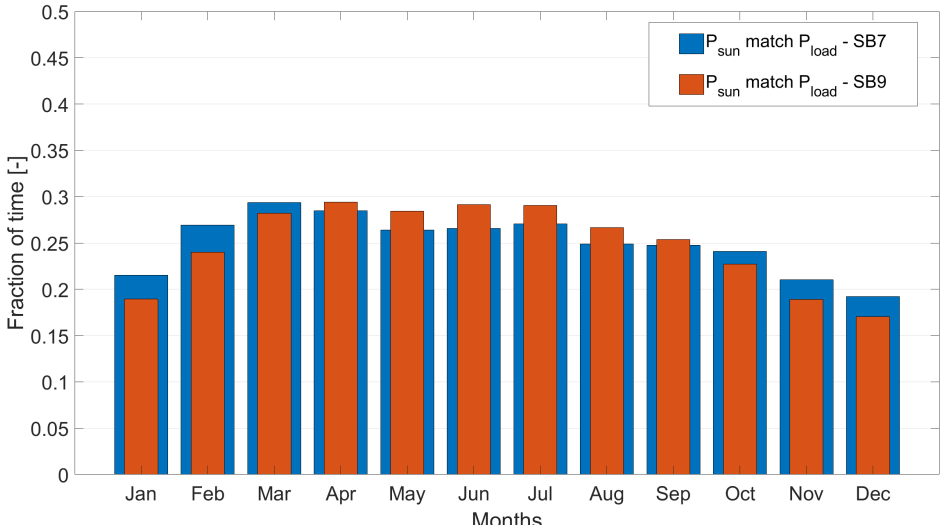

Figure 5.26: Comparison between the fraction of time in which PV generation and power demand happen simultaneously for substation 7 and 9 in Gdynia

5.2.8 Comparison between results of the two grids

This section has the aim of analysing the overall performance of the integration of PV in the two grids and drawing some conclusion on the reasons of the different results obtained for the two traction systems, located in Arnhem and Gdynia.

In table Table 5.9 and Table 5.10 the results of PV integration are provided for all the substations of the two grids. In Table 5.8, a synthesis is made of the most important findings. The potential of integrating PV in the Gdynia trolleygrid is higher than in the Arnhem trolleygrid. By observing the data reported in this summarising table, it is possible to see that Gdynia is outperforming Arnhem on all the parameters, with better results both in terms of PV utilization and load coverage.

The more centralised traction system that can be found in Gdynia favours the integration of PV. In fact, this characteristics of the system causes the increase in the rating of the substations and therefore of the expected power requirements under each of them. The Gdynia grid is characterised on average by a higher amount of sections and of total km covered by each substation. Also, the higher number of lines and buses running in the grid improves the results of PV since the increase in traffic is not followed by an increase in sections and of substations.

Table 5.8: Results of PV integration in the Arnhem and Gdynia grid

	Arnhem	Gdynia
Average PVU	41.3%	54.1%
Average LC	16.7%	23.3%
Load covered with PV [MWh]	1100	1827
Fraction of total load [%]	18.8%	24.6%
PV Energy Excess [MWh]	1608	1377
Fraction of total PV Energy [%]	66.5%	42.9%

Table 5.9: PV integration results in Arnhem trolleygrid - PV Utilization and Load Coverage effects on energy demand and PV energy excess

Substation Number	PV capacity [kWp]	PVU [-]	LC [-]	PV covered load [MWh]	Remaining load [MWh]	PV energy [MWh]	PV Excess [MWh]
1	78	0.302	0.120	20.1	147.9	70.3	12.4
2	192	0.469	0.192	78.9	333.1	173.2	112.6
5	97	0.330	0.134	28.0	181.0	87.6	51.4
7	110	0.399	0.162	38.1	197.9	99.6	51.8
8	97	0.378	0.153	31.9	176.1	87.6	58.8
10	73	0.318	0.124	19.5	137.5	66.2	27.7
11	133	0.452	0.182	52.2	234.8	120.1	59.2
12	100	0.385	0.156	33.8	182.2	90.5	65.1
13	99	0.280	0.115	24.3	187.7	89.3	56.0
14	218	0.460	0.187	88.0	382.0	196.6	151.1
15	126	0.398	0.161	43.5	226.5	113.9	83.7
16	157	0.414	0.169	57.0	281.0	141.9	83.4
17	119	0.419	0.169	43.3	213.7	107.4	68.4
18	38	0.146	0.06112	0.0	81.0	0.0	0.0
19	82	0.353	0.140	24.5	150.5	74.0	9.0
20	142	0.425	0.172	52.7	253.3	128.3	79.3
CS (4,9,21)	432	0.625	0.256	237.7	690.3	389.6	284.3
HQ (3,6)	424	0.607	0.249	226.7	685.3	382.6	353.5
Total		**41.26%**	**16.70%**	**1100.1**	**4741.9**	**2418.8**	**1607.6**

Table 5.10: PV integration results in Gdynia trolleygrid - PV Utilization and Load Coverage effects on energy demand and PV energy excess

Substation Number	PV capacity [kWp]	PVU [-]	LC [-]	PV covered load [MWh]	Remaining load [MWh]	PV energy [MWh]	PV Excess [MWh]
1	412	0.575	0.247	223.8	680.4	390.9	166.5
2	591	0.591	0.255	330.6	967.2	560.4	229.2
3	280	0.508	0.218	134.0	481.5	265.5	130.9
4	395	0.576	0.248	215.0	651.9	374.4	158.9
5	312	0.550	0.236	162.1	523.0	295.8	133.3
6	592	0.633	0.273	354.5	945.9	561.2	206.4
7	122	0.423	0.180	48.2	219.1	115.9	67.0
8	25	0.142	0.0624	0.0	0.0	23.8	20.4
9	141	0.387	0.165	51.2	257.9	134.0	82.3
10	517	0.630	0.271	307.7	827.5	490.3	182.0
Total		**54.14%**	**23.25%**	**1827.2**	**5554.4**	**3212.2**	**1376.9**

To conclude this section, a comparison between the fraction of time in which the load and the PV generation match is provided. The bar charts provided in Figure 6.10 show the fraction of time in which the substation load is covered partially (20%) 5.27a or fully (100%) 5.27b by the PV generation for each substation (substation numbers indicated on the x-axis). On average only 21% of the time the load is partially covered and 11% of the time is fully covered. For Gdynia only the two values are of 22% and 10.4% and for Arnhem 20.8% and 11.72%. On average Arnhem substations have a higher full coverage of the load but lower partial. This could be related to the shift of one hour in the sunset and sunrise times which probably allows to increase the number of fully covered runs during the summer. As a matter of fact, the time periods are all moved of plus one hour for Arnhem, moving the first time period starting time to 5 and the ending time of the evening period at 22. This allows to have more runs

in light period during summer since fewer runs are found to be happening between 4 and 5 compared to 21 and 22.

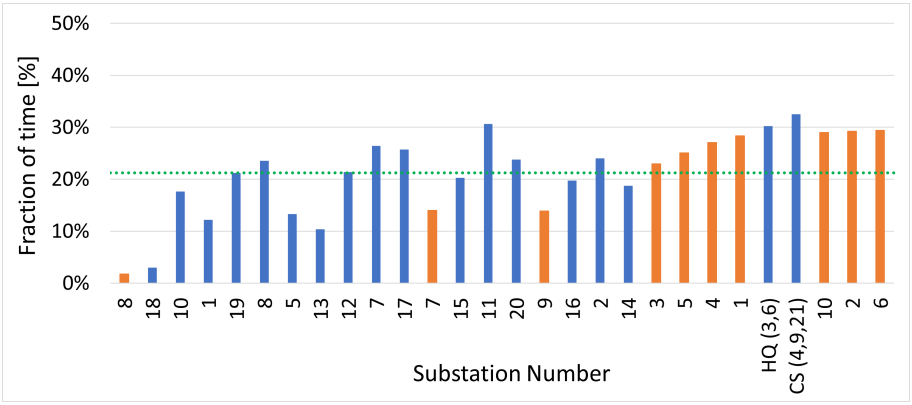

(a) Fraction of time in which the PV generation can supply at least 20% of the load throughout the year for each substation

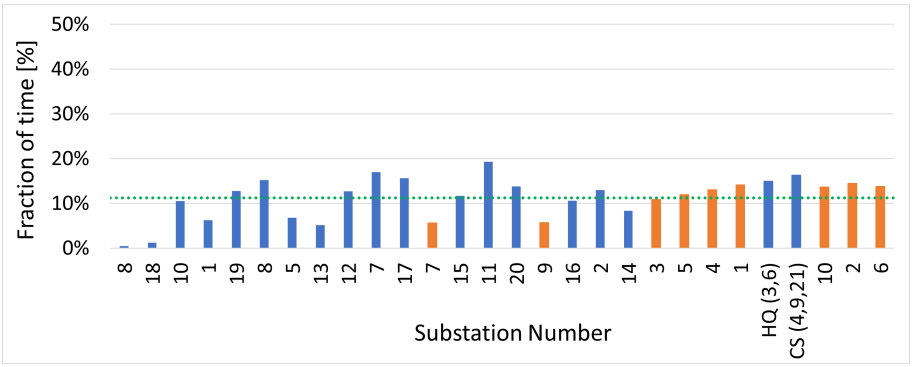

(b) Fraction of time in which the PV generation can supply the whole load throughout the year for each substation

Figure 5.27: Temporal mismatch between PV generation and load: fraction of time in which PV covers the load through the year - Arnhem in blue and Gdynia in orange

5.3 Summary and takeaway points of the chapter

In this chapter the reader finds the analysis conducted on the impact of selected Key Performance Indicators on the potential of integrating PV systems in trolleybus traction grids. The indicators studied in this chapter are: the environmental-related parameters, the substation power requirements, the number of sections supplied by the substation, the average section length of the sections supplied, the average bus traffic under the section, the HVAC requirements and the activation of bilateral connections.

The increase in average radiation levels and sunshine duration causes the **increase in load coverage** (Figure 5.4) and better PV performance in terms of amount of energy used to supply the load. However, the **PV utilization is constant or lower** (Figure 5.3) when the generation is increased due to the increase of sun hours and irradiance. This is due to the increase in excess generation which is dumped in the grid.

The substation load demand and its configuration has a strong impact on the potential of integrating PV. For very small substations the variation in power/energy requirements cause strong variations in PVU and LC. The values of PVU and LC seem to **reach a plateau** after a certain substation size (Figure 5.10 and 5.11). The increase in number of sections fed by a substation also causes the **improvement of both PVU and LC**, as noticeable from the values plotted in Figure 5.7. The increase in section length instead **does not affect** the integration of PV (Figure 5.8). As a matter of fact, not trend is found in the output values of PVU and LC.

Higher average bus traffic levels induce higher PVU and LC. Similar trends of the data are found for this indicator as well, causing a **rapid increase in PVU and LC for small values** and reaching a peak and a **plateau** after the value of 3 buses supplied simultaneously on average. This trend is visible in **??**.

Removing the HVAC demand causes the **reduction of the PV utilization (Figure 5.19) and Load coverage (Figure 5.20)** for all the substations. This is an unexpected result, probably due to the flattening of the load curve caused by the HVAC removal.

Finally, bilateral connections are only partially studied. The introduction of bilateral supply seems to be **favouring the integration of PV** although it causes the overall reduction of the substations' loads.

To conclude, 3 comparisons are made between different substations of the grids, analysing the potential of integrating PV for each of them. An overview of the performance of the two trolleygrids is given as conclusion to the chapter. The lower average substation energy demand, the bus traffic distribution and the substation configuration in Arnhem grid generate a **lower potential for PV integration** in comparison to Gdynia trolleybus system.

6 RESULTS: PV AND STORAGE INTEGRATION

In this chapter, first the effects of adding storage (coupled with the PV system at substation level) on the potential of integrating PV is assessed. Then, a brief analysis of the feasibility of integrating these systems in the grids is presented.

6.1 Storage integration effects on the PV potential

In this section, the reader can find a study on the effects of integrating storage coupled with PV at substation level. The storage system taken into consideration in this study is a battery energy stationary storage system (BESS), which is placed on the AC side with the PV system. The BESS is seen from the DC side as an AC source of electricity together with PV and the grid. The feed in point of the three generation units (grid, PV and storage) is the same. The integration of storage is meant to increase the self-consumption and therefore the PV utilization and reduce both the grid power requirements and the PV power dump into the AC grid. As mentioned in Chapter 2, one of the drawbacks of installing stationary storage compared to on-board storage is the reduction of the possibilities of increasing the utilization of regenerative braking energy. In this case, with stationary storage installed on the AC side, there is no possibility of recovering and storing braking energy due to the unidirectional operation of the inverter. The effectiveness of the BESS is therefore only associated to the increased use of PV energy and has no impact on the reduction of energy consumption due to energy recuperation. As mentioned in the Models chapter (4) the battery systems taken as reference are the Tesla Powerpack systems, due to their modularity to the fact that they provide utility scale highly performative energy storage systems.

The impact of storage introduction is studied with respect to its effect on the potential of PV integration. Therefore the PV utilization and the Load Coverage factors are used also in this case to assess the impact of storage in the grid. In Figure 6.1a and Figure 6.1b the same substations (2 and 9 of Gdynia grid) presented at the beginning of the previous chapter are shown. The curves represent the variation of PVU and LC at varying PV capacity installed when storage is included. Multiple lines are plotted to represent the increase in storage capacity which is done in steps of 230 kWh, capacity of one Tesla Powerpack. In both cases the solid line is the case with no storage installed (discussed in the previous chapter). The number of batteries is varied based on the PV generation. The maximum number of batteries represents, for each substations, the capacity that is necessary to install in order to avoid dumping PV energy in the MVAC grid. Indicated with a vertical red line in the two plots is the PV capacity size selected from the previous analysis on PV integration, based on Equation 5.4. For substation 2 this is approximately 590 kWp and for substation 9 140 kWp.

The two substations have different sizes: substation 2 and 9 have respectively 1298 MWh and 310 MWh yearly energy requirements, an average of 6.6 buses supplied against 1, 3 sections fed compared to 1 and a km range of 3.45 km against the 1.37 of substation 9. The comparison between the two is proposed to see the effect of including storage in two substations with opposite characteristics. What can be observed comparing the plots, is that the introduction of one battery in the smaller substation allows to increase the PVU up to values of 90%. On the other side, for the larger substation the increase in PVU and LC are less significant due to the higher load. What can be noticed in both cases is that increasing the number of batteries does not linearly improve the PVU and the LC. The improvement of these two indicators reaches a saturation point and from that point onward installing extra batteries causes only a slight variation of PV utilization and load coverage. In order to evaluate

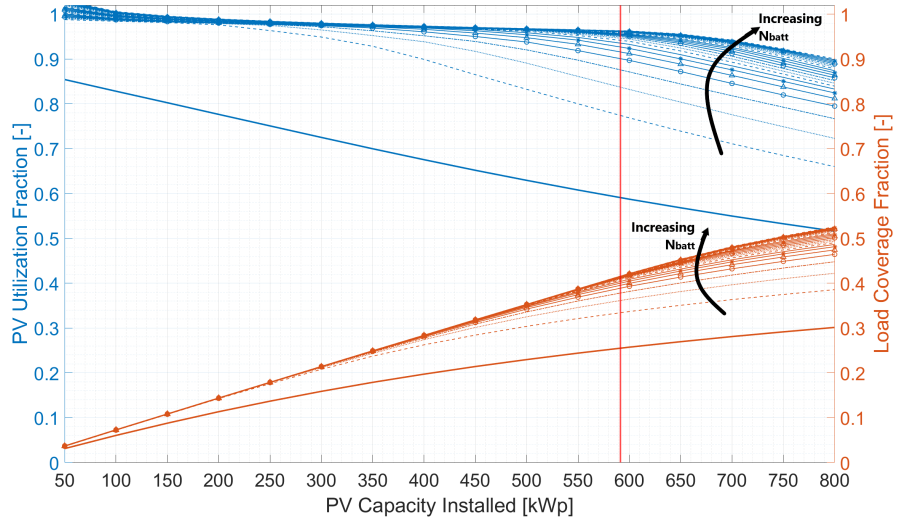

(a) PV Utilization and Load coverage with varying PV capacity [50-800]kWp and number of batteries (N_{batt}) between [0-22]·230kWh - substation 2 Gdynia (PV system size indicated by the red line)

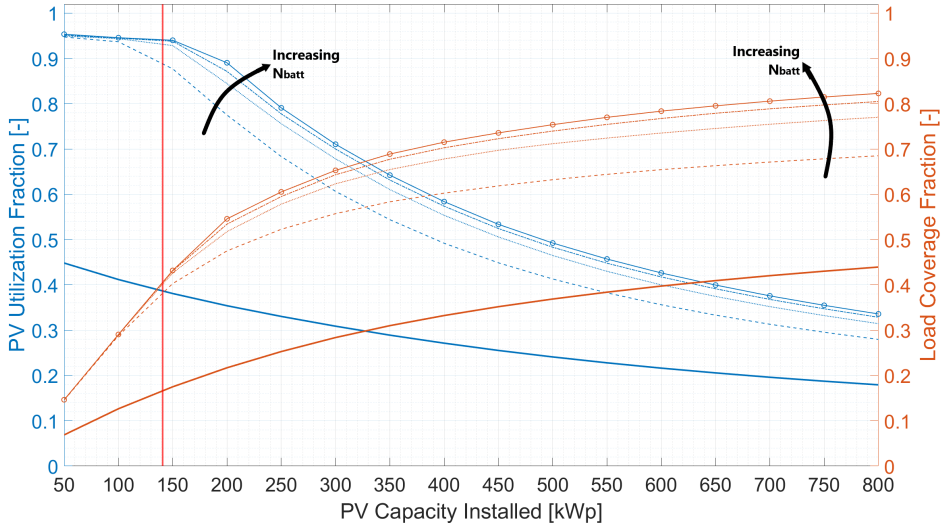

(b) PV Utilization and Load coverage with varying PV capacity [50-800]kWp and number of batteries (N_{batt}) between [0-4]·230kWh - substation 9 Gdynia (PV system size indicated by the red line)

Figure 6.1: PV Utilization and Load coverage with varying PV capacity and number of batteries installed for substations of different sizes

also the performance of the battery system connected to the PV, another indicator is defined: the battery energy storage system utilization.

This is defined as:

$$BESSU = \frac{\int_t P_{\text{discharge}}\, dt}{\text{Days of the year} \cdot \text{Cap} \cdot \text{DoD}} = \frac{\text{Energy Discharged}}{\text{Available Capacity}} \tag{6.1}$$

Where, $P_{discharge}$ is the power discharged every second from the battery system, 366 are the days in 2020, Cap is the total capacity of the battery system (which is 230kWh multiplied by the number of batteries) and DoD (0.9) is the Depth of Discharge.

Through this indicator the cycles of discharge of the battery are estimated [44]. The utilization of the battery provides information on the amount of storage capacity that is used. This means that the indicator can reach values that are higher than one if multiple charge/discharge cycles a day are performed. If the BESS experiences a full discharge cycle on a daily basis then the battery utilization will be 100%. This allows us to understand to what extent the battery is being used and avoid over-sizing the storage system. In Figure 6.2a and Figure 6.2b, the levels of utilization of the batteries are

shown. Again, in the plots the number of batteries is varied from one to the maximum amount, which represents the capacity that is necessary to avoid PV excess dump in the AC grid.

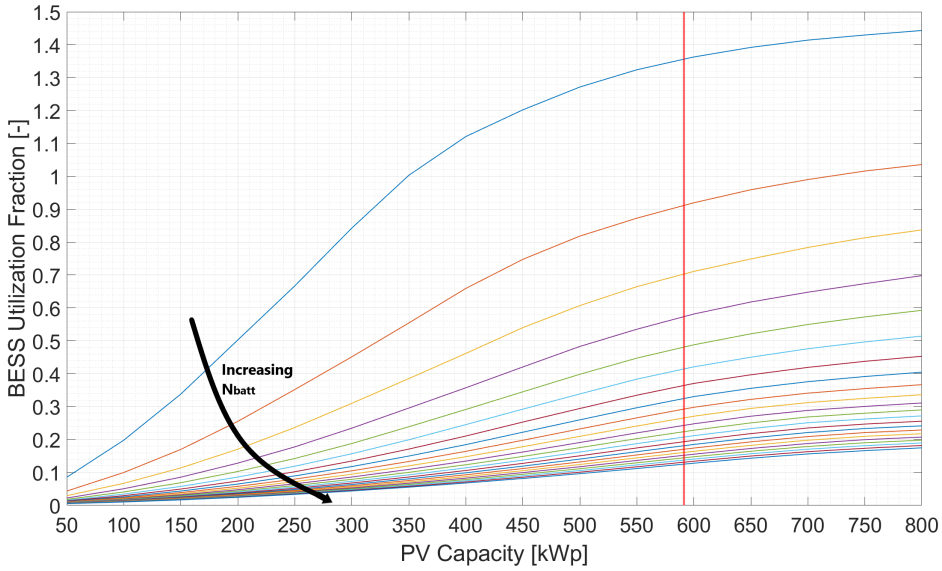

(a) Battery utilization with varying number of batteries (N_{batt}) between [0-22]·230kWh - substation 2 Gdynia (PV system size indicated by the red line)

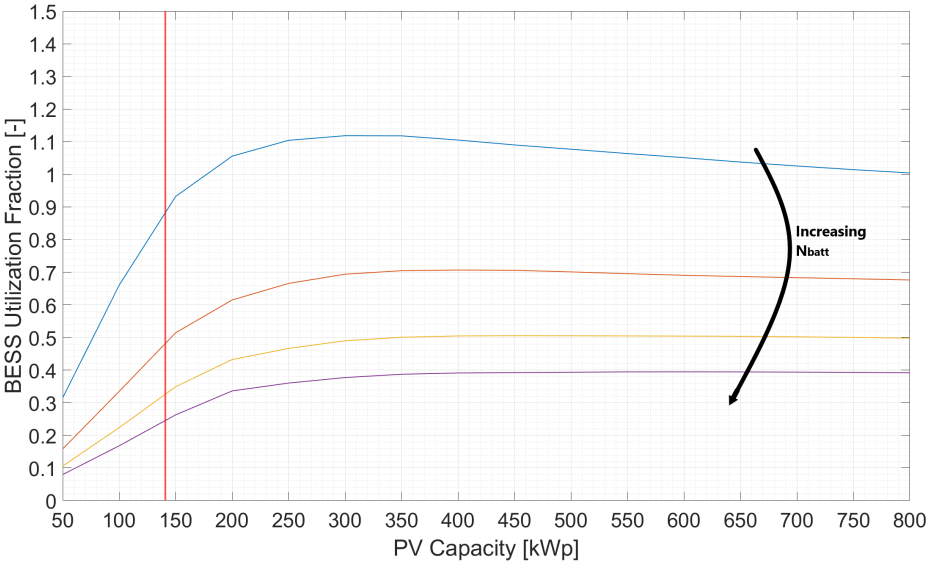

(b) Battery utilization with varying number of batteries (N_{batt}) between [0-4]·230kWh - substation 9 Gdynia (PV system size indicated by the red line)

Figure 6.2: Utilization of the Battery Energy Storage Systems integrated in two substation of different sizes

What can be seen is that increasing the number of batteries causes the reduction of the utilization of the storage system, namely the reduction of the charge and discharge cycles carried out throughout the year. The number of batteries in the two plots goes from 1 to maximum, from the top to the bottom line. The vertical red line represents the PV capacity size, for substation 2 590 kWp and for substation 9 140 kWp. If we fix these values and check the BESS utilization, we see that the maximum number of batteries that can be installed to have at least 50% utilization are 4 and 1 respectively for the large substation (2) and the small one (9). Installing more batteries, in both cases, would cause a rapid decrease of the utilization of the storage system and a minor increase in PV utilization and load coverage. In Table 6.1 and Table 6.2 an overview of the effects of introducing storage in the two substations is presented. In particular, the results of the case in which the number of batteries is selected to have zero dump are provided in Table 6.1 and the case in which it is picked to have at least 50%utilization are given in Table 6.2.

Table 6.1: Substation 2 and 9 in Gdynia grid - comparison between performance without and with BESS in the zero energy dump case

	Without BESS - baseline				With BESS - Zero dump				
Substation number	**PV cap [kWp]**	**PVU [%]**	**LC [%]**	**PV dump [MWh]**	**Batteries [number]**	**PVU [%]**	**LC [%]**	**PV dump [MWh]**	**BESSU [%]**
2 - Gdynia	591	59.14	25.47	229	22	96.32	41.57	0	12.52
9 - Gdynia	141	38.71	16.53	82	4	94.19	40.65	0	24.53

Table 6.2: Substation 2 and 9 in Gdynia grid - comparison between performance without and with BESS in the BESS utilization (BESSU) >50%

	Without BESS - baseline				With BESS - BESSU >50%				
Susbtation number	**PV cap [kWp]**	**PVU [%]**	**LC [%]**	**PV dump [MWh]**	**Batteries [number]**	**PVU [%]**	**LC [%]**	**PV dump [MWh]**	**BESSU [%]**
2 - Gdynia	591	59.14	25.47	229	4	90.11	38.89	37	57.40
9 - Gdynia	141	38.71	16.53	82	1	89.41	38.58	7	89.67

Although in the tables the data for only two substations are reported, it is possible to see that the increase of number of batteries from one case to the other induces limited variations in the PVU and LC values, respectively by 5% and 2 percentage points. On the other hand, in order to have zero energy dump in the AC grid the number of batteries is increased to a point in which the utilization of the storage system drops to values of less than a third than what is found in the optimised case of utilization ¿50%. The beneficial effect of introducing storage is seen not only in the PVU and LC values that are effectively increased in both cases, but also when looking at the energy dump. In fact, also in the case in which the number of batteries is optimised to have an utilization of more than 50% the PV energy dump in the AC grid is reduced by 84% and 91%, respectively for substation 2 and 9.

The reduced utilization of the battery storage system when increasing the number of batteries included, is visible also by the state of charge variation throughout the year. The State of Charge of the BESS in the two cases proposed, no excess dump in the grid and battery utilization higher than 50%, is plotted both for substation 2 in Figure 6.3 and substation 9 in Figure 6.4. The significant increase in the number of charge and discharge cycles occurring when the number of batteries is decreased is clear from the plots. Another observation that can be done is on the seasonal mismatch. It is possible to notice how the battery operation is concentrated between March and October. In the winter months all the PV generated energy, which is limited compared to the rest of the years generation as shown in Figure 6.10, is directly used by the load. Thus the battery is never charged and therefore never used to supply the load either. As expected, in order to increase the load coverage further it would be necessary to introduce either a long term storage system to shift the load from summer to winter months and which would compensate for the low PV output during the colder and darker months.

After the analysis proposed for the two substations in Gdynia, some general conclusions are drawn on the potential of integrating PV systems coupled with storage for all the substations in the two grids. The two cases used to assess the performance of storage introduction in the traction grid are presented in the previous sections and here summarised:

- Battery energy storage system is sized to avoid PV excess to be dumped in the MVAC grid. The sizing condition used is: P_{dump}=0.
- The Battery energy storage system is sized based on the battery utilization. Therefore, the sizing condition for this case is: BESSU>50%

In the plots that are presented next, these two cases are analysed and compared to the no battery scenario. In Figure 6.5, the PV utilization variation is presented for the three cases. In the previous chapter, the effects of the substation size on the PV system effective integration are studied. It is concluded that the increase in energy requirements induces higher levels of PVU and LC. As can be seen in Figure 6.5, the introduction of storage is more effective for smaller substations that had limited potential with only PV. As a matter of fact, the battery systems, appropriately sized for each substation, bring all the substations, independently from the size, to similar levels of PV utilization. In Figure 6.6,

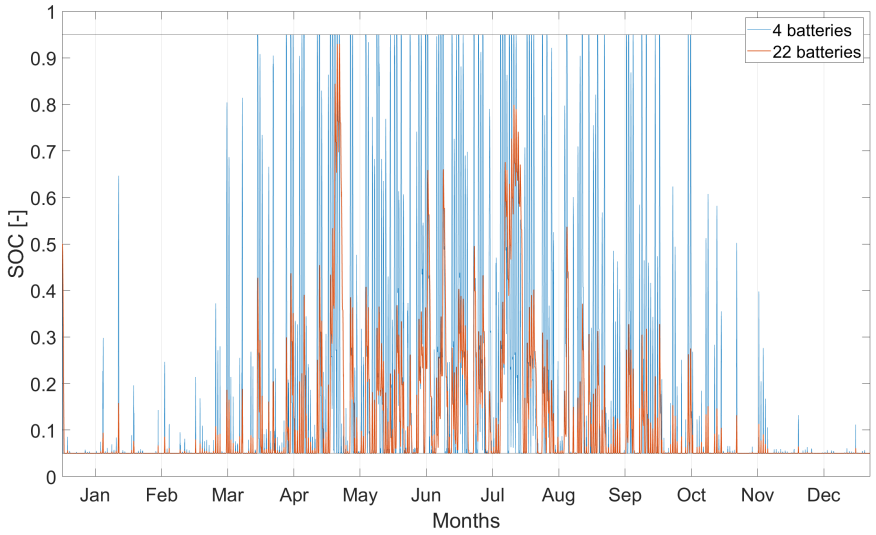

Figure 6.3: State of Charge variation for the Battery energy storage systems installed in substation 2 in Gdynia grid for the two cases proposed in the analysis (no dump and BESSU >50%)

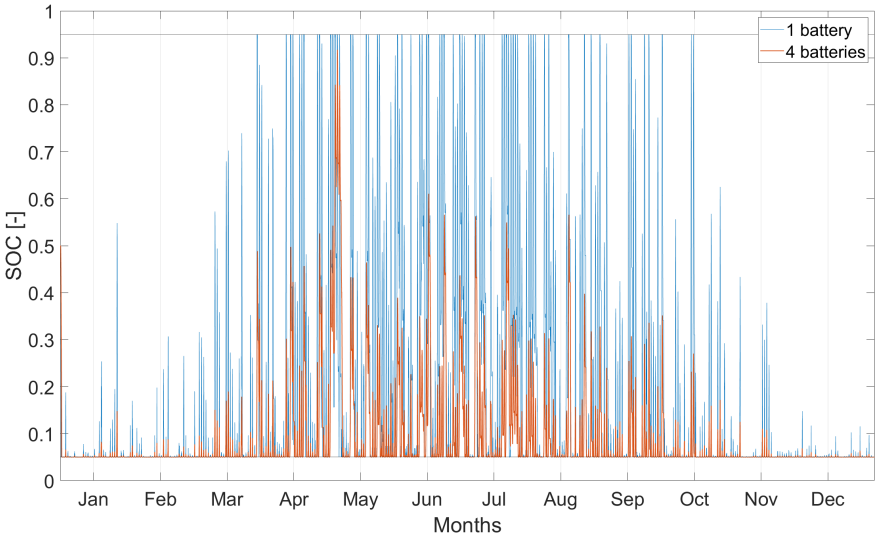

Figure 6.4: State of Charge variation for the Battery energy storage systems installed in substation 9 in Gdynia grid for the two cases proposed in the analysis (no dump and BESSU >50%)

the LC variation for all the substations after the introduction of the BESS is plotted. The observations done so far for the PVU can be made for the LC also. From the two plots the comparison between the two cases, zero dump and high battery utilization, can also be done. The increase in the number of batteries to reduce to zero the PV excess energy dump in the grid does not bring along significant improvement of the performance of the PV and storage coupled system.

In Figure 6.7, the number of batteries for the two cases is shown. It can be seen that in order to have zero dump of PV excess the number of batteries can be increased by 15 batteries, which corresponds to 3.45 MWh of storage capacity. However, the additional battery capacity not only does not significantly increase the PVU and the LC but causes the battery utilization to drop. The plot in Figure 6.8 shows the increase in utilization that the battery system experiences when the capacity is reduced. Imposing the BESSU to be higher than 50% causes an increase in BESSU of around 45 percentage points on average. It has to be noted also that smaller substations never reach a battery utilization of 50% or higher. This is why some points lay on the x-axis. These substations are excluded from the analysis, since their dimensions do not allow to have significant PV integration potential, not even when storage is added.

The number of batteries to reach the 'zero dump' condition presents some peaks. If we look at Figure 6.7, there are 3 cases in which the increase in number of batteries is higher than expected, the

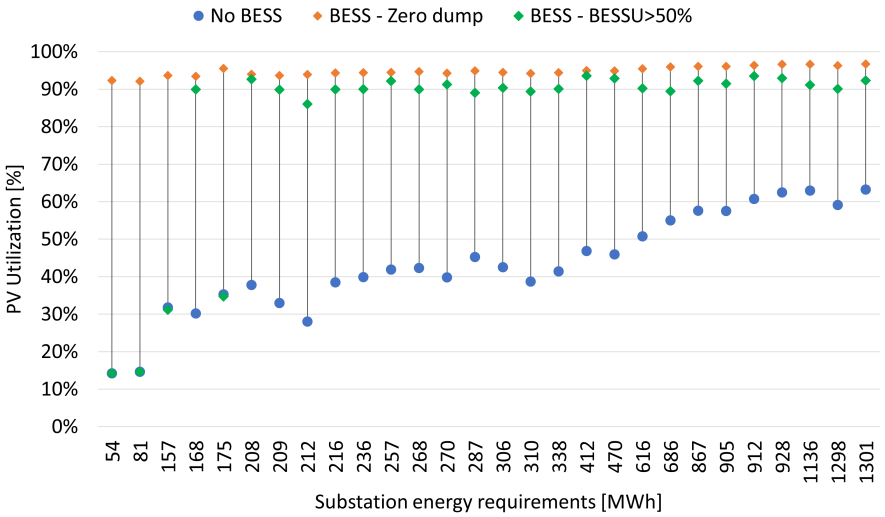

Figure 6.5: PV Utilization levels without battery energy storage system (BESS), in the zero dump and in the BESSU>50% scenarios

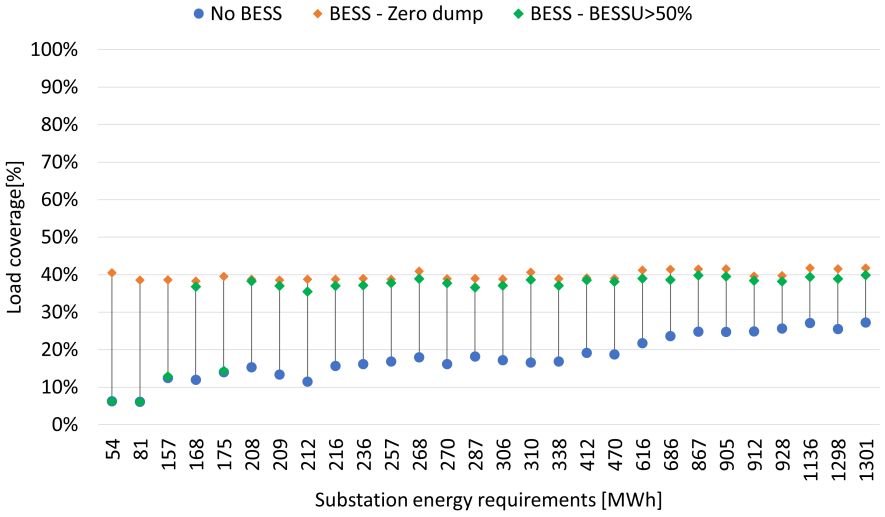

Figure 6.6: Load coverage levels without battery energy storage system (BESS), in the zero dump and in the BESSU>50% scenarios

substations with 175 MWh, 212 MWh and 1298 MWh energy requirements. When we look at the distribution of the load in the day we can see that these three substations have higher shares of runs happening during night hours. In particular, going in order of increasing energy demand, the first substation presents 12.5% of its runs during night time against an average of 8.4% for all the substations. The second substation (212 MWh) shows better results due to the fact that the fraction of runs happening in the night has a share of 10.2%. Finally, the substation with 1298 MWh energy demand, is the high demand substation with the highest rate of night runs, accounting for 9.1% of the runs of the day on average throughout the year. In all three cases this not only implies lower match with the PV profile, but also a decrease in the runs happening through out the day and in PV direct use.

The next plot provides some interesting insights related to the dump of PV excess energy that is not used by the load. In Figure 6.9, the energy dump in the two cases for all the substations is shown, compared to the dump happening when no storage is included. The increase in the size of the substations causes a linear increase in the excess energy. The introduction of batteries induces a strong reduction of the energy dumped. In the zero dump scenario there is no energy dump, since this is the sizing condition. However, one can see that the energy excess is extremely reduced also when the storage capacity is selected based on the battery utilization.

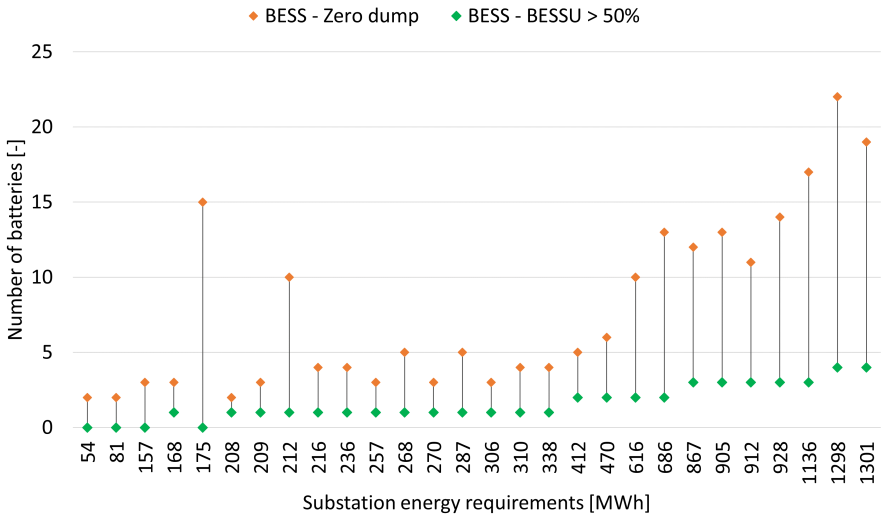

Figure 6.7: Comparison between the number of batteries installed in the two scenarios: zero energy dump and battery utilization > 50%

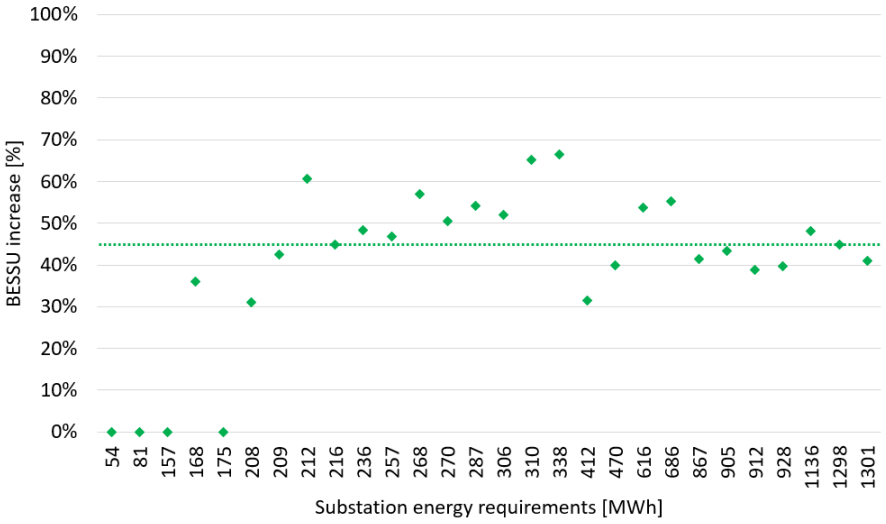

Figure 6.8: Battery utilization increase when reducing the number of batteries from zero dump scenario to high battery utilization scenario condition

To conclude, the introduction of storage is highly effective in terms of PV performance and of management of the excess energy generation. The smaller substations are the ones that are mostly affected by the integration of batteries, seeing increases in PVU by more than 60 percentage points in some cases and in LC by 20 percentage points and higher. The energy dump is strongly reduced for all the substations also in the case in which the sizing of the battery system is done through the condition on its utilization. The further increase in batteries to reach zero energy dump is not a feasible solution due to the high amounts of extra capacity required. Not only it is not feasible, but it is also not interesting in terms of performances since it does not cause significant improvements in the PV utilization and load coverage. The final conclusions can be drawn looking at Figure 6.10a and 6.10b. These bar charts represent the fraction of time in which the PV and storage system are able to supply the load. What can be seen in first place is that the fraction of time in which the load is partially covered by the PV generation, for at least 20%, increased by 3 percentage points. However, the fraction of time in which the load is completely covered improved by 7 percentage points. This means that the introduction of battery storage systems induces an improvement in the temporal mismatch, especially favouring the overall load coverage. The increase in the fraction of time in which the load is partially covered is limited by the seasonal mismatch between PV generation and demand, and as we have observed from the SOC plots, the storage system does not allow major improvements. This is due to the short-term characteristics of the storage method chosen.

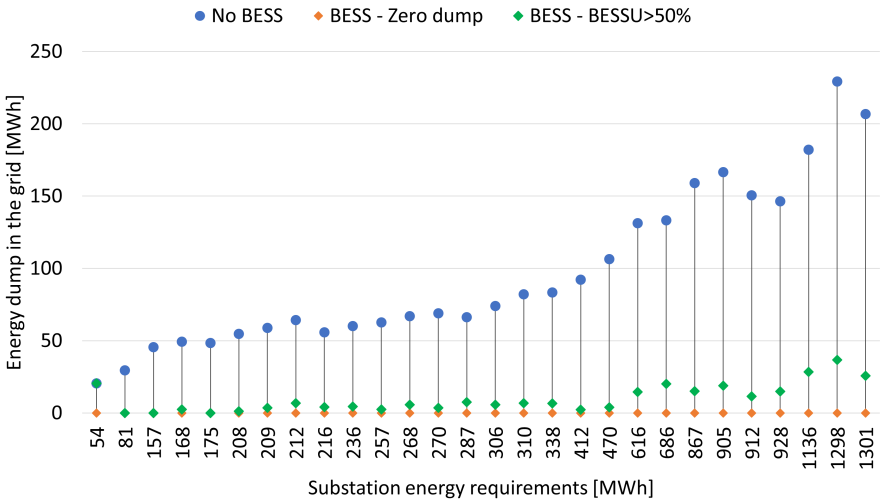

Figure 6.9: Comparison between the PV excess energy dumped between the two scenarios (zero energy dump and battery utilization $> 50\%$) and the no storage case

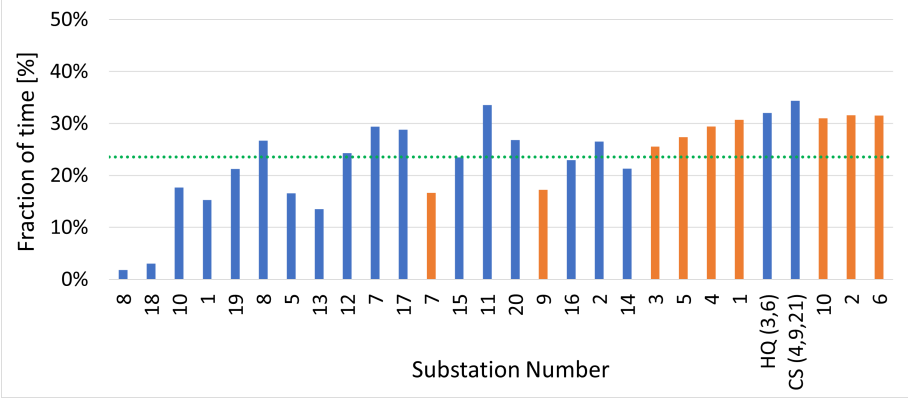

(a) Fraction of time in which the PV generation can supply at least 20% of the load throughout the year for each substation

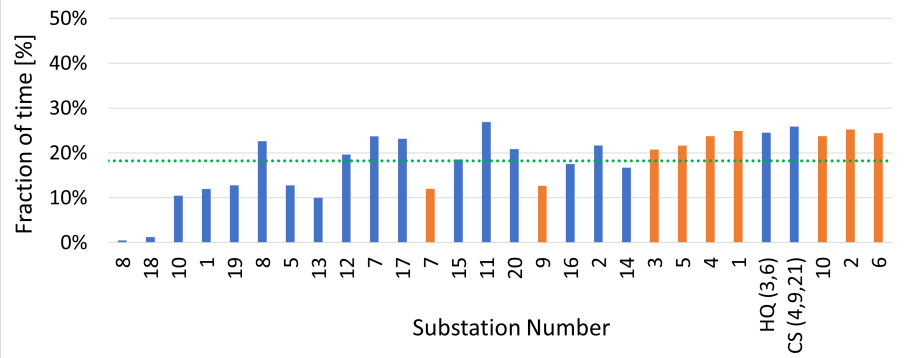

(b) Fraction of time in which the PV generation can supply the whole load throughout the year for each substation

Figure 6.10: Temporal mismatch between PV generation and load: fraction of time in which PV covers the load through the year - Arnhem in blue and Gdynia in orange

The integration of storage in this project is functional to the PV potential. This means that the aim is to assess its impacts on the variation of the PV performance. However, it is possible to see in the plots that substations have different responses to storage integration. It would be interesting to study what are the causes of successful integration of storage and if any of the KPIs plays a role on this. In Figure 6.11 and 6.12, two plots are provided showing the variation of BESSU and of Energy dump with the size of the substation. As one can see, some possible trends can be found. However, it would be interesting to perform this study through a sensitivity analysis, varying the storage size of smaller and

equal steps for all the substations to see what the effects are on each of them. This will be included in the recommendations for future work.

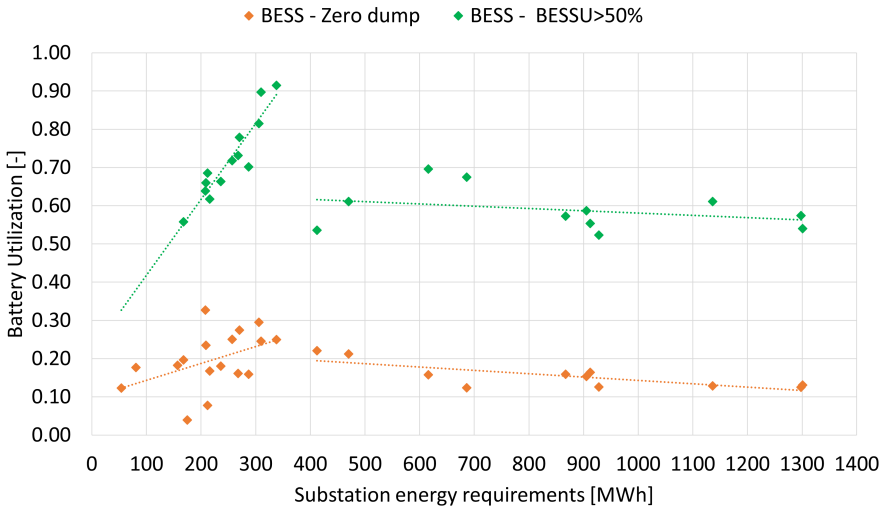

Figure 6.11: Battery utilization in the two scenarios used for the sizing of the storage system

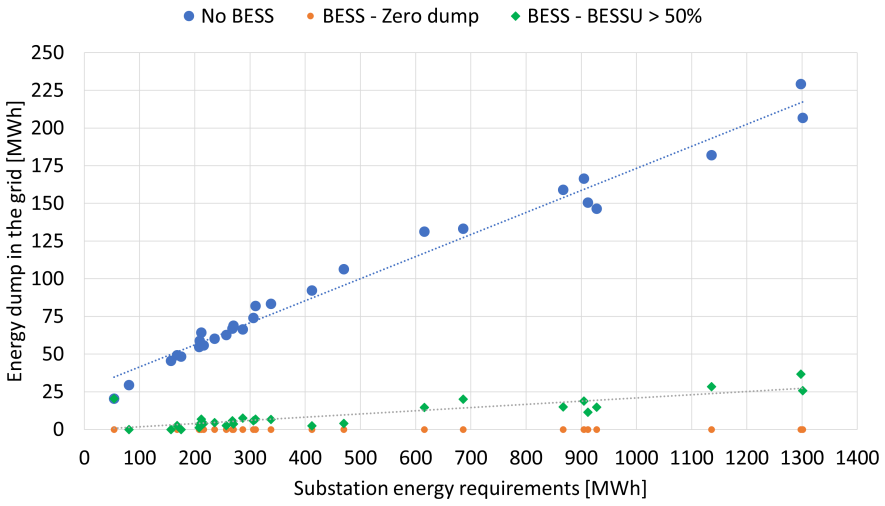

Figure 6.12: Energy dump trends for the two sizing options and the case with no storage

6.2 Feasibility of installing PV and Storage in the traction grids

This last section is dedicated to a brief analysis on the feasibility of the PV and storage integration. In Table 6.3 and 6.4, an overview of the size of the PV and battery systems installed for each substation in Arnhem an Gdynia are provided.

The results show that a total surface of 2.6 hectares and 3.4 hectares are required to install the systems in Arnhem and in Gdynia. This value is obtained considering an area of approximately 3.7 m2 per module which is found to be the optimal installation in the Groningen PV system project using the same PV modules [55]. These numbers all refer to the case in which all the substations are fed by a PV+battery system (excluding the smaller substations for which 50% battery utilization cannot be reached). In Gdynia 3.4 MWp of PV modules and 5.3 MWh of battery storage would be necessary to supply the traction grid. The traction grid is not autonomous with the integration of PV and storage, but is still dependant on the MVAC grid. Overall in Gdynia 3 GWh per year would be supplied by the PV and battery system out of a total demand of 7.4 GWh. In Arnhem, a total of 2.5 MWp and 4.8

MWh PV and battery systems would be required to supply the load, with storage sized based on its utilization. Also in this case the load would be covered partially from these sources and would still be dependant on the MVAC grid. Overall, 2.2 Gwh out of 5.8 GWh of total demand would be supplied from the PV plus storage system. Both in Gdynia and in Arnhem, the smallest and less performative substations are excluded. In these substations it is not possible to reach a battery utilization of more than 50% and therefore they are considered not appropriate for the analysis.

To conclude, in Table 6.5, the investment costs and payback time for the two systems are shown. This calculation is done very roughly, just to provide an idea of the investment costs and the time in which the system would be paid back. The installation costs for PV are taken as 700€/kWp [37] and compared to [30], while storage costs are estimated considering a system price of around 250€/kWh of capacity installed [50], considering the reduction in price that the Li-ion battery systems are undergoing in these years. Finally, to compute the yearly savings the commercial electricity prices are used, 13.76 cent€/kWh in the Netherlands [57] and 13.43 cent€/kWh in Poland in 2019 [56].

It is possible to see that only after 9 and 10 years, for Gdynia and Arnhem, the installation would generate revenues. If one considers 20/25 years of lifetime, this makes the investment effective since it would generate revenues for half of the installation lifetime. These numbers are a very rough estimation of the actual costs. The study of the feasibility and optimization of the installations should be performed again in a more precise way. For example, location issues and land permission and costs are not considered. In many cases one PV+battery system could be supplying multiple substations, minimizing space and costs of the Balance of System. It is found by playing with the numbers, that installing the PV+storage systems in only a few substations could reduce the Payback time further. For future work, it would be interesting to study an optimization method accounting also for costs and availability of space.

Table 6.3: PV and storage system sizing for every substation in Arnhem grid

Substations	PV capacity [kWp]	PV modules	Surface [m²]	Batteries (BU>50%)	Storage capacity [kWh]
1	78.4	215	799	1	230
2	191.6	525	1950	2	460
HQ (3,6)	424	1162	4316	3	690
CS (4,9,21)	431.6	1183	4394	3	690
5	96.8	266	988	1	230
7	109.6	301	1118	1	230
8	96.8	266	988	1	230
10	0	0	0	0	0
11	133.2	365	1356	1	230
12	100.4	276	1026	1	230
13	98.8	271	1007	1	230
14	218.4	599	2225	2	460
15	125.6	345	1282	1	230
16	156.8	430	1598	1	230
17	119.2	327	1215	1	230
18	0	0	0	0	0
19	0	0	0	0	0
20	142.4	391	1453	1	230
Total	**2523.6**	**6922**	**2.6 hm²**	**21**	**4830**

Table 6.4: PV and storage system sizing for every substation in Gdynia grid

Substations	PV capacity [kWp]	PV modules	Surface [m2]	Batteries (BU>50%)	Storage capacity [kWh]
1	412	1129	4194	3	690
2	591.2	1620	6018	4	920
3	280.4	769	2857	2	460
4	394.8	1082	4019	3	690
5	312	855	3176	2	460
6	592.4	1624	6032	4	920
7	122	335	1245	1	230
8	0	0	0	0	0
9	140.8	386	1434	1	230
10	517.2	1417	5264	3	690
Total	**3362.8**	**9217**	**3.4 hm2**	**23**	**5290**

Table 6.5: Payback time and investment costs

Gdynia	
PV investment	2.35 M€
Storage investment	1.36 M€
Yearly savings	-0.41 M€
Payback time	9.2 years

Arnhem	
PV investment	1.77 M€
Storage investment	1.24 M€
Yearly savings	-0.30 M€
Payback time	9.9 years

6.3 Summary and takeaway points of the chapter

The integration of Battery Energy Storage Systems coupled with PV at substation level is discussed in this chapter, in which a study is conducted on the effect that the integration of battery energy storage systems (BESS) has on the PV performance. The effectiveness of introducing BESS is also measured through the PV Utilization (PVU) and the Load Coverage (LC), since the aim is to study its **impact on the PV integration**.

The analysis of two scenarios is proposed. In the first one, the battery system is sized based on the amount of capacity required to avoid any PV generation excess to be dumped in the grid ('**Zero dump**'). The second scenario is the one in which the BESS is sized based on the utilization of the system, so the number of batteries is chosen to have at least **50% of battery utilization**. This analysis allowed us to conclude, that increasing the storage capacity installed over a certain limit **reduces the battery system utilization** (Figure 6.8) and does not bring significant improvements in the PV performance (Figure 6.5 and 6.6).

The introduction of BESS coupled with the PV systems at substation level increases substantially the performance of the PV systems, reaching values of **PV utilization in the range of 90%** or higher and levels of **load coverage of approximately 40%**. The enhancement of PVU and LC is high especially for smaller substations which see increases by up to **60 and 30 percentage points** respectively.

Finally, the feasibility of the introduction of PV and storage is studied. The rough estimation of the investment costs provide a total payback time of **9-10 years** for the two grids. This makes the project cost-effective if the lifetime considered is 20-25 years.

7 CONCLUSIONS AND FUTURE WORK

In this last chapter the conclusions drawn through this research project are summarised, followed by an overview of the limitations of the project and the possibilities of extension of the work.

The transport sector in EU is responsible for 30% of total energy consumption and 27% of greenhouse gas emissions. Investigating in possible solutions to reduce the energy consumption and the emissions of urban transport is the context in which this thesis project is developed. Electrifying and supplying through emission-free sources urban means of transport is a possible solution. In this research project, we investigated on the potential of introducing Photovoltaic (PV) systems in trolleybus traction grids in different cities. In particular, Arnhem and Gdynia trolley-grids are used as case studies. When speaking about PV system integration potential, the intention is to investigate the effectiveness of the PV generation in supplying the load. This is measured investigating both what fraction of the PV generated energy is used by the trolleybus system compared to the total generation (PV Utilization 5.1) and what fraction of the load is covered by the PV generated energy (Load Coverage 5.2). These two elements provide an overview of how well the PV systems can perform in relation to the traction grid operation.

Different solutions for PV integration are possible, here we study the effects of the structure of the grid and of the characteristics of the city on the integration of PV at substation level on the AC side. Finally, the impact of coupling the PV systems with battery energy storage systems (BESS) is assessed. The storage system is studied in terms of PV performance, however also the battery utilization is assessed considering the daily charge and discharge cycles performed throughout the year 6.1.

A number of challenges is faced during the project, which induces the increase in the time that is necessary to prepare the modelling inputs and the simulation program structure. The limited amount of available data of the grids and measurements from the grid operation, required us to generate data ourselves in order to simulate the trolleygrid system operation. In relation to this data on bus routes, schedules and city topography are used to create velocity profiles of the trolleybuses. The introduction of simulated input data increases the error in the outputs and some limitations to the model which will be further discussed in the next section. Overall, the main contributions of this Master Thesis project are:

- An extensive review of the existing literature on the causes of electric vehicles energy demand variations and on the integration of PV and storage systems in traction grids of different types
- The definition of a set of Key Parameter Indicators (KPIs) that can be used to evaluate the potential of integrating PV systems in different cities
- A model generating velocity profiles for different city and route characteristics, based on existing measured velocity cycles
- A study on some selected KPIs, between the identified ones, to assess their impact on PV integration in trolleygrids
- A study on the effect of storage introduction coupled with the PV systems integrated at substation level
- An comparison between the results of different substations and of the two trolleygrids in Arnhem and in Gdynia.

We answered to the research questions we identified in Chapter 1.

Question 1
What parameters have an impact (qualitatively) on the PV integration in a trolleygrid, and to what extent?

An extensive research is done on the parameters, identified as **Key Parameter Indicators (KPIs)**, to determine the effects that they are expected to have on the traction grids. The effects are studied in terms of expected intensity of the impact and also on which component of the system is expected to be affected more. A set of KPIs is defined based on the literature study performed and on the available data of the two trolleygrids. This **set of parameters** can be used as base to **determine the effectiveness of the PV integration** based on the values found for each city. They are classified in terms of effects on the system components and on the relation between different parts of the trolleygrid system. They are divided in three groups based on if they are considered environmental-, city- or trolleybus-system-related parameters. In Figure 3.6, the table with the outputs of this study is given. The table is colour coded based on the **intensity of the impact** of each indicator. A brief explanation of what is the cause of the impact of the parameter on the system component is also provided.

Not all the parameters are selected and used further in the quantitative assessment of the impact on the PV integration due to limited availability of data, time limitations and appropriate method of analysis suggested. The analysis of the impact of all the KPIs should be concluded in future works in order to **develop a framework** which would allow to draw general recommendations on the application of PV. Based on the values found for each indicator, it will be possible to define the expected potential of integrating PV. For the KPIs which have not been studied yet, possible analysis and research methods are briefly proposed.

Question 2
How does the potential of PV integration vary for different cities in respect to selected study- indicators (quantitatively)?

1. *How do **environmental parameters** affect the potential of PV integration in trolleygrids?*
   It is possible to conclude that the environmental parameters, as sunshine duration and yearly irradiance, have a strong impact on the Load Coverage (LC), while do not affect noticeably the PV Utilization (PVU). The increase in average radiation levels and sunshine duration induce a linear increase in the Load Coverage (LC) factor. The PV Utilization, as mentioned, is less affected and sees a slight reduction in cities in which the radiation levels are much higher. In Figure 5.4 and 5.3, the reader can find the two plots representing the LC and PVU variation with respect to the radiation and the daily sunshine duration. The maximum **variation of LC reaches values of 10 percentage points**, while only **1 percentage point PVU variation** is registered for the weather data analysed. The trend found for these two parameters is caused by the fact that the same PV system installed in cities with different irradiance data will present an **increase in the generation**, however since the load is constant this will be followed by an **increase in excess** energy dumped in the grid. The **load coverage increase** is limited by the **temporal mismatch and the seasonal mismatch** of load and generation.

2. *How does the **configuration of the substations** (power, number, length of supplied sections) affect the potential of PV integration in in trolleygrids?*
   The average power/energy requirements of the substation strongly affect the integration of PV and its performance. The increase in energy and power demand induces the **increase of both PV utilization (PVU) and load coverage (LC)**. This is shown in Figure 5.11 and Figure 5.10. The decentralization of trolleybus systems causing the increase in number and the reduction in size of the substations will reduce the potential of integrating PV in the trolleygrid.

   The conclusion on the **negative effect on PV performance of decentralising** the traction-grid, is confirmed when the effect of the number of sections supplied by a substation is studied. In Figure 5.7, the trends for the PVU and LC with varying number of sections is shown. The increase in number of sections fed by a substation induces a **parabolic increase in the PVU and LC fractions**.

Increasing the length of the sections is expected to have a positive impact, due to the increase in the probability of having more buses under the substation and therefore having a higher power requirement. Moreover, the increased transmission losses should also favour the integration of PV, inducing an increase in the demand. However, as can be seen from Figure 5.8, making the sections longer seems to have no impact on the performance of PV. As a matter of fact, **no trend is found** in the data. This could be related to the face that the increased probability of having an extra bus on the section causes also a higher chance of power exchange between buses. The increased rates of regenerative breaking probably balance out the other elements.

An overall **'service coefficient'** is defined as the product of the total km of overhead lines supplied and the average power requirements of a substation. This parameter is used to obtain an indication of the effect of substation size both in terms of spatial and quantitative power requirement distribution. The trends found when plotting this indicator for all the substations of the two grids, show a fractional function trend which reaches a plateau for sizes larger than 500 kWkm. When comparing the effect of km and kW, the power requirements play a bigger role and have a stronger effect on the potential of integrating PV at substation level.

The size of the substation and the distribution of substations in the trolleygrids have a strong impact on the potential of integrating PV. All the curves used to fit the data found for the substation seem to **reach a plateau and a saturation point** over which the increase of the studied indicator has a very limited or null effect on the performance of PV.

3. *How does **bus traffic** affect the potential of PV integration in trolleygrids ?*
   The increase in the average bus traffic under a substation causes the **improvement of the PV system performance**. In Figure 5.14 the values of PV utilization and Load Coverage found for all the substations are provided and a fitting model is proposed. A very similar regression model is found, as the one discussed for the substation size and configuration. Also the impact of bus traffic is strong for variations in low number of buses supplied and reach a **saturation after the value of 3 buses**. The PVU and LC seem to both reach a plateau after this point, and therefore any further increase in bus traffic does not improve the PV performance anymore.

4. *How do the **HVAC requirements** affect the potential of PV integration in trolleygrids?*
   The HVAC power demand of a bus causes the **seasonal variability of the load**. In Figure 6.10, one can see the opposite curves presented by the HVAC requirements and the PV generation throughout the year. Through this study it is demonstrated that, in spite of the opposite trends characterising the HVAC requirements and the PV generation, removing the HVAC demand **reduces the potential of integrating PV**. As a matter of fact, although switching off the HVAC system causes a more constant load throughout the year, both the PV utilization and the load coverage experience a reduction when this test is done. **The PVU variation can reach values of up to 35 percentage points drop and the LC of maximum 14 percentage points**. The increase in the fraction of the total substation energy demand covered by the HVAC system on average induces a higher drop in the PV performance.

   It is also concluded that the better characteristics in terms of substation configuration and bus traffic, cause a limited variation when removing the HVAC. As a matter of fact, the characteristics of some substations in Gdynia allow to confine the negative effect of removing the HVAC power demand.

5. *How does the introduction of **bilateral connections** between sections affect the PV integration in trolleygrids?*
   The effect of introducing bilateral connections between sections of different substations is studied only partially due to modelling and time constraints. The model to simulate the operation of all the sections of the grid with and without bilateral connections is not complete yet and this does not allow to simulate the operation of the whole grid. The results for 3 substations are plotted in Figure 5.21. The reduction in energy demand induced by the bilateral connections for the three substations is not necessarily followed by a decrease in PV performance. The variation in PVU and LC are negligible although reductions in energy demand are significant.

Although it is difficult to draw conclusions by the observation of the performance of 3 substations only, it is possible to say that the introduction of bilateral connections seem to be **beneficial for the performance** of the trolleygrid and the integration of PV. This because the reduction in energy demand (and in losses) induces a **reduction of PV capacity** required without undermining the performance of the system.

Question 3
How does the introduction of stationary storage affect the integration of PV in trolleygrids?
Stationary storage (battery energy storage system or BESS) is introduced coupled with PV at substation level. This means that the battery system is used only to increase the PV self-consumption and improve the match between PV generation and load. The storage system is not used to supply any other service to the trolleygrid.

The introduction of BESS coupled with the PV systems at substation level increases substantially the performance of the PV systems, reaching values of PV utilization in the range of 90% or higher and levels of load coverage of approximately 40%. The enhancement of PVU and LC is high especially for smaller substations which see increases by up to 60 and 30 percentage points respectively for the former and the latter. In Figure 6.5 and 6.6, the plots related to the increase in PVU and LC are shown.

The analysis of two scenarios is proposed. In the first one, the battery system is sized based on the amount of capacity required to avoid any PV generation excess to be dumped in the grid. The second scenario is the one in which the BESS is sized based on the utilization of the system. The number of batteries is chosen to have at least 50% of battery utilization. When comparing the results of these two cases, some conclusions are drawn:

- The increase in capacity to reach zero energy dump does not induce high variations in the PV utilization (PVU) and in the load coverage (LC). An average of +3.5 percentage points increase in PVU and of +1.5 percentage points in LC are registered. Therefore, the PV performance is not affected significantly (Figure 6.5 and 6.6).
- The battery system utilization (BESSU) drops considerably, with reductions in the utilization by -45.5 percentage points, when increasing the battery size to avoid dumping energy in the MVAC grid (Figure 6.8).
- The reduction in energy dump experienced by the system in the second scenario is on average of 93.5% (Figure 6.9).

This allows us to conclude that increasing the storage capacity installed over a certain limit reduces the battery system utilization and does not bring significant improvements in the PV performance.

The introduction of storage enhances PV performance, increasing the utilization of PV, the temporal match between PV and load (from 20% to 24%) and the load coverage. However, it is possible to observe that both PVU and LC reach limits. The first is restrained by efficiencies and losses while the second one is strongly affected by the seasonal mismatch between load and PV.

7.1 Recommendations and Future Work

Starting from the data in input and the models used, some limitations are found in the proposed research method. Moreover, the developed methods to assess the potential of integrating PV in trolley-bus traction grids can be used to extend the results to other cities and should be completed though the study of the missing KPIs.

The first limitation in this work is the amount of available data. One of the recommendations is to repeat the work with an increased number of measurements. In particular, this is true for the Gdynia grid, for which everything was simulated due to the complete absence of measured data. This **limits the precision of the power profiles** obtained for the runs of the buses throughout the grid. The recreation of power profiles has two main limitations. The first is related to the fact that the velocity

profiles are generated without taking into account the road gradients, the presence of other vehicles and traffic congestion in the streets and passenger flow. Therefore, the power profiles generated might see peaks in power due to high accelerations in steep roads which would not be there in real conditions. Also, the power profiles are generated with a fixed passenger load. The second thing reducing the accuracy of the generated power profiles is the error introduced when using the HAN University model. Although this model is adapted to the buses used in the two grids, with the respective power and torque control curves, this model is subject to errors up to 30% especially when regenerative energy is concerned. To conclude, the first suggestion for future work is to **increase the amount of measurements** or to **increase the accuracy of the model** used to generate the velocity profiles and the one created by HAN university to create power curves from the velocities.

Secondly, the study **develops a set of KPIs** that can be used to assess the potential of PV integration in trolleygrids. However, although the indicators have been identified and the set developed and organised, not all the KPIs have been studied to define the impacts that they have on the PV integration. Due to the limitations in time and data, 5 indicators have been studied thoroughly and 1 has been briefly discussed. In order to complete the table, which can then be used to identify directly the potential of PV integration, the **investigation on the other KPIs** should be completed, starting from the bilateral connections effect. Some research methods are proposed for the indicators that have not yet been studied.

The third recommendation is to complete the work and confirm the obtained results once the **power flow calculations model** for all the types of sections is completed. For this research only linear sections are modelled through power flow calculations. Once the models to simulate all the types of sections and of connections are ready, the work should be repeated. Through these models the hypothesis made on the bilateral effects can also be confirmed or proven to be wrong.

Moreover, the study has been conducted for two cities. The **introduction of other trolleygrids** in the analysis would not only allow to confirm the results but also to understand if the **plateau trend** found in the PV utilization and Load coverage are actually a good representation of the data. The introduction of a very centralised trolleybus traction grid could allow us to understand whether after reaching a certain value of power, number of sections and bus traffic the PVU and LC are still constant or whether they start decreasing.

Another future work that would be interesting to perform is to repeat the analysis introducing **PV and storage on the DC side**. This should increase the utilization of both PV and storage, since the efficiency would be increased and the battery would perform also ancillary services as voltage regulation and increase in the regenerated power use. However, this would require a model to simulate the voltage control in the network which would be necessary when connecting everything on the DC side.

In relation to the introduction of storage in the grid, as mentioned in Chapter 6, some additional study could be performed. It is found that substations have different reactions to the integration of storage based on their energy demand. However, future work could focus on the **effects that the KPIs have on the effectiveness of storage** integration. A sensitivity analysis, with smaller and constant variation of the storage capacity, can be used to understand why the BESS works better in some substations and what potential storage has when integrated coupled with PV. Another check that should be performed is on the **distribution of the dumped power** throughout the year, instead of focusing only on the total energy dump.

To conclude, once the KPI study and the table is completed this framework to assess the potential of PV introduction in trolleygrids should be **tested and verified** for other traction grids. This would allow to have a general overview of the elements to consider before deciding whether to introduce PV and storage in the trolleygrids.

BIBLIOGRAPHY

[1] Refrigerating American Society of Heating and Air Conditioning. Ashrae standard, "ventilation for acceptable indoor air quality," ashrae standard 62, 1999.

[2] Refrigerating American Society of Heating and Air Conditioning. *ASHRAE Handbook of Fundamental*. 2001.

[3] Olindo Isabella René van Swaaij Miro Zeman Arno Smets, Klaus Jäger. *Solar Energy, The physics and engineering of photovoltaic conversion technologies and systems*. Uit Cambridge Ltd, 2016.

[4] The World Data Bank. Population, female (% of total population) - netherlands, 2019.

[5] The World Data Bank. Population, female (% of total population) - poland, 2019.

[6] The World Data Bank. Population, male (% of total population) - netherlands, 2019.

[7] The World Data Bank. Population, male (% of total population) - poland, 2019.

[8] Ricardo Barrero, Xavier Tackoen, and Joeri Van Mierlo. Stationary or onboard energy storage systems for energy consumption reduction in a metro network. *Proceedings of the Institution of Mechanical Engineers, Part F: Journal of Rail and Rapid Transit*, 224(3):207–225, 2010.

[9] Mikołaj Bartłomiejczyk. Bilateral power supply of the traction network as a first stage of smart grid technology implementation in electric traction. In *MATEC Web of Conferences*, volume 180, page 02003. EDP Sciences.

[10] Mikołaj Bartłomiejczyk. Practical application of in motion charging: Trolleybuses service on bus lines. In *2017 18th International Scientific Conference on Electric Power Engineering (EPE)*, pages 1–6. IEEE.

[11] Mikołaj Bartłomiejczyk. Super capacitor energy bank medcom ucer-01 in gdynia trolleybus system. In *IECON 2016-42nd Annual Conference of the IEEE Industrial Electronics Society*, pages 2124–2128. IEEE.

[12] Mikołaj Bartłomiejczyk. Potential application of solar energy systems for electrified urban transportation systems. *Energies*, 11(4):954, 2018.

[13] Mikołaj Bartłomiejczyk. *Dynamic charging of electric buses*. Sciendo, 2019.

[14] Mikołaj Bartłomiejczyk, Piotr Hołyszko, and Piotr Filipek. Measurement and analysis of transmission losses in the supply system of electrified transport. *Journal of Ecological Engineering*, 17(5), 2016.

[15] Mikołaj Bartłomiejczyk and Leszek Jarzebowicz. Energy savings by application of supercapacitor storage in trolleybus supplying station–analysis of experimental results. *Czasopismo Techniczne*, 2016(Elektrotechnika Zeszyt 1-E (2) 2016):17–32, 2016.

[16] Mikołaj Bartłomiejczyk and Robert Kołacz. The reduction of auxiliaries power demand: The challenge for electromobility in public transportation. *Journal of Cleaner Production*, 252:119776, 2020.

[17] Mikołaj Bartłomiejczyk and Marcin Połom. Spatial aspects of tram and trolleybus supply system. In *8th International Scientific Symposium on Electrical Power Engineering (ELEKTROENERGETIKA)*, pages 223–227.

[18] Mikołaj Bartłomiejczyk and Marcin Połom. Multiaspect measurement analysis of breaking energy recovery. *Energy conversion and management*, 127:35–42, 2016.

[19] Mikołaj Bartłomiejczyk and Marcin Połom. The impact of the overhead line's power supply system spatial differentiation on the energy consumption of trolleybus transport: planning and economic aspects. *Transport*, 32(1):1–12, 2017.

[20] Chris Bingham, Chris Walsh, and Steve Carroll. Impact of driving characteristics on electric vehicle energy consumption and range. *IET Intelligent Transport Systems*, 6(1):29–35, 2012.

[21] Mark Bolinger, Samantha Weaver, and Jarett Zuboy. Is 50$/mwh solar for real? falling project prices and rising capacity factors drive utility-scale pv toward economic competitiveness. *J Progress in photovoltaics: research and applications*, 23(12):1847–1856, 2015.

[22] NBG Brinkel, MK Gerritsma, TA AlSkaif, Ioannis Lampropoulos, AM van Voorden, HA Fidder, and WGJHM van Sark. Impact of rapid pv fluctuations on power quality in the low-voltage grid and mitigation strategies using electric vehicles. *International Journal of Electrical Power and Systems, Energy*, 118:105741, 2020.

[23] Massimo Ceraolo and Giovanni Lutzemberger. Stationary and on-board storage systems to enhance energy and cost efficiency of tramways. *Journal of Power Sources*, 264:128–139, 2014.

[24] Flavio Ciccarelli, Luigi Pio Di Noia, and Renato Rizzo. Integration of photovoltaic plants and supercapacitors in tramway power systems. *Energies*, 11(2):410, 2018.

[25] Maria Vittoria Corazza, Umberto Guida, Antonio Musso, and Michele Tozzi. A european vision for more environmentally friendly buses. *Transportation Research Part D: Transport and Environment*, 45:48–63, 2016.

[26] World Data. Body size by country, 2019.

[27] AA Hossam El-din, CF Gabra, and Ahmed HH Ali. Effect of ambient temperature on performance of different types of pv cells at different location in egypt. *solar energy*, 83:604–624, 2013.

[28] Mohammad Ali Fayazbakhsh and Majid Bahrami. Comprehensive modeling of vehicle air conditioning loads using heat balance method. Report 0148-7191, SAE Technical Paper, 2013.

[29] NOAA National Centers for Environmental Information. State of the climate: Global climate report for 2020, 2021.

[30] Ran Fu, David J Feldman, and Robert M Margolis. Us solar photovoltaic system cost benchmark: Q1 2018. Report, National Renewable Energy Lab.(NREL), Golden, CO (United States), 2018.

[31] Marc Gallet, Tobias Massier, and Thomas Hamacher. Estimation of the energy demand of electric buses based on real-world data for large-scale public transport networks. *Applied energy*, 230:344–356, 2018.

[32] Krzysztof Grzelec and F Birr. Development of trolleybus public transport in gdynia as part of a sustainable mobility strategy. *Zeszyty Naukowe. Transport/Politechnika Śląska*, 2016.

[33] Hitoshi Hayashiya, Hiroshi Itagaki, Yuichi Morita, Yoshihisa Mitoma, Takayuki Furukawa, Takuya Kuraoka, Yuta Fukasawa, and Takatoshi Oikawa. Potentials, peculiarities and prospects of solar power generation on the railway premises. In *2012 International Conference on Renewable Energy Research and Applications (ICRERA)*, pages 1–6. IEEE.

[34] Hitoshi Hayashiya, Takashi Suzuki, Keiji Kawahara, and Takashi Yamanoi. Comparative study of investment and efficiency to reduce energy consumption in traction power supply: A present situation of regenerative energy utilization by energy storage system. In *2014 16th International Power Electronics and Motion Control Conference and Exposition*, pages 685–690. IEEE.

[35] IEA. Data overview, electricity statistics, 2020.

[36] IRENA. Innovation landscape brief: Utility-scale batteries. 2019.

[37] Arnulf Jäger-Waldau. Pv status report 2019. page 85, 2019.

[38] Hamed Jafari Kaleybar, Hossein Madadi Kojabadi, Morris Brenna, Federica Foiadelli, and Dario Zaninelli. An intelligent strategy for regenerative braking energy harvesting in ac electrical railway substation. In *2017 5th IEEE International Conference on Models and Technologies for Intelligent Transportation Systems (MT-ITS)*, pages 391–396. IEEE.

[39] Kiran Kambly and Thomas H Bradley. Geographical and temporal differences in electric vehicle range due to cabin conditioning energy consumption. *Journal of Power Sources*, 275:468–475, 2015.

[40] Beyhan Kilic and Erkan Dursun. Integration of innovative photovoltaic technology to the railway trains: A case study for istanbul airport-m1 light metro line. In *IEEE EUROCON 2017-17th International Conference on Smart Technologies*, pages 336–340. IEEE.

[41] Yasunori Kume, Kai Yokoyama, Takahiro Sata, and Eiichi Morita. Lithium ion battery application for regenerative energy utilization in traction power supply system. In *IECON 2017-43rd Annual Conference of the IEEE Industrial Electronics Society*, pages 3884–3888. IEEE.

[42] Reinhart Kühne. Electric buses–an energy efficient urban transportation means. 35(12):4510–4513, 2010.

[43] Antti Lajunen and Timothy Lipman. Lifecycle cost assessment and carbon dioxide emissions of diesel, natural gas, hybrid electric, fuel cell hybrid and electric transit buses. 106:329–342, 2016.

[44] Matthew T Lawder, Vilayanur Viswanathan, and Venkat R Subramanian. Balancing autonomy and utilization of solar power and battery storage for demand based microgrids. *Journal of Power Sources*, 279:645–655, 2015.

[45] Tzu-Ping Lin, Ruey-Lung Hwang, Kuo-Tsang Huang, Chen-Yi Sun, and Ying-Che Huang. Passenger thermal perceptions, thermal comfort requirements, and adaptations in short-and long-haul vehicles. *International Journal of Biometeorology*, 54(3):221–230, 2010.

[46] Kai Liu, Jiangbo Wang, Toshiyuki Yamamoto, and Takayuki Morikawa. Modelling the multilevel structure and mixed effects of the factors influencing the energy consumption of electric vehicles. *Applied energy*, 183:1351–1360, 2016.

[47] Kai Liu, Jiangbo Wang, Toshiyuki Yamamoto, and Takayuki Morikawa. Exploring the interactive effects of ambient temperature and vehicle auxiliary loads on electric vehicle energy consumption. *Applied Energy*, 227:324–331, 2018.

[48] Kai Liu, Toshiyuki Yamamoto, and Takayuki Morikawa. Impact of road gradient on energy consumption of electric vehicles. *Transportation Research Part D: Transport and Environment*, 54:74–81, 2017.

[49] Walter Naranjo, Luis E Muñoz Camargo, Javier E Pereda, and Camilo Cortes. Design of electric buses of rapid transit using hybrid energy storage and local traffic parameters. *IEEE Transactions on Vehicular Technology*, 66(7):5551–5563, 2016.

[50] Pablo Ralon, Michael Taylor, Andrei Ilas, Harald Diaz-Bone, and K Kairies. Electricity storage and renewables: Costs and markets to 2030. 2017.

[51] M Salih, M Koch, D Baumeister, Mahjar Wazifehdust, Philippe Steinbusch, and Markus Zdrallek. Adapted newton-raphson power flow method for a dc traction network including non-receptive power sources and photovoltaic systems. In *2019 IEEE PES Innovative Smart Grid Technologies Europe (ISGT-Europe)*, pages 1–5. IEEE.

[52] Mohammed Salih, D Baumeister, M Wazifehdust, P Steinbusch, M Zdrallek, S Mour, P Deskovic, T Küll, and C Troullier. Impact assessment of integrating novel battery-trolleybuses, pv units and ev charging stations in a dc trolleybus network. In *2nd E-Mobility Power System Integration*

Symposium.

[53] Pedro Mota Santos, Joao P Trovao, and Paulo G Pereirinha. Sustainable trolleybus system: Rectifier substation technology improvement for energy efficiency and operational cost reduction. In *2014 IEEE Vehicle Power and Propulsion Conference (VPPC)*, pages 1–6. IEEE.

[54] Bram Scheurwater. The potential of renewable energy sources for powering of trolleybus grids - an arnhem case-study. Master thesis report, TU Delft, 2020.

[55] Chint Solar. Midden-groningen project, 2019.

[56] Statista. Prices of electricity for industry in poland from 2000 to 2019 (in euro cents), 2019.

[57] Statista. Prices of electricity for industry in the netherlands from 2008 to 2020 (in euro cents), 2020.

[58] Nicem TANYERİ and Çağlar BAŞLAMIŞLI. Prediction of the annual heat load of an articulated electric urban bus. 40(1):27–36, 2020.

[59] Tesla. Powerpack - utility and business energy storage.

[60] Abhishek Singh Tomar, Bram PA Veenhuizen, Lejo Buning, and Ben Pyman. Viability of traction battery for battery-hybrid trolleybus.

[61] Zheming Tong and Hao Liu. Modeling in-vehicle vocs distribution from cabin interior surfaces under solar radiation. 12(14):5526, 2020.

[62] E Vuerich, JP Morel, S Mevel, and J Oliviéri. Updating and development of methods for worldwide accurate measurements of sunshine duration. In *WMO Technical Conference of CIMO (TECO–2012), Brussels, Belgium*, pages 16–18.

[63] Can Wang, Wenjia Cai, Xuedu Lu, and Jining Chen. Co2 mitigation scenarios in china's road transport sector. *Energy Conversion and Management*, 48(7):2110–2118, 2007.

[64] Mahjar Wazifehdust, Dirk Baumeister, Mohammed Salih, Philippe Steinbusch, Markus Zdrallek, Stan Mour, and Conrad Troullier. Potential analysis for the integration of renewables and ev charging stations within a novel lvdc smart-trolleybus grid. 2019.

[65] M Wołek, A Szmelter-Jarosz, M Koniak, and Golejewska. Transformation of trolleybus transport in poland. does in-motion charging matter? 2020.

[66] Marcin Wołek and Olgierd Wyszomirski. The trolleybus as an urban means of transport in the light of the trolley project. *Wydawnictwo Uniwersytetu Gdańskiego, Gdańsk*, 2013.

[67] Bingfang Wu, Shufu Liu, Weiwei Zhu, Mingzhao Yu, Nana Yan, and Qiang Xing. A method to estimate sunshine duration using cloud classification data from a geostationary meteorological satellite (fy-2d) over the heihe river basin. *Sensors*, 16(11):1859, 2016.

[68] SC Yang, M Li, Y Lin, and TQ Tang. Electric vehicle's electricity consumption on a road with different slope. *Physica A: Statistical Mechanics and its Applications*, 402:41–48, 2014.

A | PV MODULE DATASHEET

AstroSemi™

Incredible Power for Small Body

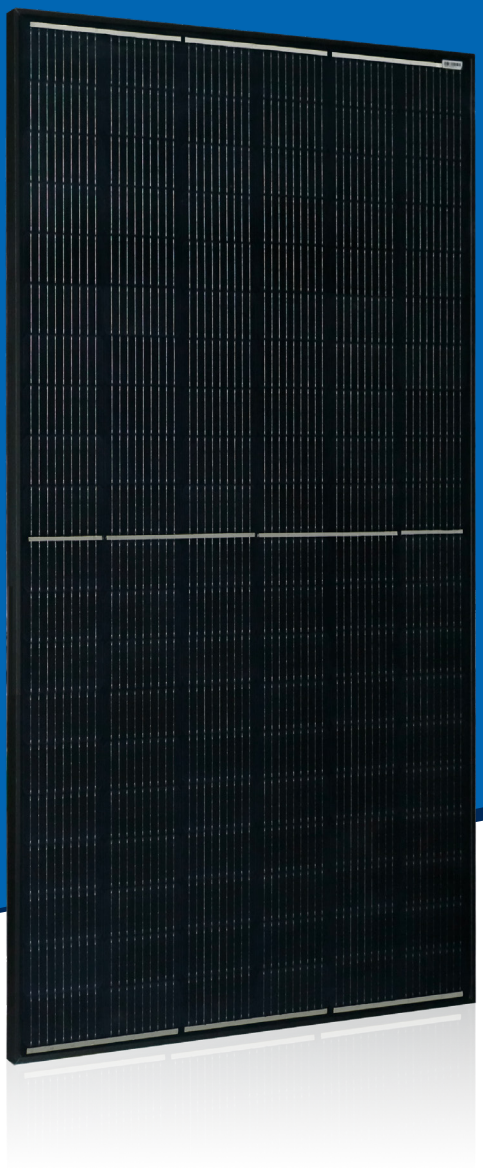

355W~365W

Monocrystalline PV Module

CHSM60M(BL)-HC Series (166)

Tier 1 Bloomberg | No.1 PHOTON | Underwritten by International Insurer | DNV GL 2020 TOP Performance

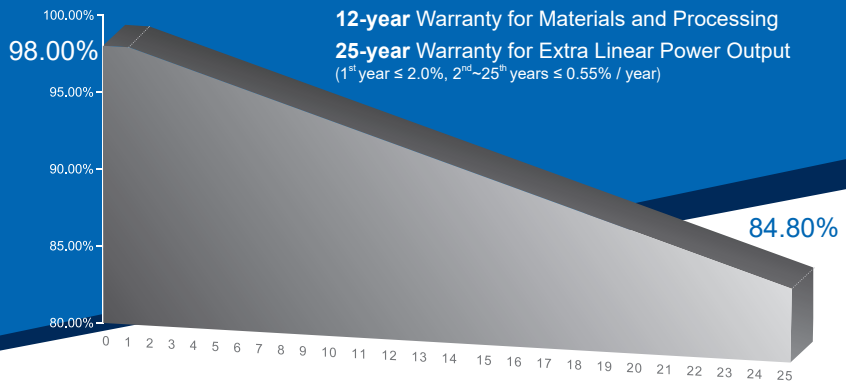

12-year Warranty for Materials and Processing

25-year Warranty for Extra Linear Power Output

(1st year ≤ 2.0%, 2nd~25th years ≤ 0.55% / year)

COMPREHENSIVE CERTIFICATES

First solar company which passed the TUV Nord IEC/TS 62941 certification audit.

KEY FEATURES

OUTPUT POSITIVE TOLERANCE
Guaranteed 0~+5W positive tolerance ensures power output reliability.

INNOVATIONAL HALF-CELL TECHNOLOGY
Improves the module output, decreases the risk of mirco-crack, enhances the module reliability.

INNOVATIVE PERC CELL TECHNOLOGY
Excellent cell efficiency and output.

REDUCE SHADOW LOSS
Effectively reduces the effect of shadow on the module surface.

REDUCE INTERNAL MISMATCH LOSS
Reduces mismatch loss and improves output.

THE-STATE-OF-THE-ART APPEARANCE
Full black designed for a better aesthetic appearance and building integration.

PID RESISTANCE
Excellent PID resistance at 96 hours (@85℃ /85%) test, and also can be improved to meet higher standards for the particularly harsh environment.

ASTRONERGY
A CHINT COMPANY

For Global Market

ELECTRICAL SPECIFICATIONS

STC rated output (P_{mpp})*	355 Wp	360 Wp	365 Wp
Rated voltage (V_{mpp}) at STC	33.24 V	33.49 V	33.73 V
Rated current (I_{mpp}) at STC	10.68 A	10.75 A	10.82 A
Open circuit voltage (V_{oc}) at STC	39.80 V	40.14 V	40.41 V
Short circuit current (I_{sc}) at STC	11.15 A	11.21 A	11.29 A
Module efficiency	19.2%	19.5%	19.7%
Rated output (P_{mpp}) at NMOT	264.7 Wp	268.5 Wp	272.2 Wp
Rated voltage (V_{mpp}) at NMOT	30.99 V	31.22 V	31.45 V
Rated current (I_{mpp}) at NMOT	8.54 A	8.60 A	8.65 A
Open circuit voltage (V_{oc}) at NMOT	37.42 V	37.74 V	37.99 V
Short circuit current (I_{sc}) at NMOT	8.97 A	9.02 A	9.08 A
Temperature coefficient (P_{mpp})	- 0.34%/°C		
Temperature coefficient (I_{sc})	+0.04%/°C		
Temperature coefficient (V_{oc})	- 0.27%/°C		
Nominal module operating temperature (NMOT)	44±2°C		
Maximum system voltage (IEC/UL)	1000V_{DC}		
Number of diodes	3		
Junction box IP rating	IP 68		
Maximum series fuse rating	20 A		

STC: Irradiance 1000W/m^2, Cell Temperature 25°C, AM=1.5
NMOT: Irradiance 800W/m^2, Ambient Temperature 20°C, AM=1.5, Wind Speed 1m/s

CURVE

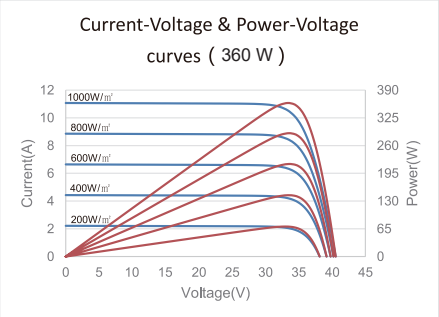

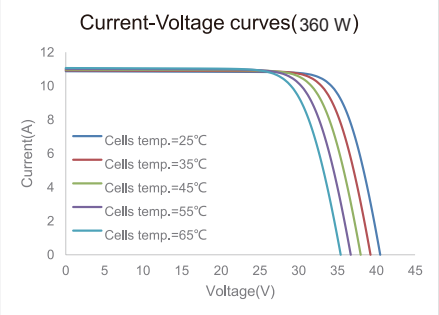

MECHANICAL SPECIFICATIONS

Outer dimensions (L x W x H)	1765 x 1048 x 35 mm
Frame technology	Aluminum, black anodized
Module composition	Glass / EVA / Backsheet (black)
Front glass thickness	3.2 mm
Cable length (IEC/UL)	Portrait: 350 mm Landscape: 1200 mm
Cable diameter (IEC/UL)	4 mm² / 12 AWG
① Maximum mechanical test load	5400 Pa (front) / 2400 Pa (back)
Fire performance (IEC/UL)	Class C (IEC) or Type 1 (UL)
Connector type (IEC/UL)	MC4 compatible

① Refer to Astronergy crystalline installation manual or contact technical department.
Maximum Mechanical Test Load=1.5×Maximum Mechanical Design Load.

PACKING SPECIFICATIONS

① Weight (module only)	20.0 kg
② Packing unit	31 pcs / box
Weight of packing unit (for 40'HQ container)	661 kg
Number of modules per 40'HQ container	806 pcs

① Tolerance +/- 1.0kg
② Subject to sales contract

MODULE DIMENSION DETAILS

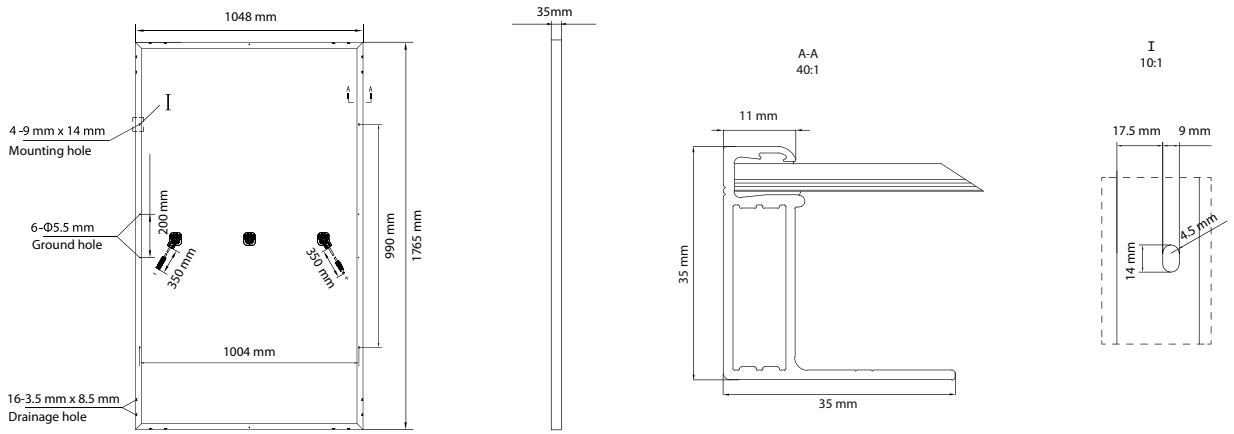

B LOAD MODEL - VELOCITY AND POWER PROFILES ELECTRIC MOTOR DATA-SHEETS

In this Appendix additional details on the load models are provided. In particular, the reader can find in this chapter the data-sets used to simulate the Velocity profiles, the equations used in the HAN university power model to find the bus powers and the motor data-sheets for the electric motors of Arnhem and Gdynia buses.

B.1 Velocity Profiles data-sets

Here the reader can find the data used as input to the velocity profile generator model. The isolated velocity cycles, defined as one travelling cycle from one stop to the other, are used to generate the complete velocity profiles. This is done by combining the individual velocity profiles based on their duration and the distance travelled.

In Figure B.1, B.2 and B.3 the plots of the data-sets are shown. The Braunschweig, the Arnhem - maximum and the Arnhem - minimum single velocity cycles grouped together are shown. As one can see, the data-sets coming from Arnhem measurements contain much more elements. As a matter of fact, the Braunschweig velocity cycle is a simulated velocity profile and therefore some of the isolated cycles are repeated. The measured data coming from Arnhem are real measured data, and present all the variability and unpredictability of real life data. Therefore, no single velocity cycle (form 0 m/s to 0 m/s velocity) presents the same characteristics. These vary in terms of maximum speed, acceleration and deceleration moments, length in time and travelled distances.

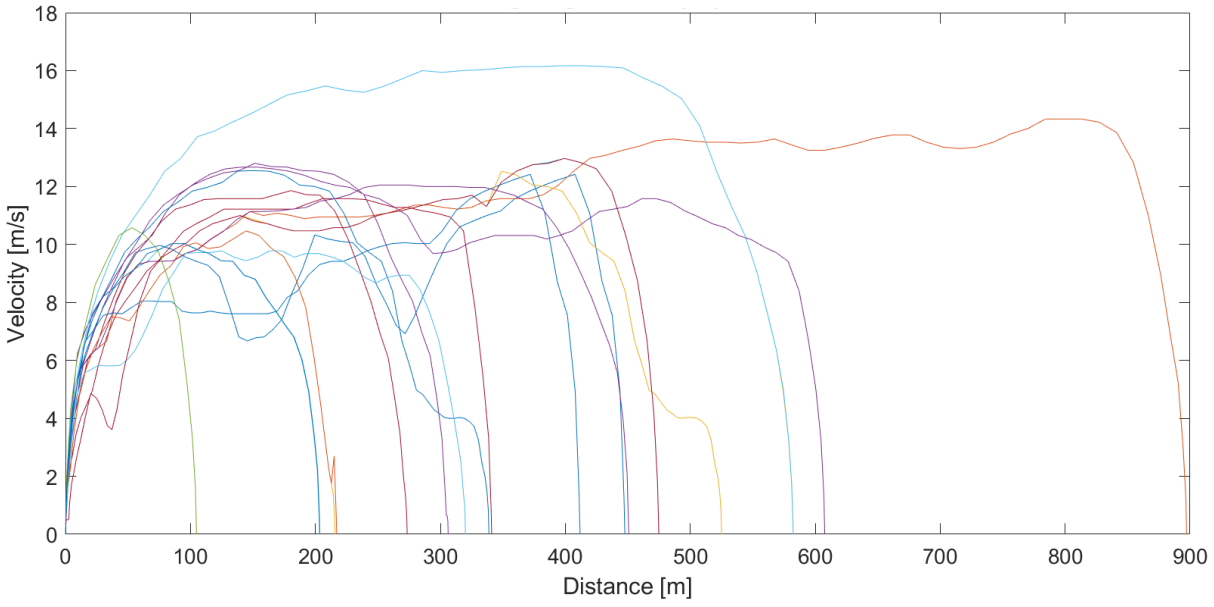

Figure B.1: Braunschweig single velocity cycles data-set, plotted versus the travelled distance

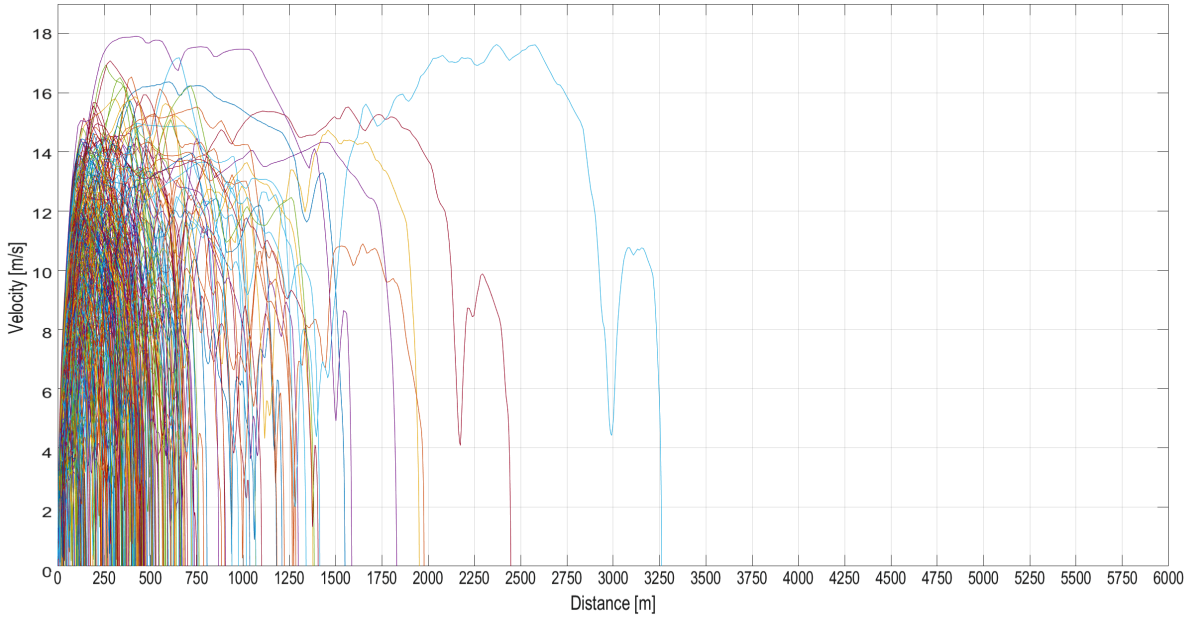

Figure B.2: 'Arnhem maximum' measurements single velocity cycles data-set, plotted versus the travelled distance

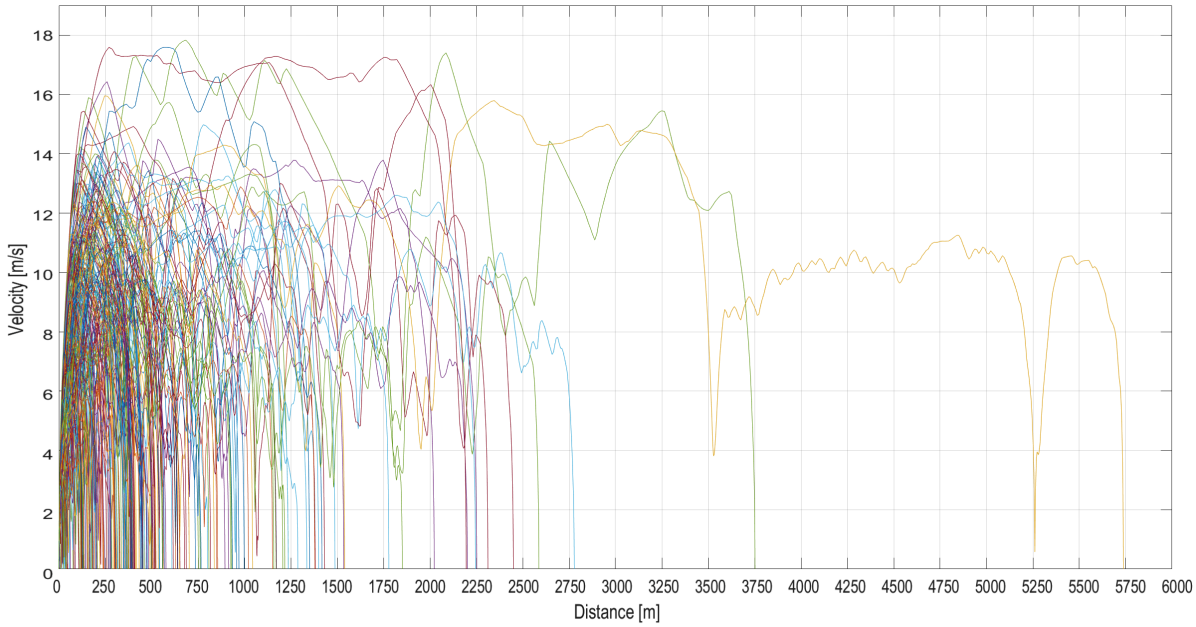

Figure B.3: 'Arnhem minimum' measurements single velocity cycles data-set, plotted versus the travelled distance

B.2 HAN University bus power model equations

This model is used to calculate the power requirements of the buses from their velocity characteristics. Through this set of equations the motor torque and rotational speed are computed. First the forces on the bus are calculated:

- Rolling resistance force

$$F_{\text{roll}} = M_{\text{bus}} \cdot g \cdot C_{\text{roll}} \cdot cos\theta \tag{B.1}$$

  with M_{bus} the bus mass, g the gravitational acceleration, C_{roll} the rolling coefficient and θ the road inclination

- Gravitational force (due to road gradients)

$$F_{\text{grav}} = M_{\text{bus}} \cdot g \cdot sin\theta \tag{B.2}$$

- Aerodynamic force

$$F_{\text{aero}} = \frac{1}{2}(v_{\text{bus}} + v_{\text{wind}})^2 \cdot \rho \cdot C_{\text{d}} \cdot A_{\text{f}} \tag{B.3}$$

with v_{bus} the bus speed, v_{wind} the wind speed, A_f the bus frontal surface and C_d the drag coefficient

- Inertia force

$$F_{\text{inertia}} = M_{\text{bus}} \cdot C_{\text{inertia}} \cdot a_{\text{bus}} \tag{B.4}$$

with $C_{inertia}$ the inertia coefficient and a_{bus} the bus acceleration

From these four components the traction force is computed as:

$$F_{\text{traction}} = F_{\text{roll}} + F_{\text{grav}} + F_{\text{aero}} + F_{\text{inertia}} \tag{B.5}$$

The wheel torque can then be found as:

$$T_{\text{wheel}} = F_{\text{traction}} \cdot r_{\text{wheel}} \tag{B.6}$$

with r_{wheel} the wheel radius.

After this the motor torque and rotational speed can be computed. The latter is found through Equation B.7, while the former as in Equation B.8 is the gear torque is positive (and the electric motor is working as a generator) or through Equation B.9 if negative (with electric motor consuming power).

$$w_{\text{motor}} = n_{\text{gear}} \cdot \frac{v_{\text{bus}}}{r_{\text{wheel}}} \tag{B.7}$$

with n_{gear} the gear ratio and r_{wheel} the tire radius.

$$T_{\text{motor}} = \frac{T_{\text{gear}}}{\eta_{\text{gear}}} \tag{B.8}$$

with η_{gear} the gearbox efficiency.

$$T_{\text{motor}} = T_{\text{gear}} \cdot \eta_{\text{gear}} \tag{B.9}$$

with η_{gear} the gearbox efficiency.

The gearbox torque is computed as the sum of T_{wheel}, as in B.6, over the gear ration, $T_{friction}$ and $T_{inertia}$. These two terms are found respectively as:

$$T_{\text{friction}} = \frac{P_{\text{gear}}}{w_{\text{motor}}} \tag{B.10}$$

with w_{motor} the rotational speed of the motor and P_{gear} the idling power loss due to friction,

$$T_{\text{inertia}} = I_{\text{gear}} \cdot (\Delta w_{\text{motor}}) \tag{B.11}$$

with I_{gear} the gear inertia and Δw_{motor} the motor rotational speed variation in time.

Now that both motor torque and rotational speed are found the mechanical power is computed as the product of the two.

B.3 Arnhem Electric motor datasheet

In onderstaande tabel zijn de technische gegevens weergegeven van de Swiss Trolley III.

Mechanical Part	
Vehicle design	Three-axle articulated trolleybus with a 100 % low-floor share
Type	Swiss Trolley III BGT-N2C
Length of vehicle	17,934 mm
Width of vehicle	2,550 mm
Turning circle	23,930 mm
Transport capacity	123 (48 seating, 75 standing)
Boarding height	327 mm
Gear ratio	1: 9.817
Mass of empty vehicle	18,920 kg
Mass of vehicle full to capacity	28,000 kg
Electrical Part	
Max. speed at flat level	65 km/h
Acceleration	1.3 m/s² (adjustable)
Braking deceleration	1.3 m/s² (adjustable)
Max. climbing capability	> 15 %
Traction motors	Two force-ventilated three-phase asynchronous motors
Type	ML 3450 K/4
Nominal output	2 x 160 kW
Max. torque	1335 Nm
Nominal voltage	3 AC 420 V
Nominal speed	1477 min⁻¹
Max. speed	4400 min⁻¹
Weight	560 kg5
Roof equipment container on trailer	Kiepe DGG 414
Dimensions	1736 x 920 x 446 mm
Design	Container mounted in an insulated way with internal double insulation
Roof equipment container on front car	Kiepe DGG 335
Dimensions	3000 x 1640 x 553 mm
Design	Internal double insulation with device carrier fitted in an insulated way

Traction inverters	Two IGBT direct pulse inverters of the type Kiepe DPU 500
Input voltage	DC 600 V (+ 25 %, - 30 %)
Output	
Cooling	Forced air cooling
Characteristics	- IGBT technology - Triggering of the drive units via optical waveguides - Pulse pattern given by the inverter control module - Jerkfree starting and braking - Combined regenerative and rheostatic brake - Wheel slip/slide protection (ABS/TCS function)
On-board converter	Static on-board converter
Type	Kiepe BNU 500
Input voltage	DC 600 V (+ 25 %, - 30 %)
Output voltage	DC 24 V / 5.7 kW AC 400 V / 230 V, 50 Hz, 16 kW
Characteristics	- Double insulation for fitting on the roof - Electrical isolation of the outputs from the contact line system - Separate battery charge according to constant voltage/constant current curve
Current collector system	Kiepe OSA 200
Characteristics	- Automatic fast lowering in case of dewirement - Centration of the trolley poles in the middle in case of lowering - Lowering from the driver's workplace
Diesel generator unit	Four-cylinder series diesel engine with flange-mounted synchronous generator energised permanently
Type	Kirsch
Diesel engine	IVECO
Mechanical power	95 kW
Certification	according to EURO3
Speed range	1300 - 2700 min⁻¹
Type of generator	G80 PME
Electrical power	80 kW
Output voltage	DC 400 V - 900 V

B.4 Gdynia Electric motor datasheet

STDa280-4A

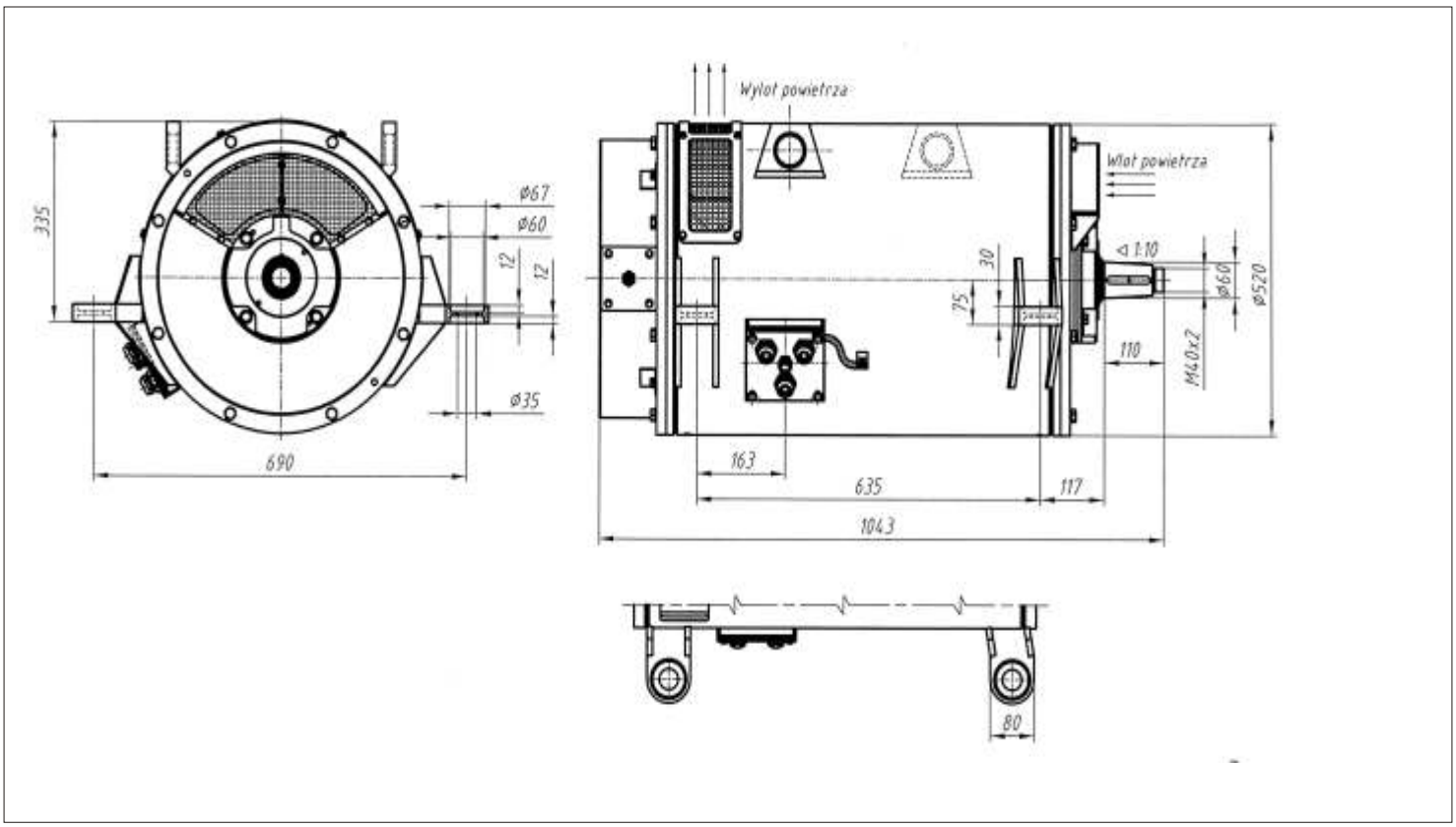

3-phase induction motor designed for driving of trolleybus. Motor in special execution, hanging, with feet. Motor desinged for supply from frequency inverter.

Power Output	Duty	Current	Voltage	Connection	Number of Leads	Rated Current	Rated Speed of Rotation	Frequency	Efficiency	Power Factor	Weight (with clutch)	Direction of Rotation	Ambient Temperature	Relative Humidity
kW	-	-	V	-	-	A	rpm	Hz	%	-	kg	-	°C	%
125	S1	3-phase	400	人	3	226	1784	60	93,8	0,85	650	**Both**	:#Ş Č°H	95

- ***Type of motor*** **-** asynchronous, squirrel cage, low voltage
- ***Design*** **-** special
- ***Mechanical execution*** **-** *f*or horizontal operation
- ***Shaft end*** **-** *o*ne, conic
- ***Cooling*** **-** IC01
- ***Bearings*** **-** *roller bearings*: “DE” side NU 314 Em1 C3
  “NDE” side 6312 C3
- Motor with supply cables type Radox 4GKW-AX-EMC-L
- ***Rotation speed sensor:*** MHRM 12G2501
- ***Speed control:***
  from 0 to 1780rpy at T=const.;
  from 1780 to 3800 rpm at P=const.

C PARALLEL LINES APPROXIMATION STUDY

In this Appendix some additional plots for the Total distance approximation method are provided, followed by the brief analysis of the other method studied to approximate the voltage drops along the overhead lines in the case in which parallel connections are implemented.

C.1 Total distance approximation error analysis

In this section some additional plots related to the analysis of the total distance approximation and the error committed when applying it are provided. In Figure C.1, C.2, C.3 and C.4 the plots of the error in the approximation are shown. The curves represent the error introduced in the simulations when the total distance approximation is used with varying bus power and position. The four plots differ by the distance between the parallel connections, going respectively from 100 m to 250 m in steps of 50 m. As one can see the increase in power and in distance from the supply point (at 0 m) cause the increase in the error introduced. Also, the higher the distance between two subsequent connections the higher the error committed when making the assumptions for this approximation.

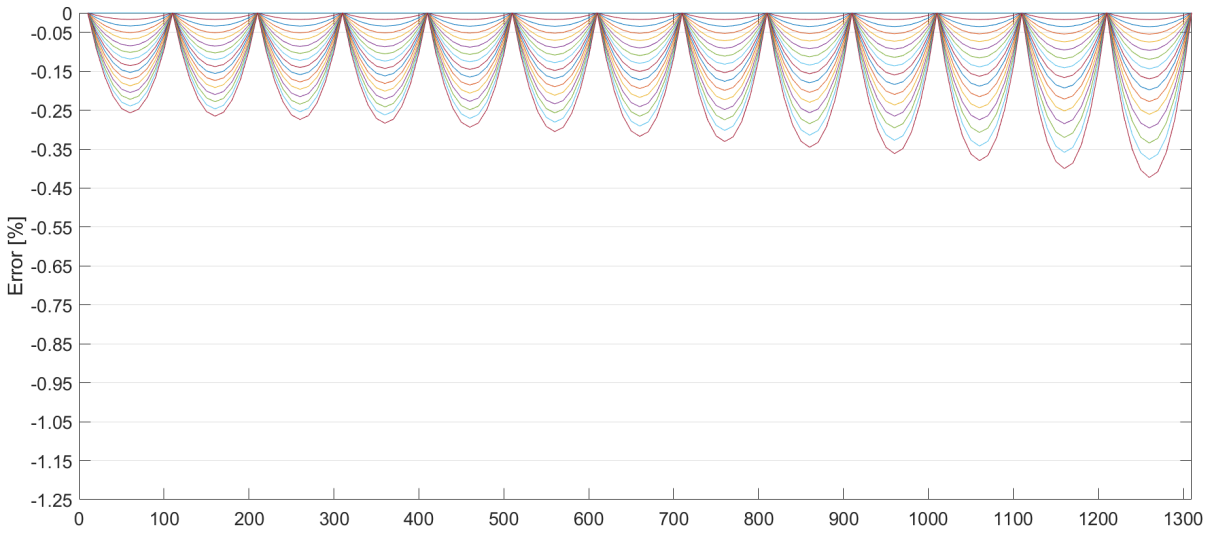

Figure C.1: Error introduced using the total distance approximation of the bus voltage, plotted as a function of the distance from the supply point (0 m), with parallel connections every 100 m. Increasing power requirements are shown, with every curve representing a power demand level

C.2 Total current approximation error analysis

The same analysis presented for the Total distance approximation method is now briefly proposed for the total current approximation. In Chapter 4, the assumptions introduced for this method are explained. Here only the results are provided.

In Figure C.5 and **??**, the variation of the error introduced with this method are shown. As one can see also in this case the error is increasing with:

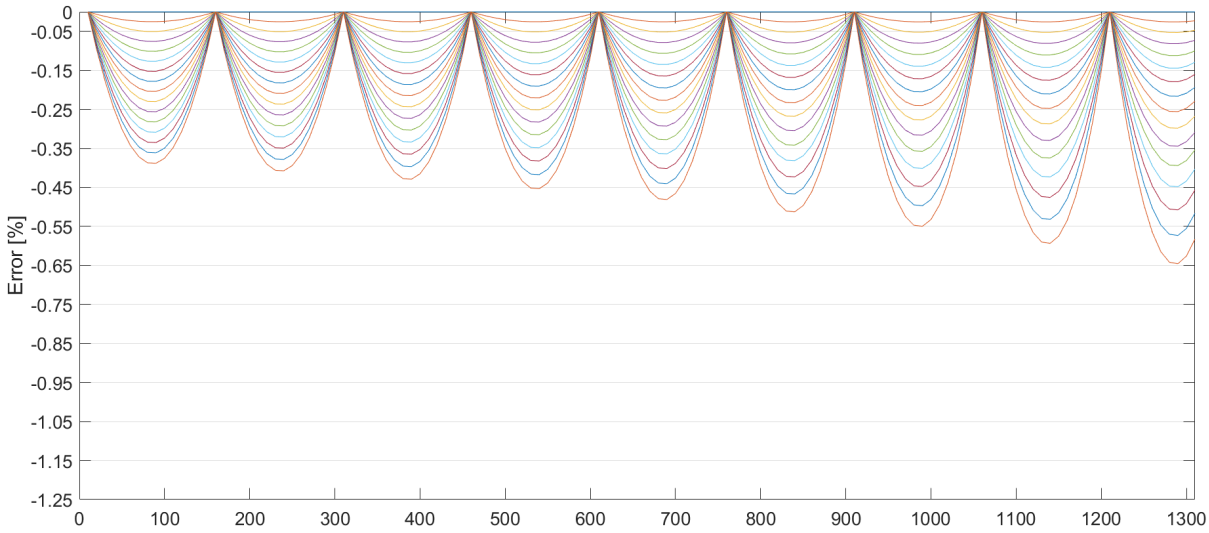

Figure C.2: Error introduced using the total distance approximation of the bus voltage, plotted as a function of the distance from the supply point (0 m), with parallel connections every 150 m. Increasing power requirements are shown, with every curve representing a power demand level

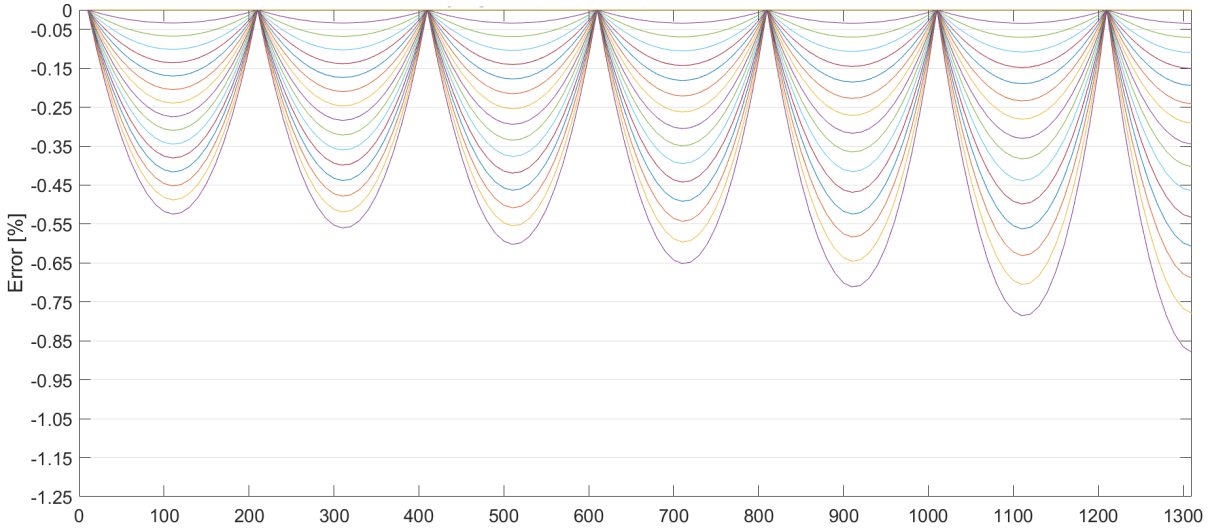

Figure C.3: Error introduced using the total distance approximation of the bus voltage, plotted as a function of the distance from the supply point (0 m), with parallel connections every 200 m. Increasing power requirements are shown, with every curve representing a power demand level

- Distance of the bus from the supply point (the higher the voltage drop, the worse is the expected performance of the model compared to the actual voltage levels),
- Distance between subsequent parallel connections. In both plots different connection points are simulated and it is possible to see that increasing the distance between parallel connections the error committed by using the approximation method increases,
- Power requirements of the bus. In C.5 the error is plotted for a bus demand of 100 kW, while in C.6 the error for 300 kW is shown. It is possible to see that the increase in power requirements causes always an increase in the error introduced.

Also, by observing these plots it can be concluded that this approximation is **always overestimating** the voltage drop.

When picking a random point in the supply section, it is possible to demonstrate that not only the absolute position of the bus plays a role but also its relative position within each fraction of line between

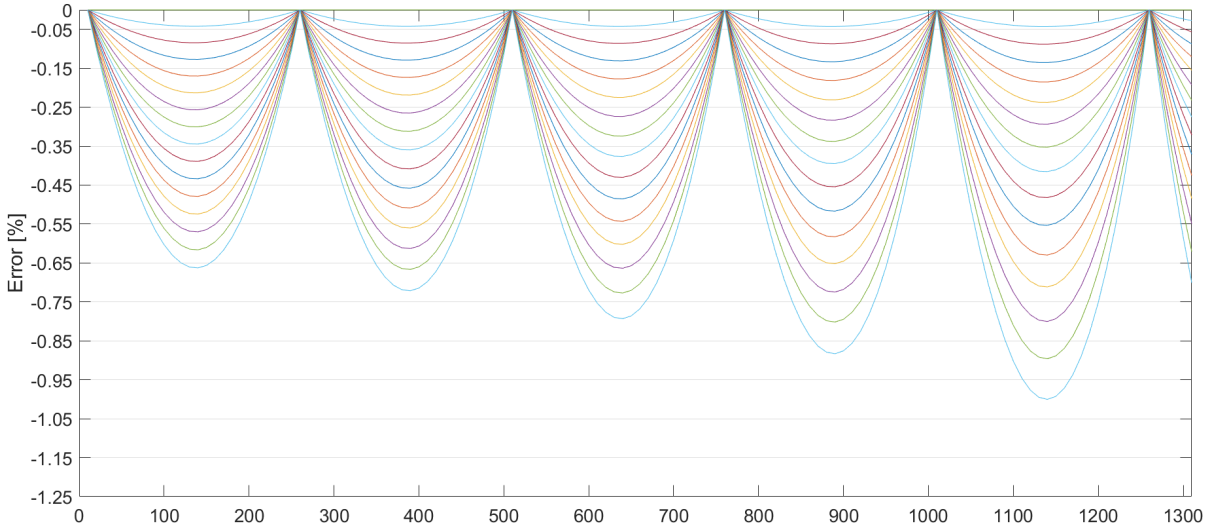

Figure C.4: Error introduced using the total distance approximation of the bus voltage, plotted as a function of the distance from the supply point (0 m), with parallel connections every 250 m. Increasing power requirements are shown, with every curve representing a power demand level

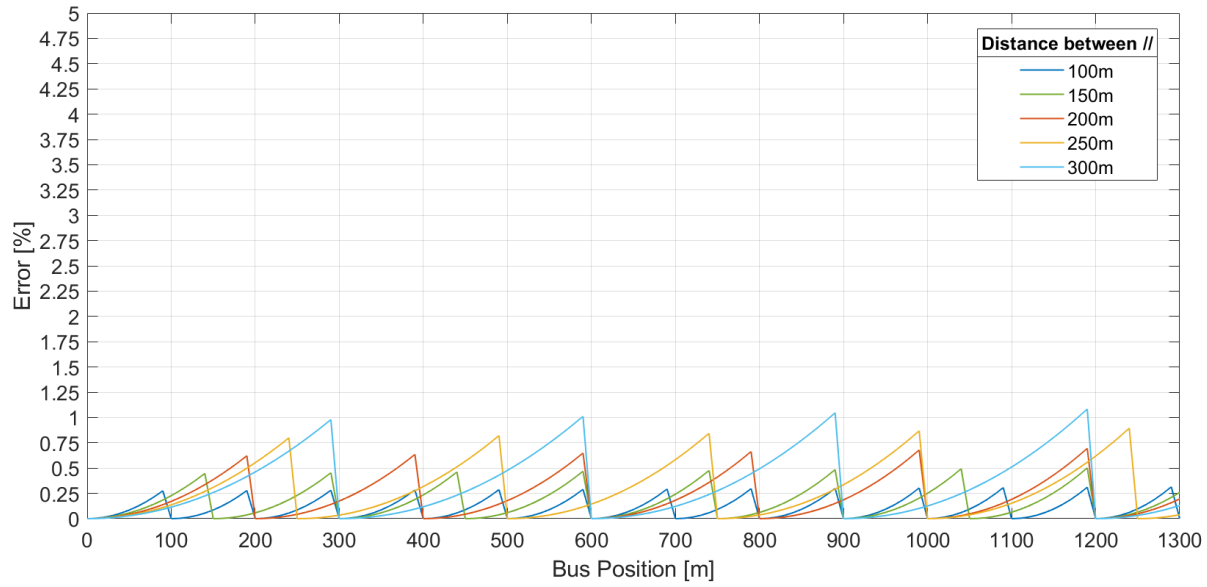

Figure C.5: Error in the Total current approximation with varying distance from the supply and distance between parallel connections, at 100 kW bus power demand

to subsequent connections. This is demonstrated, in Chapter 4, also for the other approximation method. Although the error is higher overall if the distance between the parallel connections is longer, based on the relative position of the bus within two connections it can happen that this is not the case. As an example, 700m distance from the supply point is taken. In Figure C.7a and C.7b one can see where this point is located along the 1300m supply section and where is is relatively located within two parallel connections. When the bus is at 700m distance from the supply, the error in the approximation is lower for the case in which parallel connections are at 250m one from the other rather than in the case in which they are at 200m from each other, as shown in Figure C.7c.

To conclude this analysis, a research on the effects of varying the supply voltage is performed. The reduction of the line voltage causes the overall increase in current for the same power requirements of the bus and therefore and increase in transmission losses and in the voltage drop. Moreover, if the same voltage difference between the approximation and the actual value is found at lower voltage levels, this will have in percentage a higher error. Therefore, it is expected that at lower voltages the

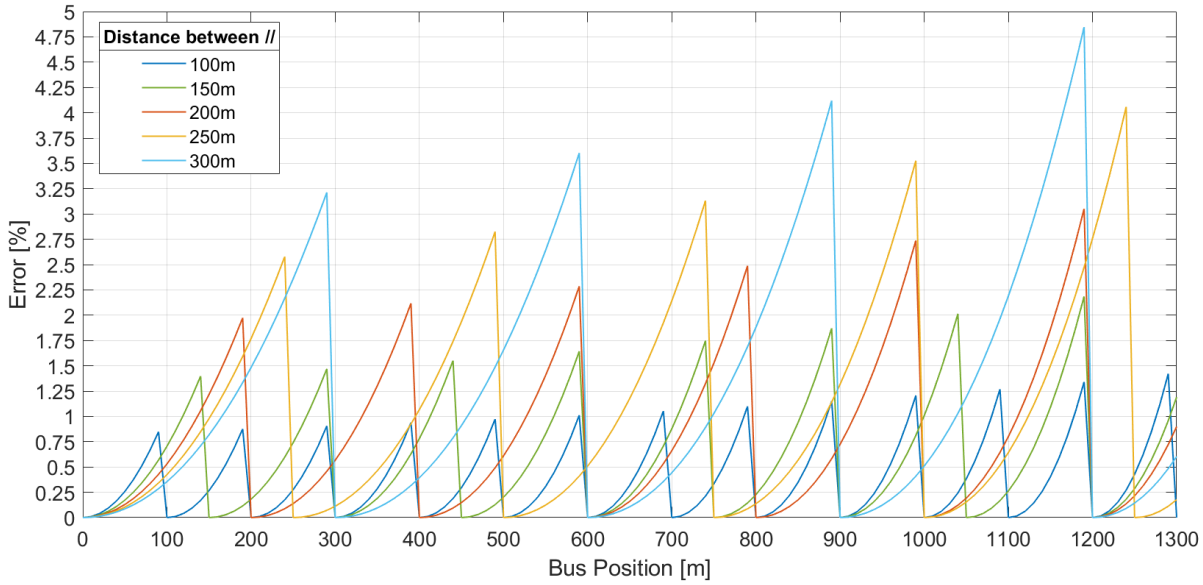

Figure C.6: Error in the Total current approximation with varying distance from the supply and distance between parallel connections, at 300 kW bus power demand

error in the approximation will increase. This is confirmed by the simulations and is represented in Figure C.8.

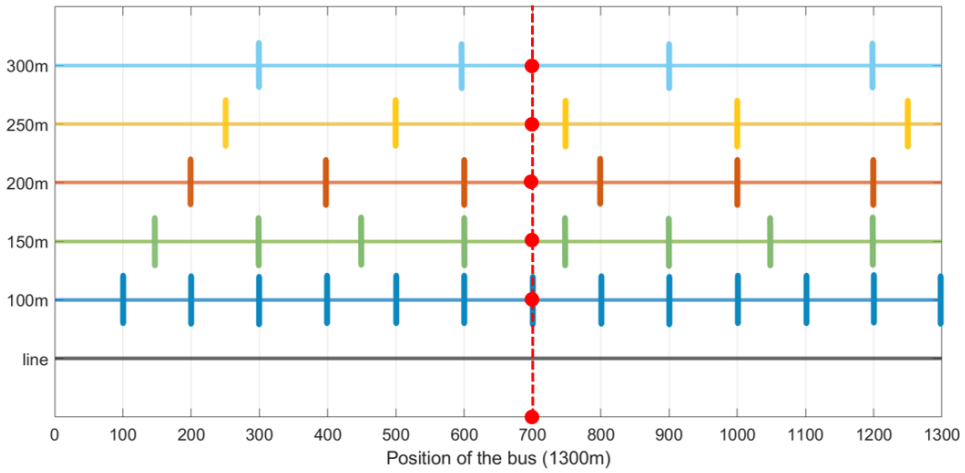

(a) Characteristics of the position based on the distance between parallel connections along the line

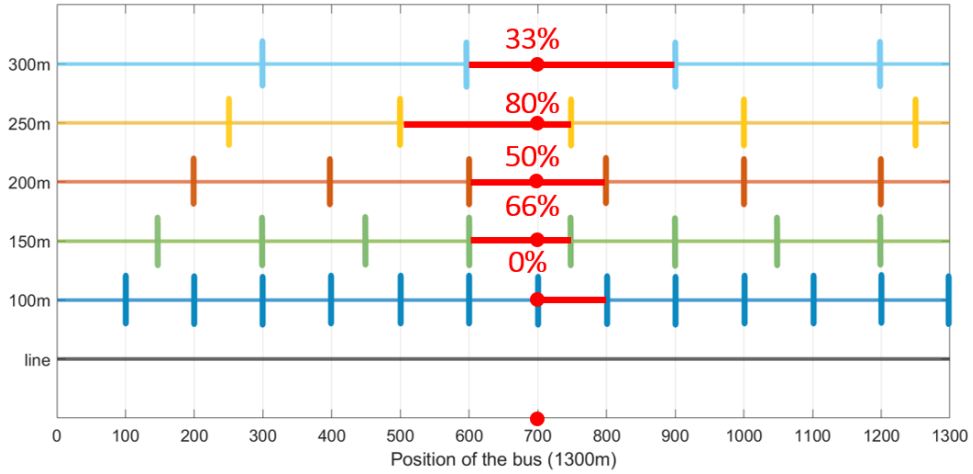

(b) Fraction of section between two subsequent parallel connections travelled by the bus

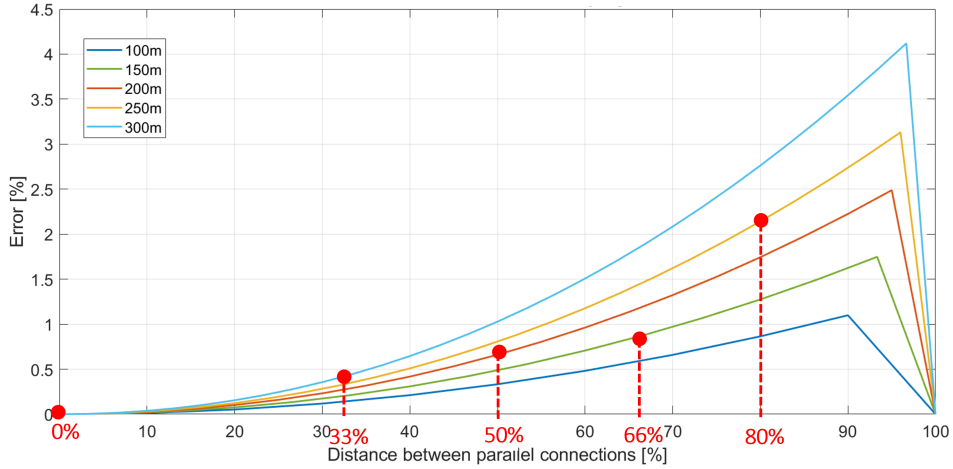

(c) Error variation in relation to the position of the bus between two subsequent parallel connections

Figure C.7: Error introduced using the total current approximation of the bus voltage, varying in relation to the position between two subsequent parallel connections. Example: bus at 700m from the supply point.

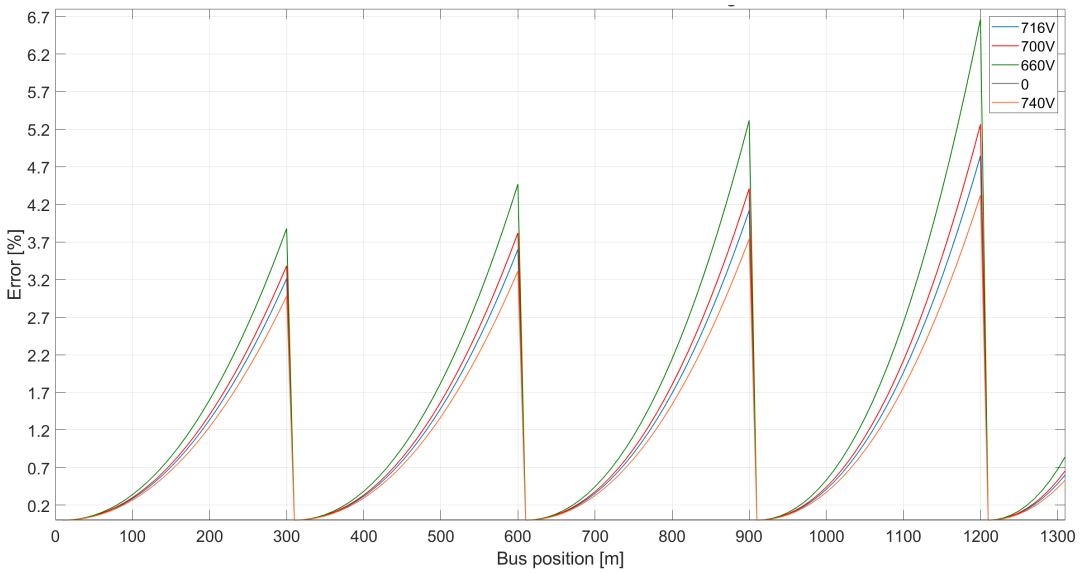

Figure C.8: Error introduced using the total current approximation of the bus voltage as a function of bus distance from the supply point (0 m) and supply voltage, at 300 kW power requirement and with parallel connections every 300m

D GRID OPERATION - DATA IN INPUT AND OUTPUTS

In this Appendix an example of the tables used to simulate the grid operation (schedules, distribution of bus stops and traffic lights in the grid) is provided. The tables of the simulation outputs with all the characteristics of the grid are then provided.

D.1 Input data organization

One line is taken as example to show the work that is done for all the lines of the two grids. The data is organised in tables containing information on the bus stops and traffic lights location along the lines, the sections and respective substations crossed while travelling along the lines and the timetables of the buses throughout the different days of the week. The line used as example is line 22 of Gdynia grid.

Bus Stops and Traffic Lights
First the bus stop position along each line are found. The distance between the stops and the distance of each stop from the starting point are retrieved through Google Maps. In Figure D.1 and D.2, the tables for line 22 of Gdynia grid are shown. This work is done for both directions of each line. As one can see, the position of the traffic lights is also registered in the tables. The location is identified as the distance travelled from the bus before meeting the traffic light.

Another thing included in these two tables is the timestep between two subsequent bus stops. These 3 timetables (weekday, saturday and sunday) together with the distance between each stop, are used to pick the appropiate single velocity cycle. This should be matching the distance travelled and ahould fit in the timestep.

Section lengths and substations
The second set of data required to simulate the grid operation is the information on the distribution of the sections in the grid. To do this, the sections crossed by the bus along each line are saved. Together with this the distance travelled by the bus in each section crossed, are also measured through Google Maps. In Figure D.3 and D.4, the tables containing this information for line 22 of Gdynia grid are provided. One can see that the location in terms of section and substation of each stop are given, together with the length covered by each section in the line. The substation voltage is also included in this type of table.

Timetables per line and per bus
The bus schedules for the different day types are downloaded and saved from the respective transport companies Breng and ZKM, in Arnhem and Gdynia respectively. The timetables though, have to be organised in terms of bus runs. This is done by matching with a specific bus each trip. In Figure D.5, D.6 and **??** the timetables organised per leaving and arriving time at the terminals are shown, respectively for Weekday, Saturday and Sunday schedules. These tables are shown for Gdynia, in which 3 different schedules are found. For Arnhem grid, the same is done for 6 schedules (Summer Weekday, Summer Holiday, Summer Saturday, Saturday, Weekday and Holiday).

As one can see, the timetables are colour coded based on the buses that are performing each run. The arrival time at the terminal station is adapted to the duration of the full run with the respective velocity profile (High traffic, medium traffic or low traffic) used for each day. In this way, the runs performed by each bus for each line are defined. Indicated in red are the bus runs which are delayed. In Figure D.8, D.9 and D.10 the timetables of the buses serving line 22 of Gdynia grid are shown. In the tables, **step**

represents the second in the day at which the run starts and **string** is the code of the velocity profile to chose. It identifies the line and the direction of the run of the bus.

Gdynia Dworzec Gł. PKP - Cisowa						
Bus Stops	**Distance [m]**	**Cum. distance [m]**	**Traffic lights [m]**	**Timestep [s]**		
				Weekday	Saturday	Holiday
Cisowa SKM 06	0	0	405	0	0	0
Cisowa SKM 91 (NŻ)	50	50	1475	60	60	60
Piaskowa 01	450	500	3125	60	60	60
Kcyńska 01	350	850	3225	120	120	110
Chylonia Dworzec PKP 01	600	1450	3805	60	60	60
Pucka 01	460	1910	4355	60	60	60
Leszczynki SKM 01	550	2460	4655	60	60	60
Zamenhofa 01	350	2810	4895	120	110	110
Węzeł Żołnierzy Wyklętych 01	300	3110	5355	120	120	120
Morska - Estakada 01	700	3810	6255	60	60	60
Kalksztajnów 01	500	4310	6655	110	60	60
Mireckiego 01	550	4860	7195	120	120	120
Uniwersytet Morski 01	500	5360	7375	60	60	60
Stocznia SKM - Morska 01	450	5810	7595	60	60	60
Bpa Okoniewskiego 01	450	6260	7825	120	120	120
Gdynia Dworzec Gł. PKP - Wolności 02	550	6810	8075	60	60	60
Warszawska 02	280	7090	8180	60	60	60
Witomińska 02	550	7640	8380	120	120	120
Węzeł Franciszki Cegielskiej 04	500	8140	8490	200	180	180
Urząd Miasta - Świętojańska 01	600	8740	8650	60	60	60
Traugutta 01	450	9190	8690	60	60	60
Żwirki i Wigury 01	400	9590	8790	110	100	100
Skwer Kościuszki - InfoBox 01	290	9880	9800	90	60	60
Plac Kaszubski - Świętojańska 01	500	10380	10040	60	60	60
Plac Kaszubski - Jana z Kolna 02	130	10510	10290	120	120	120
Gdynia Dworzec Gł. PKP - Hala 06	650	11160	10750	60	60	60
Gdynia Dworzec Gł. PKP 02	290	11450				

Figure D.1: Table containing the bus stop and traffic light positions along line 22 in Gdynia grid - Direction 1

Cisowa - Gdynia Dworzec Gł. PKP						
Bus Stops	Distance [m]	Cum. distance [m]	Traffic lights [m]	Timestep [s]		
				Weekday	Saturday	Holiday
Gdynia Dworzec Gł. PKP 03	0	0	350	60	60	60
Gdynia Dworzec Gł. PKP - Hala 03	170	170	580	120	120	120
Plac Kaszubski 03	550	720	910	80	60	60
Plac Kaszubski - Świętojańska 02	340	1060	1190	120	110	100
Skwer Kościuszki - InfoBox 02	260	1320	1430	100	90	60
Wybickiego 02	220	1540	2330	60	60	60
Żwirki i Wigury 02	300	1840	2870	60	60	60
Traugutta 02	350	2190	3150	120	120	120
Wzgórze Św. Maksymiliana SKM 03	450	2640	3250	190	180	180
Witomińska 01	700	3340	3550	100	90	90
Warszawska 01	500	3840	4150	60	60	60
Gdynia Dworzec Gł. PKP - Wolności 01	350	4190	4300	120	120	120
Bpa Okoniewskiego 02	550	4740	4650	60	60	60
Stocznia SKM - Morska 02	350	5090	5650	70	60	60
Uniwersytet Morski 02	700	5790	6050	100	60	60
Mireckiego 02	450	6240	6350	60	60	60
Kalksztajnów 02	550	6790	6550	70	60	60
Morska - Estakada 02	300	7090	7050	120	120	120
Węzeł Żołnierzy Wyklętych 02	600	7690	7750	100	60	60
Zamenhofa 02	450	8140	9450	60	60	60
Leszczynki SKM 02	450	8590	10450	60	60	60
Pucka 02	600	9190		120	110	110
Chylonia Dworzec PKP 02	500	9690		60	60	60
Kcyńska 02	500	10190		60	60	60
Piaskowa 02	350	10540		60	60	60
Cisowa SKM 02	250	10790				

Figure D.2: Table containing the bus stop and traffic light positions along line 22 in Gdynia grid - Direction 2

D.2 Output data tables for Gdynia and Arnhem grids

The section and substation data output from the simulations in terms of grid structure, losses, section lengths, energy requirements and bus traffic are shown in the next tables.

Cisowa - Gdynia Dworzec Gł. PKP							
Bus Stops	**Section number**	**Substation number**	**Section lengths (subsequent)**	**Section number**	**Substation number**	**Substation voltage**	**Sections cum. distance**
Cisowa SKM 06	1	1	1250	1	1	685	1250
Cisowa SKM 91 (NŻ)	1	1	380	3	1	685	1630
Piaskowa 01	1	1	1100	4	1	685	2730
Kcyńska 01	1	1	1460	1	2	675	4190
Chylonia Dworzec PKP 01	3	1	850	2	2	675	5040
Pucka 01	4	1	1100	3	2	675	6140
Leszczynki SKM 01	4	1	850	2	3	690	6990
Zamenhofa 01	1	2	960	1	5	684	7950
Węzeł Żołnierzy Wyklętych 01	1	2	450	2	5	684	8400
Morska - Estakada 01	1	2	550	3	5	684	8950
Kalksztajnów 01	2	2	1200	2	4	685	10150
Mireckiego 01	2	2	810	1	4	685	10960
Uniwersytet Morski 01	3	2	490	3	3	690	11450
Stocznia SKM - Morska 01	3	2					
Bpa Okoniewskiego 01	2	3					
Gdynia Dworzec Gł. PKP - Wolności 02	2	3					
Warszawska 02	1	5					
Witomińska 02	1	5					
Węzeł Franciszki Cegielskiej 04	2	5					
Urząd Miasta - Świętojańska 01	3	5					
Traugutta 01	2	4					
Żwirki i Wigury 01	2	4					
Skwer Kościuszki - InfoBox 01	2	4					
Plac Kaszubski - Świętojańska 01	1	4					
Plac Kaszubski - Jana z Kolna 02	1	4					
Gdynia Dworzec Gł. PKP - Hala 06	3	3					
Gdynia Dworzec Gł. PKP 02	3	3					

Figure D.3: Table containing the sections and substations crossed by the buses travelling along line 22 in Gdynia grid - Direction 1

Gdynia Dworzec Gł. PKP - Cisowa							
Bus Stops	**Section number**	**Substation number**	**Section lengths (subsequent)**	**Section number**	**Substation number**	**Substation voltage**	**Sections cum. distance**
Gdynia Dworzec Gł. PKP 03	3	3	350	3	3	690	350
Gdynia Dworzec Gł. PKP - Hala 03	3	3	700	1	4	685	1050
Plac Kaszubski 03	1	4	1200	2	4	685	2250
Plac Kaszubski - Świętojańska 02	2	4	700	3	5	684	2950
Skwer Kościuszki - InfoBox 02	2	4	80	2	5	684	3030
Wybickiego 02	2	4	960	1	5	684	3990
Żwirki i Wigury 02	2	4	850	2	3	690	4840
Traugutta 02	2	4	1100	3	2	675	5940
Wzgórze Św. Maksymiliana SKM 03	3	5	850	2	2	675	6790
Witomińska 01	1	5	1300	1	2	675	8090
Warszawska 01	1	5	1100	4	1	685	9190
Gdynia Dworzec Gł. PKP - Wolności 01	2	3	380	3	1	685	9570
Bpa Okoniewskiego 02	2	3	1220	1	1	685	10790
Stocznia SKM - Morska 02	3	2					
Uniwersytet Morski 02	3	2					
Mireckiego 02	2	2					
Kalksztajnów 02	1	2					
Morska - Estakada 02	1	2					
Węzeł Żołnierzy Wyklętych 02	1	2					
Zamenhofa 02	4	1					
Leszczynki SKM 02	4	1					
Pucka 02	3	1					
Chylonia Dworzec PKP 02	1	1					
Kcyńska 02	1	1					
Piaskowa 02	1	1					
Cisowa SKM 02	1	1					

Figure D.4: Table containing the sections and substations crossed by the buses travelling along line 22 in Gdynia grid - Direction 2

Departures from Monday to Friday (except public holidays):							
Gdynia Dworzec Gł. PKP - Cisowa			Cisowa - Gdynia Dworzec Gł. PKP				
Gdynia Dworzec Gł. PKP 03	Cisowa SKM 02	string	Cisowa SKM 06	Gdynia Dworzec Gł. PKP 02	string		BUS
08:21	09:00	GD_C	08:01	08:41	C_GD		1
08:36	09:15	GD_C	08:16	08:56	C_GD		2
08:51	09:30	GD_C	08:31	09:11	C_GD		3
09:06	09:45	GD_C	08:46	09:26	C_GD		4
09:21	10:00	GD_C	09:01	09:41	C_GD		5
09:36	10:15	GD_C	09:16	09:56	C_GD		6
09:51	10:30	GD_C	09:31	10:11	C_GD		
10:06	10:45	GD_C	09:46	10:26	C_GD		
10:21	11:00	GD_C	10:01	10:41	C_GD		
10:35	11:14	GD_C	10:16	10:56	C_GD		
10:50	11:29	GD_C	10:31	11:11	C_GD		
11:05	11:44	GD_C	10:46	11:26	C_GD		
11:20	11:59	GD_C	11:01	11:41	C_GD		
11:35	12:14	GD_C	11:16	11:56	C_GD		
11:50	12:29	GD_C	11:31	12:11	C_GD		
12:05	12:44	GD_C	11:46	12:26	C_GD		
12:20	12:59	GD_C	12:01	12:41	C_GD		
12:35	13:14	GD_C	12:16	12:56	C_GD		
12:50	13:29	GD_C	12:31	13:11	C_GD		
13:05	13:44	GD_C	12:46	13:26	C_GD		
13:20	13:59	GD_C	13:01	13:41	C_GD		
13:34	14:13	GD_C	13:16	13:56	C_GD		
13:48	14:27	GD_C	13:32	14:12	C_GD		
14:03	14:42	GD_C	13:47	14:27	C_GD		
14:18	14:57	GD_C	14:02	14:42	C_GD		
14:33	15:12	GD_C	14:17	14:57	C_GD		
14:48	15:27	GD_C	14:32	15:12	C_GD		
15:03	15:42	GD_C	14:47	15:27	C_GD		
15:18	15:59	GD_C	15:02	15:42	C_GD		
15:34	16:15	GD_C	15:17	15:57	C_GD		
15:49	16:30	GD_C	15:32	16:12	C_GD		
16:04	16:45	GD_C	15:47	16:27	C_GD		
16:19	17:00	GD_C	16:02	16:42	C_GD		
16:34	17:15	GD_C	16:17	16:57	C_GD		
16:49	17:30	GD_C	16:32	17:12	C_GD		
17:04	17:44	GD_C	16:47	17:27	C_GD		
17:19	17:58	GD_C	17:02	17:42	C_GD		
17:34	18:13	GD_C	17:18	17:58	C_GD		
17:49	18:28	GD_C	17:33	18:13	C_GD		
18:07	18:46	GD_C	17:47	18:27	C_GD		
18:28	19:07	GD_C	18:07	18:47	C_GD		
18:48	19:27	GD_C	18:25	19:05	C_GD		
19:08	19:47	GD_C	18:44	19:24	C_GD		
19:28	20:07	GD_C	19:04	19:44	C_GD		
19:48	20:27	GD_C	19:24	20:04	C_GD		
20:08	20:47	GD_C	19:47	20:27	C_GD		
20:30	21:09	GD_C	20:04	20:44	C_GD		
21:04	21:43	GD_C	20:24	21:04	C_GD		
21:34	22:13	GD_C	20:54	21:34	C_GD		
22:05	22:44	GD_C	21:25	22:05	C_GD		
22:35	23:14	GD_C	21:55	22:35	C_GD		
			22:25	23:05	C_GD		

Figure D.5: Weekday schedule, adaptation of the timetable to the bus runs for each direction of line 22 in Gdynia

Departures on Saturdays (except public holidays):							
Gdynia Dworzec Gł. PKP - Cisowa			Cisowa - Gdynia Dworzec Gł. PKP				
Gdynia Dworzec Gł. PKP 03	Cisowa SKM 02	string	Cisowa SKM 06	Gdynia Dworzec Gł. PKP 02	string		BUS
05:49	06:25	GD_C	05:00	05:37	C_GD		1
06:19	06:55	GD_C	05:30	06:07	C_GD		2
06:43	07:19	GD_C	06:00	06:37	C_GD		3
07:03	07:39	GD_C	06:25	07:00	C_GD		4
07:23	07:59	GD_C	06:43	07:20	C_GD		5
07:43	08:19	GD_C	07:02	07:39	C_GD		6
08:03	08:39	GD_C	07:22	07:59	C_GD		
08:23	08:59	GD_C	07:42	08:19	C_GD		
08:45	09:21	GD_C	08:00	08:37	C_GD		
09:05	09:41	GD_C	08:19	08:56	C_GD		
09:25	10:01	GD_C	08:39	09:16	C_GD		
09:45	10:21	GD_C	08:59	09:36	C_GD		
10:00	10:36	GD_C	09:15	09:52	C_GD		
10:13	10:54	GD_C	09:27	10:04	C_GD		
10:28	11:04	GD_C	09:41	10:18	C_GD		
10:43	11:19	GD_C	09:56	10:33	C_GD		
10:58	11:34	GD_C	10:11	10:48	C_GD		
11:13	11:49	GD_C	10:26	11:03	C_GD		
11:28	12:04	GD_C	10:41	11:18	C_GD		
11:43	12:19	GD_C	10:56	11:33	C_GD		
11:58	12:34	GD_C	11:11	11:48	C_GD		
12:18	12:54	GD_C	11:26	12:03	C_GD		
12:28	13:04	GD_C	11:41	12:18	C_GD		
12:43	13:19	GD_C	11:56	12:33	C_GD		
12:58	13:34	GD_C	12:11	12:48	C_GD		
13:13	13:49	GD_C	12:26	13:03	C_GD		
13:28	14:04	GD_C	12:41	13:18	C_GD		
13:43	14:19	GD_C	12:56	13:33	C_GD		
13:58	14:34	GD_C	13:11	13:48	C_GD		
14:13	14:49	GD_C	13:26	14:03	C_GD		
14:28	15:04	GD_C	13:41	14:18	C_GD		
14:43	15:19	GD_C	13:56	14:33	C_GD		
14:53	15:29	GD_C	14:11	14:48	C_GD		
15:12	15:48	GD_C	14:26	15:03	C_GD		
15:32	16:08	GD_C	14:46	15:23	C_GD		
15:52	16:28	GD_C	15:06	15:43	C_GD		
16:12	16:48	GD_C	15:25	16:02	C_GD		
16:33	17:09	GD_C	15:48	16:25	C_GD		
16:53	17:29	GD_C	16:08	16:45	C_GD		
17:13	17:49	GD_C	16:28	17:05	C_GD		
17:34	18:10	GD_C	16:48	17:25	C_GD		
17:54	18:30	GD_C	17:05	17:42	C_GD		
18:11	18:47	GD_C	17:25	18:02	C_GD		
18:31	19:07	GD_C	17:42	18:19	C_GD		
18:50	19:26	GD_C	18:02	18:39	C_GD		
19:10	19:46	GD_C	18:24	19:01	C_GD		
19:28	20:04	GD_C	18:47	19:24	C_GD		
19:48	20:24	GD_C	19:07	19:44	C_GD		
20:08	20:44	GD_C	19:27	20:04	C_GD		
20:30	21:06	GD_C	19:46	20:23	C_GD		
21:03	21:39	GD_C	20:04	20:41	C_GD		
21:33	22:09	GD_C	20:24	21:01	C_GD		
22:03	22:39	GD_C	20:54	21:31	C_GD		
22:33	23:09	GD_C	21:25	22:02	C_GD		
			21:55	22:32	C_GD		
			22:25	23:02	C_GD		

Figure D.6: Saturday schedule, adaptation of the timetable to the bus runs for each direction of line 22 in Gdynia

Departures on Sundays and public holidays:							
Gdynia Dworzec Gł. PKP - Cisowa			Cisowa - Gdynia Dworzec Gł. PKP				
Gdynia Dworzec Gł. PKP 03	Cisowa SKM 02	string	Cisowa SKM 06	Gdynia Dworzec Gł. PKP 02	string		BUS
06:03	06:37	GD_C	05:21	05:59	C_GD		1
06:33	07:07	GD_C	05:51	06:29	C_GD		2
07:03	07:37	GD_C	06:21	06:59	C_GD		3
07:33	08:07	GD_C	06:51	07:29	C_GD		4
08:03	08:37	GD_C	07:21	07:59	C_GD		5
08:33	09:07	GD_C	07:51	08:29	C_GD		6
09:03	09:37	GD_C	08:20	08:58	C_GD		
09:33	10:07	GD_C	08:50	09:28	C_GD		
10:03	10:37	GD_C	09:20	09:58	C_GD		
10:33	11:07	GD_C	09:50	10:28	C_GD		
10:53	11:27	GD_C	10:08	10:46	C_GD		
11:13	11:47	GD_C	10:23	11:01	C_GD		
11:33	12:07	GD_C	10:44	11:22	C_GD		
11:53	12:27	GD_C	11:07	11:45	C_GD		
12:13	12:47	GD_C	11:27	12:05	C_GD		
12:33	13:07	GD_C	11:47	12:25	C_GD		
12:53	13:27	GD_C	12:07	12:45	C_GD		
13:13	13:47	GD_C	12:27	13:02	C_GD		
13:33	14:07	GD_C	12:47	13:25	C_GD		
13:53	14:27	GD_C	13:07	13:45	C_GD		
14:13	14:47	GD_C	13:27	14:05	C_GD		
14:33	15:07	GD_C	13:47	14:25	C_GD		
14:53	15:27	GD_C	14:04	14:42	C_GD		
15:13	15:47	GD_C	14:24	15:02	C_GD		
15:33	16:07	GD_C	14:44	15:22	C_GD		
15:53	16:27	GD_C	15:07	15:45	C_GD		
16:13	16:47	GD_C	15:24	16:02	C_GD		
16:33	17:07	GD_C	15:44	16:22	C_GD		
16:53	17:27	GD_C	16:04	16:42	C_GD		
17:13	17:47	GD_C	16:27	17:05	C_GD		
17:34	18:08	GD_C	16:44	17:22	C_GD		
17:54	18:28	GD_C	17:04	17:42	C_GD		
18:11	18:45	GD_C	17:27	18:05	C_GD		
18:31	19:05	GD_C	17:42	18:20	C_GD		
18:50	19:24	GD_C	18:02	18:40	C_GD		
19:10	19:44	GD_C	18:24	19:02	C_GD		
19:28	20:02	GD_C	18:45	19:23	C_GD		
19:48	20:22	GD_C	19:05	19:43	C_GD		
20:08	20:42	GD_C	19:24	20:02	C_GD		
20:30	21:04	GD_C	19:44	20:22	C_GD		
21:03	21:37	GD_C	20:04	20:42	C_GD		
21:33	22:07	GD_C	20:24	21:02	C_GD		
22:03	22:37	GD_C	20:54	21:32	C_GD		
22:33	23:07	GD_C	21:25	22:03	C_GD		
			21:55	22:33	C_GD		
			22:25	23:03	C_GD		

Figure D.7: Sunday schedule, adaptation of the timetable to the bus runs for each direction of line 22 in Gdynia

Departures from Monday to Friday (except public holidays):																	
1			2			3			4			5			6		
time	step	string	time	step	string	time	step	string	time	step	string	time	step	string	time	step	string
07:56	28560	Turnon	08:11	29460	Turnon	08:31	30660	Turnon	08:26	30360	Turnon	08:41	31260	Turnon	08:16	29760	Turnon
08:01	28860	C_GD	08:16	29760	C_GD	08:36	30960	GD_C	08:31	30660	C_GD	08:46	31560	C_GD	08:21	30060	GD_C
08:51	31860	GD_C	09:06	32760	GD_C	09:16	33360	C_GD	09:21	33660	GD_C	09:36	34560	GD_C	09:01	32460	C_GD
09:31	34260	C_GD	09:46	35160	C_GD	10:06	36360	GD_C	10:01	36060	C_GD	10:16	36960	C_GD	09:51	35460	GD_C
10:21	37260	GD_C	10:35	38100	GD_C	10:46	38760	C_GD	10:50	39000	GD_C	11:05	39900	GD_C	10:31	37860	C_GD
11:01	39660	C_GD	11:16	40560	C_GD	11:35	41700	GD_C	11:31	41460	C_GD	11:46	42360	C_GD	11:20	40800	GD_C
11:50	42600	GD_C	12:05	43500	GD_C	12:16	44160	C_GD	12:20	44400	GD_C	12:35	45300	GD_C	12:01	43260	C_GD
12:31	45060	C_GD	12:46	45960	C_GD	13:05	47100	GD_C	13:01	46860	C_GD	13:16	47760	C_GD	12:50	46200	GD_C
13:20	48000	GD_C	13:34	48840	GD_C	13:47	49620	C_GD	13:48	49680	GD_C	14:03	50580	GD_C	13:32	48720	C_GD
14:02	50520	C_GD	14:17	51420	C_GD	14:33	52380	GD_C	14:32	52320	C_GD	14:47	53220	C_GD	14:18	51480	GD_C
14:48	53280	GD_C	15:03	54180	GD_C	15:17	55020	C_GD	15:18	55080	GD_C	15:34	56040	GD_C	15:02	54120	C_GD
15:32	55920	C_GD	15:47	56820	C_GD	16:04	57840	GD_C	16:02	57720	C_GD	16:17	58620	C_GD	15:49	56940	GD_C
16:19	58740	GD_C	16:34	59640	GD_C	16:47	60420	C_GD	16:49	60540	GD_C	17:04	61440	GD_C	16:32	59520	C_GD
17:02	61320	C_GD	17:18	62280	C_GD	17:34	63240	GD_C	17:33	63180	C_GD	17:47	64020	C_GD	17:19	62340	GD_C
17:49	64140	GD_C	18:07	65220	GD_C	18:25	66300	C_GD	18:28	66480	GD_C	18:48	67680	GD_C	18:07	65220	C_GD
18:44	67440	C_GD	19:04	68640	C_GD	19:08	68880	GD_C	19:24	69840	C_GD	20:24	73440	C_GD	18:12	65520	Turnoff
19:28	70080	GD_C	19:48	71280	GD_C	19:47	71220	C_GD	20:08	72480	GD_C	20:29	73740	Turnoff			
20:24	73440	C_GD	20:54	75240	C_GD	20:30	73800	GD_C	20:13	72780	Turnoff						
21:04	75840	GD_C	21:34	77640	GD_C	21:25	77100	C_GD									
21:55	78900	C_GD	22:25	80700	C_GD	22:05	79500	GD_C									
22:35	81300	GD_C	22:30	81000	Turnoff	22:10	79800	Turnoff									
22:40	81600	Turnoff															

Figure D.8: Weekday schedule, bus runs coded with steps and strings for each run of line 22 in Gdynia

Departures on Saturdays (except public holidays):																	
1			2			3			4			5			6		
time	step	string	time	step	string	time	step	string	time	step	string	time	step	string	time	step	string
04:55	17700	Turnon	05:25	19500	Turnon	05:55	21300	Turnon	06:38	23880	Turnon	09:10	33000	Turnon	09:51	35460	Turnon
05:00	18000	C_GD	05:30	19800	C_GD	06:00	21600	C_GD	06:43	24180	C_GD	09:15	33300	C_GD	09:56	35760	C_GD
05:49	20940	GD_C	06:19	22740	GD_C	06:43	24180	GD_C	07:23	26580	GD_C	10:00	36000	GD_C	10:28	37680	GD_C
06:25	23100	C_GD	07:02	25320	C_GD	07:22	26520	C_GD	08:00	28800	C_GD	10:41	38460	C_GD	11:11	40260	C_GD
07:03	25380	GD_C	07:43	27780	GD_C	08:03	28980	GD_C	08:45	31500	GD_C	11:28	41280	GD_C	11:58	43080	GD_C
07:42	27720	C_GD	08:19	29940	C_GD	08:39	31140	C_GD	09:27	34020	C_GD	12:11	43860	C_GD	12:41	45660	C_GD
08:23	30180	GD_C	09:05	32700	GD_C	09:25	33900	GD_C	10:43	38580	GD_C	12:58	46680	GD_C	13:28	48480	GD_C
08:59	32340	C_GD	09:41	34860	C_GD	10:11	36660	C_GD	11:26	41160	C_GD	13:41	49260	C_GD	14:11	51060	C_GD
09:45	35100	GD_C	10:13	36780	GD_C	10:58	39480	GD_C	12:28	44880	GD_C	14:28	52080	GD_C	14:53	53580	GD_C
10:26	37560	C_GD	10:56	39360	C_GD	11:41	42060	C_GD	13:11	47460	C_GD	17:05	61500	C_GD	14:58	53880	Turnoff
11:13	40380	GD_C	11:43	42180	GD_C	12:18	44280	GD_C	13:58	50280	GD_C	17:54	64440	GD_C			
11:56	42960	C_GD	12:26	44760	C_GD	12:56	46560	C_GD	15:06	54360	C_GD	17:59	64740	Turnoff			
12:43	45780	GD_C	13:13	47580	GD_C	13:43	49380	GD_C	15:52	57120	GD_C						
13:26	48360	C_GD	13:06	47160	C_GD	14:26	51960	C_GD	16:28	59280	C_GD						
14:13	51180	GD_C	14:43	52980	GD_C	15:12	54720	GD_C	17:13	61980	GD_C						
14:46	53160	C_GD	15:25	55500	C_GD	15:48	56880	C_GD	18:02	64920	C_GD						
15:32	55920	GD_C	16:12	58320	GD_C	16:33	59580	GD_C	18:50	67800	GD_C						
16:08	58080	C_GD	16:48	60480	C_GD	17:25	62700	C_GD	19:27	70020	C_GD						
16:53	60780	GD_C	17:34	63240	GD_C	18:11	65460	GD_C	20:08	72480	GD_C						
17:42	63720	C_GD	18:24	66240	C_GD	18:47	67620	C_GD	20:54	75240	C_GD						
18:31	66660	GD_C	19:10	69000	GD_C	19:28	70080	GD_C	20:59	75540	Turnoff						
19:07	68820	C_GD	19:46	71160	C_GD	20:04	72240	C_GD									
19:48	71280	GD_C	20:23	73380	GD_C	21:33	77580	GD_C									
20:24	73440	C_GD	21:25	77100	C_GD	22:25	80700	C_GD									
21:03	75780	GD_C	22:02	79320	GD_C	22:30	81000	Turnoff									
21:55	78900	C_GD	22:07	79620	Turnoff												
22:33	81180	GD_C															
22:38	81480	Turnoff															

Figure D.9: Saturday schedule, bus runs coded with steps and strings for each run of line 22 in Gdynia

Departures on Sundays and public holidays:																	
1			2			3			4			5			6		
time	step	string	time	step	string	time	step	string	time	step	string	time	step	string	time	step	string
05:16	18960	Turnon	05:46	20760	Turnon	06:16	22560	Turnon	07:16	26160	Turnon	13:59	50340	Turnon			
05:21	19260	C_GD	05:51	21060	C_GD	06:21	22860	C_GD	07:21	26460	C_GD	14:04	50640	C_GD			
06:03	21780	GD_C	06:33	23580	GD_C	07:03	25380	GD_C	10:23	37380	C_GD	14:53	53580	GD_C			
06:51	24660	C_GD	08:03	28980	GD_C	07:51	28260	C_GD	11:13	40380	GD_C	15:44	56640	C_GD			
07:33	27180	GD_C	08:50	31800	C_GD	08:33	30780	GD_C	11:47	42420	C_GD	16:33	59580	GD_C			
08:20	30000	C_GD	09:33	34380	GD_C	09:20	33600	C_GD	12:33	45180	GD_C	17:42	63720	C_GD			
09:03	32580	GD_C	10:08	36480	C_GD	10:03	36180	GD_C	13:07	47220	C_GD	18:31	66660	GD_C			
09:50	35400	C_GD	10:53	39180	GD_C	10:44	38640	C_GD	13:53	49980	GD_C	19:05	68700	C_GD			
10:33	37980	GD_C	11:27	41220	C_GD	11:33	41580	GD_C	14:44	53040	C_GD	19:48	71280	GD_C			
11:07	40020	C_GD	12:13	43980	GD_C	12:07	43620	C_GD	15:33	55980	GD_C	19:53	71580	Turnoff			
11:53	42780	GD_C	12:47	46020	C_GD	12:53	46380	GD_C	16:44	60240	C_GD						
12:27	44820	C_GD	13:33	48780	GD_C	13:27	48420	C_GD	17:34	63240	GD_C						
13:13	47580	GD_C	14:24	51840	C_GD	14:13	51180	GD_C	18:24	66240	C_GD						
13:47	49620	C_GD	15:13	54780	GD_C	15:24	55440	C_GD	19:10	69000	GD_C						
14:33	52380	GD_C	16:04	57840	C_GD	16:13	58380	GD_C	20:24	73440	C_GD						
15:07	54420	C_GD	16:53	60780	GD_C	17:04	61440	C_GD	20:29	73740	Turnoff						
15:53	57180	GD_C	17:27	62820	C_GD	17:54	64440	GD_C									
16:27	59220	C_GD	18:11	65460	GD_C	19:44	71040	C_GD									
17:13	61980	GD_C	18:45	67500	C_GD	20:30	73800	GD_C									
18:02	64920	C_GD	19:28	70080	GD_C	21:25	77100	C_GD									
18:50	67800	GD_C	20:04	72240	C_GD	22:03	79380	GD_C									
19:24	69840	C_GD	21:03	75780	GD_C	22:08	79680	Turnoff									
20:08	72480	GD_C	21:55	78900	C_GD												
20:54	75240	C_GD	22:33	81180	GD_C												
21:33	77580	GD_C	22:38	81480	Turnoff												
22:25	80700	C_GD															
22:30	81000	Turnoff															

Figure D.10: Sunday schedule, bus runs coded with steps and strings for each run of line 22 in Gdynia

Section	Substation	Substation Voltage [V]	Code	Number of sections per substation
Cisowa	Podstacja Polnocna	685	1/1	6
Kcynska			1/2	
Poczta			1/3	
Gazownia			1/4	
Wiejska			1/5	
Pustki			1/6	
Baza	Podstacja Grabowek	675		3
Leszczynki			2/1	
Grabowek			2/2	
Mleczarnia			2/3	
Stocznia	Podstacja Dworzec	690	3/1	3
Dr_Towarowy			3/2	
Pl_Konstytucji			3/3	
Pl_Kaszubski	Podstacja Wendy	685	4/1	3
Swietojanska			4/2	
10 Luty (10 lutego)			4/3	
Warszawska	Podstacja Kielecka	684	5/1	3
Slaska (Węzeł)			5/2	
Wzgorze_Sw_Maks			5/3	
Redlowo	Podstacja Redlowo	680	6/1	3
Maly_Kack			6/2	
Wielkopolska_Klif			6/3	
Kamienny Potok	Podstacja Sopot	690	7/1	2
Sopot			7/2	
Reja	Podstacja Sopot Reja	704	8/1	1
Wajdeloty	Podstacja Wielkopolska	690	9/1	1
Zrodto Marli	Podstacja Chwaszczynska	690	10/1	5
Nowowiczlinska			10/2	
Mietowa			10/3	
Rdestowa			10/4	
Chwaszczynska			10/5	

Figure D.11: Gdynia outputs: section codes, substation voltages, number of sections per substation

Section	Substation	Average system transmission losses	Substation transmission losses [%]	Section transmission losses [%]
Cisowa	Podstacja Polnocna	8.50	9.10	4.90
Kcynska				9.80
Poczta				3.40
Gazownia				9.10
Wiejska				7.80
Pustki				14.00
Baza	Podstacja Grabowek		8.90	
Leszczynki				6.00
Grabowek				5.00
Mleczarnia				15.30
Stocznia	Podstacja Dworzec		9.30	8.20
Dr_Towarowy				13.60
Pl_Konstytucji				2.80
Pl_Kaszubski	Podstacja Wendy		7.00	5.70
Swietojanska				9.50
10 Luty (10 lutego)				5.50
Warszawska	Podstacja Kielecka		6.00	8.70
Slaska (Węzeł)				2.50
Wzgorze_Sw_Maks				4.80
Redlowo	Podstacja Redlowo		9.10	7.70
Maly_Kack				11.70
Wielkopolska_Klif				7.80
Kamienny Potok	Podstacja Sopot		8.00	5.70
Sopot				9.50
Reja	Podstacja Sopot Reja		4.10	4.10
Wajdeloty	Podstacja Wielkopolska		7.20	7.20
Zrodto Marli	Podstacja Chwaszczynska		9.20	10.90
Nowowiczlinska				8.40
Mietowa				6.10
Rdestowa				7.20
Chwaszczynska				9.50

Figure D.12: Gdynia outputs: system, section and substation transmission losses

Section	Substation	Section Length [km]	Km covered by substation	Average section length substation
Cisowa	Podstacja Polnocna	1250	8540	1423
Kcynska		1660		
Poczta		380		
Gazownia		1100		
Wiejska		1700		
Pustki		2450		
Baza	Podstacja Grabowek		3450	1150
Leszczynki		1500		
Grabowek		850		
Mleczarnia		1100		
Stocznia	Podstacja Dworzec	1450	3020	1007
Dr_Towarowy		920		
Pl_Konstytucji		650		
Pl_Kaszubski	Podstacja Wendy	900	2700	900
Swietojanska		1200		
10 Luty (10 lutego)		600		
Warszawska	Podstacja Kielecka	1160	2380	793
Slaska (Węzeł)		470		
Wzgorze_Sw_Maks		750		
Redlowo	Podstacja Redlowo	2550	5150	1717
Maly_Kack		1700		
Wielkopolska_Klif		900		
Kamienny Potok	Podstacja Sopot	2200	4200	2100
Sopot		2000		
Reja	Podstacja Sopot Reja	1100	1100	1100
Wajdeloty	Podstacja Wielkopolska	1370	1370	1370
Zrodto Marli	Podstacja Chwaszczynska	1980	6965	1393
Nowowiczlinska		1680		
Mietowa		705		
Rdestowa		1300		
Chwaszczynska		1300		

Figure D.13: Gdynia outputs: section lengths, substation average section length and substation total overhead km fed

Section	Substation	Energy Requirements sections [kWh]	Energy requirements substation [MWh]
Cisowa	Podstacja Polnocna	145940	905
Kcynska		151367	
Poczta		65637	
Gazownia		100606	
Wiejska		243219	
Pustki		179934	
Baza	Podstacja Grabowek		1298
Leszczynki		432482	
Grabowek		404072	
Mleczarnia		435842	
Stocznia	Podstacja Dworzec	102520	616
Dr_Towarowy		382432	
Pl_Konstytucji		118813	
Pl_Kaszubski	Podstacja Wendy	267927	867
Swietojanska		425185	
10 Luty (10 lutego)		156901	
Warszawska	Podstacja Kielecka	344602	686
Slaska (Węzeł)		82883	
Wzgorze_Sw_Maks		244325	
Redlowo	Podstacja Redlowo	710401	1301
Maly_Kack		421512	
Wielkopolska_Klif		142826	
Kamienny Potok	Podstacja Sopot	148620	268
Sopot		114038	
Reja	Podstacja Sopot Reja	53155	54
Wajdeloty	Podstacja Wielkopolska	303427	310
Zrodto Marli	Podstacja Chwaszczynska	463454	1136
Nowowiczlinska		256802	
Mietowa		72291	
Rdestowa		150322	
Chwaszczynska		170266	

Figure D.14: Gdynia outputs: section and substation energy demand

Section	Substation	NB section max	NB section mean	NB substation max	NB substation mean
Cisowa	Podstacja Polnocna	3	0.7	9	3.3
Kcynska		3	0.6		
Poczta		3	0.2		
Gazownia		3	0.4		
Wiejska		4	0.8		
Pustki		3	0.6		
Baza	Podstacja Grabowek			18	6.6
Leszczynki		8	2.6		
Grabowek		9	2.5		
Mleczarnia		9	1.6		
Stocznia	Podstacja Dworzec	2	0.3	11	2.7
Dr_Towarowy		8	1.7		
Pl_Konstytucji		5	0.7		
Pl_Kaszubski	Podstacja Wendy	7	1.1	12	3.4
Swietojanska		8	1.7		
10 Luty (10 lutego)		5	0.6		
Warszawska	Podstacja Kielecka	7	1.7	10	3.2
Slaska (Węzeł)		4	0.4		
Wzgorze_Sw_Maks		6	1.1		
Redlowo	Podstacja Redlowo	11	2.6	14	4.7
Maly_Kack		6	1.6		
Wielkopolska_Klif		4	0.5		
Kamienny Potok	Podstacja Sopot	4	0.6	5	0.9
Sopot		3	0.4		
Reja	Podstacja Sopot Reja	3	0.5	3	0.5
Wajdeloty	Podstacja Wielkopolska	6	1.0	6	1.0
Zrodto Marli	Podstacja Chwaszczynska	8	1.8	13	4.3
Nowowiczlinska		5	0.9		
Mietowa		3	0.3		
Rdestowa		4	0.5		
Chwaszczynska		5	1.1		

Figure D.15: Gdynia outputs: section and substation average and maximum bus traffic

Section	Substation	Substation Voltage [V]	number of sections per substation
2	1	698	2
3			
14	2	698	3
15			
16			
12	HQ (3,6)	630	4
36			
9		660	
32			
5	CS (4,9,21)	*685*	5
6		685	
8			
25		677	
37		685	
38			
17	5	700	3
18			
35			
20	7	724	2
21			
13	8	700	2
19			
22	10	716	1
30	11	659	2
31			
23	12	686	2
24			
28	13	673	2
29			
26	14	628	3
27			
41			
33	15	684	2
34			
42	16	705	2
43			
39	17	728	2
40			
46	18	700	2
47			
44	19	700	2
45			
48	20	700	2
49			

Figure D.16: Arnhem outputs: substation voltages and number of sections per substation

Section	Substation	Average system transmission losses	Section transmission losses [%]	Substation transmission losses [%]
2	1	6.00	7.05	6.19
3			5.33	
14	2		8.70	6.00
15			3.98	
16			5.32	
12	HQ (3,6)		8.48	7.51
36			8.48	
9			6.53	
32			6.53	
5	CS (4,9,21)		*0.00*	3.51
6			3.45	
8			2.21	
25			4.37	
37			3.77	
38			3.77	
17	5		5.64	5.70
18			6.92	
35			4.55	
20	7		4.22	5.46
21			6.70	
13	8		4.81	6.71
19			8.61	
22	10		7.41	7.41
30	11		6.08	6.08
31			6.08	
23	12		4.13	5.03
24			5.93	
28	13		4.14	5.22
29			6.30	
26	14		6.16	6.16
27			6.16	
41			6.16	
33	15		6.32	7.52
34			8.72	
42	16		5.29	4.22
43			3.15	
39	17		4.85	4.47
40			4.08	
46	18		5.74	5.71
47			5.67	
44	19		6.79	7.25
45			7.70	
48	20		7.13	7.42
49			7.71	

Figure D.17: Arnhem outputs: system, section and substation transmission losses

Section	Substation	Section Length [km]	Km covered by substation	Average section length substation
2	1	1300	2180	1090
3		880		
14	2	1320	3340	1113
15		1120		
16		900		
12	HQ (3,6)	1120	4450	1113
36		1370		
9		900		
32		1060		
5	CS (4,9,21)	*0*	2340	468
6		440		
8		100		
25		860		
37		590		
38		350		
17	5	1030	2980	993
18		1250		
35		700		
20	7	960	2660	1330
21		1700		
13	8	1670	4510	2255
19		2840		
22	10	1590	1590	1590
30	11	950	2350	1175
31		1400		
23	12	850	2250	1125
24		1400		
28	13	970	2070	1035
29		1100		
26	14	1000	3610	1203
27		1300		
41		1310		
33	15	1110	3090	1545
34		1980		
42	16	1220	1970	985
43		750		
39	17	1150	2100	1050
40		950		
46	18	1000	2310	1155
47		1310		
44	19	1400	2650	1325
45		1250		
48	20	1680	3190	1595
49		1510		

Figure D.18: Arnhem outputs: section lengths, substation average section length and substation total overhead km fed

Section	Substation	Energy Requirements sections [kWh]	Energy requirements substation [MWh]
2	1	95171	168
3		73231	
14	2	153137	412
15		104508	
16		154522	
12	HQ (3,6)	344449	912
36		225595	
9		216544	
32		125680	
5	CS (4,9,21)		928
6		263208	
8		15100	
25		150062	
37		45919	
38		454141	
17	5	81745	209
18		95041	
35		31823	
20	7	78911	236
21		157384	
13	8	159201	208
19		48970	
22	10	157479	157
30	11	125249	287
31		161367	
23	12	65732	216
24		150054	
28	13	96540	212
29		115698	
26	14	182535	470
27		121237	
41		165971	
33	15	155752	270
34		114702	
42	16	221104	338
43		116639	
39	17	134210	257
40		122410	
46	18	43383	81
47		37567	
44	19	77154	175
45		98162	
48	20	136189	306
49		170157	

Figure D.19: Arnhem outputs: section and substation energy demand

Section	Substation	NB section max	NB section mean	NB substation max	NB substation mean
2	1	2	0.3	3	0.5
3		3	0.2		
14	2	2	0.5	6	1.2
15		3	0.3		
16		4	0.5		
12	HQ (3,6)	7	1.2	10	2.8
36		3	0.7		
9		5	0.6		
32		3	0.4		
5	CS (4,9,21)			14	4.6
6		7	1.0		
8		2	0.1		
25		4	0.5		
37		2	0.1		
38		10	2.9		
17	5	3	0.2	4	0.6
18		2	0.3		
35		1	0.1		
20	7	2	0.2	2	0.8
21		2	0.5		
13	8	2	0.4	3	1.0
19		3	0.6		
22	10	3	0.5	3	0.5
30	11	3	0.3	5	1.3
31		4	1.0		
23	12	2	0.1	3	0.7
24		3	0.6		
28	13	2	0.2	3	0.5
29		3	0.3		
26	14	4	0.4	5	1.1
27		3	0.2		
41		3	0.4		
33	15	3	0.4	3	0.8
34		2	0.3		
42	16	4	0.7	4	1.1
43		4	0.4		
39	17	3	0.4	3	1.0
40		3	0.6		
46	18	1	0.1	1	0.2
47		1	0.1		
44	19	1	0.2	2	0.8
45		2	0.6		
48	20	2	0.4	5	1.1
49		3	0.7		

Figure D.20: Arnhem outputs: section and substation average and maximum bus traffic

Colophon

This document was typeset using LaTeX. The document layout was generated using the arsclassica package by Lorenzo Pantieri, which is an adaption of the original classicthesis package from André Miede.